Australian Geomechanics Volume 58 No 3 SEPTEMBER 2023

ISSN 0818-9110

AUSTRALIAN GEOMECHANICS

JOURNAL AND NEWS OF THE AUSTRALIAN GEOMECHANICS SOCIETY ISSN 0818-9110

VOLUME 58: NO.3 SEPTEMBER 2023

INCLUDING

AUSTRALIAN GEOMECHANICS SOCIETY

A technical society of
ENGINEERS AUSTRALIA

Reducing geotechnical uncertainty

INSITU GEOTECH SERVICES

reducing geotechnical uncertainty

COMPREHENSIVE RANGE OF
IN SITU TESTING, SAMPLING
AND GEOTECHNICAL SERVICES

mick@insitu.com.au
0407 467 025

mark@insitu.com.au
0437 824 776

www.insitu.com.au

BRISBANE | MELBOURNE | SYDNEY | HOBART | PERTH | TOWNSVILLE | PNG

Ranger Mine-Supply and Install Wicks in Pit 3, Jabiru, NT

Menard continues to deliver ground improvement solutions to the mining sector. For our recent project at Ranger Mine we installed 41,484 wick drains in a highly unconsolidated young hydraulic fill that is below water level. Fine cohesive soils have low permeability and it takes relatively long periods for them to consolidate under loads. Installation of PVDs greatly shortens the water drainage path and significantly reduces the consolidation time.

Ground Improvement Specialist

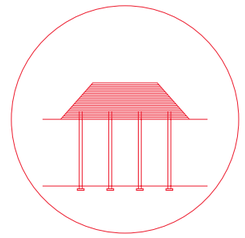

At Menard Oceania, we have a proven track record in delivering ground improvement works for complex structures. On this occasion, providing the foundations for the mining market.

Connect with us

Sydney (head office) +61 2 9491 7100
Brisbane +61 7 3354 9100
Melbourne +61 3 9321 1350
Perth +61 4 5040 2239
Christchurch (NZ) +64 3 365 3005

www.menardoceania.com.au

menard

AUSTRALIAN GEOMECHANICS

JOURNAL AND NEWS OF THE AUSTRALIAN GEOMECHANICS SOCIETY

VOLUME 58: NO.3 SEPTEMBER 2023

Cover Photo: Dolphin pile and anchor installation, Dampier, Western Australia
Photography and story: Stephen Kariuki

The existing Dampier Fuel Wharf in the Pilbara region of Western Australia was designed and built in 2010/2011 and consisted of a mooring system designed for vessels up to 46 kDWT. Upgrade works were completed in early 2023 and included the construction of new additional mooring dolphins and associated catwalk to allow for Panamax size vessels. The installation of raked driven steel piles was undertaken as part of the upgrade works. Where the driven piles did not achieve sufficient geotechnical uplift capacity, tension anchors were installed through the pile toe. Typical ground conditions at the pile toe consisted of high to very high strength granite/granophyre/dolerite.

The cover photo was taken from the crew transfer vessel and shows the barge setup in preparation for anchor installation.

AUSTRALIAN GEOMECHANICS SOCIETY

Published by

The Australian Geomechanics Society, National Secretariat

PO Box 7, The Gap, QLD 4061

ISSN 0818-9110

ENGINEERS AUSTRALIA

The Australian Geomechanics Society is a technical society of Engineers Australia.

CONTENTS

TECHNICAL PAPERS

INTERNATIONAL SOCIETIES

[All papers have been refereed in accordance with the full HERDC review process, unless stated otherwise]

AUSTRALIAN GEOMECHANICS SOCIETY NATIONAL COMMITTEE

TITLE	NAME	BUSINESS PHONE/MOBILE	EMAIL
Dr	David LACEY *Chair*	Tel: 07 3831 4600 Mob: 0499 819 991	dlacey@fsg-geotechnics.com.au
Dr	Nina LEVY *Immediate Past Chair*	Tel: 08 9423 3338 Mob: 0419 910 733	n.levy@fugro.com
Mr	Timothy THOMPSON *Vice Chair and Treasurer*	Tel: 07 3023 6284	timothy.thompson@arup.com
Mr	John JOHNSTON *Newcastle Elected Member*	Tel: 0411 210 727	j.a.johnston@live.com
Dr	Ali PARSA *New South Wales Elected Member*	Mob: 0424 573 014	aparsa@jkgeotechnics.com.au
Dr	Amir SHAHKOLAHI *Queensland Elected Member*	Mob: 0450 751 095	amir@globalsynthetics.com.au
Mr	Rod FYFE *South Australia & NT Elected Member*	Mob: 0408 100 225	r.fyfe@geofabrics.com.au
Dr	Ali TOLOOIYAN *Tasmania Elected Member*	Tel: 03 6226 2429	ali.tolooiyan@utas.edu.au
Dr	Daniel KING *Victoria Elected Member*	Mob: 0408 990 122	dking@golder.com.au
Dr	Harun MEER *Western Australia Elected Member*	Mob: 0425 545 508	harun.meer@localgeotechnics.com.au
Mr	Graham SCHOLEY *ISSMGE Vice President for Australasia*	Tel: 02 9478 3900 Mob: 0417 460 667	gscholey@golder.com.au
Dr	Sevda DEHKHODA *ISRM Vice President for Australasia*	Tel: 08 6436 8591 Mob: 0449 174 195	sevda.dehkhoda@uqconnect.edu.au
Mr	Anthony BOWDEN *IAEG Vice President for Australasia*	Tel: 02 9320 9320 Mob: 0418 411 749	anthonyjh.bowden@gmail.com
Dr	Hugo E ACOSTA MARTINEZ *Interim Editor, Australian Geomechanics*	Mob: 0423 528 174	editor@australiangeomechanics.org
Ms	Eleni GKELI *NZGS Chair*		chair@nzgs.org
Mr	Jon GIBBS *National Secretariat*	Tel: 07 3705 5971	secretary@australiangeomechanics.org

VIEW FROM THE CHAIR

SEPTEMBER 2023

Welcome to the 3rd issue of *Australian Geomechanics* for 2023. I hope everyone is well, enjoying their spring and having a productive second half of 2023.

With the 2022-2023 financial year having recently concluded, it is a good time to reflect on the status of the society. I am pleased to be able to report that the society's membership has grown to nearly 2,600 individuals as of 30 June 2023. This represents a very impressive increase of over 10 % in total membership for the preceding 12 months; and has been driven by an increased membership across all levels (professional, retired, post-graduate and student). I welcome all our new members, and I hope that these increased membership number reflects the AGS' ability to provide relevant information and professional development opportunities.

Since the last edition of the journal, the undoubtable highlight of the AGS event calendar was the successful delivery of the *14th Australia New Zealand Conference on Geomechanics* in Cairns, Queensland. This event saw over 480 geomechanics practitioners, from at least 16 countries, converge to tropical North Queensland in the first week of July to attend the largest regular event that is organized by AGS. In addition, with Cairns playing host to this iteration of the ANZ quadrennial conference series, the 2023 edition was also the first time that the event was held outside of a state capital city.

Unfortunately, the much-anticipated warm winter sun did not entirely eventuate; but the 3-day technical program and multiple social events of the conference more than made up for the overcast skies. I hope everyone who attended had a good time and were able to take the opportunity to broaden both their technical awareness and network of colleagues.

A longer conference report has been compiled by the local organising committee and appears later in this edition of *Australian Geomechanics*. However, it would be remiss of me to thank, on behalf of the entire AGS, all of those involved in the organisation of this event – led by Dr. Richard Kelly. From all the feedback that I have heard, the attendees thoroughly enjoyed themselves.

I also wanted to briefly highlight other contributions directly made by the AGS to the ANZ2023 conference. As per recent national and international conferences hosted by the AGS, the society also took the opportunity to provide full sponsorship for a geotechnical engineer from within the Oceanic region to attend the conference. Ms. Lorin Tuilakepa from Fiji attended, and it was a delight to meet her at the event. This support aligns with the aims to expand the ISSMGE reach within the Oceanic region (beyond solely Australia and New Zealand), and is fully supported by both the AGS and NZGS. A brief conference report has been prepared by Lorin, which the AGS has chosen to republish herein

Similarly, the AGS supported the attendance of Ms. Denise Hayes to introduce the *Scott Sloan Memorial Session* at ANZ2023. From a personal viewpoint, it was lovely to meet Denise in person and, as everyone who attended the session will attest, it was very emotional to hear her discuss the passion that Scott unwaveringly demonstrated for geomechanics. Equally, the fondness that all the session's presenters had in remembering Scott was universal – both as a prolific and high-quality researcher, contributor to the development of the wider industry, and also as a personal friend to so many of our technical leaders.

Finally, the AGS also directly funded and facilitated the *Women in Engineering* Sundowner event on the second evening of the conference. During this event, slides prepared by over 60 inspiring women were presented to the crowd – highlighting the diverse group, and extensive contributions made by, women in our industry. Thanks for Dr. Nina Levy and her team for spearheading this event, which, in my opinion, was a great example of how to celebrate a specific subset of our widely varied fraternity.

At the close of ANZ2023, the NZGS announced that the *15th Australia New Zealand Conference on Geomechanics* will be hosted in Christchurch, New Zealand. I wish the NZGS organiser's all the best and look forward to seeing everyone 'across the ditch' in 2028.

A final takeaway from the ANZ0203 was the reinforcement of demand (and requirement) for the geomechanics industry to offer a robust program of practical professional development opportunities for our practitioners. This was the feedback received from both the workshop held to evaluate the interest in reviewing / updating the AGS' *Australian Landslide Risk Management Guidelines* (hosted by Darren Paul and Tony Miner, with AGS subsidising the cost of attendance for interested parties) and the ISSMGE's Heritage Time Capsule (HTC) organised panel session on *Education of the next generation of geomechanics professionals in ANZ* (with representatives from both Australian and New Zealand education institutions). This feedback relates back to both the provision of industry experienced personnel to assist with the delivery of relevant courses within the tertiary education environment, as well as the provision of additional, relevant training opportunities to professionals. This feedback also correlates well with the response to the 2023 (and prior years) training courses being co-ordinated by AGS, in which we have seen registrations exceed well above 90% of available spaces.

To build on this momentum, the AGS is looking to nationally co-ordinate a wider range of single-day training events over future years. The included program and rollout of such events is still currently taking shape, but examples of such events that would be added to the existing courses are anticipated to include events similar to the "Geotechnical Laboratory Testing Course" and "Short course on simple Field Testing" events which were developed and trialled by the QLD Chapter this year. The AGS is also keen to hear from suitably experienced practitioners that are interested in developing and presenting similar technical courses –

please email the National Secretary with ideas / expressions of interest in such roles.

Another role in which the AGS is seeking expressions of interest for is the Editor (or an editorial team) of this publication – *Australian Geomechanics*. A call for applications is included in this edition, and I encourage anyone interested to submit an expression on interest to the AGS secretariat. In addition, and as indicated in previous editions from my 'View from the Chair', there is also the intention is to widen both the pool of reviewers and a group of sub-editors / assistants associated with the publication. So, anyone who is keen to be involved in the quarterly production of this journal should not be afraid to put their hand up.

Mid-2023 has also seen the announcement of significant awards by both the AGS and ISSMGE, and I would like to publicly announce them to our membership.

The recipient of the 2022 'AGS Practitioner Award' is John Wagstaff. The awards committee unanimously agreed that John's contribution to the AGS – a relationship that has ensured nearly the entire 52-year history of the AGS – was almost unparalleled. Coupled with his commitment to the success of Australian civil and commercial development projects, and the nationwide footprint of his contributions, John truly has made a "significant contribution to the geotechnical profession" throughout Australia. The announcement and presentation of this award was made to John at the gala dinner of the ANZ2023 – and it was fitting that this announcement could be made in front of a truly national audience.

In early July it was formally announced that **Professor Harry Poulos is to be an inaugural recipient of the 'Lifetime Achievement Medal' of the International Society for Soil Mechanics and Geotechnical Engineering.** Professor Poulos joins Professor Michele Jamiolkowski (Italy) – whom unfortunately passed away the day prior to the award announcement by the ISSMGE Board – as the 2023 award recipients, with the award recognising their full career contribution and, specifically, the "manner in which their work has touched and shaped the lives and views of many". Congratulations Harry! The AGS were delighted when you accepted our approach to be the Australian nominee for this global award, and as mentioned in our nomination letter, we believe that Harry embodies the eligibility criteria associated of the award. Full details of the local investiture event will follow in due course.

Although I have previously publicly announced the award, **ANZ2023 saw Professor Mark Jaksa formally present the honour lecture associated with the John Jaeger Memorial Award**. This represents the first time in 8 years that the award has been presented and only the 11th time it has been presented since its inauguration in 1980. As the weight of the award itself is 8 kg, this makes it both the most rarely bestowed and "weightiest" award made by the AGS. From my audience viewpoint, Professor Jaksa effectively demonstrated his "contribution of the highest order over a lifetime commitment to the geotechnical profession in Australia" during his lecture entitled *Geotechnical variability: In the ground and throughout a career*. Mark continually appears to be a pioneer in each of the fields he has chosen to research, as demonstrated by his compilation of a quasi-site investigation database for the Adelaide CBD in order to evaluate spatial variability of Keswick Clay (undertaken in the 1990's) through to the in-depth assessment of potential soil compaction issues associated with proposed lunar development. I recommend anyone looking for an interesting geomechanics read over a variety of geomechanics topics to seek out his keynote paper which is published within the ANZ2023 proceedings.

Presentation of John Jaeger Memorial Award after Award Lecture at ANZ2023 – David Lacey (L) and Prof Mark Jaksa (R)

As per the AGS' perpetual calendar of nationally coordinated awards, the nomination period for the 2023 E.H. Davis Memorial Lecturer is now open. Please refer the call for nominations contained within this edition of *Australian Geomechanics* or the awards section on the AGS website for further details. I strongly encourage any interested members to consider providing nominations.

Finally, Jay Ameratunga, who has acted as the AGS nominee on Standards Australia's Committee CE-020 (Geosynthetics) for over a decade has recently indicated that he no longer wishes to continue in the position. Jay's role included acting as Chair of the committee during the initial compilation and release of AS8700. With a revision to this standard now being considered, Jay has identified that it is an opportune time to pass the baton to another experienced AGS practitioner. On behalf of the AGS, I would like to sincerely thank Jay for this extensive service on this committee!

Until next time,

DAVID LACEY

National Chair, Australian Geomechanics Society

CHAPTER NEWS

NEW SOUTH WALES

A repeat of the 61st Rankine Lecture

The AGS Sydney Chapter hosted a repeat of the 61st Rankine Lecture on May 10th at the UTS lecture hall in Sydney. The lecture, titled "Constitutive Modelling in Computational Geomechanics," was presented by Emeritus Professor John Carter from the University of Newcastle and attracted over 80 attendees. In his excellent lecture, Professor Carter provided a comprehensive state-of-the-art summary of existing constitutive models and major developments over the past 50 years. He also discussed the specific limitations of these models, reminding the audience that they are merely imperfect idealisations of reality. Professor Carter's lecture was very engaging and informative. He avoided going into complex numerical detail, instead focusing on the physical basis of constitutive models and their practical applications. He also highlighted the importance of using constitutive models correctly, noting that a variety of models are available in commercial packages. In addition to hearing the Rankine Lecture in person, attendees were given the opportunity to ask questions and delve deeper into the lecture's subject matter - a unique opportunity to learn from one of the leading experts in the field of constitutive modelling.

The AGS Sydney Chapter would like to thank Professor John Carter for his time and availability. The chapter is proud to have hosted another successful repeat of the Rankine Lecture, and it is pleased that the number of Rankine lecturers from the Sydney & Newcastle Chapter is now reaching a very satisfying proportion in this prestigious event.

Repeated Rankine Lecture

ATS/AGS Seminar - Building around existing tunnels

The one-day seminar on Building Around Existing Tunnels was held successfully on April 2023 in Sydney with the participation of +70 professionals from government bodies, developers, consultants, contractors, and suppliers to share their knowledge and experiences in this area.

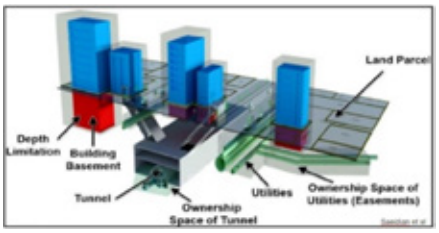

Building around existing tunnels

As there is an increasing demand for the assessment of the potential impact of new building construction, on the existing tunnels and other underground infrastructure, this seminar covered a wide range of topics and introduced new horizons for innovation and further developments in this area.

The seminar discussed the impact assessment guidelines and cases studies on the following type of tunnels:

- Major underground caverns
- Metro Tunnels
- Historical Tunnels
- Pressurised water tunnels
- Brick Tunnels
- Sewer Tunnels
- Sewer Tunnels
- Road Mined tunnels

AGS and ATS would like to thank all the speakers to provide great papers and presentations for the seminar: Strath Clarke (PSM), Don Cooper & Adrian Chau (Aurecon), Paul Hewitt (WSP), Owen Davies (Mott MacDonald), Peter Bourke (Sydney Metro), Jiping Pan (WSP), Lesley Yang (Aurecon), Carlos Sanchez (UNAM- Mexico), Mark Sheffield (Aurecon), Arun Sarathchandran (AECOM), Ted Nye (Nyeconsulting), Chenhui Lee (SMEC), Mohammad Khoshini (SMEC).

Also thanks to the organising Committee, in particular, Ted Nye for his significant contribution to organising the event:

- Ted Nye (Nyeconsulting)
- Philip Clark (TfNSW)
- Sam Mirlatifi (GHD)
- Asal Bidarmaghz (UNSW)
- Alexandre Gomes (SMEC)
- Sam Jones (Ghella)

The event was jointly sponsored by Engineers Australia, the Australian Tunnelling Society (ATS) and the Australian Geomechanics Society (AGS).

AGS Sydney Soil and Rock logging course 2023

Recognizing the crucial role of robust site investigation practices, the University of Technology Sydney (UTS) organised a highly successful and comprehensive Soil and Rock Logging Course on May 17th. Led by esteemed professionals Fred Barnes and Ian Shipway, the course received tremendous interest and garnered overwhelmingly positive feedback from its participants.

In line with the Australian Standard AS1726 - Geotechnical Site Investigations, the course offered participants an extensive range of knowledge and skills essential for precise soil and rock logging. The meticulously designed curriculum encompassed theoretical lectures, practical demonstrations, and hands-on exercises, resulting in a truly engaging and enriching learning experience for all attendees.

The successful planning and execution of the course were made possible by the invaluable contributions of three dedicated volunteers: Myles Harris-Ayling, Natalia Ramirez, and Troy Credlin.

2023 AGS Sydney Chapter Soil and Rock Logging Course

Young Geomechanical Professionals' Night

The YGPN, hosted by the Australian Geomechanics Society (AGS) - Sydney Chapter, took place on 14th June 2023 at the EA auditorium. This event holds a prominent position on the AGS calendar, providing early and mid-career geotechnical engineers and engineer geologists with an excellent opportunity to showcase their work and bolster their professional portfolios.

The YGPN 2023 witnessed a remarkable turnout of AGS members, and the speakers delivered exceptional, high-quality, and technical presentations. The 1st prize was jointly awarded to Michael Egan and Ken Chen for their outstanding contributions. Hamid Mortazavi Bak and Mehrnoush Rafei secured the 3rd and 4th positions, respectively.

The organizing committee members of YGPN included Navid Yeganeh (Event Coordinator), Mehdi Tamadon, Rhys McMillan, Natalia Ramirez, and Chanaka Gunasekara. The AGS – Sydney Chapter and YGPN committee extend their gratitude to the judging panel members: Idy Li (EIC Activities), Behzad Fatahi (University of Technology Sydney, UTS), Tanya Strate (SMEC), and AHM Kamruzzaman (Zaman) (Transport for NSW, TfNSW) for their valuable contribution in the judging process.

The full list of talks presented at YGPN 2023 is as follows:

- Mehrnoush Rafei (Engineering Geologist – Jacobs) Topic: "Secular Change In Mineral Composition Of A Mesoproterozoic Shale Controlling The Primary Rock Properties."
- Michael Egan (Senior Geotechnical Engineer – JK Geotechnics) Topic: "A Case Study On The Geotechnical Challenges Of A Deep Excavation In Parramatta, New South Wales, Australia."
- Ken Chen (Associate Geotechnical Engineer – WSP) Topic: "Strain Softening And Navigating Karstic Risks In The Design And Construction Of Large Retaining Walls."
- Hamid Mortazavi Bak (PhD Candidate – UNSW; Team Lead, Geotechnical Design – Geotesta) Topic: "Enhancing Soil-Construction Material Interface Shear Strength Parameters Through Bio-cementation."

AGS Sydney Chapter YGP night

Geo-conversation on "Chat GPT and Geotechnical Engineering Practice"

On 21 June 2023, a roundtable panel discussion was organised and facilitated by the Australian Geomechanics Society – Sydney Chapter, on the topic of ChatGPT and Geotechnical Engineering Practice: Navigating Opportunities and Challenges in the AI Era. Over 115 people from our Geotech community attended. The panel discussion brought together perspectives from different sectors to explore the opportunities, challenges, and future implications of generative AI on geotechnical engineering practice, design, and construction.

The panel discussion provided an in-depth overview of the current state of Generative AI adoption within geotechnical engineering, revealing a landscape punctuated by immense opportunities, notable challenges, and transformative future implications. The panellists, leveraging their respective areas of expertise and professional backgrounds, engaged in a robust dialogue that ranged from theoretical aspects to practical applications. Opportunities identified by the panellists included AI's potential to augment human intelligence, the ability to automate routine tasks and improve decision-making processes. However, the panel also recognised several challenges such as the risk of over-reliance on AI, the necessity for high-quality data, and the urgency for professionals to adapt to this evolving technological environment. Furthermore, the conversation delved into the future implications of AI within the industry. The panellists emphasised the pace at which AI technology is progressing, and the need for geotechnical engineers to stay abreast of these changes. They also highlighted the importance of further discussions on risk mitigation, data security, and the creation of company-specific models. The panel concluded with a call to action for engineers to embrace AI as a supplementary tool and to engage in continuous learning to ensure the safe and effective deployment of generative AI in geotechnical engineering.

A replay of the discussion can be accessed via the following link on the AGS Clubhouse page:
https://www.clubhouse.com/room/MO2q9IrL?utm_medium=ch_room_xr&utm_campaign=PuxHPeVFk8ajD4iXpyXAVA-772809

New Book from AGS Sydney Symposium

The Proceedings of the 2021 AGS Sydney Annual Symposium on Geotechnical Lessons Learnt: Building and Transport Infrastructure Projects has now been published as Lecture Notes in Civil Engineering, Volume 325 by Springer. The book contains 12 papers that are indexed by Scopus and EI Compendex database to enhance the visibility for future citations. These Proceedings were the cooperative effort of many authors and qualified reviewers. The editors and organising committee wish to thank the authors, who have generously contributed their time to prepare the various papers and the colleagues of the authors, who have assisted with time, secretarial, drafting and other facilities. The organising committee included Ali Parsa, Cholachat Rujikiatkamjorn, Sam Mirlatifi, Hadi Khabbaz, Adrian Hulskamp, AHMK Zaman, Puvaneswary Rajarathnam, Kourosh Kianfar, Mehdi Tamadon, Saman Zargarbashi.

The Lecture Notes in Civil Engineering publishes the latest developments in Civil Engineering—quickly, informally and in top quality. Volumes published in the series embrace all aspects and subfields of, as well as new challenges in, Civil Engineering.

AGS Sydney Chapter 2nd Geo-conversation

2021 AGS Sydney Chapter Symposium book

Ali Parsa, AGS NSW Chapter Chair

QUEENSLAND

This report includes the QLD Chapter news between January and July 2023. The activities included celebrating women in geotechnical engineering, technical presentations, short courses, awards, collaborating with universities, students' events, and hosting ANZGeo2023. Please visit the AGS QLD Chapter webpage for updates.

Women in the AGS Networking Breakfast

Wednesday 8 Mar 2023

AGS QLD started 2023 with a celebration of the International Women's Day with a coffee and scone. The morning was being held at Spoon Deli Café (Fortitude Valley). Throughout the morning, guests were able to partake in a few 'get-to-know' their neighbour games and be inspired by the women of the AGS. This event was organised by AGS QLD women sub-committee: Natalie Quinlisk (chair), Hannah Down and Arsh Kaur.

With special thanks to Aurecon for sponsoring this event.

Women in the AGS networking breakfast and group photo

Technical Talk: Earthworks - Theory to Practice – Design and Construction

Tuesday 28 Mar 2023

By Dr. Burt Look, from Foundation Specialist Group (FSG)

The technical presentation was based on the latest book by Dr. Burt Look. This 2022 book aims to connect earthworks theory with practice by providing examples of inconsistencies that occur on a regular basis.

This 1-hour overview sampled a few case studies relevant to Queensland practice, with a background on the Main Roads Earthworks specifications for placement and control. The overview covered the introduction chapters on acquiring data with investigation and laboratory testing to obtain the correct information prior to the ground model development, as well as construction quality monitoring. A few (mis)understandings and limitations on common practices and tests were highlighted.

Dr. Burt Look presenting at AGS QLD technical talk

Technical talk: Computational Slope Stability Analysis

Wednesday 3 May 2023

By Prof. Vaughan Griffiths, Professor of Civil Engineering, Colorado School of Mines-USA, Fulbright Distinguished Chair, University of Newcastle-NSW

The lecture described two simple slope stability analyses that can lead to unconservative (unsafe) solutions. Firstly, a classical problem solved by Taylor was revisited using (i) simple optimization, (ii) elastic-plastic finite elements with strength reduction and (iii) upper- and lower-bound finite element limit analysis. The results showed the benefits of the finite element approaches, especially as the slope becomes relatively flat where the simple approach starts to overestimate the factor of safety. Secondly, a probabilistic slope stability analysis was performed using (i) a simple analytical approach and (ii) the random finite element method (RFEM). For the case considered, the analytical approach was shown to underestimate the probability of failure, by failing to account for spatial variability in the form of a correlation length.

This event was organised in collaboration with QLD University of Technology (QUT).

Prof. Vaughan Griffiths presenting at QUT

Technical Talk: The Probability of Failure in Geotechnical Analysis

Thursday 4 May 2023

By Prof. Vaughan Griffiths

The lecture reviewed some of the techniques to make probabilistic geotechnical predictions and discuss some of their benefits and shortcomings. Since Random Finite Element Method (RFEM) is the only method able to explicitly account for spatial variability, the lecture focused on cases where it could have a significant influence on outcomes. In particular, examples were given of geotechnical applications that indicated a "worst case" spatial correlation length.

This event was jointly organised by the University of Queensland (UQ) School of Civil Engineering and SMEC Australia, and supported by the AGS QLD Chapter.

Prof. Vaughan Griffiths presenting at UQ

AGS-University Joint Academic Seminar and Networking event

Thursday 4 May 2023

The focus of this event was to showcase the breadth of opportunities within the industry, and to provide information on how students/young professionals can engage with the AGS. The format of the seminar was a 30-minute presentation, followed by a 30-minute open forum, followed by an hour for casual networking.

This event was heavily supported by the industry and AGS QLD chapter technical committee, with five presentations by Amir Shahkolahi (Global Synthetics, QLD Chapter chair), Hannah Down (AECOM), Allan McConnell, (Insitu Geotech Services, IGS), Vincent Blanchet (WSP), Adam Deacon (KCB), and the support from Natalie Murphy (WSP), Prof. David Williams (UQ), and Prof. Alexander Scheuermann (UQ).

This event was organised by the UQ Civil Engineering Student Association (UQ CESA) and the AGS QLD Chapter.

Students enjoying presentations from industry and networking with the presenters at UQ campus

AGS QLD Cruise Night on Brisbane River

Thursday 18 May 2023

The AGS QLD chapter organised a networking night on Brisbane River (The MV Lady Brisbane vessel) for its members and their guests.

The cruise was chartered for AGS QLD. Each member could buy extra tickets for their guests at the same price.

With special thanks to AGS QLD annual sponsors Wagstaff Pilling, EDG Consulting Engineers, Insitu Geotech Services, ConeTec and Aurecon for their support.

An unforgettable night on Brisbane river for AGS members

Soil and Rock logging course

Friday 19 May 2023

The soil and Rock Logging Course in Brisbane was hosted by the AGS QLD chapter on 19 May 2023 at QLD Transport and Main Road (TMR) Laboratory, with the QLD Committee member Simon Foley from ENGEO being the coordinator of the event. Soil samples and cores were provided by QLD TMR.

Presented by Ian Shipway from EDG Consulting and Fred Baynes, the course was aimed at educating the profession and was particularly relevant to geotechnical and mining consultants, geotechnical contractors and laboratory geo-technicians and other professionals. The course included presentations to explain the basic principles as well as practical session where course participants worked in small groups to log a variety of donated soil and rock core samples under the guidance and instruction of experienced industry professionals.

Ian Shipway and Fred Baynes presenting the course for students

Short Course: Geotechnical near surface field tests

Thursday 15 June 2023

AGS QLD chapter has planned for a series of short courses for graduate students and young engineers. To start with, a half-day short course on geotechnical near surface field tests was organised. This was designed to be an opportunity for attendees to try a number of techniques to evaluate the near-surface material condition via common hand-operated tools, including LFWD, vane shear, LWD, etc.

The course was presented by Dr. David Lacey, Clinton Chan and Ernesto Urbaez, at Port of Brisbane.

Dr. David Lacey talking about LFWD testing

International Women in Engineering Day: Technical Evening

Thursday 22 Jun 2023

AGS QLD celebrated International Women in Engineering (+ Geology) Day on Thursday 22nd June at 5:30pm at City Winery. The evening included a number of short technical presentations by women in the ground engineering industry.

Presentations of the night included:

- Elisabeth Simbolon (AECOM) & Michelle Philipson (Jacobs): "A Forensic Investigation on a Pipeline Corridor Impacted by a Landslip"
- Adelaide Fielden (Aurecon): "Utilising geological principles for effective geotechnical design modelling"
- Ramathi Gunasekera (EDG Consulting): "A challenge is an opportunity in disguise"

This event was organised by AGS QLD women sub-committee: Natalie Quinlisk (chair), Hannah Down and Arsh Kaur.

AGS QLD International Women in Engineering Day speakers (from left to right): Elisabeth Simbolon, Adelaide Fielden, Ramathi Gunasekera, Michelle Philipson

Attendees enjoying the great night at Brisbane City Winery

AGS QLD Women sub-committee (from left to right): Natalie Quinlisk (chair), Hannah Down and Arsh Kaur.

14th Australia and New Zealand Conference on Geomechanics

It was in 1975, almost midway through the first decade of the society's existence, that QLD hosted its first international conference under the AGS banner – namely the 2nd Australia and New Zealand Conference on Geomechanics. which welcomed 243 registered attendees to Brisbane in late July 1975, at which 61 papers were presented over 4 days.

Now in 2023, the 14th Australia and New Zealand Conference on Geomechanics (ANZGeo2023) was held in QLD between 2nd and 5th July 2023 in Cairns, with about 500 attendees and more than 200 papers.

AGS QLD had an active collaboration in ANZGeo2023. The organising committee included Richard Kelly (conference chair, and active member of AGS QLD Technical Committee), David Lacey (conference co-chair, AGS National chair, and active member of AGS QLD Technical Committee), Amir Shahkolahi (AGS QLD Chair), Robert May (Chair of the Technical Committee), and Jon Gibbs (AGS National Secretary). The conference was heavily promoted through AGS QLD chapter activities and events since 2022 by the whole team and AGS QLD Committee members, who were actively following up the event and assisted during the conference as well.

Congratulations and special thanks to the whole team for the very successful event.

ANZGeo2023 organising committee

AGS QLD Distinguished Service Award

To celebrate decades of service and collaboration and support, AGS QLD team awarded the AGS QLD Distinguished Service Award to two of their valuable members, Allan McConnell and John Wagstaff.

Allan McConnell, who can specifically remember that he started working in QLD on 01 July 1969, recalls that he "tagged along" with Peter McAnally (then of Ground Test) to the AGS' events from the time of the society's inception. Allan has been a member of AGS QLD Committee since 1981.

The longstanding relationship between AGS QLD and John Wagstaff was also established by early 1983, with co-hosted technical events and seminars on piling related topics occurring on a semi-regular basis from this time onwards.

Congratulations and special thanks to both John Wagstaff and Allan McConnell for their long-standing support.

The award ceremony was held during the ANZGeo2023 Gala Dinner in Cairns.

AGS QLD Distinguished Service Award winners John Wagstaff (left) and Allan McConnel (right).

Technical Talk:

Rockfall Mitigation Using Flexible-Net Systems

Wednesday 12 July 2023

By Ahren Bichler, Trumer Schutzbauten Canada

This technical talk had two parts:

Part 1: "Standardized approach to rockfall fence design": This part focused on summarising the parts of the ONR 24810 application guide specific to catchment fences beginning with the initial site investigation through to establishing maintenance and inspection schedules.

Part 2: "Long-term relationships with rockfall catchment fences": The extent of deformations related to 3 major rockfall events impacting a single structure over the span of a decade were summarised in this part. In addition, the performance of the system in relation to the characteristics of natural events, site geometry, efficiency of flexible-net systems and the deformability of both the anchorage and the post base supports were discussed.

Ahren Bichler presenting at AGS QLD technical talk

Please feel free to provide your comments and feedback to the QLD chapter team (contact details in the AGS QLD Chapter webpage).

Amir Shahkolahi, AGS Queensland Chapter Chair

SOUTH AUSTRALIA & NORTHERN TERRITORY

John Jaeger Memorial Award

The AGS SA/NT Chapter congratulates Professor Mark Jaksa, conferred the 2023 John Jaeger Memorial Award by the AGS. The award was presented at the ANZ2023 conference in Cairns in early July and recognises an individual who has demonstrated ''a lifetime commitment of the highest order to the geotechnical profession in Australia''.

Chapter Events

Monthly chapter events continued in May with FMG Consultants kindly hosting a tour of their soil testing laboratory, located in Marleston SA.

The new state of the art facility was designed for fast and efficient output of soils analysis. The FMG Research and testing laboratory tour included the sample receival area, sample preparation and compaction area, Density Gauge, Shrink Swell area, concrete testing area and classification testing area for PSD, Atterberg's and CBR. As a founding member of FMG Research, Gary Turnbull explained how research was integral to the ongoing development, management and continued accreditation of the laboratory. He has led the FMG Research team in delivering high quality NATA accredited compaction and materials testing for civil construction projects throughout South Australia, on a number of major key infrastructure projects.

FMG Research Laboratory tour May 2023.

The June event saw a presentation on Computational Slope Stability Analysis from renowned Professor Vaughan Griffiths. Slope stability analysis remains a central activity for geotechnical practitioners and a continued area of interest and research for academics. A wide range of methodologies for slope stability analysis have been developed, ranging from Taylor's charts from the 1930s to state-of-art random finite element methods for probabilistic analysis. The lecture covered a general discussion on factors of safety and discussed the significant contrast between factors on loads, as opposed to factors on strength. A classical slope problem solved by Taylor was revisited using (i) simple optimization assuming circular failure mechanisms, (ii) elastic-plastic finite elements with strength reduction and (iii) upper- and lower-bound finite element limit analysis. The results showed the benefits of the finite element approaches, especially as the slope becomes relatively flat where a simple approach starts to over estimate the factor of safety.

Vaughan Griffiths PhD, DSc, PE, D.GE, C.Eng, FICE, Dist.M.ASCE is a Professor of Civil Engineering at the Colorado School of Mines. His

research interests lie in application of finite element and risk assessment methodologies in geotechnical engineering, and his papers on slope stability analysis are among the most highly cited in the geotechnical engineering literature.

Design Philosophies in Geotechnics was the topic for July, presented by Sergei Terzaghi, grandson of the renowned Karl Terzaghi, known as the father of soil mechanics. Sergei's early years were spent in Oregon USA and he has enjoyed a much travelled career with tenures in New Zealand, USA and Australia.

Sergei presented thoughts and practices from Karl Terzaghi discoveries and findings. Whilst 2nd October is commonly recognized as Karl Terzaghi's birthday – at least in the geotechnical community, it is important to recognize that we are also in the midst of a number of key 100 year anniversaries based around his key discoveries and findings. These include Consolidation Theory (1916-1919), validation of lateral earth pressure theory, Erdbau Mechanik (1925) and filter rules amongst others. While it is always a good opportunity to reflect on some of his thoughts, ways of operation, discussed in context of the time and today, it more opportune now than ever before as the pace of evolution/change increases in our profession.

Soil and Rock Logging Course

Presented by Ian Shipway and Fred Baynes, the AGS SA/NT Chapter hosted a course on Soil and Rock Logging for 8 industry attendees. The one-day course aims to educate geotechnical engineers, engineering geologists, geo-technicians and other relevant professionals in logging and/or interpreting soil and rock logs in accordance with AS1726 – Geotechnical Site Investigations. In addition, the significant changes to AS 1726 contained within the 2017 Revision were discussed in detail. Thanks to Brendan Scott and the University of Adelaide for their generous time and access to their facilities on the day.

Soil and Rock Logging Course May 2023.

Rod Fyfe; AGS SA and NT Chapter Chair

WESTERN AUSTRALIA

In the last quarter AGS WA chapter has three technical presentations. All the the events were very successful and houseful audiences. In May Peter Kingston presented on "A specialist contractor's view to managing geotechnical risk in design and construction", in June Dr. Anna-Carin Brink Pavements in the Public Domain.

The WA Chapter of the AGS arranged the 22nd Dr Baden Clegg Award for the Young Geotechnical Professionals' on Tuesday 11 July 2023. Competition named after Dr Baden Clegg was a lecturer for 30 years at UWA. He developed Perth Sand Penetrometer and the Clegg Impact Soil Tester ("Clegg Hammer") which have been extensively used in Perth. This annual event gives a platform for our younger geo-professionals to present their work, gain feedback from experienced colleagues and become involved in AGS activities.

Abstracts for the award were collected via open invitation and a total of nine abstracts were received. Abstracts were reviewed anonymously and ranked by each committee members and three abstracts with the highest scores qualified for the final. Sam Shahin presented on "Structural analysis and modelling in an evolving mineral resources operation"; Shengsheng Fan presented on "Understanding the effect of monopile installation process on the subsequent lateral response through experimental and numerical approaches"; and Wilson Jiang presented on "Clay liner construction challenges and lessons learned". The winner for the 22nd Dr Baden Clegg Award was **Wilson Jiang**, congratulations Wilson.

At the end of the presentation a trophy was given to the winner and prize money was given to all finalists. The award was presented by Stephanie Clegg, a daughter of Dr. Baden Clegg. Thanks to all participants. A photo of the finalists with Stephanie Clegg is presented below.

22nd Dr Baden Clegg Award 2023. (l-r) Wilson Jiang, Stephanie Clegg, Shengsheng Fan and Sam Shahin.

In addition, the WA Chapter arranged Soil and Rock Logging course. The course were presented by Fred Baynes and Ian Shipway. Thirty engineers from different companies in WA attended the course.

Four volunteers: Eddy Yong, Ben Follet, Rachel Westnidge and Andrew Economo assisted during the course. A photo during the course is shown below:

Soil and Rock Logging Course. (l-r) Ian Shipway, Rachel Westnidge, Eddy Yong, Andrew Economo, Ben Follet and Fred Baynes.

AGS WA chapter is fully booked with the monthly technical sessions. In addition to monthly technical sessions, this year AGS WA Chapter is also arranging a one-day workshop related to earthworks and land developments, field trips for the local engineers and the Annual Symposium 2023.

Harun Meer, AGS Western Australia Chapter Chair

ANZ 2023 CONFERENCE REPORT

14TH AUSTRALIA AND NEW ZEALAND CONFERENCE ON GEOMECHANICS (ANZ2023)

Introduction (The Path to Cairns …)

Every four years the Australian Geomechanics Society (AGS) or New Zealand Geotechnical Society (NZGS) host an *Australia and New Zealand Conference on Geomechanics*. This has been the established sequence since 1971, with the current iteration – the *14th Australia and New Zealand Conference on Geomechanics (ANZ2023)* – held in Cairns, Queensland, between 02 and 06 July 2023.

As per the status bestowed on similar national / Australasian events since 1952, the current series of ANZ conferences are designated the Australasian Regional Conference of the International Society for Soil Mechanics and Geotechnical Engineering (ISSMGE). The ANZ conferences on geomechanics typically represent the largest regular gathering of geomechanics professionals in the Australasian region, and are the largest regularly scheduled event that is organised by the AGS.

The hosting of ANZ2023 in Cairns, Queensland was announced at the closing session of ANZ2019 (Perth, Western Australia), and was based on a bid submitted to the AGS National Committee by interested members of the AGS' Queensland Chapter. Specifically, this bid realised AGS' stated desire for the event to be hosted by a suitable regional centre within Australia, rather than be held at a state capital city (as all state capitals had previously hosted ANZ conference events).

Although there was some initial uncertainty amongst the local organisers and the AGS about how the move to a regional city may impact the conference attendance, this was quickly swamped by the immense uncertainty presented by the global pandemic. Impacts of the border closures due to COVID included the loss of direct flights between the host city and New Zealand / Asian population centres, which (worryingly) had been one of principal reasons Cairns had been chosen.

Following on from the uncertainty of 2020-22, the organising committee decided the primary aim of the conference should be to reconnect ANZ based geomechanics practitioners post-COVID. It was for this reason that there was no remote attendance or 'streaming' option offered for the conference, with the organisers wishing to maximise in-person attendance.

Summary of Attendance (Statistics)

Initial (2020) planning estimates from the Local Organising Committee (LOC) were that, based on location and previous events, ANZ2023 would likely attract 300 to 400 attendees to Cairns in July 2023.

Attendee registrations tracked approximately along the anticipated pathway until approximately four (4) weeks out from the conference. From this point onwards, the registrations continued to surpass expectations, suggesting that many delegates only committed to attending the conference once their personal short-term schedules and work demands had been determined.

By the end of the conference it was confirmed that there were:

- A total of 480 attendees (inclusive of speakers and exhibitors);
- 16 Nationalities represented – unsurprisingly Australia (394) and New Zealand (at least 62) made up the vast majority of the registrations;
- 22 Tertiary Institutions were represented as the primary affiliation listed by conference attendees; and
- Over 165 companies were listed within the primary delegate affiliation – with WSP (42); TfNSW (20); SMEC (20); GHD (12): and Aurecon (11) being the top five represented companies.

Obviously, these final attendance figures well exceeded the organisers' expectations. This was a wonderful outcome for the conference and confirmation of the widespread appeal in the delivered technical program (or, at least, interest in spending a week in Cairns in the middle of winter).

Technical Workshops (Day 1)

Day 1 (Sunday, 02 July 2023) of ANZ2023 saw three half-day workshops being presented. Even though the workshops were only confirmed approximately two months prior to the conference, all workshops were well attended and fully booked.

The topics and presenters at the workshops included:

- *Designing Mechanically Stabilised Earth (MSE) Walls*, presented by Professor Richard Bathurst from Royal Military College of Canada. The workshop included separate presentations on "The new AASHTO stiffness method for internal stability design of MSE walls", as well as "Probabilistic reliability-based analysis and design of MSE walls".
- *Review of Australian Landslide Risk Management Guidelines,* presented by Darren Paul (WSP) and Tony Miner (A.S. Miner Geotechnical). The impetus for this workshop was to bring together those with experience using AGS' Guidelines for Landslide Risk Management (AGS, 2007) in order to share their experiences and to assess the need for future revision of the guidelines. The AGS subsidised attendance at this event, with the view that the workshop may become the catalyst for the formation of a dedicated working group to update the AGS' guidelines, now that they have been implemented in practice over a 15-year period.
- *Earthworks: Theory to Practice – Design and Construction*, by Dr. Burt Look, which provided a summary of theory and case studies relevant to understanding several of the influential aspects of achieving positive outcomes in the construction of earthworks formations.

The conclusion of the workshops was timed to coincide with the commencement of the conference welcoming drinks, which was the first opportunity for all attending delegates to meet and socialise.

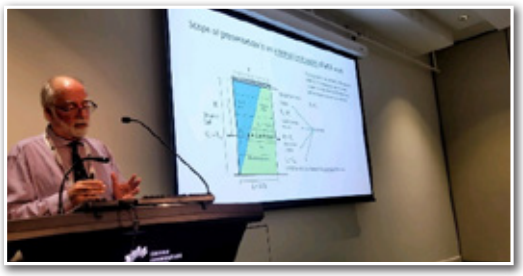

Professor Richard Bathurst presenting during his Designing Mechanically Stabilised Earth (MSE) Walls workshop

Keynote Speakers who delivered Honorary Lectures with their awards and the National Chairs of the host organisations – Left to Right: David Lacey (AGS, National Chair), Professor Mark Jaksa (AGS Jon Jaeger Memorial Award), Ann Williams (2022 Geomechanics Lecturer), and Eleni Gkeli (NZGS, National Chair).

Keynote Speaker Professor Anna Giacomini presenting during the special plenary session dedicated to the late Professor Scott Sloan.

Technical Program (Day 2 through Day 4)

Days 2 to 4 of the conference (Monday through Wednesday) largely saw the delivery of the technical program of the conference. Each day saw a number of plenary sessions, presented by invited keynote speakers, interspersed with sessions split over five (5) parallel streams.

The Technical Committee, headed by Dr. Robert May, prepared an excellent selection of keynote speakers, including (in alphabetical order):

- Dr Fred Baynes (Baynes Geological) – *The use of the IAEG EGM Guidelines to anticipate Engineering Geological Conditions* for Projects in Australia (pre-recorded presentation due to illness of Dr. Baynes, with onsite assistance from Darren Paul);
- Dr Shiaohuey Chow (University of Melbourne) – *Plate Anchors for Offshore Floating Renewable Energy Devices;*
- Professor Anna Giacomini (University of Newcastle) – *Rockfall Monitoring and Mitigation Measures Design for the Civil and Resource Sectors;*
- Professor Mark Jaksa (University of Adelaide), presenting the AGS' Jon Jeager Memorial Award – *Geotechnical Variability: In the Ground and throughout a Career;*
- Dr Daniel King (WSP) – *Risk assessment of Ground Movement Rebound Effects Associated with Hazelwood Mine Closure and Mine Pit Flooding;*
- Dr Ellen Rathje (University of Texas) – *Learning from earthquakes and other natural hazards: Past, present, and Future;*
- Dr Merrick Taylor (Beca) – *Implementing Performance Based Design to Achieve Seismic Engineering Solutions for Foundations in Sandy Soils;*
- Ann Williams (Beca), presenting the NZGS' 2022 Geomechanics Lecture – *The Question of Risk*

The wide-ranging nature of this keynote program effectively meant that there was something of interest for all attendees. A corresponding outcome for the conference, and a conscious decision of the organisers, was that the mix of keynote speakers represented a approximately equal mix of genders and included speakers from varied career progressions, backgrounds and field of expertise (e.g. geotechnical engineers, engineering geologists, primarily tertiary or industry based practitioners).

Within the keynote speaker program, both the AGS and NZGS nominated recipients of each society's most prestigious award (each awarded quadrennially) to make honour lectures. The AGS recognised Professor Mark Jaksa as the 11th recipient of the *John Jaeger Memorial Award* for "contributions of the highest order over a lifetime commitment to the geotechnical profession in Australia", whilst the NZGS celebrated Ann Williams as the 17th *NZGS Geomechanics Lecturer* for her "long-

standing contribution to the geotechnical profession in New Zealand, especially to understanding the geotechnical hazard and risk issues".

Across the sessions of parallel stream held over the three days of ANZ2023, 185 individual authors were each afforded 15-minute presentation slots, curated by the Technical Committee into themed sessions. Each presentation included a summary of the key points detailed within the associated peer-reviewed technical paper, and included a brief question and answer question from the attending audience.

In addition to the oral presentations, another 48 peer-reviewed papers were accepted into the conference technical program and presented throughout the conference as electronic posters. Multiple terminals where these posters could be perused by all attendees (with the facility to submit questions directly to the author) were included both in the main exhibition area and at key communal areas of the conference facility. A compilation session that highlighted many of the quality posters submitted to the conference was also included as part of the parallel session, which was presented by the Technical Committee.

Professor Scott Sloan Memorial Session

A special plenary session was held on the last afternoon of the technical program of ANZ2023 to celebrate the recent passing of an international renowned researcher and leader within the Australian geomechanics community – Professor Scott William Sloan AO.

Professor Sloan died suddenly and unexpectedly on 23 April 2019 whilst on holiday in far North Queensland and, due to the global pandemic, ANZ2023 represented the first appropriate chance for the industry he was so passionate about to reflect and remember both his extensive research contributions and his personal qualities – including his friendliness, wit, intelligence, warmth and approachable demeanour.

The memorial session was organised and opened by Associate Professor George Kouretzis, one of Scott's close University of Newcastle colleague. Attending as the guest of the AGS, Scott's wife Denise Hayes (nee Sloan) next shared some brief reflections of Scott and thanked all the people who assisted him throughout his long-term passion for geomechanics.

Left to Right: Denise Hayes (nee Sloan), Anna Giacomini and George Kouretzis during the plenary session dedicated to the late Professor Scott Sloan.

Presentations that allowed reflection upon Professor Sloan's research, while simultaneously providing some insight into each of the speaker's personal observations and memories of working alongside Scott, were then made by some of his long-term collaborators. These speakers included Professor Anna Giacomini, Professor Mark Randolph, Professor Vaughan Griffiths, Professor Ian Moore, Professor John Carter, Professor Buddhima Indraratna, Professor Daichao Sheng and Professor Harry Poulos.

Many of the anecdotes delivered during this special session were recalled with great affection and, unanimously, the speakers remembered Professor Sloan as both a focussed and brilliant researcher whilst being generous and supportive to all those around him.

Geo-Education Session (organised by ISSMGE Heritage Time Capsule, HTC)

A special session was held within the parallel session schedule of Day 2 of ANZ2023 that was entitled "Geo-Education, a way forward".

This session was organised by and hosted by members of the Heritage Time Capsule (HTC) project group within the ISSMGE, and was aimed at exploring the specific educational requirements that would result in the the next generation of geotechnical engineers being appropriately knowledgeable such that they can become effective and productive professionals. This was discussed in the context of the current state of geotechnical engineering programs across ANZ universities, alongside the current interactions that occur between tertiary institutions and industry that aim to communicate and manage ongoing resourcing and professional development demands.

The format of this session varied from the remainder of the conference in that both short presentations and a panel discussion with audience interaction were included. The panel members included representatives from academia – Dr. Negin Yousefpour (University of Melbourne) and Professor Liam Wotherspoon (The University of Auckland), industry - Dr. Jason Surjadinata (John Holland), representing Australia; and Ms. Eleni Gkeli (Stantec), representing New Zealand), and; Young Professionals - Ms. Xue Le (Keller), Australia; and Mr. Christoph Kraus (Beca), New Zealand. Opening and Closing remarks were made by Mr. Graham Scholey (WSP and ISSMGE VP for Australasia) and Professor David Airey (The University of Sydney) respectively.

Feedback provided from the session was that robust discussion was had between all participants, and that there was a clear demand by industry for the development of additional, practical and relevant training opportunities for geomechanics professionals (especially early-career professionals). Reciprocally, session attendees identified that industry experienced personnel should be endeavouring to assist tertiary institutions with the development and delivery of such courses (and ensure their relevance to industry requirements is maximised).

It is envisaged that the conversations commenced at this ANZ2023

session will continue post-conference, such that strategic goals and a key, tangible actions can be established and delivered. The AGS, alongside the NZGS and ISSMGE, are key stakeholders in achieving these outcomes – as any increased training opportunities, or alteration to the scope of tertiary geo-education will directly impact our membership and community. As such, the AGS are keen to capitalise upon the momentum established during this special session and will directly assist in achieving the identified tangible outcomes.

Sponsors and exhibitors

Twenty-one conference sponsors and 37 exhibitors directly supported the ANZ2023 conference. This represented a sell-out of the available exhibition space, and the AGS are grateful for their support to our flagship event. To encourage maximum interaction between sponsors and delegates, and to ensure all the cutting-edge technology on display was remained within the line of sight of attendees throughout the conference, all meals were served within the exhibitor area.

Women in Engineering, Sundowner Drinks

On the Monday evening, at the conclusion of the Day 2 Technical Program, a sundowner social event was held with the aim of celebrating the achievements and diversity of Women in Engineering (WiE) and, more specifically, Women in Geomechanics.

In preparation of the event, summary slides were sought from women working in geomechanics focussed roles throughout the Australasian region – with the each slide including their name, a brief description of the authors current role and, most importantly, the answer to "what drives me?".

Approximately 60 slides were returned in a very short timeframe, and these were then presented as a rotating show on multiple large screens at the sundowner event to showcase and highlight the inspiring women present throughout our community and industry – effectively offering all attendees a snapshot of the diverse roles and significant contribution being made by women. This approach was a resounding success, and represented a definite point of difference to other social events held in recent conferences.

This event was a comparatively late addition to the conference program, and organised by the AGS largely external to the main conference program. Thanks go to the dedicated team of Dr. Nina Levy, Dr. Asal Bidarmaghz, Clare Bridgeman, Hannah Down, Christoph Kraus and Eleni Gkeli for the organisation of this enjoyable event.

Kuranda Rail Tour (Fieldtrip)

On the morning of Day 5 (Thursday, 06 July 2023) a smaller group of ANZ2023 attendees departed Cairns and embarked upon the Kuranda Scenic Railway for the mountain village of Ngunbay (Kuranda). This heritage railway is recognised as an Australian National Engineering Landmark (NEL), and the ride is picturesque trip through the ancient World Heritage-listed Wet Tropics Rainforest of the Din Din (Barron Gorge) National Park during the trains steep ascent towards the Atherton Tablelands.

Of particular interest to the geomechanics contingent was the geo-engineering heritage of the railway – which, during the construction of the 37 km line between 1881 and 1886, saw the completion of 106 rock cuttings, 15 hand-formed tunnels (totalling 1.75 km length) and over 55 bridges (that combined have over 2.0 km of spanned length). As the alignment of the railway was constructed over unstable geology, significant geo-engineering challenges were required to be overcome during the initial construction and have continued to influence the required maintenance program delivered in the intervening 137 years.

In addition to the official (mainly historical) commentary provided by the railway, Sam Bogue (WSP) provided the ANZ2023 party with an interesting, geo-themed technical commentary that detailed several interesting aspects of the rail line.

Upon arrival at Kuranda village, attendees got to spend some time sightseeing prior to returning to Cairns (and sea level) via the 7.5 km glide down the Skyrail Cableway. This return journey included stops to see rainforest boardwalks and views at Red Peak and Barron Falls.

The conference committee recognises and thanks Sam Bouge for his local knowledge and contribution in the organisation of the fieldtrip.

ANZ2023 Conference Dinner

On the evening of Day 3 (Wednesday, 04 July 2023) the conference dinner was held in the Grand Ballroom of the Pullman International in Cairns CBD. 380 of the conference delegates attended the dinner, which represented the use of the full capacity of the venue. All attendees appeared to happily take this opportunity to relax, unwind and socialise with colleagues.

The busy Exhibitor Hall at the ANZ2023 Conference

Kuranda Scenic Railway on the Stoney Creek Falls Bridge during its ascent up the Barron Gorge (Photo credit: Timothy Thompson) 2022

AGS Practitioner Award

As ANZ2023 represented the largest gathering of geomechanics professionals from around the ANZ region in 2023, the conference dinner was the opportune moment for the recipient of the 2022 'AGS Practitioner Award' to be announced. This honour was conferred upon John Wagstaff, to reflect his almost unparalleled contribution to the AGS (and the wider Australian geomechanics community) over the past 40+ years.

As identified on the evening, the awards committee agreed unanimously that John, through Wagstaff Piling, has embodied the basis of the award – in that his efforts in foundation design, research and construction practice across Australia undoubtably represents a "significant contribution of the highest order, over an extended period, to the geotechnical profession in Australia".

AGS QLD Distinguished Service Awards

The AGS Queensland Chapter also took the opportunity presented by the conference dinner to recognise the multiple decades of service provided to the AGS by two of their long-standing committee members – Allan McConnell and John Wagstaff. Both Allan and John were presented with a Distinguished Service Award for their extensive contribution to AGS QLD Chapter – with Allan and John having been involved in the chapter committee for at least 42 and 44 years respectively.

It was interesting to note that during their brief acceptance remarks, both of the award recipients reflected on how important the training and opportunities provided by the AGS were to developing the next generation of geo-professionals.

ANZ2028 – Announcement of Host City

As per the established tradition of New Zealand hosting every third ANZ regional geomechanics conference, the *15th Australia and New Zealand Conference on Geomechanics* is due to be hosted by NZGS.

During the closing session of ANZ2023, Eleni Gkeli (Chair, NZGS) announced that the City of Christchurch would be the venue for the conference, and that the event would be hosted in the 2028 calendar year. This five-year gap between ANZ conferences is being implemented at the request of the ISSGME, such that the two-year gap between their quadrennial *International Conference on Soil Mechanics and Geotechnical Engineering* (ICSMGE) and the Australasian regional conference is re-established.

Acknowledgements and thanks from ANZ Local Organising Committee

The Organising Committee thanks all the delegates, speakers, voluntary reviewers, sponsors and exhibitors for their contribution to the success of this event.

We hope all attendees found the technical program interesting and enjoyed connecting and reuniting with aligned professionals.

A special acknowledgement s also made to Arinex, who acted as the Professional Conference Organiser for ANZ2023. Their support in the organisation and running of the conference was invaluable to the Local Organising Committee.

ANZ2023 Conference Dinner Attendees enjoying each other's company

John Wagstaff, left, receiving the 2022 'AGS Practitioner Award' from David Lacey (Chair, AGS National Committee)

Allan McConnell, right, receiving an AGS QLD Distinguished Service Award from Amir Shahkolahi (Chair, AGS QLD Chapter)

The key members of the ANZ2023 Local Organising Committee included:

- Dr. Richard Kelly, Co-Chair ANZ2023 Organising Committee
- Dr. David Lacey, Co-Chair ANZ2023 Organising Committee & Chair AGS National Committee
- Dr. Robert May, Chair, ANZ2023 Technical Committee
- Amir Shahkolahi, Chair AGS Queensland
- Jon Gibbs, Secretary AGS

REPORT ON CONFERENCE ATTENDANCE

14TH ANZ CONFERENCE ON GEOMECHANICS (2023)

A Fiji Engineer's Experience

2nd – 5th July, 2023, Cairns, Australia

I wish to acknowledge the ISSMGE, AGS and NZGS for the opportunity to attend the 14th ANZ Conference on Geomechanics 2023 which was held in Cairns, Australia from 2nd to 5th July, 2023. The entire Conference experience was awe-inspiring and impactful!

The highlights of the 14th ANZ Conference on Geomechanics were: the Pre-Conference Workshop on 2nd July, 2023, conducted by Dr. Burt Look – this started off an exciting week. The interactive and engaging discussions during the workshop were thought provoking and insightful which I enjoyed immensely. I was also captivated by the Keynote presentations, particularly by Professor Ellen Rathje and Professor Mark Jaksa and, the 15-minute presentations by participants from the Industry and Academia which covered a number of case studies on slopes, soft soils, climate change, ground improvement and ground engineering.

Attendance at a conference such as this event marks a significant milestone for Fiji Geotechnical Engineers as it provides an avenue at the international level for Fiji Geotechnical Engineers to gain access to international leaders in the geotechnical engineering field. It also enables us to participate, learn and share the local knowledge with highly qualified professionals. Of equal importance, it provides a platform for Fiji Geotechnical Engineers to gain a better understanding on potential workable solutions to better address the geotechnical engineering challenges and improve geotechnical engineering and investigations in Fiji (and the South Pacific region).

It is anticipated that the benefits for future ongoing ties between geotechnical engineers in Fiji and the AGS, NZGS and ISSMGE would generally include:

- A continued involvement and active participation of Fiji geotechnical engineers at the international level;
- The possibility of the creation of a qualified group of geotechnical engineers in Fiji with direct link to the overarching *Engineers Fiji;*
- Enables a connection to and with Geotechnical Engineers from neighbouring Pacific Island Countries.
- Provides new opportunities for Fiji Geotechnical Engineers to explore with its connection to AGS, NZGS and ISSMGS;
- Provides exposure for Fiji Geotechnical Engineers, particularly women, to enhance their learned technical skillset and knowledge;
- Enables a learning environment for Fiji Geotechnical Engineers via direct connection and networks with well-established Experts within the Industry and Academia;
- Improves the calibre of Geotechnical Engineers in Fiji by creating a better-informed community in Fiji.
- Strengthens Fiji's growth within the engineering community and awareness in Geotechnical Engineering.

The above list of benefits is non-exhaustive. There is great potential within Fiji to grow the Geotechnical Engineering community and many benefits for both the International Societies and those actively working in the geotechnical field within the Fiji (and South Pacific) region.

Honoured to have been introduced to the widely respected and recognised, Emeritus Professors and Experts, Professor John Carter and Professor Harry Poulos.

Author: Lorin Tuilakepa (Engineer at Erasito Consultants Limited, Fiji)

WORKSHOP REPORT

AUSTRALIAN GEOMECHANICS SOCIETY GUIDELINES FOR LANDSLIDE RISK MANAGEMENT 2007

Outcomes of workshop held at the 14th Australian and New Zealand Conference on Geomechanics, July 2023

Darren Paul
WSP, Australia, Darren.Paul@wsp.com

Tony Miner
A.S. Miner Geotechnical, Australia, aminer@asmg.com.au

In response to the publication of the Australian Geomechanics Society Guidelines for Landslide Risk Management, 2007 (AGS 2007) a group of concerned practitioners wrote to *Australian Geomechanics* to convey some issues they perceived with the document and to suggest it be immediately revised following its initial publication. In response, the taskforce responsible for producing the AGS 2007 guidelines had this response (ref: AGS 2008).

The Letter Authors suggest revising the documents. This is considered unnecessary in the short term and impractical given the extensive critical input that interested practitioners have already provided. No doubt, a review in say 5 years will be wise as the geotechnical community and regulators gain more experience in using LRM.

The geotechnical community in Australia has now accrued 15 years of experience implementing the AGS 2007 guidelines and it would seem a review might be well overdue. Furthermore, owing to the La Niña events experienced in Australia over the past three years, there has been an increase in landslide frequency and a number of fatalities which has raised community awareness of landslides and landslide hazard management.

A workshop to gauge opinion on the need for a review was organised by the authors and was held on 2 July 2023 in conjunction with the 14th Australia and New Zealand Conference on Geomechanics. The workshop was attended by 44 geotechnical practitioners from across Australia and New Zealand with a broad range of backgrounds. It should be noted that those attending represented approximately 10% of the total numbers attending the conference and highlighted the industry interest in the discussion. The objective of the workshop was to answer three questions:

- Do the AGS 2007 guidelines on Landslide Risk Management require a revision?
- If yes, what are the key areas that need to be revised?
- How will we go about revising the guidelines?

To help answer these questions, Mr Darren Paul provided an overview of the content and structure of AGS2007 documents which comprise 5 separate parts dealing with zonation, risk assessment and general information. Mr Tony Miner and Dr Fred Baynes gave presentations on issues they have come across with implementation of the guidelines through their careers. Darren Paul and Tony Miner also submitted a paper to the conference (Paul and Miner 2023) setting out their experiences of issues with LRM in Australia with a view to sparking debate and discussion on whether a revision is required and what that revision should include. After two hours of engaging debate, as well as some written and verbal inputs from eminent practitioners unable to attend, the workshop reached the following conclusions.

- The guidelines do require a revision in some form, a point the workshop attendees were unanimous on. There were a range of views as to how extensive that revision should be, ranging from a complete re-write to a minor supplement. However, the majority opinion was noted to be somewhere in between these two extremes. Most of what is in the current document should be carried forward to a revision, but updated to reflect learnings over the past 15 years and to modernise and streamline the document.
- Many opinions were put forward as to what aspects of AGS2007 require revision, but the workshop was able to distil those opinions down to a few key areas, including:
    * The document can at its worst be impenetrable to many readers, and some experienced reviewers indicated they have reviewed many reports that don't follow the guidelines well. This was thought to be a consequence of some practitioners' inability to understand and to apply the guidance set out in the document.
    * The current guidelines could use more useful information on hazard identification, including geomorphology and understanding slope forming processes and process rates.
    * The risk assessment techniques in the AGS 2007 guidelines seem to mostly apply to residential applications. Some practitioners report difficulty when applying the guidelines to other situations, such as roads, walking tracks, railways or hazards that present a risk to large numbers of people. There is scope to have the guidelines better cover non-residential applications, for example through clear, worked examples.
    * The guidelines should include more guidance on managing temporal change, including changes that may be induced by climate change and environmental factors such as bushfire.
    * The uncertainty associated with landslide risk assessment is very well known, including the ability to accurately or consistently estimate input parameters such as landslide likelihood. The guidelines could use more information on how to communicate uncertainty to end users of landslide risk assessment reports.

    - Overall, it was felt that the document needs to be simplified and be made more concise with a broader applicability and flexibility in choice of assessment methodology undertaken.
- In support of the majority consensus reached at the workshop and to effect an update, a submission will be made to the AGS national committee to seek approval and funding to commence a revision of AGS2007. It was recognised that a broad range of stakeholders may wish to provide input and submissions to revised guidelines, including:
    - Geotechnical practitioners including engineering geologists and geotechnical engineers.
    - The geo-spatial community.
    - Emergency management authorities.
    - The insurance industry.
    - Ultimately a range of end user s (including state and local government authorities and possibly even homeowners) who commission these reports and then need to interpret the outcomes.

Subject to approval to proceed with an update, strategies will be developed around the structure and terms of reference for a working group dedicated to updating the guidelines. We expect this process to commence in late 2023.

The authors would also like to invite any further submission, thoughts and comments from interested stakeholders as we commence the process of revision.

You may make a submission by emailing the AGS Secretariat at secretary@australiangeomechanics.org. Please note landslide guidelines in the subject line of your email.

References

- Australian Geomechanics, Vol 42, No 1, March 2007.
- Australian Geomechanics, Vol 43, No 1, March 2008.
- Paul, D., Miner, A.S. Landslide risk assessment in Australia: background, current practice and future developments, *Proceedings of the 14th Australia and New Zealand Conference on Geomechanics,* Cairns, July 2023

Darren Paul presenting during workshop in Cairns.

PhD Thesis Abstracts for publication in *Australian Geomechanics*

AUSTRALIAN GEOMECHANICS SOCIETY

The Australian Geomechanics Society invites PhD students to submit an abstract of their thesis completed in 2023 to *Australian Geomechanics*.

This invitation is restricted to PhD theses submitted to Australian universities and accepted as partial fulfilment of the requirements for the degree of Doctor of Philosophy and to PhD theses by Australian students submitted at overseas institutions.

The thesis should have been completed and accepted within one year of the abstract being published in Australian Geomechanics.

The invitation is open to all theses related to geomechanics topics. AGS requests promotion of this initiative among PhD students and academic networks.

The abstracts will be published in the March 2024 issue of *Australian Geomechanics*.
The following information is required for publication:

- Author's name (with current affiliation and contact information)
- Thesis title
- Date submitted/approved
- Sponsoring Professor / Academic Supervisor and University (contact address, telephone and e-mail address)
- A brief abstract (strictly max 250 words)
- Scanned page of Title Page of thesis.
- Information should be submitted to the *Australian Geomechanics* Editor, via email: editor@australiangeomechanics.org. Please attach as a MS Word document.

Deadline: Friday 2nd February 2024

OBITUARIES

JOHN PHILLIPS
1940 – 2023

John began his career as a structural engineer with the Commonwealth Government, working on rocket launching facilities at Woomera, the design of foundations for several Reserve Bank buildings and the international terminals at Tullamarine and Mascot. John felt that the most challenging aspect of his work was foundation engineering, so he returned to university to complete a Master's degree in soil mechanics. This expertise would carry through to the rest of his career.

Joining GHD in 1967 in Melbourne, he worked on the largest dam project GHD had completed at the time, the Bungal Dam in Victoria, and then on several other projects in Victoria, Tasmania and Queensland.

In 1979 John relocated to Perth with his family to work on five dams for the Worsley Alumina Refinery near Collie. At the time, relatively few tailings dams had been built in Australia, so John set out on a study tour to Germany and the United States to learn more. He brought back key learnings that informed the successful delivery of this project and resulted in GHD taking out two patents in dam building. The Worsley Alumina project would go on to win two prestigious engineering awards and John became a technical authority in tailings and dams.

Over a 40-year career, John worked in 11 countries covering almost 100 major tailings dams, more than 20 major water dams and three dams built into the sea. He was sought out as an expert to advise on dam collapses around the world, including the Opuha Dam in New Zealand. He was an Honorary Life Member of the Australian National Committee on Large Dams (ANCOLD) in recognition of his contribution to the industry, and also represented Australia on the International Commission on Large Dams in Paris.

Thanks to his outstanding leadership, John quickly rose to be GHD's WA Regional Manager and was appointed Chairman in 1999, the first Perth-based Chairman in the company's history. Speaking at Engineering Week in Perth that year, John predicted the globalisation of just about every market, including professional services. *"Globalisation will have an impact either on the nature of engineering services, or a changed attitude from engineers, or an alternate method of evaluating the worth of engineering products."* he said. GHD was determined to compete globally while remaining employee-owned – a business model that continues today.

John was also an early adopter of what today would be known as ESG. *"It seems self-evident that our use of resources should not diminish the opportunities for our children and grandchildren",* he commented in 2000. "GHD has committed itself to both pursue projects with strong sustainability components and to assist our clients by demonstrating viable sustainability concepts in our design and operations."

After stepping down as Chairman, John continued working in GHD's Dams & Tailings team in Western Australia until shortly before his passing.

In addition to his roles at GHD, John was a member of the National Board for the Centre of Engineering Leadership and Management. He was a past President of the WA Division of Engineers Australia and a past Chairman of the Association of Consulting Engineers in WA (now Consult Australia).

John will be fondly remembered across Australia and internationally by family, friends, clients, work colleagues and those he helped though his volunteer activities.

Note: This obituary is based on a media release from global professional services company GHD.

PETER BERNARD HILLS
1959 – 2023

Peter Hills was born in Sydney but spent most of his youth in Launceston. He attended the University of Tasmania between 1978 and 1981, achieving an Honours degree in geology.

From University he obtained a cadetship with Renison Goldfields, and after a short stint in Queensland, was posted to the Mt Lyell copper mine in western Tasmania, where he was in his element as an underground geologist. He met his wife Helen there and they remained a devoted couple. Rugby was a passion, in that tough west coast environment and he both managed and played for the local team on that infamous gravel oval. A teammate described him as *'always committed, dependable and organised'.*

From Mt Lyell, he was next posted to the Porgera gold mine in the highlands of Papua New Guinea, then one of the world's largest gold producers. It was a FIFO arrangement – common enough today, but back then Hobart to PNG Highlands and back was quite a commute. After Porgera, he and Helen moved to Sydney where Peter was at Plutonic Resources. At this time their two children were born – Daniel and Emma.

In 1993 Peter earned a Masters degree in Engineering Science from James Cook University.

A few years later, the fabled Beaconsfield gold mine in northern Tasmania was slated to re-open, and Peter's manager at Porgera invited Peter to join him there as Senior Mine Geologist. He and Helen quickly agreed. Being a deep mine, Peter brought his developing geotechnical skills to bear in the mine re-opening process and thereafter. 2006 and the Beaconsfield mine disaster caused a step-change in the complexity and detail of rock mechanics and geotechnical studies at Beaconsfield and Peter became an authority on deep mine seismicity and related subjects and presented papers at numerous Australian and overseas conferences.

When the Beaconsfield mine closed, Peter joined consulting firm Pitt & Sherry as a Senior Consultant and carried out many projects mainly involving rock mechanics and geotechnical engineering. Tunnel studies were a favourite, probably reminding him of being down a mine!

During this time, and until he died, Peter was active in both the Australian Geomechanics Society (AGS) and the Australasian Institute of Mining and Metallurgy (AusIMM). He was Secretary and then President of the re-constituted AusIMM Tasmania Branch, which he helped originate.

Professionalism was a core passion of Peter's. He was a long serving member of the AusIMM's Chartered Professionals program committee and its chair from 2016 to 2018. He served for two years on the Professional Accreditation Advisory task force, and for many years was an assessor for the chartered professionals program. He was the chair of the Consultant's Society committee for 2019-2020 and helped organise many conferences, with a special interest in the Underground Operator's Conference. For his many and varied contributions, he was awarded the AusIMM Service Award in 2010 and the prestigious Beryl Jacka Award in 2020.

In the AGS, while not holding any office, Peter was active for many years, attending and presenting technical papers and mentoring younger members.

It would be remiss not to mention Peter's appreciation of a crisp Riesling and a full-bodied shiraz – or a carménère, which he discovered when visiting South America – and finishing off with a 'sticky'. He loved to fish and a good bushwalk. His projects around the house usually ended up being substantial undertakings because, as in his work, there was never a question of a job done by halves.

Peter leaves his wife Helen, children Daniel and Emma, grandson Charlie, father Norm, sister Jennie and a large number of friends and work colleagues grieving at the loss of a fine man.

E.H. Davis Memorial Lecture

Call for Nominations

AUSTRALIAN GEOMECHANICS SOCIETY

www.australiangeomechanics.org

SUBMISSION DEADLINE
30th Nov 2023

This biennial lecture commemorates the work in geomechanics by Professor Edward Hughesdon Davis. Professor Davis was one of the pioneers of geomechanics in Australia. He perceived that progress and understanding of the theoretical basis of geomechanics would only come if consistent, sound, but simple models of soil behaviour were used. The two topics that were the central focus of his research were the application of the theory of elasticity to foundation deformation and the theory of plasticity to stability. He also made a major contribution to the theory of consolidation of clay soils. Ted Davis was always extremely conscious of the link between theory and practice, the relationship between the idealised and the real material, and the engineering significance of his work.

BASIS OF THE AWARD

The lecturer is a person selected by the National Committee as having made a distinguished recent advancement to geomechanics knowledge in Australia.

NOMINATION

Nominations should be made through the Chapter Committees, or by individuals, to the secretary of the National Committee, following a call for nominations in Australian Geomechanics. Determination of the award is by a subcommittee of the National Committee. The nominee is expected to be a member of the Australian Geomechanics Society.

SELECTION

The Chairman of the National Committee shall promulgate a sub-committee of 3 members of the National Committee to consider nominations for the award.

PRESENTATION & AWARD

The award includes a National Lecture tour of AGS Chapters, to be undertaken primarily in the 12 months following the award announcement being made. The award memento will be presented by a representative of the National Committee at a mutually agreed event. The Lecturer shall also distill his lecture into a technical paper that will be published in *Australian Geomechanics* at the conclusion of each tour.

SUBMISSION DEADLINE

30th Nov 2023

FOR MORE INFORMATION VISIT

https://australiangeomechanics.org/awards/e-h-davis-memorial-lecture/

CALL FOR EXPRESSION OF INTEREST (EOI)

Position of Editor of *Australian Geomechanics*

AUSTRALIAN GEOMECHANICS SOCIETY

The National Committee of the Australian Geomechanics Society (AGS) invites expressions of interest from individuals interested in taking on the Editor role of our quarterly journal, *Australian Geomechanics*. The position would suit an experienced (Senior or Principal) geotechnical professional who is retired, on the cusp of retirement or works part-time. However, anyone with the requisite ability and the opportunity to devote the necessary time to the position is encouraged to apply. **Applications open 1st September 2023.**

The journal is published quarterly - in March, June, September and December. Generally, the deadline for receiving final content is the 5th day of the month prior to publication and putting together the issue, with the direct support of a graphic designer, takes up to 2 weeks. The average effort is approximately 4- 5 hours / week, but varies from week to week depending upon the timing of the journal production cycle and the timing of submissions received.

Full training will be provided, and a modest stipend applies to the role.

General responsibilities of the Editor role include:

- Managing article peer review and editing of articles. *Australian Geomechanics* uses the Scholastica journal peer review management system.
- Resolving problems that arise from time to time, such as plagiarism and ensuring articles are original and have not been previously published.
- Minor final formatting of papers to be print-ready, and proof reading of other content for the journal. Applicants should have a good eye for detail and experience in writing, editing, and proof reading.
- Liaison with AGS Chapters, Secretariat, Vice-Presidents (or liaisons) of international societies (ISSMGE, ISRM and IAEG) and Executive for content other than articles to be included in the journal.
- Content registration (DOI and associated metadata of articles) in Crossref.
- Liaison with Advertisement Coordinator for advertisement matters.
- Contributing to strategic development of the Journal.
- Attracting submissions and themed issue proposals to the Journal to ensure continued relevance and quality of content. Themed issues normally have a champion (guest editor), but standard peer-review process and requirements are applicable.
- Maintaining regular communication with the AGS Executive.
- Prepare reports and attend meetings of the AGS National Committee.

Interested applicants should send a short CV and a statement outlining their interest in seeking the position of Editor of *Australian Geomechanics*, and their overall objectives for the role. Ideally, applications should explicitly address the individual's aims and vision for *Australian Geomechanics*, suggested steps to be taken to sustain the pool of high-quality papers, and the expansion of the readership of the journal.

The AGS is seeking an initial term for the role of three years. The AGS is also seeking to fill the position of Assistant Editor/s to provide support with the tasks.

Enquiries regarding what the position entails can be addressed to the Interim Editor, Hugo Acosta-Martinez (editor@australiangeomechanics.org). EOI applications should be sent to Jon Gibbs, AGS Secretary (secretary@australiangeomechanics.org). The process will remain open until a suitable candidate is appointed.

CONFERENCE CALENDAR

OCTOBER 2023	
1-4	76th Annual Canadian Geotechnical Conference (GeoSaskatoon), Saskatoon, Saskatchewan, Canada *www.geosaskatoon2023.ca*
2-6	PIARC XXVIIth World Road Congress– Together on the road again, Prague, Czech Republic *www.wrc2023prague.org/*
3-5	Symposium on Energy Geotechnics (SEG23), Delft, The Netherlands *www.seg23.dryfta.com*
9-14	15th International ISRM Congress - Challenges in Rock Mechanics and Rock Engineering, Salzburg, Austria *www.isrm2023.com*
10-12	11th International Symposium on Ground Freezing, London, UK *www.iom3.org/events-awards/11th-international-symposium-on-ground-freezing.html*
10-12	10th International Conference on Ground Support in Mining, Perth, Australia *www.acggroundsupport.com*
16-18	HYDRO 2023 International Conference and Exhibition - New Ideas for Proven Resources, Edinburgh, Scotland *www.hydropower-dams.com/hydro-2023/*
24-26	1st International Conference on Geotechnics of Tailings and Mine Waste, Ouro Preto, Brazil *www.geominouropreto.com.br/2023/icgtmw2023*
25-27	21st Southeast Asian Geotechnical Conference and 4th AGSSEA Conference (SEAGC-AGSSEA 2023), Bangkok, Thailand. *www.seagcagssea2023.com*
31-3 Nov	48th Annual Conference on Deep Foundations (DFI48) - Embracing Change, Seattle, Washington, USA *www.dfi.org/annual2023*
NOVEMBER 2023	
1-3	2nd International Conference on Exploration and Utilization of Underground Space, Singapore *www.acuus2023.com*
6-10	7th International Conference on Earthquake Engineering and Seismology (7ICEES), Antalya, Türkiye *www.18wcsi-7icees.org/7icees*
14-16	Third International Slope Stability in Mining Conference (SSIM23), Perth, Australia *www.acgsurfacemining.com/*
14-17	6th World Landslide Forum - Landslide Science for Sustainable Development, Florence, Italy *www.wlf6.org*
20-23	2nd International Conference on Construction Resources for Environmentally Sustainable Technologies (CREST-2023), Fukuoka, Japan *www.ic-crest.com/*
DECEMBER 2023	
2-7	1st SLRMES Conference on Rock Mechanics for Infrastructure and Geo-Resources Development, Colombo, Sri Lanka *www.slrmes.org*
14-15	5th International Conference on Geotechnics for Sustainable Infrastructure Development, Hanoi, Vietnam *www.geotechn.vn*
FEBRUARY 2024	
25-28	Geo-Congress 2024 - Bridging Government, Industry, and Academia for Resilient Mega-Communities, Vancouver, Canada *www.geocongress.org*
MARCH 2024	
5-7	Southeast Asian Conference and Exhibition on Tunnelling and Underground Space (SEACETUS2024), Kuala Lumpur, Malaysia *www.iemtasb.weebly.com/seacetus2024.html*
APRIL 2024	
4-5	7th International Conference series on Geotechnics, Civil Engineering and Structures (CIGOS), Ho Chi Minh, Vietnam *www.cigos2024.sciencesconf.org*
19-25	World Tunnel Congress 2024 - Tunnelling for a better life, Shenzhen, China *www.wtc2024.cn*
MAY 2024	
7-10	8th International Conference on Earthquake Geotechnical Engineering (8ICEGE), Osaka, Japan *https://confit.atlas.jp/guide/event/icege8/top*
7-10	International Foundations Conference and Equipment Expo, Dallas, Texas, USA *www.ifcee2024.com*
26-29	GeoShanghai International Conference 2024, Shanghai, China *www.geo-shanghai.org*
28-30	Second annual Conference on Foundation Decarbonization and Re-use, Amsterdam, The Netherlands *www.foundationreuse.com*

CONFERENCE CALENDAR

JUNE 2024	
14-17	11th International Symposium of Geotechnical Aspects of Underground Construction in Soft Ground (IS-Macau 2024), Macao SAR, China *www.is-macau2024.skliotsc.um.edu.mo*
15-19	SuperPile '24 - Piling Design and Construction Conference, San Francisco, GA, USA *www.dfi.org/superpile2024*
18-21	7th International Conference on Geotechnical and Geophysical Site Characterization (ISC7), Barcelona, Spain *https://isc7.cimne.com/*
JULY 2024	
3-5	Third International Conference on Press-in Engineering 2024, Singapore *www.2024.icpe-ipa.org*
8-12	14th International Symposium on Landslides, Chambéry, France *www.isl2024.com*
15-19	Eurock 2024 - New Challenges in Rock Mechanics and Rock Engineering - an ISRM Regional Symposium, Alicante, Spain *www.isrm.net/conference/show/6357*
AUGUST 2024	
25-31	The 37th International Geological Congress, Busan, Republic of Korea *www.igc2024korea.org*
26-30	XVIII European Conference on Soil Mechanics and Geotechnical Engineering, Lisbon, Portugal *www.ecsmge-2024.com*
SEPTEMBER 2024	
10-12	4th International Society for Intelligent Construction Conference (ISIC 2024), Orlando, Florida, USA *www.is-ic.org/conferences/2024-isic-international-conference*
23-29	IS-Grenoble 2024 International Symposium on Geomechanics from Micro to Macro, Grenoble, France *www.is-grenoble2024.sciencesconf.org*
24-28	13th Asian Rock Mechanics Symposium "Advances in Rock Mechanics - Infrastructure Development" (ARMS13), New Delhi, India *www.isrm.net/conference/show/6356*
OCTOBER 2024	
2-4	5th European Conference on Physical Modelling in Geotechnics (ECPMG 2024), Delft, The Netherlands *www.issmge.org/events/ecpmg-2024*
6-9	18th African Regional Conference on Soil Mechanics and Geotechnical Engineering, Algiers, Algeria *www.algeos-dz.com/18ARC.html*
7-10	49th Annual Conference on Deep Foundations (DFI49), Aurora, Colorado, USA *www.dfi.org/annual2024*
30-31	1st international Rock Mass Classification Conference (RMCC), Oslo, Norway *www.isrm.net/conference/show/6371*
NOVEMBER 2024	
13-15	XVII Panamerican Conference on Soil Mechanics and Geotechnical Engineering, Pucon, Chile *www.panamgeochile2024.cl/*
20-22	5th International Conference on Transportation Geotechnics (5th ICTG), Sydney, Australia *www.ictg2024.com.au* **AGS SUPPORTED EVENT**
MAY 2025	
14-19	World Tunnel Congress (WTC2025) - Tunnelling into a sustainable future - methods and technologies, Stockholm, Sweeden *www.wtc2025.com*
JUNE 2025	
27 - 29	Eurock 2025 - Expanding the underground space - future development of the subsurface, Trondheim, Norway *www.isrm.net/conference/show/6365*
NOVEMBER 2025	
27 - 29	15th Asian Regional Conference of IAEG - "Geological Engineering for Scietal and Sustainable Development", Dhaka, Bangladesh *www.iaeg.info/event/arc-2025-dhaka*
JUNE 2026	
14-19	21st International Conference on Soil Mechanics and Geotechnical Engineering, Vienna, Austria *www.issmge.org/events/21st-international-conference-on-soil-mechanics-and-geotechnical-engineering*
OCTOBER 2027	
17-23	16th ISRM International Congress on Rock Mechanics, Seoul, Korea *http://isrm2027.website.or.kr*

AGS advises that the status of events at any time should be checked using the links to the event websites.

CORPORATE MEMBERS

The Australian Geomechanics Society gratefully acknowledges the contribution made by its Corporate Members.

FIRM	ADDRESS				PHONE
5QS Consulting Group	PO Box 63	WARNERS BAY	NSW	2282	(02) 4952 1666
A. S. James Pty Ltd	15 Libbett Avenue	CLAYTON SOUTH	VIC	3169	0408 564 597
ADE Consulting Group Pty Ltd	Unit 6, 7 Millennium Court	SILVERWATER	NSW	2128	(02) 8541 7214
AECOM Australia Pty Ltd	PO Box 1307	FORTITUDE VALLEY	QLD	4007	(02) 8934 0281
ARCADIS Australia Pacific	Level 16/580 George Street	SYDNEY	NSW	2000	(02) 8907 9150
Arup Australia Services Pty Ltd	Level 4, 108 Wickham Street	BRISBANE	QLD	4006	(07) 3023 6284
ATC Williams Pty Ltd	222-225 Beach Road	MORDIALLOC	VIC	3195	(03) 8587 0985
Aitken Rowe Testing Laboratories Pty Ltd	4/2 Riedell Street	WAGGA WAGGA	NSW	2650	(02) 6939 5555
Alliance Geotechnical Pty ltd	10 Welder Road	SEVEN HILLS	NSW	2147	1800 288 188
Anora Foundations Pty Ltd	PO Box 3282	DARRA	QLD	4076	(07) 3279 7966
Aurecon Australasia Pty Ltd	Level 2, 116 Military Road	NEUTRAL BAY	NSW	2089	(02) 9465 5386
Barrason's Engineers	1/206 Princes Hwy	PAKENHAM	VIC	3810	(03) 5940 2638
Bauer Foundations Australia Pty Ltd	Ground Floor, 154 Enoggera Road	NEWMARKET	QLD	4051	(07) 3352 7444
Butler Partners Pty Ltd	79 Doggett Street	NEWSTEAD	QLD	4006	(07) 3852 3800
CPTS	16 Charles Place	MANLY WEST	QLD	4179	0407 375 977
Chadwick Geotechnics Pty Ltd	25 Metcalf St	DANDENONG SOUTH	VIC	3175	(03) 8796 7900
Civiltest Pty Ltd	PO Box 537	MORNINGTON	VIC	3931	(03) 5975 6644
CONETEC Pty Ltd	6 Chapman Pl	EAGLE FARM	QLD	4009	0473 923 084
Construction Sciences Pty Ltd	60 Kingsford Smith Drive	ALBION	QLD	4010	1300 165 769
Core Consultants Pty Ltd	52 Second Ave	MAROOCHYDORE	QLD	4558	(07) 5475 5900
Douglas Partners Pty Ltd	96 Hermitage Road	WEST RYDE	NSW	2114	(02) 9809 0666
Durham Geo Slope Indicator	Unit 1/82 Reserve Street	WEMBLEY	WA	6014	(08) 9284 9090
EI Australia Pty Ltd	01/55 Miller St	PYRMONT	NSW	2009	(02) 9516 0722
Fugro Australia Marine Pty Ltd	Level 1, 1060 Hay Street	WEST PERTH	WA	6005	(08) 9218 2000
GEOFABRICS Australia Pty Ltd	83-93 Canterbury Road	BRAESIDE	VIC	3195	1300 60 60 20
GHD Pty Ltd	Locked Bag 2727	ST LEONARDS	NSW	1590	(02) 9462 4859
Geobrugg Australia Pty Ltd	PO Box 2468	MALAGA	WA	6944	(08) 9249 9939
Geomotion (Australia) Pty Ltd	9/31-33 Chaplin Drive	LANE COVE	NSW	2066	(02) 9950 4728
Geotech International Australia Pty Ltd	8 Argyle Place	MILLERS POINT	NSW	2000	(02) 9950 5598
Geotech Pty Ltd	174 Turner Street	PORT MELBOURNE	VIC	3207	(03) 9624 4200
Geotechnique Pty Ltd	PO Box 880	PENRITH	NSW	2751	(02) 4722 2700
Geotesta Pty Ltd	6/31-37 Howleys Road	NOTTING HILL	VIC	3168	(03) 9562 8808
Global Synthetics Pty Ltd	41 Sammut St Smithfield	SMITHFIELD	NSW	2164	(02) 9725 4321
Golder Associates Pty. Ltd.	147 Coronation Drive	MILTON	QLD	4064	(07) 3721 5400
Intrax Consulting Engineers Pty Ltd	35 Banks St	MELBOURNE	VIC	3205	(03) 8371 0100
Ischebeck Titan (Australia) Pty Ltd	197 Queens Road	KINGSTON	QLD	4114	(07) 3208 1158
JC Geotechnics Pty Ltd	Suite 3A, Level 3, 1C Grand Ave	ROSEHILL	NSW	2142	(02) 8066 0665
JK Geotechnics	115 Wicks Road	MACQUARIE PARK	NSW	2113	(02) 9888 5000
Jacobs Group (Australia) Pty Ltd	452 Flinders Street	MELBOURNE	VIC	3000	0424 446 277
Keller Pty Ltd (TS)	Suite G01-02 Ground Floor, 2-4 Lyonpark Rd	MACQUARIE PARK	NSW	2113	0430 445 486

FIRM	ADDRESS				PHONE
Menard Oceania Pty Ltd	Level 5, 13-15 Lyon Park Road	MACQUARIE PARK	NSW	2113	(02) 9491 7100
Mott MacDonald Australia Pty Ltd	Level 3, 707 Collins Street	MELBOURNE	VIC	3008	(03) 9037 7575
Norwegian Geotechnical Institute Pty Ltd	Level 7, 40 St Georges Terrace	PERTH	WA	6000	(08) 6559 6499
Pells Sullivan Meynink	G3, 56 Delhi Rd	NORTH RYDE	NSW	2113	(02) 9812 5000
Piling and Concreting Australia	PO Box 1605	RUNAWAY BAY	QLD	4216	(07) 5500 5898
Probedrill Pty Ltd	9 Baling Street	COCKBURN CENTRAL	WA	6164	(08) 9417 9933
Reinforced Earth P/L	Level 5, 13-15 Lyonpark Road	MAQUARIE PARK	NSW	2113	(02) 9910 9910
Roads and Maritime Services	99 Phillip Street	PARRAMATTA	NSW	2150	(02) 8837 0246
SCT Operations Pty Ltd	131a Kembla Street	WOLLONGONG	NSW	2500	(02) 4222 2777
Sixense Oceania	92 Thistlethwaite Street	SOUTH MELBOURNE	VIC	3205	(03) 9510 0582
SMEC Australia Pty. Ltd	Level 5 20 Berry Street	NORTH SYDNEY	NSW	2060	(02) 9925 5555
Scherzic Ground Investigations	PO Box 555	HOBART NORTH	TAS	7002	(03) 6273 6565
Shirley Consulting Engineers Pty Ltd	PO Box 6160	PYMBLE	NSW	2073	(02) 9449 5577
Site Geotechnical Pty Ltd	Factory 3, 8 Cannery Court	TYABB	VIC	3913	1300 557 260
Statewide Geotechnical Pty Ltd	17-20 Summer Lane	RINGWOOD	VIC	3134	(03) 9879 2999
Terrascan Pty Ltd	37 Day Street North	SILVERWATER	NSW	2128	0408 723 340
Tetra Tech Coffey Pty Ltd	Level 19, Tower B, Citadel Tower799 Pacific Highway	CHATSWOOD	NSW	2067	(02) 9406 1192
Tonkin & Taylor Pty Ltd	Level 3, 99 Coventry Street	SOUTHBANK	VIC	3006	(03) 8796 7900
Trilab Pty Ltd	346A Bilsen Road	GEEBUNG	QLD	4034	(07) 3265 5656
WSP Australia Pty Ltd	Level 4, Northbank Plaza, 69 Ann Street	BRISBANE	QLD	4001	(02) 9272 5100
Wagstaff Piling Pty Ltd	PO Box 117	ASHGROVE	QLD	4060	(07) 3366 2555

ADVERTISERS

The Australian Geomechanics Society gratefully acknowledges the support from firms that advertise in *Australian Geomechanics.*

FIRM	PAGE
Acu-Vib Electronices	37
Black Insitu Testing	140
Chadwick Geotechnics	76
ConeTec Pty Ltd	38
Construction Sciences Pty Ltd	74
Datgel Pty Ltd	39
Douglas Partners	94
Durham Geo Slope Indicator P/L	Outside back cover
ECOFINE	60
Geobrugg Australia	114
Geofabrics Australasia	75

FIRM	PAGE
Geosolve	39
GHD Geotechnics	142
Insitu Geotechnical Services	Inside front cover
Itasca Australia Pty Ltd	40
Menard-Oceania	Inside back cover
Probedrill P/L	59
Senversa	141
Terrascan Pty Ltd	96
Terratest Australia Pty Ltd	115
Tonkin & Taylor	95
Trilab P/L	116

AUSTRALIAN GEOMECHANICS SOCIETY

We need YOU!

Australian Geomechanics was established to meet the needs of the practicing geotechnical professional. As such we are keen on publishing practical papers that are of use to local consultants and researchers.

We are always pleased to receive content in the form of review articles, technical papers, letters to the Editor, original research papers, case studies, and methodologies or methods.

Submissions are required at least 4 months prior to publication and can vary in length from 1-page to 20-pages.

More details on our Editorial Policy can be found at the AGS website (australiangeomechanics.org/journal/editorial-policy/)

Technical papers may be submitted via the AGS Scholastica website: (https://ags.scholasticahq.com/for-authors)

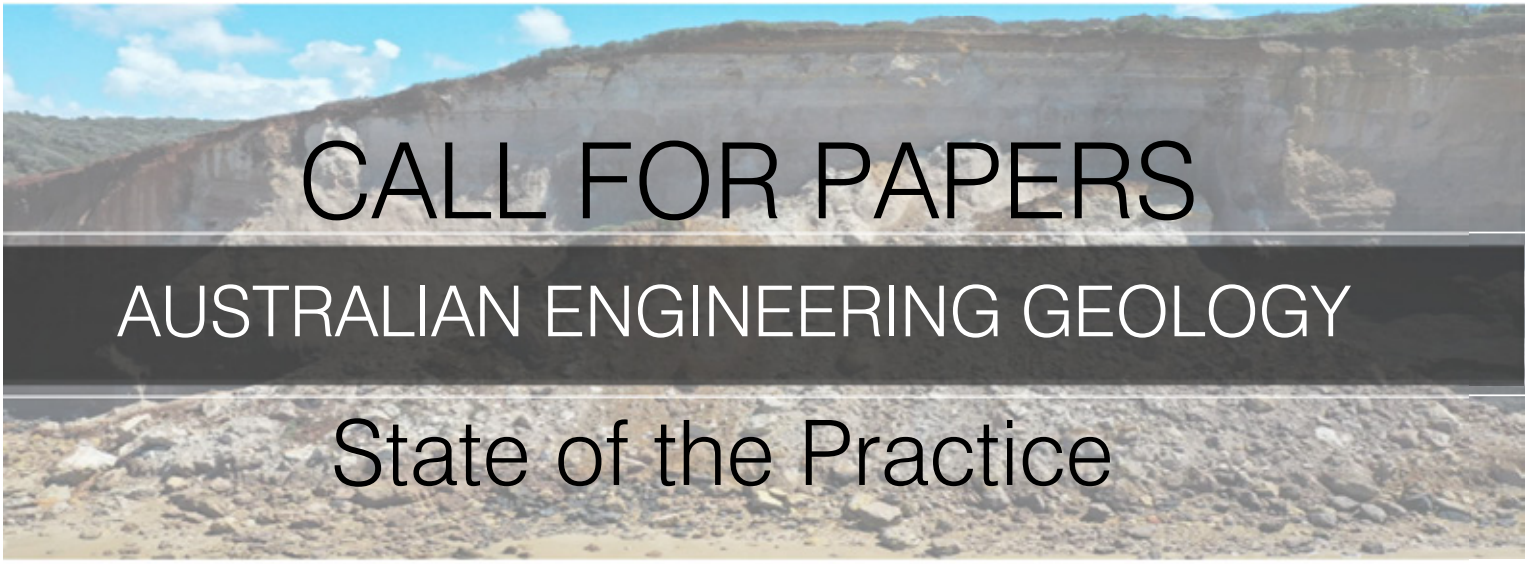

CALL FOR PAPERS

AUSTRALIAN ENGINEERING GEOLOGY

State of the Practice

In celebration of the 60th anniversary of the International Association for Engineering Geology and the Environment (IAEG), the Australian Geomechanics Society is pleased to announce a themed issue of *Australian Geomechanics* titled "Australian Engineering Geology – State of the Practice".

We encourage practitioners and academics to submit papers relating to this topic.

Unfortunately, soils are made by nature and not my man, and the products of nature are always complex…As soon as we pass from steel and concrete to earth, the omnipotence of theory ceases to exist. Natural soil is never uniform (Karl Terzaghi, 1936).

Without application of the geological sciences, geotechnical engineering lacks a design basis. A sound understanding of the ground composition, the processes that have and continue to form the ground and how the ground will respond to change are vital inputs for all geotechnical engineering.

From the design and interpretation of ground investigation and the development of engineering geological models to the identification and assessment of geohazards, skills in engineering geology are vital to our industry.

So, what is the current state of engineering geology practice in Australia? What are the key challenges facing engineering geology today and in the future?

In celebration of the IAEG's 60th anniversary, this special edition of Australian Geomechanics will seek to explore these questions.

THEMES

The following are some suggested topics for this special edition of *Australian Geomechanics*:

- Resilience against climate change, natural disasters and geological hazards.
- Engineering geology for tunneling and underground space.
- Ground characterization for Australian conditions, e.g. duricrusts, expansive soils and carbonates.
- The role of engineering geology in a sustainable future – renewable energy water security.
- Digital engineering geology.
- Construction materials – identification, investigation and exploitation.
- Growing the body of knowledge of engineering geology in Australia - education and competence.
- Ground investigation and measurement.
- Engineering geological ground models.
- Communication of geological matters to stakeholders.
- Interesting case studies highlighting the importance of engineering geology to the practice of geotechnical engineering in Australia.

PAPER SUBMISSION

Papers submitted for consideration in the special edition should be submitted via Scholastica no later than 29 February 2024. Early submissions are encouraged.

For further guidance on the preparation of papers, editorial policy and how to submit a paper, please refer to the *Australian Geomechanics* Journal webpage.

https://australiangeomechanics.org/journal/.

If you are unsure whether your paper is suitable for publication in this special edition, then please submit a 300 word abstract via Scholastica for consideration.

Papers for publication in this themed issue will be based on their quality and relevance to the topic. We encourage submissions from the geotechnical profession, other geoscience practitioners, the quarry industry, as well as academia.

Good engineering geologists must be good geologists who understand engineering needs. Good geotechnical engineers must be good engineers who understand the help that geology can bring (Peter Fookes, 2000).

AGS Applied Landslide Risk Assessment 2024

AUSTRALIAN GEOMECHANICS SOCIETY

www.australiangeomechanics.org

Melbourne, Victoria March 2024

AIMS OF THE COURSE

This course will be conducted over 2 stages: a 1-day seminar followed by a 3-day field course.

The principal objective of this course is to teach students the fundamentals of landslide risk assessment and how to collect information and make observations in the field to support effective landslide risk assessments. The teaching method is based on examples and guided field exercises, in which the students learn by carrying out realistic project related work in the classroom and/or field whilst being supervised by very experienced practitioners.

Students who complete the course should be able to achieve the following:

DAY-1 SEMINAR

- Be familiar with the Australian Geomechanics Society Guidelines for Landslide Risk Assessment (AGS 2007).
- Understand the importance of a desk study and use desk study information to inform field assessment.
- Undertake risk to life and risk to property calculations for a range of scenarios.

DAY-2–4 FIELD COURSE

- Communicate more successfully with other professionals, involved in landslide engineering and landslide risk management.
- Develop effective field techniques for mapping and observing landslides.
- Recognize a variety of landslide types and identify landslide hazards.
- Observe and understand the geological and geomorphological features associated with landslides, record them on maps and develop different types of geological models for a project area with a landslide problem.
- Understand landslide mechanisms, processes and process rates and estimate the probability of landslide processes and consequences occurring.
- Identify elements at risk from landslide
- Form judgements on what might be regarded as reasonable inputs into a landslide risk assessment using AGS 2007 or similar guidelines.

WHO SHOULD ATTEND

This course is designed for geologists and engineers involved in landslide engineering and landslide risk management. It is envisaged that participants will have some industry experience, some familiarity with assessing landslides, and wish to enhance and develop their field skills.

The field course will be limited to 24 participants on a first-come, first-served basis.

Please contact Darren Paul to discuss whether the AGS Applied Landslide Risk Assessment Course to be held in Melbourne is suitable for you.

ACCREDITATION AND PRESENTERS

The course is run by the Australian Geomechanics Society and is recognized by Engineers Australia as meeting an equivalent of 40 hours of CPD,. Engineering geologists Fred Baynes, Phil Flentje, Tony Miner and Darren Paul have developed and will present the course on behalf of the Australian Geomechanics Society. A teacher to student ratio of around 1 to 6 will be maintained throughout the course.

COURSE OUTLINE

Participants will be accommodated in hotels in and around Melbourne and will travel each day from the hotel by coach to the teaching sites. The course will be undertaken over 4 days, 3 nights and will visit a variety of landslide and rock fall sites. The indicative course outline is set out on the following page.

WHEN
Thu 22 Feb 2024 –
Sun 25 Feb 2024

WHERE:
Melbourne and various locations around Victoria

COST:
AGS Members: $4,095
Non-members: $4,295
Prices inc. GST

The fee includes all instruction, 3 nights accommodation, course notes, and transport for field trips. The fee also includes all breakfasts, 2 lunches, and 2 dinners throughout the course. Other meals and accommodation are not included in the registration fee and students will be given the opportunity to arrange their own meals.

EVENT CONTACT:
For further information about the course contact Darren Paul via darren.paul@wsp.com

RSVP:
Please RSVP via: https://australiangeomechanics.org/courses/applied-landslide-risk-assessment/

CPD:
Engineers Australia (EA) members participating in AGS technical sessions can record attendance on their personal Continuing Professional Development (CPD) logs. Members should refer to EA's CPD policy for details on CPD types, requirements and auditing guidelines.

PROGRAM

DAY 1 SEMINAR THURSDAY 22 FEBRUARY, 9:30AM – 5:30PM

Full day seminar on landslides risk assessment covering basic principles of landslides risk assessment, use of the Australian Geomechanics Society Guidelines for Landslide Risk Management (AGS 2007) and worked examples.

Course dinner and introduction to field component.

DAY 2 FRIDAY 23 FEBRUARY, 7:00AM – 9:30PM

Full day training and mapping exercise at Montrose debris flow observing source areas, mapping run out zones and identifying elements at risk.

Evening seminar and overnight accommodation in Kalorama, concluding 9:30pm.

DAY 3 SATURDAY 24 FEBRUARY, 7:00AM – 9:30PM

Mapping and LRM exercise at Plantes Hill Landslide Mooroolbark, with focus on assessing elements at risk from landslide.

Walkover and discussion at deep seated coastal landslide at The Dell, Clifton Springs.

Rockfall mapping and risk assessment exercise at The Bluff, Barwon Heads.

Evening seminar and feedback on rockfall mapping and hazard assessment exercise.

Overnight accommodation in Geelong.

DAY 4 SUNDAY 25 FEBRUARY, 7:00AM – 6:00PM

Mapping, frequency and LRM exercise on complex landslide at Cut Hill Landslide, Parwan Valley.

Visit to Niddrie quarry to observe rock fall remediation and treatment.

Airport drop off at 5pm, return to Melbourne at 6pm.

ASSESSMENT OF DELIVERABLES – FIELD COMPONENT

Most exercises will involve a deliverable which will be individually assessed by the course presenters and feedback provided in the field. Some team exercises will be presented to the group as a whole in the evening workshops. Each participant will be verbally advised as to the standard of their work. Upon successful completion of the course participants will be given a certificate of attendance.

REGISTRATION FEE

The registration fee is $4,095 for members and $4,295 for non-members.

The fee includes all instruction, 3 nights accommodation, course notes, and transport for field trips. The fee also includes all breakfasts, 2 lunches, and 2 dinners throughout the course. Other meals and accommodation are not included in the registration fee and students will be given the opportunity to arrange their own meals.
Our strong preference is for all participants to stay at the nominated hotels. If you would like to discuss making arrangements for your own accommodation, please contact Darren Paul via darren.paul@wsp.com.

ACCOMMODATION & TRANSPORT

1-Day Seminar, Thursday 22 February:
Seminar will be at or near the University of Melbourne in Carlton (venue TBA). Dinner will be held in the Melbourne University/ Carlton area. Overnight accommodation is the Travel Inn Hotel, Carlton , Cnr. Drummond and Grattan Streets Carlton. Breakfast included.

Friday 23 February:
Accommodation at A Country Place in Kalorama in the Yarra Ranges area in the outer east of Melbourne. Dinner and breakfast included.

Saturday 24 February:
Accommodation at Rydges Geelong. Breakfast and lunch included.

REGISTRATION

Members are required to log in to access the AGS member price, which is not transferable. Members may only purchase a single ticket at the member price.

Payment via credit card is available and processed by Stripe. The Australian Geomechanics Society will not store or have access to your credit card information, and Stripe adhere to strict security and PCI compliance for processing online transactions.

Upon purchase, an email and a tax invoice will be sent to the buyer. Attendees will also receive an email with their tickets attached, as well as a link to download the tickets if they are misplaced.

CANCELLATION POLICY

Fees will not be refundable if a participant is unable to attend. However, a nominated person may attend in your place. If at any time the course is cancelled, fees will be refunded in full.

AGS Members' Photography

AUSTRALIAN GEOMECHANICS SOCIETY

You too can publish your photos in *Australian Geomechanics*

We are inviting all our members to submit photos for publication in Australian Geomechanics to showcase the top class work being undertaken in our industry.

All selected photos will be published with acknowledgment of the photographer, their affiliation and with a caption describing the photo.

If you would like to promote your project and your work in this way, please submit your high resolution digital images via email to our Editor at: editor@australiangeomechanics.org

Please include:

- Name of the Photographer.
- Affiliation of the Photographer.
- A caption describing the image.
- Authorisation from end client.

Our Editor will select photos for publication.

By submitting your photo, you grant your permission for the Australian Geomechanics Society to publish the photograph in *Australian Geomechanics*. The AGS Photography Release Form needs to be completed to formalise agreement. It will be provided if submissions are selected for publication.

Photographs selected for publication will be at the sole discretion of the Australian Geomechanics Society.

SV 803

Ground and Buildings Vibrations

Smart Monitoring

Acu-Vib Electronics
ACOUSTICS AND VIBRATIONS

A new **wireless vibration monitor** from Svantek, represents the cutting edge of high-technology monitoring devices. Specifically designed for wireless vibration monitoring of both **building and ground vibrations** in a variety of environmental conditions, this device utilizes geophones as its primary vibration sensors.

- **3-year warranty** for hardware
- **3-axial vibration** measured simultaneously
- **PPV, VDV, FFT, 1 /3 OCTAVE**, and **WAV** recording
- **DIN, BS, VC** limit curves inbuilt
- User adjustable **limit curves**
- Vibration **events** compared to limit curves directly in the device
- Instant **SMS** and **email** alarms
- **Remote access** to vibration and noise data via SvanNET cloud service
- Automatic **reporting** from the SvanNET cloud service
- Powering from the internal **battery**, mains, or **solar** power
- Bluetooth modem for **mobile app**
- Up to 6 months Battery life

NATA
WORLD RECOGNISED ACCREDITATION

SVANTEK
monitoring systems

Find us at acu-vib.com.au

SAFETY. QUALITY. PEOPLE. EQUIPMENT.

GLOBAL LEADERS IN SITE CHARACTERIZATION

Brisbane, Queensland
6 Chapman Pl
Eagle Farm QLD 4009

Perth, Western Australia
113 Radium Street
Welshpool WA 6106

- 200kN Tracked CPT Rigs
- Resistivity-Seismic CPTu
- In-Situ Testing (eVST, PMT, DMT, Ball-CPT)
- Direct Push Disturbed and Undisturbed Sampling
- 200kN Portable CPT Rigs
- Mining
- Infrastructure
- Energy
- Environmental
- Commercial Development

BETTER INFORMATION
BETTER DECISIONS

PROUDLY SERVING ALL OF AUSTRALIA AND OCEANIA
CONETEC.COM.AU | 04 0720 8389

CONETEC

Geosolve

Contacts:
Daniel Borin & Duncan Noble
support@ geosolve.co.uk

London, UK
www.geosolve.co.uk

SLOPE version 12

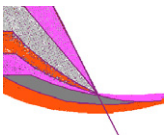

Slope Stability Analysis &
Reinforced Soil Design

Key features

Multiple water tables or piezometric surfaces
Slip surfaces: Circular, 2 and 3 part wedges, general non-circular slips
Multiple surcharges
Seismic analysis
Interactive graphical input
Reinforced soil options:
- Designs optimum reinforcement layout
- Choice of Grids, Strips, Fabric, Soil nails

GWALL Version 4

Gravity Wall **fully revised**
Reinforced Concrete walls
Multiple Load Cases and Limit State combinations
Factor of Safety on sliding and overturning.
Bending moments and Shear Forces in stem and base (including the effects of compaction)

New feature **Gabion walls**

WALLAP version 6.08

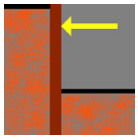

Retaining Wall Analysis
Sheet piles, Diaphragm walls
Combi walls, Soldier pile walls

Key features

Factor of Safety calculation
Bending moment and displacement analysis with 2-D quasi FE option and soil arching
Single Pile analysis with loads applied at various orientations
Complex ground profiles; Variable wall section
Thermal loading in struts; Seismic loading
Integral Bridge design to PD 6694
Limit State analysis to Eurocode 7
Change from undrained to drained conditions
Context sensitive help
Customized report generation

New features

Display of Critical Active and Passive wedges
Results include Minimum Required Free Anchor Lengths

FLAC2D 9 NEW

Version 9 now available

Solve your most complex geotechnical problems

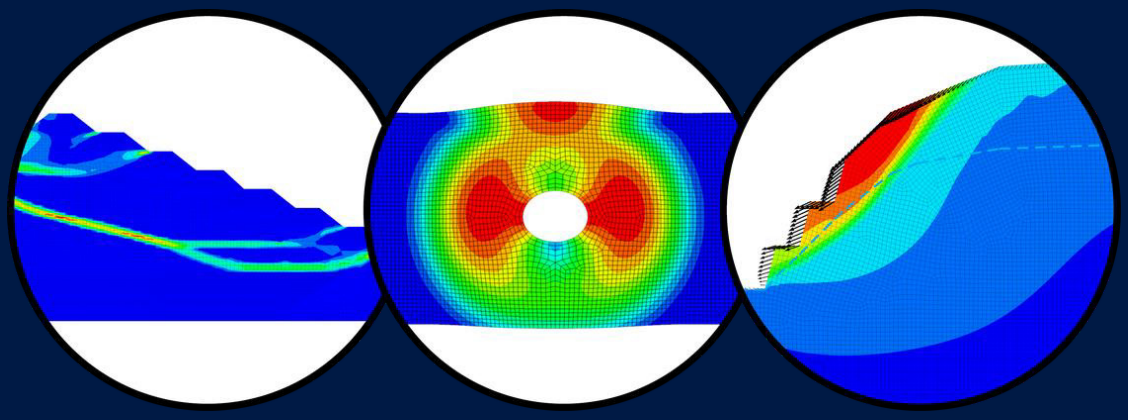

FLAC2D is designed to provide engineers and researchers with an intuitive and robust platform to simulate and analyse two-dimensional and axisymmetric geotechnical problems. It combines cutting-edge numerical solutions with a user-friendly interface, allowing users to efficiently model complex geological structures and perform advanced analyses for:

- Slope stability
- Foundation design & soil structure interaction
- Retaining walls and excavation support
- Tunnels and underground structure stability
- Seismic design and liquefaction analysis
- Ground improvement analysis
- Geotechnical hazard assessment
- Geotechnical design comparison
- Factor of safety calculations
- Groundwater flow & seepage analysis

Discover more about *FLAC2D* on our website
www.itasca.com.au/flac2d

ITASCA

SHEAR STRENGTH OF STOCKPILED COKING COAL – EXISTING DATA

John David Eckersley

James Cook University, Townsville, Australia

https://doi.org/10.56295/AGJ5831

ABSTRACT

Flowslides and stability issues have occurred periodically within stockpiles of coking (metallurgical) coal at coal processing plants and export terminals in Queensland's Bowen Basin, and to a lesser degree in New South Wales, since the early 1970s. A description of the issue and summary of research at James Cook University (JCU) from 1973 to 2000 was published in ACARP Report C4057 (Eckersley, 2000).

Eckersley (2022) partly updated that work with SEEP/W transient seepage modelling of a 12 m high coal stockpile constructed at Hay Point in late 1991 for which initial moisture content, pore water pressures at the stockpile base, outflows from subsoil drains and final density and moisture profiles were measured. This provided a good starting point for modelling of moisture movements within production coal stockpiles as required for meaningful slope stability analyses.

The current paper provides an accessible summary of available data from laboratory shear strength testing of coking coal to assist in selection and critical assessment of parameters for slope stability analyses of coal stockpiles. This includes data for saturated coal likely to form the base of a stockpile and currently limited data for unsaturated coal forming the bulk of a stockpile. It then highlights some issues in the selection of parameters for stability analyses of coal stockpiles.

1 INTRODUCTION

Metallurgical (coking) coal is typically prepared for export by crushing and washing the run-of-mine coal. It is temporarily stacked into coal processing plant (CPP) product stockpiles prior to reclamation and train loading for transport to port stockpiles and subsequent ship loading. The product has relatively low specific gravity (typically 1.33 to 1.38) and consequently the bulk density as stockpiled (typically 0.9 to 1.1 t/m^3) is relatively low. Pore water pressures in stockpiles therefore have greater impact on slope stability than for other geo-materials, whether from redistribution of initial moisture or rainwater infiltration (Eckersley, 1985, 1986, 1990a, 2000).

As a result, flowslides and slope stability issues have been observed within stockpiles of coking coal at export terminals and at processing plants located at coal mines since the early 1970s in Queensland's Bowen Basin, to a lesser degree in New South Wales (Eckersley, 1985; 1990a; Davies et al., 2013), and in Western Canada (Leeder et al., 2014). Australian Coal Association Research Program (ACARP) report C4057 (Eckersley, 2000) summarises investigations from 1973 to 2000 into coal stockpile moisture and slope stability issues. More recent work on moisture properties and SEEP/W analysis of the moisture redistribution process in stockpiles was reported by Eckersley (2022).

Instability issues (frequently referred to on site as "slips" or "slumps") have varied in scale from small events (involving some tens of cubic metres) to large flowslides in which up to 65,000 m^3 of product stockpile initially up to 25 m high has slipped and flowed up to 70m. Duration of movement may be less than 10 seconds. The volume of saturated coal slurry observed in slips post-failure, speed of movement, runout distance and collapse without apparent warning all point to liquefaction of loose saturated coal as the critical process in flowslide formation (Eckersley, 1986). Consequences have included demolishing light structures, engulfing stockpile dozers, covering railway lines and pipelines, substantial operational delays, loss of product and damage to mobile plant. A case at one NSW operation resulted in a fatality and in one event at a Central Queensland Coal Preparation Plant (CPP) a CPP worker was buried up to his neck before being rescued (Eckersley, 1990a). Typical features of these slips are illustrated in Figure 1. Topographic features of the flowslide surface can range from broad crested waves to block dislocations, both approximately perpendicular to the direction of flow.

For stockpiles subjected to heavy rain the near-surface material wets up and moisture suctions are reduced. For susceptible products this results in gully erosion and shallow slips with consequent flow of near-saturated coal, thus removing a substantial proportion of the infiltrated water. These are not shown in Figure 1 but were illustrated in Eckersley (2000). This process and field experiments performed as part of the ACARP research were described by Eckersley (1999). Unfortunately, altering the size distribution of the coal product (to substantially increase permeability) and covering the stockpile to prevent water ingress are generally impractical. Stockpile covering is sometimes used overseas (Leeder et al., 2014). Practical measures to control rain-induced erosion and slipping in large

stockpiles are therefore limited to providing sufficient space to accommodate the eroded and/or slipped material (Eckersley 1990a, 2000) and re-grading (and possibly compacting) the surface of long-term stockpiles.

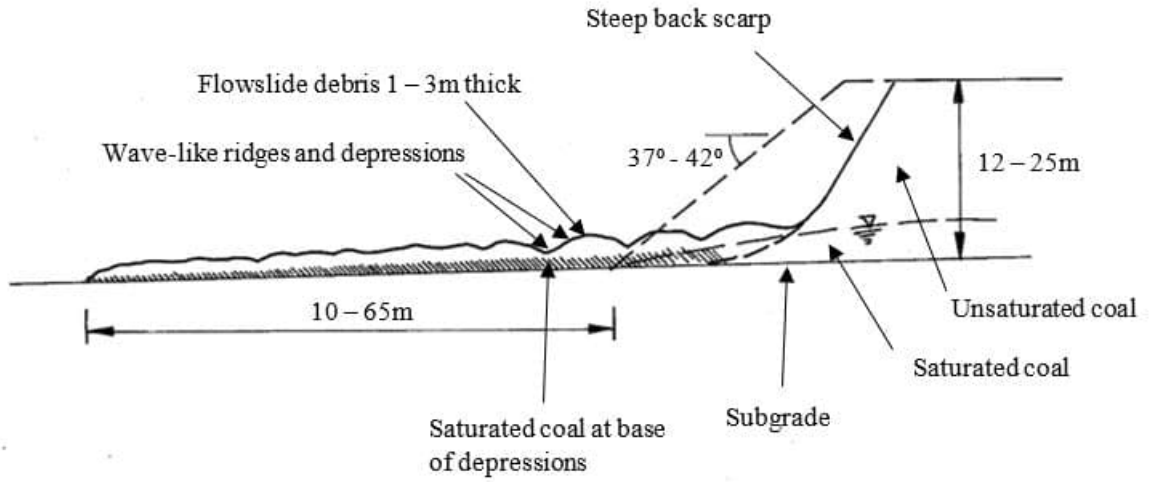

Figure 1: Typical features of coal stockpile flowslides

Redistribution of initial moisture alone (without heavy rain) can result in a sufficiently high saturated zone at the stockpile base to trigger instability (Eckersley, 1990a). Infiltrated rainwater can also penetrate into the stockpile and add to the saturated zone. Flowslides can then result for susceptible loosely placed coal when pore pressures become sufficiently high for instability to initiate under essentially drained conditions, with mobilized effective friction angles substantially less than those at the ultimate steady state shearing. If the saturated coal is sufficiently loose its contractant response to shear (i.e. tendency for volume reduction) then results in rapid generation of excess pore water pressures and liquefaction of the coal, with rapid acceleration and flow of the sliding mass. The liquefaction process within a coal stockpile context was discussed in more detail by Eckersley (1985, 1986, 1990a, 1990b) and Davies et al. (2013). Been (2016) provided insightful discussion of liquefaction in the context of tailings dam design, and Jefferies (2019) included a useful note on the transition from drained to undrained conditions.

If pore pressures in the saturated part of a stockpile (and preferably – suctions in the unsaturated part) can be quantified, stability analyses using appropriately selected strength parameters could be used to design the stockpile geometry (height, slope angle, bench dimensions) and/or drainage measures to reduce the likelihood of serious instability. The recent paper by Eckersley (2022) provided a starting point for seepage analyses.

The objective of the current paper is to summarize relevant shear strength data from the ACARP report and other sources to provide an accessible resource for stockpile slope stability analyses. Application of these parameters and validity of the approach is investigated (in at least a preliminary way) in a companion paper (Eckersley, 2023) by stability analysis of two instrumented experimental stockpiles constructed at Hay Point in 1974 and 1991.

Interested readers are referred to the ACARP Report (Eckersley, 2000) and other publications (Eckersley, 1977, 1985, 1986, 1990a, 1990b) for additional description of coal stockpile flowslides and circumstances leading to their initiation. This work was mostly conducted while the author was at James Cook University (JCU). It is of most relevance to the coal processing industry where moisture content is defined as mass of water per wet mass of coal and referred to as "% total moisture" (AS1038 - Standards Australia, 2001). However this paper follows the usual geotechnical definition (AS1289 – Standards Australia, 2005) where water content is mass of water per dry mass of solids. It is noted that geotechnical water content *w%* may be converted to % total moisture by *%TM = w%*100/(100+w%).*

2 OVERALL APPROACH

For design of stockpiles to limit the likelihood of significant flowslides occurring, the following questions are relevant:

1. Does the coal have sufficient fines to be susceptible to liquefaction? This relates to its tendency to form a loose structure with permeability (hydraulic conductivity) sufficiently low to sustain excess pore water pressures needed for liquefaction for at least a few seconds. The author's data indicates that products with a history of flowslides have d_{10}<0.35 mm.
2. Are strength and pore pressure conditions sufficiently adverse for failure to be initiated? This requires reasonable knowledge of pore water pressures in the saturated zone and moisture suctions within the unsaturated bulk of the stockpile and (in principle) is investigated by way of slope stability analyses.
3. If slipping initiates, is the saturated coal sufficiently loose for a markedly contractant response so that initiation of movement results in liquefaction (with consequent dramatic loss of strength, acceleration and rapid flow)? This requires reasonable knowledge of the density and effective stress conditions within a stockpile for comparison with those under which a contractant (liquefaction or flow) response results, as opposed to a dilatant (non-flow) response.

Eckersley (1985, 1986, 1990b) presented results from saturated isotropically consolidated undrained (CIU) triaxial tests on one coking coal product (labelled LA in the ACARP Report) with a history of instability and discussed how these demonstrate the same contractant behaviour as observed in the geotechnical literature for loose saturated sand. These results are included in the ACARP report (Eckersley, 2000), and similar triaxial tests were performed on two additional products with a history of instability (LB, LD) and one with no history of slipping (LC). This data is summarized in Section 4 below. Results are included for effective friction angles (relevant for analysis of failure initiation – see Question 2 above) and state diagrams showing dry density and effective stress conditions for which contractant rather than dilatant response to shear is likely (see Question 3 above).

Particle size distributions for the four products mentioned above are summarized in Figure 2. The products with a history of flowslides have d_{10}<0.35 mm. As noted above, the author's data indicates that for coal flowslides this is consistently the case, and so provides a first assessment of whether a coal product is susceptible to flow failure. LB is the finest product. LC is significantly coarser than the others. It is noted that for each of the products tested there is significant variation in sizing as stockpiled and the data shown is for the particular samples tested.

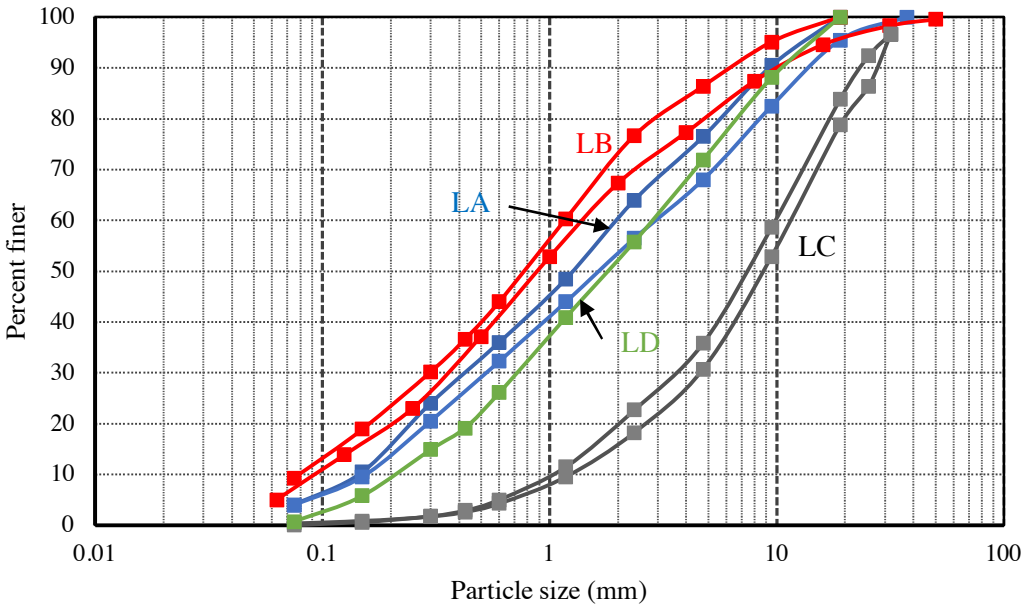

Figure 2: Product coal sizing (from Eckersley, 2000; LA, LB, LD have history of flowslides)

Except for shallow slips in response to heavy rain, the bulk of coal involved in slips is partly saturated, probably with moisture content slightly less than at the time of stockpile construction. This relates to part of Question 2 above. While the potential contribution of suction to coal stockpile stability was recognised in the ACARP report and some exploratory triaxial testing of unsaturated coal was reported, the impact on stability was not quantified and test stress paths were not ideal. A conservative approach would be to assume no cohesion in slope analyses. This may be

reasonable in civil projects. However, in the coal industry context where stockpile slope is close to its effective friction angle for shearing at constant volume, even small cohesions may significantly influence factor of safety and especially for localised slips near the toe. This might then significantly distort decisions about stockpile management. The shear strength of unsaturated coal is therefore considered in Section 5.

It is noted that as a primarily organic solid, coal differs from usual geotechnical materials. Its macerals are hydrophobic to varying degrees (Arnold & Aplan, 1989), and it also seems likely that the fines may have residual coating of chemicals used in the froth flotation process. The degree to which such effects of surface chemistry impact the shear strength of coking coal has not been investigated in the current work, but is worthy of further study. As a first approximation in view of its typical size distribution, stockpiled coking coal has been treated as a granular soil that differs from others because of its low specific gravity. The data presented below is considered to generally support this approach, but there may be subtle impacts when coal is unsaturated, or when saturated and at low effective stresses.

3 DENSITY CHANGES WITH LOADING AND SATURATION

Unfortunately, the most significant unknown relating to stockpile stability is in-situ density of the coal. It is strongly controlled by the placement method, stockpile height, size distribution and moisture content. In-situ density measurements known to the author are limited to some at Hay Point during investigations in the 1970s, to those in the 1991 experimental stockpile at Hay Point described in Eckersley (2022), and some measurements in the faces of stockpiles where erosion experiments were conducted as part of the ACARP research (Eckersley, 1999). The methodology adopted for in-situ density measurement in the 1991 experimental stockpile (Eckersley, 1994, 2000) remains relevant, and general comments on in-situ density for some stockpile construction procedures are reported by Eckersley (1977, 1986, 2000).

Possible approaches for assessing coal stockpile in-situ density include:

1. Direct measurement using sand replacement or nuclear meter techniques during staged stockpile reclamation (as done in the 1991 stockpile experiment),
2. Estimating stockpile average bulk density using weightometer records and stockpile volume survey, and
3. The bulk density prediction model developed by Standish (1990) based on stockpile height, drop height, size parameters and total moisture.

In the author's view, direct measurement for typical placement scenarios remains the best approach. Approaches 2 and 3 provide average densities with no indication of variation throughout the stockpile. Eckersley (2000) noted that Standish's (1990) model gave a good result for the 1991 experimental stockpile, but that it has limitations, being developed from products exported through Port Kembla and Port Waratah. It is therefore limited to stockpiles formed by stacker discharge with no use of dozers.

Within a coal stockpile dry density is likely to vary with burial by additional coal (as overburden stress increases) and with coal saturation. This is illustrated by the data from Eckersley (2000) presented in Figure 3. Note that this figure is presented in a form that resembles the familiar soil mechanics compression relationship in terms of void ratio. Samples of LA, LB and LD coal with 203 mm diameter and 150 mm initial thickness were prepared in a steel mould at 0.85 t/m^3 and then subjected to increasing vertical stress from 1.2 to 125 kPa, followed by resaturation due to infiltration up from the base of the specimen.

The following are noted:

- For the specimens initially at 0.85 t/m^3 dry density increased by 0.06 to 0.11 t/m^3 due to application of vertical stress approximately equivalent to 12 m of coal in a stockpile, and then by a further 0.03 to 0.04 t/m^3 with wetting to practical saturation.
- Coal initially compacted to around 0.97 t/m^3 (not shown in Figure 3) suffered only 0.01 to 0.03 t/m^3 density increase with compression, with little additional volume decrease during saturation.
- The much coarser product LC (not plotted in Figure 3) suffered much smaller loss of volume during compression compared with the products with substantial fines content (LA, LB and LD) at comparable initial dry densities.
- This data demonstrates the potential variability of in-situ density for stockpiled coal, both within an individual stockpile, and for different operational scenarios. Additional data on loss of volume due to saturation of coking coal was reported by Eckersley (1986). Coal with significant fines is also sensitive to mechanical compaction by vibration, dozer tracks and rollers.
- The strength data presented in Sections 4 and 5 illustrates the critical significance of in-situ density in performing realistic coal stockpile stability analyses.

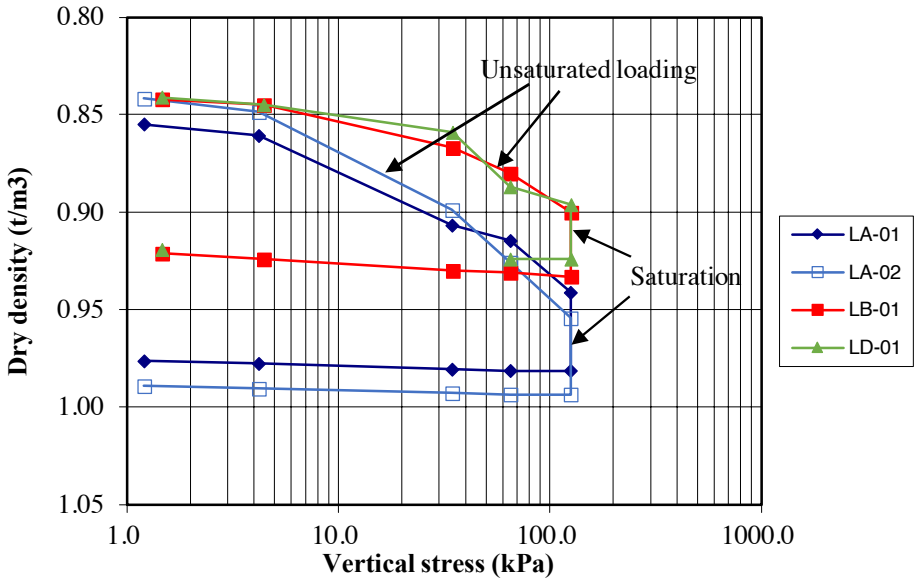

Figure 3: Volume reduction during compression and saturation (from Eckersley, 2000)

4 SHEAR STRENGTH – SATURATED COAL

4.1 TEST PROCEDURES

As noted in Section 2 and the ACARP report (Eckersley, 2000) conventional strain-controlled isotropically consolidated undrained (CIU) triaxial tests were performed on three coking coal products with a history of instability (LA, LB and LD in Figure 2) and one with no history of slipping (LC). Test specimens were nominally 102 mm in diameter and 203 mm high, prepared at moisture contents typical for that product and at a range of dry densities (typically 0.85 t/m^3 to 1.05 t/m^3). Coal forming the specimens was tamped in 25 mm layers to achieve the target density, confined at a low all-round pressure, saturated initially using infiltration from a Mariotte bottle system and then using back pressures to achieve near-saturation (Skempton's parameter B≥0.95), and finally consolidated to the desired effective stress before shearing under undrained conditions. Particles larger than 19 mm size were excluded.

Careful test procedures were found important to improve consistency of the results and those used were outlined in Appendix C of Eckersley (2000). Relevant comments include:

1. Volume reductions of more than 2% were found to occur with initial dry densities less than 0.9 to 0.95 t/m^3 as suctions in the coal were removed by wetting (as foreshadowed in Section 3). Testing at lower dry densities was therefore generally avoided in the later work (Eckersley, 1986).
2. To reduce uncertainty in estimating specimen dry density at the start of shearing, initial volume was assessed by calibrating volume of the triaxial cell and measuring the volume required to fill it to an index mark with the test specimen in place. This was checked by drying the complete specimen after testing and estimating volumes using specific gravity of the coal particles.
3. Multi-stage shearing as is often used in geotechnical consulting practice was not used, since to attempt achieving steady state shear (or critical state conditions) was considered important and especially for specimens where strain-softening occurs.

4.2 TYPICAL RESULTS

Typical results for saturated coal are illustrated in Figure 4 (plots of deviator stress and excess pore water pressure) and Figure 5 (effective stress paths). These results are from 3 tests on LB coal with compaction dry densities of 0.9 t/m^3, 0.95 t/m^3 and 1.0 t/m^3 and at effective consolidation pressure of approximately 75kPa.

The following are noted:

1. For tests LB900_03 and LB950_04 (compaction dry densities of 0.9 t/m^3 and 0.95 t/m^3) peak deviator stress was reached at approximately 2.5 mm axial deformation (1.2% axial strain), with excess pore water pressure then continuing to increase and deviator stress decreasing substantially.

2. For LB1000_05 (1.0 t/m^3) the excess pore water pressure decreased sharply after an early peak, with deviator stress continuing to increase until axial strains of around 10%.
3. Response to shearing for the 3 tests may therefore be described as contractant (F = flow or liquefaction), weakly contractant (LF = limited flow) and dilatant (NF = non-flow) respectively.
4. For the loosest case tested, mobilized effective friction angle at peak deviator stress was approximately $\phi' = 29^o$ while effective friction angle for the tests at steady state shear (critical state) was $\phi' = 38^o$ (see Figure 5).
5. For test LB1000_05 effective friction angle at peak effective stress ratio was approximately $\phi' = 41^o$.

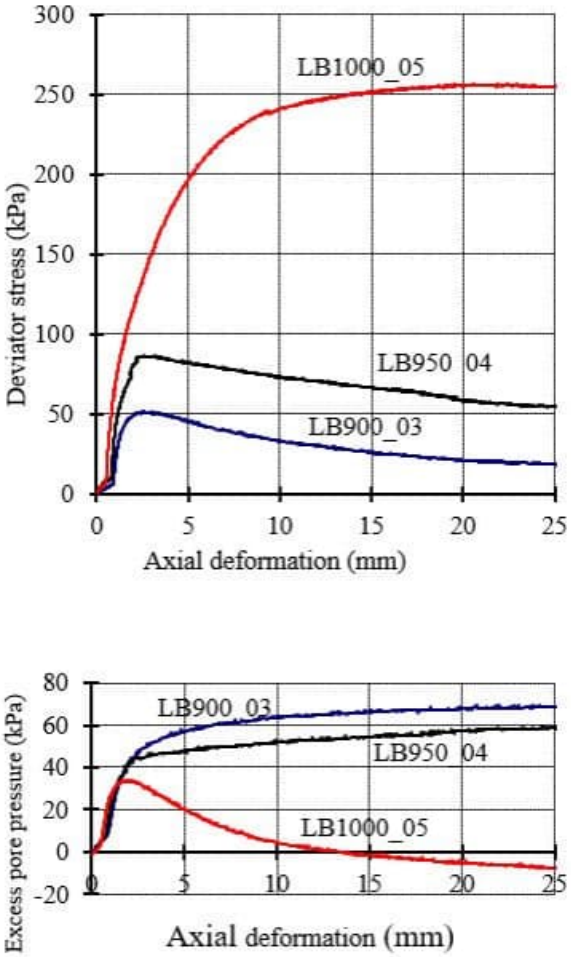

Figure 4: Deviator stress (top) and excess pore pressure (bottom) – CIU triaxial tests on LB coal (from Eckersley, 2000)

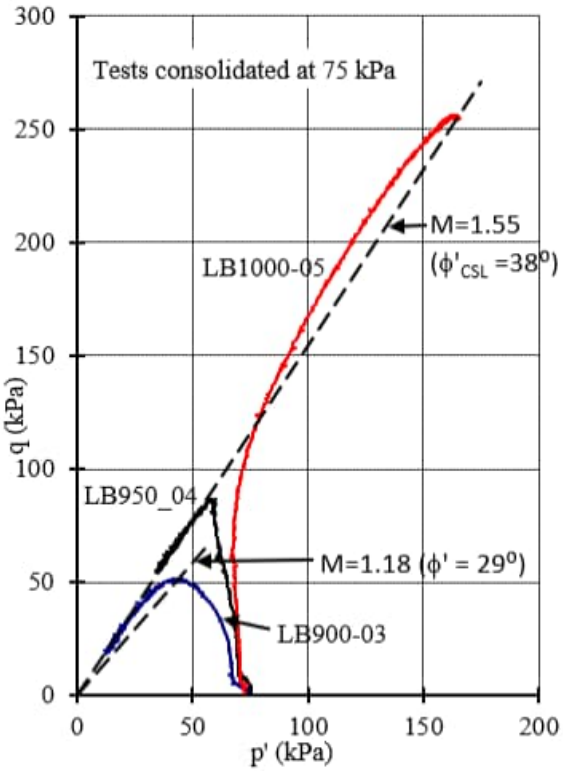

Figure 5: Effective stress paths – CIU triaxial tests on LB coal (from Eckersley, 2000)

A state diagram summarizing responses for 7 CIU triaxial tests on LB coal in terms of dry density and average effective stress (octahedral normal effective stress p') is presented in Figure 6. Contractant responses are labelled C, weakly contractant as WC and dilatant as D. For three tests consolidation prior to shearing is also shown. Note that dry density is shown increasing downwards, analogous to void ratio increasing upwards (as usually shown in geotechnical literature). The critical state line (CSL) divides contractant responses (tendency for volume reduction or liquefaction) from dilatant responses (tendency for volume increase). Note that while critical state lines are usually defined in terms of void ratio, within the coal stockpile context definition using dry density provides a practical alternative that makes use of the critical state framework. This definition of critical state line is used throughout the paper.

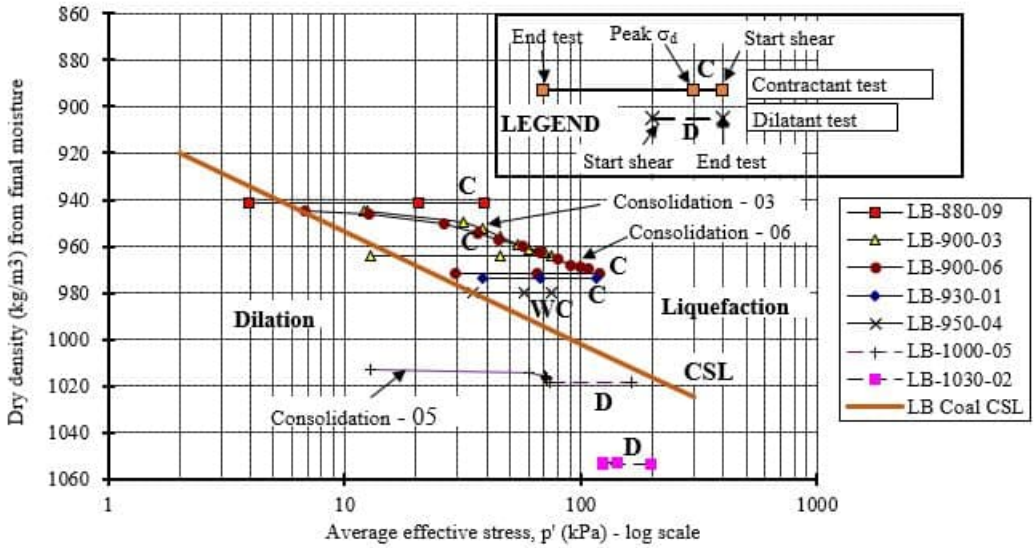

Figure 6: Dry density – effective stress state diagram - LB coal (data from Eckersley, 2000)

Further discussion is provided by Eckersley (1986, 2000). A similar pattern has been observed from testing on other coking coal products, and critical state lines for the four products with results in the ACARP Report are shown in Figure 7. Also shown for the three products with sufficient fines for liquefaction (LA, LB and LD) are a combined CSL and approximate limits of the data.

4.3 EFFECTIVE FRICTION ANGLE

Results from 33 saturated CIU triaxial tests on the four coal types tested (LA, LB, LC, LD) are summarized in Figure 8 as effective angle of shearing resistance ϕ' (assuming $c' = 0$) for varying dry density after saturation and consolidation. For contractant and weakly contractant specimens (eg. LB900_03 and LB950_04 in Figures 4 and 5), failure was defined as the point of peak deviator stress. Peak effective stress ratio was used to define failure for dilatant specimens. The same data is presented in the ACARP report (Eckersley, 2000, Figure 5.21) in terms of nominal dry density at specimen compaction (before saturation and consolidation). That plot may be more useful than Figure 8, depending on what is known about a particular stockpile.

Consistent with usual geotechnical practice for granular soils, shear strength parameters for coking coal have been expressed here in terms of ϕ' (with $c' = 0$). A useful outcome is that (apparent) cohesion values then represent the impact of suctions in unsaturated conditions. However, it is noted that effective strength is controlled by both effective stress and density (or void ratio). The data presented here is for effective consolidation pressures up to approximately 120 kPa. Been and Jefferies (1985) proposed correlating ϕ' with a state parameter (change in void ratio from initial condition to steady state at constant effective stress). Since density in a stockpile is often not known with much precision and given the scatter of laboratory data in the state diagrams, a more simplistic approach is to plot strength as a function of density only as in Figure 8.

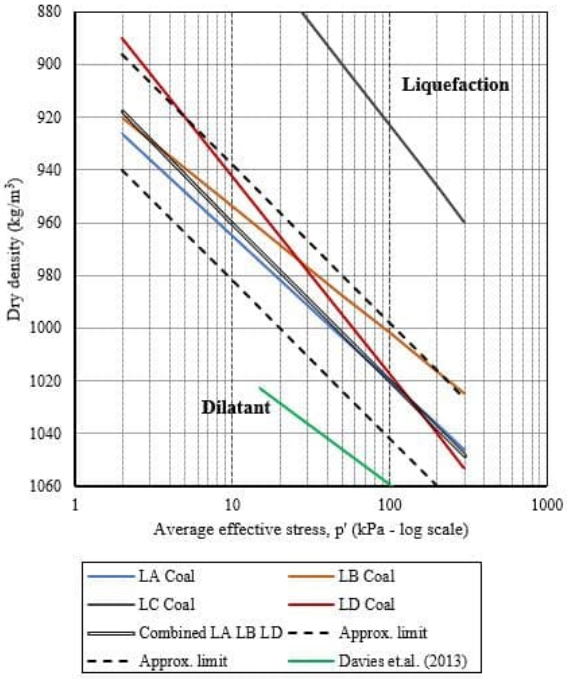

Figure 7: Summary effective stress – dry density state diagram

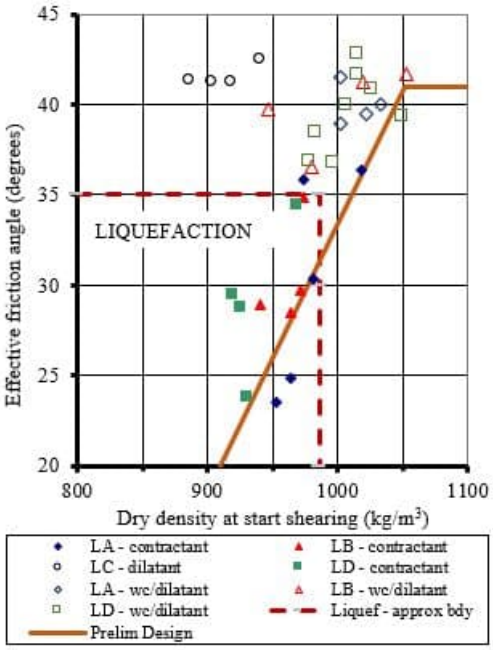

Figure 8: Effective friction angle vs. density at start of shearing for coking coal (data from Eckersley, 2000)

The following are noted:

- For the products with a history of instability (LA, LB, LD) ϕ' increases with dry density. The lower the dry density, the lower the effective friction angle at initiation of undrained failure.
- Effective friction angles of $\phi'<35^o$ and dry density less than 0.98 t/m^3 generally correspond to a contractant (F) response. Effective friction angles of $\phi'>37^o$ and dry density greater than or equal to 1 t/m^3 (1000 kg/m^3) generally correspond to a weakly contractant (LF) or dilatant (NF) response.
- For the contractant specimens peak deviator stress generally occurred at axial strains of around 1.2%.
- A preliminary design line is plotted for the three products that have sufficient fines to be susceptible to liquefaction (LA, LB, LD).
- For the product without significant fines (LC) the coal could not be placed sufficiently loose to result in a contractant response, and ϕ' values are around 41^o.

A disadvantage of relating ϕ' to dry density only is that there is significant scatter in Figure 8. This probably results from uncertainty in dry density (despite the careful procedures), variability in the product gradings as well as varying effective stress at the start of shearing. Unfortunately, the deviation of individual test points from the CSL assessed for each product is significant (eg. see Figure 6). To reduce these impacts and better illustrate the variation in ϕ' with increased dry density at constant effective stress, the results for LA, LB and LD coal have been replotted in terms of a "density state parameter" $\Delta\rho_d$. Definition of the density state parameter for one CIU test on LB coal is illustrated in Figure 9. In the coal stockpile context this is a practical alternative to the usual definition of state parameter as change in void ratio at constant p'. A line from the p'-dry density point at the end of the test (approximating the steady state for contractant specimens) was drawn parallel to the CSL assessed from tests on LB coal. The density state parameter was then defined as the change in dry density along a constant p' line from the start of shearing to its intersection with the line parallel to the CSL.

Results are shown in Figure 10. Density state parameters of 0 to 80 kg/m^3 (0 to 0.08 t/m^3) represent contractant conditions, while negative values represent initial conditions below the critical state line (dilatant). The results further illustrate that effective strength and response to shearing for stockpiled coal can change dramatically with relatively subtle changes in dry density.

Davies et al. (2013) report results from multi-stage consolidated undrained triaxial tests on saturated hard coking coal from a NSW colliery with d_{10} of 0.03 to 0.04 mm. Test specimens were prepared at dry densities of 0.9, 0.96 and 1.01 t/m^3. Their results are somewhat similar to the author's but since they are reported in terms of c' and ϕ' values from the multi-stage tests, they are not able to be directly compared with the data in Figure 8. They would also need to be used with care since at low effective stresses (close to the slope surface) the c' values may unrealistically imply reduced chance of shallow failures.

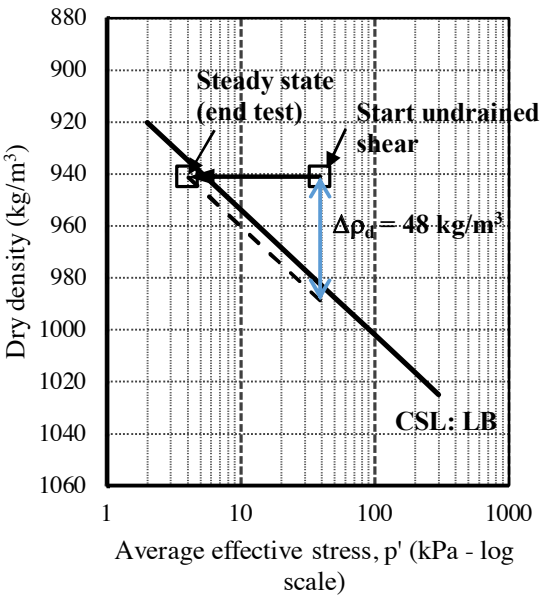

Figure 9: Density state parameter for test LB880_09 (data from Eckersley, 2000)

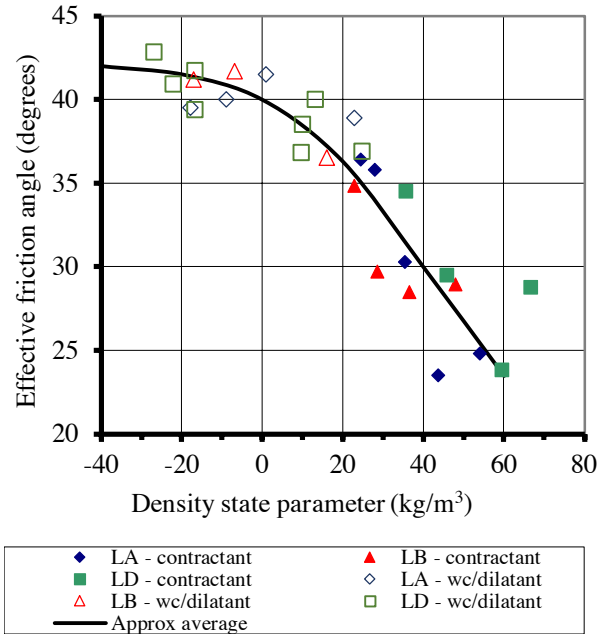

Figure 10: Effective friction angle vs. density state parameter (data from Eckersley, 2000)

Conditions within a coal stockpile involve anisotropic consolidation and (generally) drained conditions up to failure initiation. These are not replicated by undrained shearing in a CIU triaxial test. This scenario led the author and some former students to experiment with dead load (stress-controlled) testing similar to that used by Castro (1969). Limited data presented by the author and others (Eckersley, 1986; Castro, 1969) suggested that effective friction angle at peak deviator stress from CIU tests provides a reasonable first assessment of strength at initiation of failure in flowslides. Eckersley (2000) reported dead load tests in which coal specimens were saturated and isotropically consolidated, deviator stress applied using a dead load, and then brought to failure by increasing pore water pressure in stages. For loose coal specimens sudden dramatic collapse initiated at similar ϕ' values (28º to 36º) as for the conventional strain-controlled tests at comparable dry densities (Eckersley, 2000). However, a particular advantage of the stress-controlled tests was in illustrating in a laboratory test the dramatic consequences of liquefaction.

4.4 DENSITY - EFFECTIVE STRESS CONDITIONS FOR LIQUEFACTION

As noted in Section 4.2 a state diagram summarizing responses for the four coking coal products tested in terms of dry density and average effective stress is presented in Figure 7. The following are noted:

- Critical state lines (CSL) for the 3 liquefaction susceptible coals (LA, LB, LD) are similar with a dry density variation of up to ±0.03 t/m^3 (30 kg/m^3) for average effective stresses from 5 kPa to 200 kPa.
- CSL for the coarser LC product corresponds to much lower dry densities (or higher void ratios) for the same effective stress.

Given the uncertainties, for products with significant fines it is suggested that the combined CSL is used as a basis for first assessment of likelihood of liquefaction in response to shear in saturated coal. For example, for coal with d_{10}<0.35 mm within the saturated base of a stockpile with average effective stress of 100 kPa and in-situ dry density of 0.96 t/m^3, liquefaction would be likely if sliding initiates. More coarsely graded coal (such as LC) would be dilatant at the same dry density and average effective stress.

The critical state line reported by Davies et al. (2013) is also shown in Figure 7. It is located at dry densities 0.04 to 0.06 t/m^3 higher than the combined CSL from the author's tests on coal with significant fines shown in Figure 7. As noted above this was from multi-stage consolidated undrained triaxial tests.

5 SHEAR STRENGTH – UNSATURATED COAL

5.1 BACKGROUND

Except for shallow slips in response to heavy rain, the bulk of coal involved in stockpile slumps is partly saturated, probably with moisture content slightly less than at the time of stockpile construction. This section provides a brief review of how the contribution of suction may be quantified in stability analyses of coal stockpiles, prior to outlining the data available. As noted in Section 2, while coal is composed primarily of organic solids and therefore may be subject to some effects of its surface chemistry, as a first approximation it has been assumed to behave similarly to inorganic granular soil materials.

Effective stress σ' in partly saturated soil (Bishop, 1959) is usually expressed as follows:

$$\sigma' = \sigma - u_a + X(u_a - u_w) \quad (1)$$

where σ is the normal total stress, u_w is the pore water pressure, u_a is the pore air pressure and $\Psi = (u_a - u_w)$ is the matric suction pressure. X is an effective stress parameter that conceptually relates to the proportion of the shear surface area composed of water menisci over which the suction acts, and so is linked to degree of saturation. Values range from 0 (completely dry) to 1 (fully saturated).

The shear stress at failure may then be expressed as:

$$\tau_f = c' + (\sigma - u_a + X\Psi)\ tan\phi' \quad (2)$$

For cohesionless (granular) materials, $c' = 0$, and if pressures are expressed as gauge pressure so air pressure $u_a = 0$ and is assumed to be zero throughout the soil mass:

$$\tau_f = \sigma\ tan\ \phi' + X\Psi\ tan\ \phi' \quad (3)$$

$X\Psi\ tan\ \phi'$ is the "apparent cohesion" c_a which is lost by saturation of the soil. This approach was pioneered by Bishop and propounded more recently by Khalili (2018) and others.

Fredlund and Morgenstern (1977) considered $(u_a - u_w)$ as a separate state variable (also see Fredlund et al., 2012), so for granular materials, if the relationship between suction and the increase in shear strength due to suction is assumed to be linear:

$$\tau_f = \sigma\ tan\ \phi' + \Psi\ tan\ \phi_b \quad (4)$$

It is clear from equations (3) and (4) that X and $tan\ \phi_b$ are related as follows:

$$X = tan\ \phi_b\ /\ tan\ \phi' \quad (5)$$

In assessing X some authors suggest assuming that X is equal to the degree of saturation (Khalili, 2018). The similar approach of Vanapalli et al. (1996) is:

$$X = \frac{\theta - \theta_{res}}{\theta_s - \theta_{res}} \quad (6)$$

where: θ = volumetric water content

θ_{res} = residual volumetric water content below which the suction contribution to strength becomes zero

θ_s = saturated volumetric water content

While this expression has the same form as that for effective degree of resaturation S_e used in the Laliberte Corey and Brookes (1966) and the van Genuchten (1980) unsaturated moisture characteristics discussed in Eckersley (2022), the residual water content is not necessarily the same.

Khalili and Khabbaz (1998) (see also Khalili, 2018) propose using the following relationship based on the moisture suction ratio:

$$X = \frac{\psi}{PB}^{-0.55} \leq 1 \quad (7)$$

where: ψ = suction head

PB = suction head close to resaturation or desaturation (ie. approximately the air entry value)

Note that rather than the symbols used by Khalili (2018), those used here are consistent with symbols used by Eckersley (2022) and are expressed as suction heads rather than pressure.

This then leads to the following options for including the contribution of suctions to stability analyses of coal stockpiles:

1. An apparent cohesion c_a could be specified for the unsaturated coal. This would require an assessment of c_a to be made for the appropriate range of moisture suctions (or moisture contents) and density conditions throughout the relevant part of the stockpile. The complication is that while apparent cohesion will be approximately constant for a day or so after placement of fresh coal product, it will then vary throughout the unsaturated zone and with time as moisture redistributes.
2. Strength can be calculated within the slope software according to the estimated moisture suction using either Bishop's X parameter (with ϕ') or Fredlund's $tan\ \phi_b$.

Following Fredlund and others, GEO-SLOPE International (2017) suggest that for practical purposes $\phi_b = \phi'/2$ provides a reasonable estimate. However, for high suctions this may overestimate strength (as ϕ_b reduces), and for degrees of saturation approaching 1 (ie. nearly fully saturated) ϕ_b approaches ϕ'. Since in coal stockpiles the degree of saturation varies widely (S = 0.3 to 1 in the 1991 stockpile experiment described in Eckersley, 2022) the likelihood of substantially over- or under-estimating apparent cohesion seems high. For an otherwise cohesionless material this could have significant impact on calculated factor of safety.

In the case of either option above, effective friction angle ϕ' is required. Khalili (2018) indicated that ϕ' at critical state is unique and therefore the same for saturated and unsaturated conditions. He also noted that while ϕ'_{peak} may vary slightly with suction, for all practical purposes it may be taken as equal to that for saturated soils. This suggests that ϕ' does not need to be separately assessed for the unsaturated coal.

However, ϕ'_{peak} can occur at very different strains and be very different from drained and undrained tests on saturated coal. As discussed in Section 4 peak deviator stress for loose (contractant) saturated coal is typically observed at relatively small strains in CIU triaxial tests. Since the voids are much more compressible, the response of unsaturated coal to shear is generally more like that of saturated coal in drained shear. As noted in Section 5.3 below, for loose unsaturated coal in drained shear, peak deviator stress generally occurs at much greater strains than for loose saturated coal subject to undrained shear. There is therefore a question as to how ϕ' should be assessed for unsaturated coal forming the bulk of a coal stockpile if loose coal at the base is saturated with potential for liquefaction to initiate and provoke overall slipping of the stockpile.

This requires further discussion and is investigated in a limited way in a companion paper (Eckersley, 2023).

5.2 DATA FOR UNSATURATED COAL

To the author's knowledge published data for shear strength of partly saturated coking coal is limited. Two single stage tests on unsaturated LB coal at approximately 15.6% moisture content were performed as part of work for the ACARP Report (Eckersley, 2000). Davies et al. (2013) presented results from 6 unsaturated unconsolidated undrained multi-stage tests on coking coal from a colliery in NSW. As-compacted dry densities were in the range 0.9 to 1.02 t/m^3 with 6% or 12% water content. Total stress parameters of c = 0 to 27 kPa and ϕ' = 23º to 35º were reported. Unfortunately, since the parameters are from multistage tests and subject to some variability that is inconsistent with the initial density, more general applicability of the results seems limited. Since the tests were unconsolidated and undrained it also seems possible that the parameters are influenced by pore air pressures.

Prior to publication of the ACARP Report, the author hoped to assess total stress parameters for unsaturated coal over a range of stress, initial dry density and moisture content relevant to coal stockpiles at typical operations. In the absence of data for unsaturated coal from sources other than those mentioned above and in spite of potential limitations of the author's data, a summary is presented in Section 5.3 below.

However, the data from that work cannot provide a basis for assessing validity of the effective stress approaches based on predictions of suction (discussed in Section 5.1) since there were no independent assessments of effective friction angle or suction. In the absence of better data, Sections 5.4 and 5.5 present a preliminary assessment of the effective stress parameter X based on results from Jenike Cell testing used for design of bulk solids handling equipment.

5.3 TRIAXIAL TESTS ON UNSATURATED COAL

In 1994 Chris Lonergan, then an undergraduate student at James Cook University, performed triaxial tests on coking coal from BMA Coal's Goonyella Mine (Lonergan, 1994). The tests were nominally isotropically consolidated drained at axial deformation rates of 1 mm/minute (approximately 0.5% axial strain per minute). Twenty-four tests were performed at confining pressures of 30 kPa, 60 kPa and 100 kPa, moisture contents of 8%, 10% and 15%, and dry densities of 825 kg/m^3, 900 kg/m^3 and 975 kg/m^3 (Lonergan, 1994).

Results are summarised in Figure 11 (as s, t values at failure – defined as peak deviator stress). Results for the two tests on unsaturated LB coal mentioned in Section 5.2 and performed as part of work for the ACARP Report (Eckersley, 2000) are also included. Both LB and Goonyella coking coal have some history of stockpile flowslides and have d_{10} < 0.35 mm. A line corresponding to c=0 and $\phi = 40^0$ is also shown to provide some comparison. Data points are annotated with water contents to improve usefulness of the data.

Peak deviator stress in Lonergan's tests generally occurred at axial strains corresponding to the end of the test (6% to 11%) for low initial dry densities (825, 900 kg/m^3). For the tests at 975 kg/m^3 and 60 kPa or 100 kPa confining pressure peak deviator stress was at 0.5% to 2.5% axial strain. These results generally show increasing strength with increasing initial dry density and decreasing strength with increasing initial moisture content except when degree of saturation was 65% or greater (tests at 975 kg/m^3). Unfortunately, since this testing was performed with increasing axial deformation, normal stresses at failure were in the range 50 kPa to 180 kPa and so are generally higher than those in the unsaturated part of potential stockpile slip surfaces. This means that for slip surfaces less than approximately 5 m deep, strength is likely to be over-estimated. Also unfortunately, the drainage valve was not opened until the start of shearing and so volume reductions due to consolidation took place during the early part of shearing. Consolidation appeared to occur very quickly but may influence results at small strains.

The influence of moisture suctions cannot be distinguished in the data from the impact of contractant / dilatant behaviour since there were no independent assessments of effective strength parameters and measurement of suction. Appropriateness of the unsaturated strength models discussed in Section 5.1 and implemented in slope stability software therefore cannot be assessed using Lonergan's data.

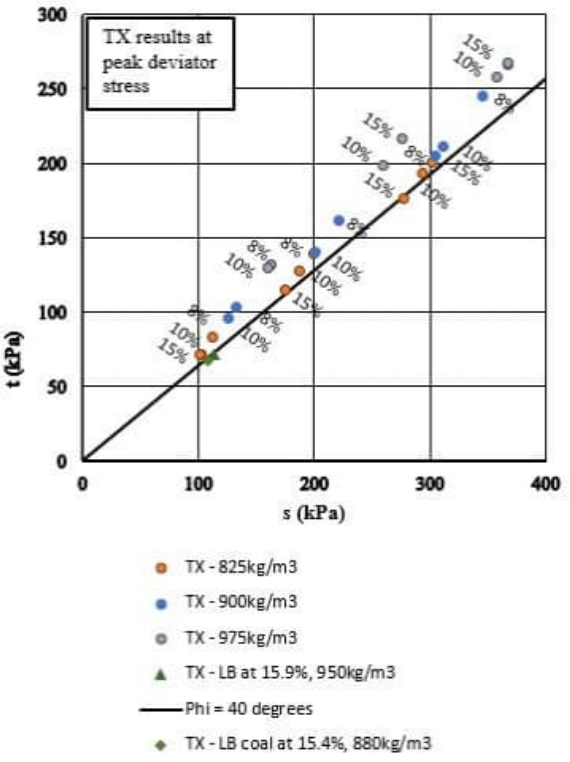

Figure 11 Triaxial test results – unsaturated coal – results at peak deviator stress (from Lonergan, 1994)

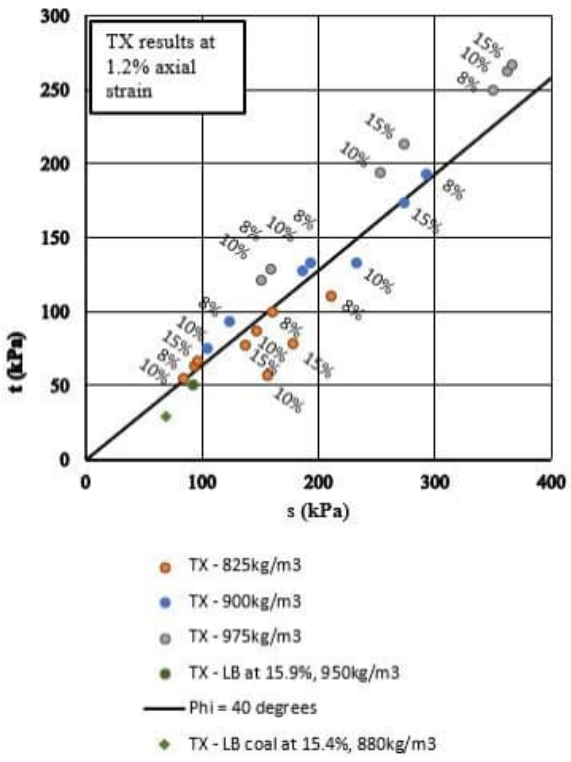

Figure 12 Triaxial test results – unsaturated coal – results at 1.2% axial strain (from Lonergan, 1994)

A question raised in Section 5.1 is whether the strength at peak deviator stress for unsaturated coal is appropriate to be used in stability analyses when it overlies loose saturated (potentially liquefiable) coal. A definitive answer cannot be provided here, but to illustrate the potential significance of the question, s and t values mobilized at axial strains of approximately 1.2% from Lonergan's tests are summarized in Figure 12. As might be implied from the description above, results at 1.2% strain are significantly less for tests at 825 and 900 kg/m^3 than in Figure 11, and especially at confining pressures of 100 kPa.

Inferred total stress angles of shearing resistance (assuming c = 0) for low density and 1.2% axial strain were in the range $\phi = 20^o$ to $\phi = 40^o$, similar to effective stress ϕ' values in Figure 8 for saturated coal that is susceptible to liquefaction. At peak deviator stress (Figure 11) values are clearly $\geq 40^o$.

5.4 JENIKE CELL TESTS ON UNSATURATED COAL

Potentially relevant data for unsaturated coal may also be derived from Jenike Cell tests, which are a form of direct shear testing not normally considered by geotechnical engineers. Jenike Cell testing is commonly performed as part of bulk solids handling investigations to provide material data for the design of bins and hoppers. As performed on coal, procedures are described in AS3880:2017 (Standards Australia, 2017), and testing is performed on unsaturated coal since this is typical for product handled by reclaim and conveyor systems. Results are interpreted in a format suited to the bulk solids handling design process.

In Jenike Cell tests remoulded specimens are first "preconsolidated" by applying a normal load and 10 to 20 twisting cycles (torsional shearing through ±45º) to bring them close to steady state shear (referred to as "critical consolidation"). Successful attainment of "critical consolidation" is indicated by shear stress increasing to a steady value within approximately half of the maximum shear displacement permitted for the test (less than 4 mm of the maximum 6 mm travel in AS3880). To obtain an instantaneous yield locus for a single consolidation stress, at least 4 additional tests are then performed on fresh specimens prepared using the same preconsolidation (normal loading and twisting) and preshearing process at the consolidation stress, with normal stress then being reduced before further shearing. In geotechnical terms this means that specimens have been prepared to critical state and then overconsolidated by reducing normal stress before additional shearing.

For coal, Jenike test specimens have 63.5 mm or 95 mm diameter (depending on normal stress required), thickness 41 mm before loading and twisting, and are prepared using the -4 mm (ie. <4 mm) size fraction (see AS3880:2017). Compared with direct shear tests used in geotechnical practice, vertical deformation is not measured and specimen density is not assessed. However, separately from Jenike Cell shearing, the relationship of bulk density to consolidation stress is measured by applying normal stress and twisting cycles to test specimens with 63.5 mm diameter and 19 mm initial thickness.

Jenike Cell tests on coking coal therefore provide a source of direct shear test data on unsaturated coal, with results from the preconsolidation and preshearing process approximating the critical state. For the current purpose, only these results (for shearing at the consolidation stress) are considered and overconsolidated specimens with their resulting dilatancy are excluded. Because of the focus on designing bins and hoppers to permit free flow of material, testing is generally performed at a moisture content that results in greatest cohesiveness.

Results from two series of Jenike Cell tests performed at the University of Newcastle by TUNRA Bulk Solids Handling Research Associates in 2020 have been made available to the author (TUNRA, 2020). These were performed on coking coal from the same operation as LE coal in the ACARP Report (Eckersley, 2000) and on reprocessed tailings from the same source. The tailings date from an earlier period at the mine when ultrafines (probably <0.5 mm) were not recovered but simply rejected as tailings. Brief details of these products as tested are as follows:

Product	Description	Moisture Content	d_{10}	d_{50}
LE	Coking coal	14.3% (12.5%TM)	0.2 mm	1.5 mm
LE tailings	Reprocessed tailings	15.5% (13.5%TM)	0.14 mm	0.4 mm

Results in terms of normal and shear stress from specified consolidation points (approximating shear at critical state) for the LE product are plotted in Figure 13. The line labelled as "Best fit phi'" has been drawn from the origin (c = 0) parallel to the best fit line through the critical consolidation points.

Points defining the yield locus for tests consolidated to 39 kPa and then sheared at reduced normal stress are also shown as an example. These show the impact of increased dilatancy with overconsolidation. Such parameters might be relevant where a new stockpile face has been formed by excavation into an existing stockpile.

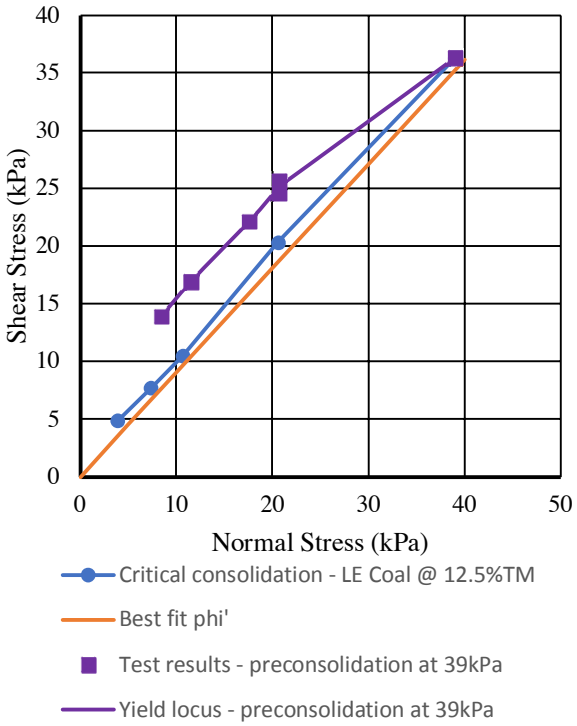

Figure 13: Results – Jenike Cell tests on unsaturated LE coal (data from TUNRA, 2020)

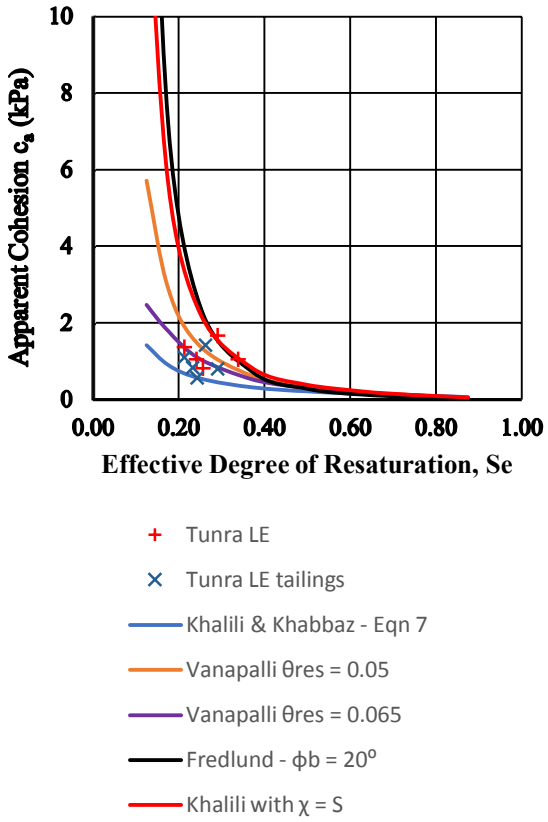

Figure 14: Suction contribution to strength of unsaturated coking coal

5.5 SUCTION COMPONENT OF STRENGTH

In the absence of better data, results from the Jenike Cell tests presented in Section 5.4 have been used to make a preliminary assessment of the contribution to shear strength from suctions in coking coal. The advantage of the Jenike Cell data is that the shear and normal stresses at critical consolidation (blue points in Figure 13) approximate shearing at the critical state and so an assessment of ϕ'_{CSL} can be made. A disadvantage is that density for the shear tests was not measured directly and so was assessed from the separate bulk density – consolidation stress testing.

Based on the literature reviewed in Section 5.1, the contribution of suction to shear strength of unsaturated coal is anticipated to be a function of matric suction Ψ and the parameter X. Since both are related to degree of saturation and no measurement of suction has been made as part of the Jenike Cell testing the following approach has been used:

1. For the Jenike Cell critical consolidation points, ϕ'_{CSL} for shearing at critical state was assessed from slope of the best fit line from each coal product (ϕ'_{CSL} = 42º for LE and 37º for reprocessed LE tailings).
2. The strength increment due to suction (apparent cohesion) was then assessed as the shear stress at failure minus $\sigma \tan \phi'_{CSL}$ for each data point.
3. The apparent cohesion was then plotted against effective degree of resaturation S_e defined as in Equation (8) with θ_{res} = 0.05 consistent with Eckersley (2022). S_e for the test moisture content was assessed from results of bulk density – consolidation stress testing in the Jenike cell as noted in Section 5.4. Consistent with Eckersley (2022), θ_s was assessed including 5% entrapped air voids.

$$S_e = \frac{\theta - \theta_{res}}{\theta_s - \theta_{res}} \quad (8)$$

The results are plotted in Figure 14. Apparent cohesion values assessed are in the approximate range 0.6 to 1.7 kPa for effective degrees of resaturation in the range 0.2 to 0.35.

To make better sense of the data in Figure 14 the expressions outlined in Section 5.1 have been used to estimate the apparent cohesion for unsaturated coal over a range of effective degrees of resaturation S_e and these are also plotted in Figure 14. Unsaturated moisture parameters for LA coal at a dry density of approximately 0.97 t/m^3 (see Eckersley,

2022) have been used to estimate the suction for a given degree of resaturation. The unsaturated effective stress parameter X has been estimated using four different options: degree of saturation S (as per Khalili, 2018), Equation 7 (Khalili and Khabbaz, 1998), Equation 6 (Vanapalli et al. 1996) using residual volumetric water content (below which the suction component of strength becomes zero) θ_{res} = 0.05 or 0.065, and Fredlund's ϕ_b approach (assuming $\phi_b = \phi'/2$). For estimating apparent cohesion from X and for Fredlund's approach, effective friction angle ϕ'=40º was assumed as appropriate for LA coal at the critical state.

It is acknowledged that Figure 14 compares experimental apparent cohesions for LE coal and LE tailings with estimated apparent cohesion for LA coal. However, all are for shearing at the critical state (so effective friction angles are not greatly different) and d_{10} values are similar. It is also noted that the background presented in Section 5.1 implies that X does not depend on ϕ'.

The following are noted:

1. Apparent cohesion implied from Jenike Cell data plots between the Fredlund (with ϕ' = 40º) and Khalili and Khabbaz predictions.
2. Since using 0.05 for the residual water content (consistent with the unsaturated moisture characteristics derived by Eckersley, 2022) tended to overestimate the strength increase for S_e in the range 0.2 to 0.35, the value was varied with 0.065 providing a better fit.
3. The apparent cohesion values assessed are much less than the total stress cohesion values that would be inferred from Lonergan's triaxial data in Figure 11.

It seems obvious that better data is required to reasonably describe the shear strength of unsaturated coal, but until this becomes available it is suggested that the Vanapalli et al. (1996) relationship is used with θ_{res} = 0.065. It is also worth noting that while friction angle at critical state shear applies for the Jenike tests discussed above, it may not be appropriate within the unsaturated bulk of coal stockpiles. This was foreshadowed in Section 5.1.

6 ADDITIONAL COMMENTS ON SELECTION OF STRENGTH PARAMETERS

Sections 4 and 5 provide a summary of currently available product coking coal shear strength data to facilitate stability analyses of stockpiles, and to provide opportunity for critical assessment of strength data from new testing. It should be obvious that reasonable knowledge of in-situ dry density throughout the stockpile being considered is critical for stability analysis outputs to be representative of reality. Despite flowslides in coal stockpiles being an ongoing hazard for the past 50 years, this remains the single greatest uncertainty in quantitative assessment of the potential for coal stockpile instability, and therefore limits ability to use data such as that in Figures 8, 10 and 11 to assess strength parameters for stockpiled coking coal.

The following significant questions are also worth noting:

1. Are effective strength parameters at peak deviator stress from CIU triaxial tests on loose saturated coal realistic for conditions where liquefaction initiates in a stockpile since the undrained shearing in the test does not replicate field conditions? (This was foreshadowed in Section 4.4).
2. Is the assessment of apparent cohesion in unsaturated coal outlined in Section 5.5 reasonable?
3. Where a stockpile base contains saturated contractant coal, should effective friction angle for the overlying loose unsaturated coal be assessed at strains similar to those at peak deviator stress in CIU tests on saturated contractant coal (e.g. around 1.2%), or simply represent peak deviator stress for unsaturated tests? (This was foreshadowed in Section 5.1).

Additional discussion and investigation of these issues is presented in a companion paper by Eckersley (2023) in the context of stability analyses of two experimental stockpiles.

7 SUMMARY AND CONCLUSIONS

Eckersley (2022) presented a basis for analysis of transient moisture movements in coal stockpiles with the objective of permitting realistic slope stability analyses for coal stockpiles where the product is prone to flowsliding. The ultimate objective is development of rational stockpile management procedures that simultaneously address the need for appropriately low risk of significant instability and the need for practical and cost-efficient handling of coal products.

The current paper presents a summary of shear strength data for coking coal available to the author to provide a basis for selection of strength parameters for stockpile stability analyses and critical assessment of results from testing of products not previously investigated. It is clear from the data that in-situ density and moisture content of coal stockpiles

need to be considered in assessing appropriate strength parameters. These will be strongly influenced by the processes used in forming the stockpile. It is strongly recommended that direct measurement of in-situ density is made in at least one production stockpile representative of the main stockpile formation practices (see Section 3.1).

Data for strength of saturated coking coal is presented in Section 4, with Figure 8 (or Figure 5.21 in Eckersley, 2000) providing a basis for preliminary selection of effective angle of shearing resistance ϕ' (assuming c'=0) at the initiation of failure, or for checking data from product-specific laboratory testing. Importantly, for loosely placed coal with sufficient fines to render the product prone to liquefaction, ϕ' is likely to be significantly less than the critical state value. Figure 7 provides a basis for preliminary assessment of whether saturated coal has density and effective stress conditions such that liquefaction is likely. If the critical state line (in dry density – effective stress space) is known or can be reasonably estimated, Figure 10 provides an alternative basis for selection of ϕ' within saturated coal at the stockpile base.

Data for strength of unsaturated coal is presented and assessed in Section 5. It is noted that significant additional investigation is required in this area. Data currently available to the author is derived from triaxial testing at James Cook University and from Jenike Cell testing at the University of Newcastle performed as part of bulk solids handling investigations. For unsaturated coal it is tentatively concluded that the strength contribution from suctions may be assessed using the Vanapalli et al. (1996) expression for the unsaturated effective stress parameter X with residual volumetric water content $\theta_{res} = 0.065$.

Significant questions remain with regard to selection of strength parameters for stability analyses, as noted in Section 6. These are discussed in a companion paper (Eckersley, 2023) and subject to preliminary investigation within the context of stability analyses of two experimental stockpiles.

8 ACKNOWLEDGEMENTS

BHP Australia Coal and its predecessor companies provided the opportunity for the research conducted at James Cook University over many years, with substantial financial support and encouragement. The Australian Coal Association Research Program provided specific support and several member companies (including BHP) provided opportunity to investigate their stockpile conditions and test selected products during the period 1995 to 2000. Since that time the author has had opportunity to review and observe stockpile conditions at numerous BHP and Glencore coal operations. The support and encouragement from these organisations and their staff at the times of that work are gratefully acknowledged. Glencore's approval to make use of the Jenike Cell results in Section 4 and TUNRA's provision of the data are gratefully acknowledged.

Chris Lonergan, a former student at James Cook University, performed the previously unpublished testing described in Section 5.3. His work is gratefully acknowledged.

The author's involvement in coal stockpile work would not have commenced without the pioneering work of (the late) Dr Keith Wallace and (the late) Professor Hugh Trollope at James Cook University. In particular, Dr Wallace mentored the author during 1975 to 1986 and provided insightful review comments on the author's work prior to his death in June 2022. I remain most grateful for their contribution. More recently Dr John Simmons has provided helpful input.

The author is grateful for comments by the reviewers of this paper prior to publication.

James Cook University provided the physical context in which this work could take place – mostly from 1975 to 2000, but more recently in providing access to software. Associate Professor Nagaratnam (Siva) Sivakugan assisted greatly in facilitating recent arrangements.

9 REFERENCES

Arnold, B.J. and Aplan, F.F. (1989). "The hydrophobicity of coal macerals." Fuel, Vol.68, Issue 5, May 1989, pp.651-658.

Been, K. (2016). "Characterizing mine tailings for geotechnical design." Australian Geomechanics, Vol.51, No.4, December 2016, pp.59-78.

Been, K. and Jefferies, M.G. (1985). "A state parameter for sands." *Geotechnique*, Vol.35, No.2, pp.99-112.

Bishop, A.W. (1959). The principle of effective stress." *Technish Ukeblad*, 106, pp.859-863.

Castro, G. (1969). "Liquefaction of sands." Ph.D. Thesis. Harvard University.

Davies, P, Zargarbashi, S and McQueen, L 2013, "Flow failure in coal stockpiles – how to reduce risk', in PM Dight (ed.), *Slope Stability 2013: Proceedings of the 2013 International Symposium on Slope Stability in Open Pit Mining and Civil Engineering*, Australian Centre for Geomechanics, Perth, pp. 881-895.

Eckersley, J.D. (1977). "Transient moisture movements in stockpiled granular materials", M.Eng.Sc. Thesis, James Cook University of North Queensland.

Eckersley, J.D. (1985). "Flowslides in stockpiled coal", *Engineering Geology*, Vol.22, pp.13-22. (Originally published in 4th Australia - New Zealand Conference on Geomechanics, Perth, May 1984, Vol.2, pp.607-611.)

Eckersley, J.D. (1986). "The initiation and development of slope failures with particular reference to flowslides", Ph.D. Thesis, James Cook University of North Queensland, Dec. 1986.

Eckersley, J.D. (1990a). "Flowslide hazards in coal stockpiles", *Mechanical Engineering Transactions, I.E.Aust*., Vol. ME 15, No.4, Dec. 1990, pp.302-306. (Originally published in Institution of Engineers, Australia, 1990 International Coal Engineering Conference, Sydney. June 1990, pp.35-39.)

Eckersley, J.D. (1990b). "Instrumented laboratory flowslides", *Geotechnique*, Vol.40, No.3, pp.489-502.

Eckersley, J.D. (1994). "Moisture movement in coal stockpiles - 2: instrumented stockpile experiment". *Australian Coal Journal*, No.44, pp.9-25.

Eckersley, J.D. (1999). "Coal erosion experiments 1995 – 1997". School of Engineering, James Cook University of North Queensland. ACARP Project C4057 Report. Jan 1999.

Eckersley, J.D. (2000). "Moisture Changes & Stability Problems in Coal Stockpiles", ACARP Report C4057, June 2000.

Eckersley, J.D. (2022). "Moisture movement analyses for coal stockpiles". *Australian Geomechanics*. Vol.57, No.3, September 2022, pp.33-48.

Eckersley, J.D. (2023). "Shear strength of stockpiled coking coal – insights from stability analysis of two instrumented stockpiles." *Australian Geomechanics*. Vol.58, No.3, September 2023. (https://doi.org/10.56295/AGJ5832).

Fredlund, D.G. and Morgenstern, N.R. (1977). "Stress state variables for unsaturated soils". *ASCE, Journal of Geotechnical Engineering*, Vol.103, No.GT5, pp.447-466.

Fredlund, D.G.; Rahardjo, H. and Fredlund, M.D. (2012). "*Unsaturated Soil Mechanics in Engineering Practice*". John Wiley & Sons.

GEO-SLOPE International (2017). "Stability modelling with GeoStudio", GEO-SLOPE International Ltd.

Jefferies, M.G. (2019). "Utility of critical state soil mechanics". *Proceedings, 13th Australia New Zealand Conference on Geomechanics* – Acosta-Martinez & Lehane (Eds). Perth, April 2019. Australian Geomechanics Society, pp.51-56.

Khalili, N. (2018). "Guidelines for the application of effective stress principle to shear strength and volume change determination in unsaturated soils." *Australian Geomechanics*, Vol.53, No.1, March 2018, pp.37-47.

Khalili, N. and Khabbaz, M.H. (1998). "A unique relationship for X for the determination of shear strength of unsaturated soils." *Geotechnique*, Vol.48. No.5, pp.681-688.

Laliberte, G.E., Corey, A.T. and Brooks, R.H. (1966). "Properties of unsaturated porous media". Hydrology Paper No. 17, Colorado State University, Fort Collins. November 1966.

Leeder, R., Howey, C., Todoschuk, T., Gransden, J., Giroux, L. and Ng, K.W. (2014). "Coal stockpile moisture and cokemaking". *AISTech - Iron and Steel Technology Conference Proceedings*. 1. 357-365.

Lonergan, C. (1994). "Shear strength testing of unsaturated coal." B.Eng Thesis, Dept. of Civil & Systems Engineering, James Cook University of North Queensland. September 1994.

Standards Australia (2001). "Australian Standard AS1038.1-2001 – Coal and coke – Analysis and testing. Higher rank coal – Total moisture." Standards Australia Ltd, Sydney. 2001.

Standards Australia (2005). "Australian Standard AS1289 - Methods of testing soils for engineering purposes. Method 2.1.1: Soil moisture content tests – Determination of the moisture content of a soil – Oven drying method (standard method)." Standards Australia Ltd, Sydney. 2005.

Standards Australia (2017). "Flow properties of coal. AS 3880:2017." Standards Australia Ltd, Sydney. 2017.

Standish, N. (1990). "The bulk density of Australian export coal." Commonwealth of Australia, National Energy Research, Development & Demonstration Program. End of Grant Report No. 1017, Dec. 1990.

TUNRA (2020). (Confidential) Results from Jenike Cell tests performed at the University of Newcastle by TUNRA Bulk Solids Handling Research Associates, 2020.

Vanapalli, S.K., Fredlund, D. and Pufahl, D.E. (1996). "The relationship between the soil water characteristic curve and the unsaturated shear strength of a compacted silt." ASTM International, Vol.19, No.3, pp.259-268.

van Genuchten, M.Th. (1980). "A closed-form equation for predicting the hydraulic conductivity of unsaturated soils". *Soil Science Society of America Journal*, Vol. 44, pp.892-898.

PROBEDRILL
GEOTECHNICAL SURVEY

The Leaders in Geotechnical Site Investigation

Excavator Platform CPT

CPT mounted to platform suitable for Excavator quick hitch

Ideal for hard to reach test locations

Up to 10t push

Seabed CPT

Pushing Capacity:
150kN (15 tonnes)
2.3m x 2.3m x 2.8m
(L x W x H); 5700kg
Testing Services:
CPTu; SCPTu; Ball CPT;
T-bar; DMT, Piston
Sampling (76mm dia x 3m)

Services:

- Electric Friction Cone Penetration Testing (CPT) including: 15cm (10t); 10cm (10t, 5t, 1t) cones.
- Piezocone (CPTu) and Dissipation testing
- Dilatometer (DMT) testing
- Seismic testing (SCPT & SDMT)
- Electrical Shear Vane Testing
- Dual Tube (Percussive) Soil sampler (50mm x 1000mm)
- Ball and T-bar testing
- Soil Sampling (25mm x 500mm; 35 x 1500mm)
- Water Sampling
- 50m, 32mm & 20mm Standpipe installation
- Vibrating Wire Piezometer installation (Single, Multiple; inverted)

New Services:

- Piston Sampler (60mm x 500mm)
- Multi-level VWP installation
- DGPS test location & Live data streaming
- Electronic Plate Load testing (up to 20 tonnes)

+61 8 9417 9933 · info@probedrill.com.au · www.probedrill.com.au

ECOFINE®

SPECIALISED MICROFINE CEMENTS

EcoFine® is your premier Australian, locally produced and trusted supplier of specialised Microfine Cements.

EcoFine Materials Pty Ltd
Landsdale WA 6065
1300 931 524
sales@ecofine.com.au
www.ecofine.com.au

Made in Western Australia

NATA

AUSTRALIAN MADE AND OWNED

SHEAR STRENGTH OF STOCKPILED COKING COAL – INSIGHTS FROM STABILITY ANALYSIS OF TWO INSTRUMENTED STOCKPILES

John David Eckersley

James Cook University, Townsville, Australia

https://doi.org/10.56295/AGJ5832

ABSTRACT

ACARP Report C4057 (Eckersley, 2000) describes flowslides and other stability issues in stockpiles of coking (metallurgical) coal at Australian coal operations and export terminals, and summarizes 1973 to 2000 research at James Cook University (JCU). Eckersley (2022) partly updated that work with SEEP/W transient seepage modelling of a 12m high coal stockpile constructed at Hay Point in late 1991.

Eckersley (2023) summarized available laboratory strength data for saturated and unsaturated coking coal to assist in selection and critical assessment of parameters for slope stability analyses of coal stockpiles. The current paper explores application of this data to stability analyses of two instrumented experimental stockpiles constructed at Hay Point, one of which collapsed suddenly and completely by flowsliding after extensive wetting. The stability analysis results tentatively confirm that the parameters and approach proposed are reasonable where stockpiles are subject to potential liquefaction-induced collapse.

Significant questions raised by Eckersley (2023) regarding how the coking coal strength data should be applied are considered in the context of the stability analyses. The analyses tentatively confirm that effective strength parameters for saturated coal derived from peak deviator stress in isotropically consolidated, undrained (CIU), strain controlled triaxial tests are reasonable. For loose saturated coal these are at low strains and substantially less than critical state values. However, for unsaturated coal forming the bulk of a stockpile, unsaturated strength and apparent cohesion should be assessed from the effective friction angle at critical state and not the value mobilized at low strains. Use of total stress parameters derived from testing unsaturated coal may over-estimate factor of safety.

1 INTRODUCTION

Flowslides and slope stability issues have been observed within stockpiles of coking (metallurgical) coal at export terminals and at processing plants located at coal mines since the early 1970s in Queensland's Bowen Basin, to a lesser degree in New South Wales (Eckersley, 1985; 1990a; Davies et al., 2013), and in Western Canada (Leeder et al., 2014). Australian Coal Association Research Program (ACARP) report C4057 (Eckersley, 2000) summarises investigations from 1973 to 2000 into coal stockpile moisture and slope stability issues. Metallurgical coal prepared for export typically has particle sizes ranging from silt through sand to gravel, and has relatively low specific gravity (typically 1.33 to 1.38). Its bulk density as stockpiled is therefore relatively low (typically 0.9 to 1.1 t/m^3). Stockpiles can therefore be susceptible to extensive erosion and shallow slipping due to rainfall, and dramatic deep-seated flowslides in loosely placed coal due to moisture redistribution and/or rainfall infiltration. A simplified illustration is presented in Figure 1.

The nature of coal stockpile instability, scale of the problem and circumstances generally contributing to failure are described by Eckersley (1977, 1985, 1986, 1990a, 2000). The liquefaction process fundamental to coal flowslides is discussed by Eckersley (1985, 1986, 1990b and 2000).

Recent work has focussed on making results of the 1973 to 2000 research accessible and in a format that will facilitate realistic stockpile slope stability analyses by geotechnical engineers currently practising in the Australian coal industry.

To facilitate analysis of transient, saturated and unsaturated moisture movements, Eckersley (2022) utilised previous laboratory permeability and column drainage tests to develop moisture characteristics suitable for use in seepage modelling. Reasonable confirmation was reported by way of SEEP/W analyses of moisture redistribution in a 12m high instrumented coal stockpile. Results of these analyses are used in stability analyses later in this paper.

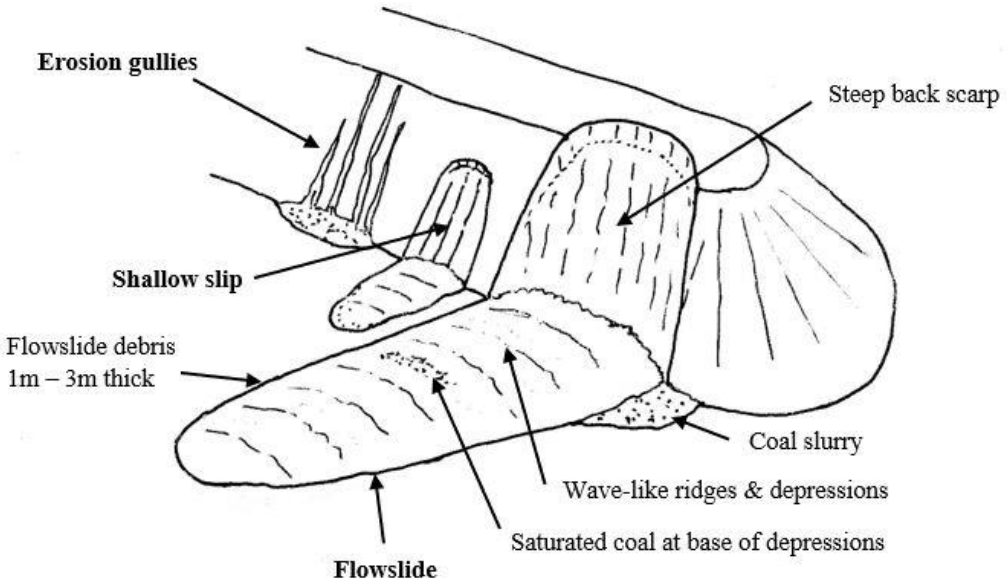

Figure 1: Typical features of coal stockpile instability

To facilitate coal stockpile stability analyses, Eckersley (2023) summarized available data on laboratory shear strength testing of saturated coal (as typical of the base of stockpiles) and unsaturated coal (as typical of the bulk of stockpiled coal above the saturated base). This forms a companion to the current paper. For saturated coal it includes effective strength parameters over the range from contractant to dilatant responses, and effective stress–dry density state diagrams to facilitate assessment of whether stockpiled coal is sufficiently loose to be prone to liquefaction. Strength data for unsaturated coal is mostly limited to total stress results from triaxial tests on a single product at a range of dry densities and water contents. To provide a basis for explicit inclusion of suctions in stability analyses, Eckersley (2023) also made a preliminary assessment of the unsaturated effective stress parameter X based on limited results from Jenike Cell testing.

The purpose of the current paper is to apply the shear strength data in Eckersley (2023) to slope stability analysis of two instrumented experimental coal stockpiles constructed at Hay Point in 1974 and 1991. Both cases included conventional geotechnical testing of in-situ density and moisture content, either during construction or during reclamation. Both included measurement of pore water pressures above the stockpile subgrade. Both were constructed from coal products with a history of instability and flowslides, and d_{10} values less than 0.35 mm. Following extensive wetting, the 1974 stockpile collapsed dramatically and completely by flowsliding. The 1991 stockpile remained stable apart from surface erosion and shallow slipping. The stability analyses are presented in Section 3 for the 1974 stockpile, and Section 4 for the 1991 experiment.

However, even where in-situ dry density is reasonably well known, in assessing strength parameters for stability analyses significant questions remain:

1. Are effective strength parameters at peak deviator stress from isotropically consolidated undrained (CIU) triaxial tests on loose saturated coal (as reported by Eckersley, 2023) realistic for conditions where liquefaction initiates in a stockpile?
2. Is the assessment of unsaturated effective stress parameter X and therefore apparent cohesion in unsaturated coal reasonable?
3. Where a stockpile base contains saturated contractant coal, should strength parameters for the overlying loose unsaturated coal be assessed at strains similar to those at peak deviator stress in CIU tests on saturated contractant coal (e.g. around 1.2%), or simply represent peak deviator stress for unsaturated tests? This includes the selection of effective friction angle for assessment of apparent cohesion.

These questions were raised in the companion paper (Eckersley, 2023) and are discussed in Section 2 below to provide context for the stability analyses. A specific objective of the current paper is then to provide insight into these questions using stability analyses for the 1974 and 1991 experimental coal stockpiles. While being far from a comprehensive assessment, the analyses provide at least limited confirmation of the approach suggested in the companion paper.

This work is of most relevance to the coal processing industry where moisture content is defined as mass of water per wet mass of coal and referred to as "% total moisture" (AS1038 - Standards Australia, 2001). However, this paper follows the usual geotechnical definition (AS1289 – Standards Australia, 2005) where water content is mass of water per dry mass of solids. It is noted that geotechnical water content *w%* may be converted to % total moisture by *%TM = w%*100/(100+w%).*

2 QUESTIONS ON SELECTION OF STRENGTH PARAMETERS

As noted in Section 1 above, while results of laboratory triaxial testing of saturated and unsaturated coal have been summarized by Eckersley (2023), significant questions arise in their application to stability analyses.

The first question arises since in coal stockpiles, conditions are not undrained from the start of shearing (as occurs in conventional strain controlled isotropically consolidated undrained (CIU) tests). Rather, the undrained conditions are preceded by anisotropic consolidation with pore water pressure increasing as redistributed moisture collects at the stockpile base. The undrained condition and associated liquefaction results from initiation of failure in loose saturated coal. This is discussed by Eckersley (1986), and Been (2016) and Jefferies (2019) provide helpful discussion of the transition from drained to undrained conditions. It is therefore not a given that effective friction angle ϕ' mobilized at peak deviator stress in CIU tests on saturated coal (or loose sand, for that matter) is appropriate for use in stability analyses. However, while to assess ϕ' from stress-controlled testing with essentially drained conditions up to the point of collapse seems preferable (at least in principle), ϕ' at peak deviator stress from conventional CIU triaxial testing seems a reasonable approximation. Limited data supporting this view is reported by Castro (1969) and Eckersley (1986, 2000). This is never-the-less worth confirming by way of stability analysis of a stockpile failure, which is presented in Section 3 below. It is also worth noting that careful attention should be paid to testing procedures (see Eckersley, 2000, 2023) and single-stage testing should be used.

Regarding estimation of apparent cohesion in unsaturated coal, the data presented by Eckersley (2023) is clearly limited and based on Jenike cell testing of small specimens in which the particles > 4 mm size have been removed. However, to the author's knowledge there is currently no alternative data and so this was considered a reasonable starting point.

It is also worth noting that while inclusion of an apparent cohesion in the partly saturated coal is important (the likelihood of localised slipping at the toe may otherwise be unrealistically overestimated), the apparent cohesion values assessed were quite small. As a result, stockpile stability is likely to be dominated by effective friction angle in the loose saturated base and effective friction angle for the unsaturated coal.

With regard to Question 3 in Section 1 above: if liquefaction initiates in saturated coal in a stockpile base at small strains, should strength parameters (ϕ' or ϕ) mobilised at similarly small strains also be adopted for loose unsaturated coal higher in the stockpile? A slope stability analysis to investigate the likelihood of liquefaction (flow failure) within saturated coal at the stockpile base would presumably adopt ϕ' at peak deviator stress from CIU tests on saturated coal (as discussed above). This value would correspond to relatively small strains. However, strength parameters reported from triaxial tests on loose unsaturated coal forming the bulk of the stockpile would correspond to much larger strains. Should these parameters be used? At strains similar to those at failure of the saturated coal, strength mobilized in the unsaturated coal would be substantially less than usually reported. While loose unsaturated coal will mobilize additional strength with displacement, the liquefying saturated coal in the base will suffer a dramatic loss of shear resistance. Ideally a full stress-deformation analysis with coupled pore pressure generation (for water and air) and proper constitutive modelling of the coal is required. However, this is beyond the scope of the current work and would require work on suitable constitutive models that has not been done for coal. Instead, a simplistic preliminary assessment is attempted using stability analyses of the 1974 and 1991 experimental stockpiles described in Sections 3 and 4 respectively.

A potentially useful reality check is provided by the observation that most stockpiles are formed by coal spilling down the face of the slope, either from being bulldozed over the advancing crest or discharged high into the face from a stacking conveyor. Provided that apparent cohesion is relatively small, fresh stockpile slopes (typically 35º to 41º) are therefore formed at close to the effective friction angle at critical state conditions (ϕ'_{CSL} – 38º to 41º for the products reported by Eckersley, 2000). This suggests that use of ϕ'_{CSL} might be appropriate for the unsaturated coal, at least for parts of the stockpile formed in this way and within a few metres of the slope surface.

3 STABILITY ANALYSES OF 1974 EXPERIMENTAL STOCKPILE

3.1 1974 STOCKPILE – CONSTRUCTION AND HISTORY

Late in 1974 James Cook University geotechnical engineering staff conducted an experiment at Hay Point in which a small 1740 tonne stockpile 6 m high (footprint 32 m long and 20 m wide) with slopes initially at 36º to 39º was constructed from coking coal. It was subjected to wetting initially by 5 irrigation sprinklers at the stockpile crest, and later by infiltration from 5 wells drilled into the top of the stockpile. The stockpile eventually collapsed 7 days after construction. A detailed account of the experiment is provided by Trollope and Wallace (1975) and an abbreviated description is presented in ACARP Report C4057 (Eckersley, 2000). Figure 2 shows a plan view of the stockpile and its instrumentation, and Figure 3 shows a cross-section.

Hydraulic piezometers were installed on a 150 mm to 300 mm thick platform of coal above the heavily compacted subgrade and monitored periodically up to an hour before the time of collapse. Coal was discharged from the stacker at low height with the pile being formed in 3 layers each approximately 2 m thick, and in-situ density and moisture content tests were performed in the top of each layer before addition of the next. Average dry density of the stockpile from the tests was 0.88 t/m^3 (range 0.77 to 1.04 t/m^3) with average moisture content 11%. Since the density tests were performed in the top of each layer it is noted that these probably underestimate in-situ density. Some volume compression would have occurred for layers 1 and 2 as the overlying thickness of coal was added. However, the density-effective stress state is likely to plot above the combined critical state line (CSL) in Figure 7 of Eckersley (2023), implying likely contractant behaviour when sheared.

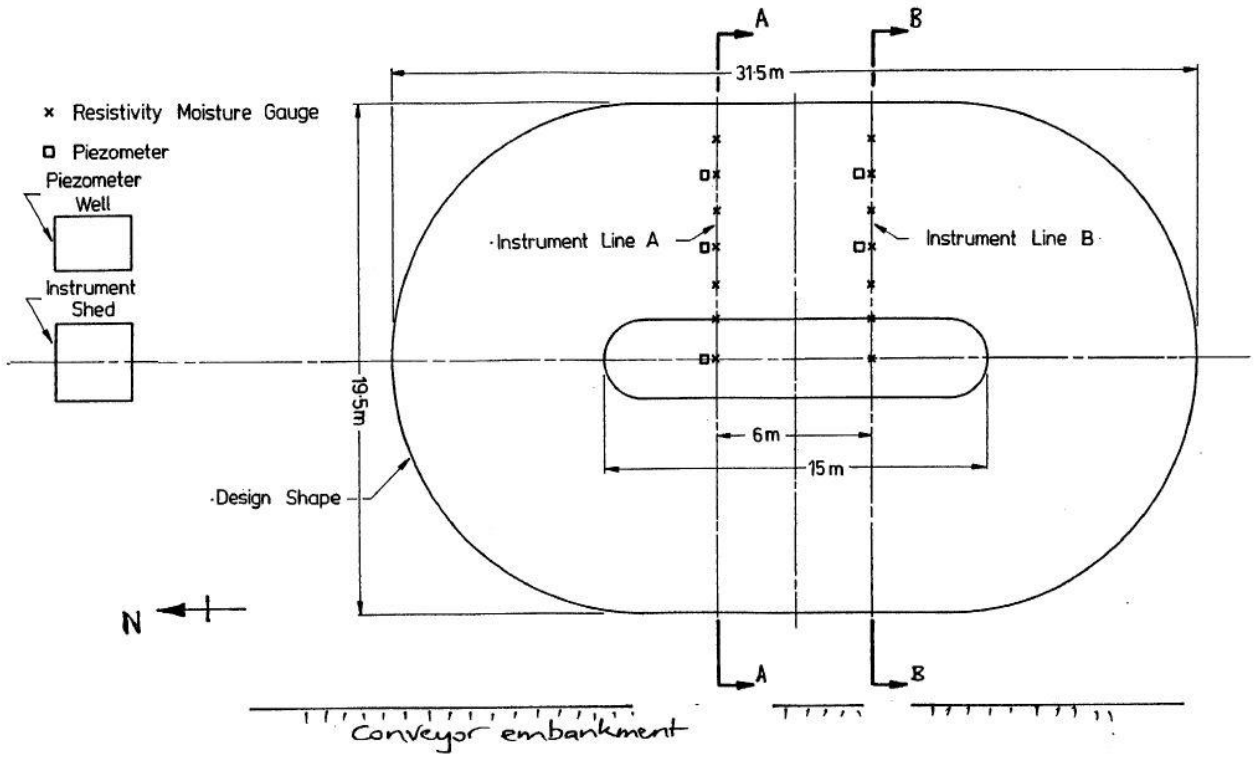

Figure 2: Initial layout of 1974 experimental stockpile (from Trollope & Wallace, 1975)

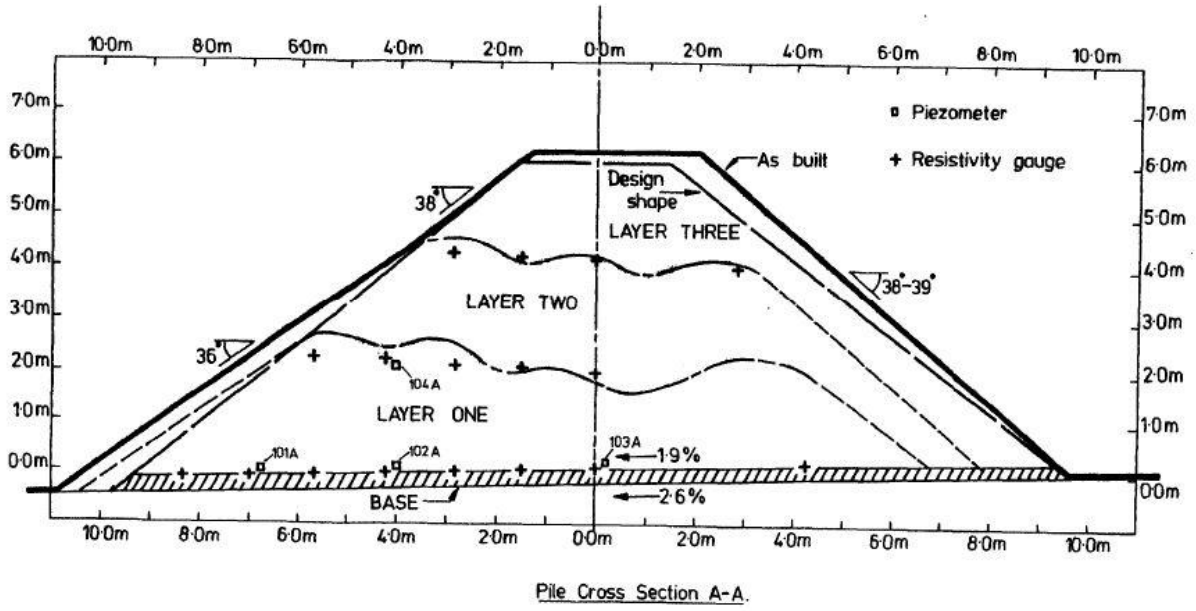

Figure 3: Cross-section AA - 1974 experimental stockpile as-constructed (from Trollope & Wallace, 1975)

Initial suction heads registered by the piezometers in the unsaturated coal before the start of water addition were approximately 0.4 m to 0.5 m.

After less than an hour of artificial rain at approximately 25 mm/h from 5 sprinklers, shallow slips approximately 200 mm thick formed in the slightly steeper western slopes (right-hand side in Figure 3), with most of the slightly flatter (36º) eastern slope suddenly slipping after 2.5 hours. The slips formed flows of coal slurry that ran down to the toe, and erosion and shallow slipping worsened until the sprinklers were turned off after 3.75 hours. There was a total of approximately 75 mm of artificial rain from the sprinklers, with a further 38mm of rain during the following night. Three days later the slipped coal was dozed back up and the top hand-shaped to form slightly flatter (30º) slopes. Five wells were subsequently drilled into the top of the stockpile to introduce water into the centre of the stockpile (approximately 63,000 litres over two days) without causing further surface erosion and shallow slipping.

The reinstated stockpile cross-section (AA) showing instrument and well locations is shown in Figure 4. As in Figure 3, the eastern slope is on the left and the subgrade slopes down to the left.

On day 8 of the experiment (7 days after construction), after a second long day observing results of water infiltration from the wells with seepage from the toe in several locations and cracking in the crest but no overt signs of failure, the research team left site. Most inconveniently - the stockpile completely collapsed within the next hour with no immediate observers! Flowslides formed from the NE and SE corners (adjacent to the left side of the section in Figure 4) with coal flowing up to 10 m from the original toe (see Eckersley, 2000). Post-failure features were typical of those observed in slips that have formed in production stockpiles. The last piezometer readings before failure indicated that the lower 0.5 m to 1.8 m of the stockpile was saturated. For the major flowslide the bottom 0.05 to 0.15 m of coal outside the stockpile initial footprint was saturated (as observed on the day following the collapse), with up to 0.6 m under the centre of the stockpile.

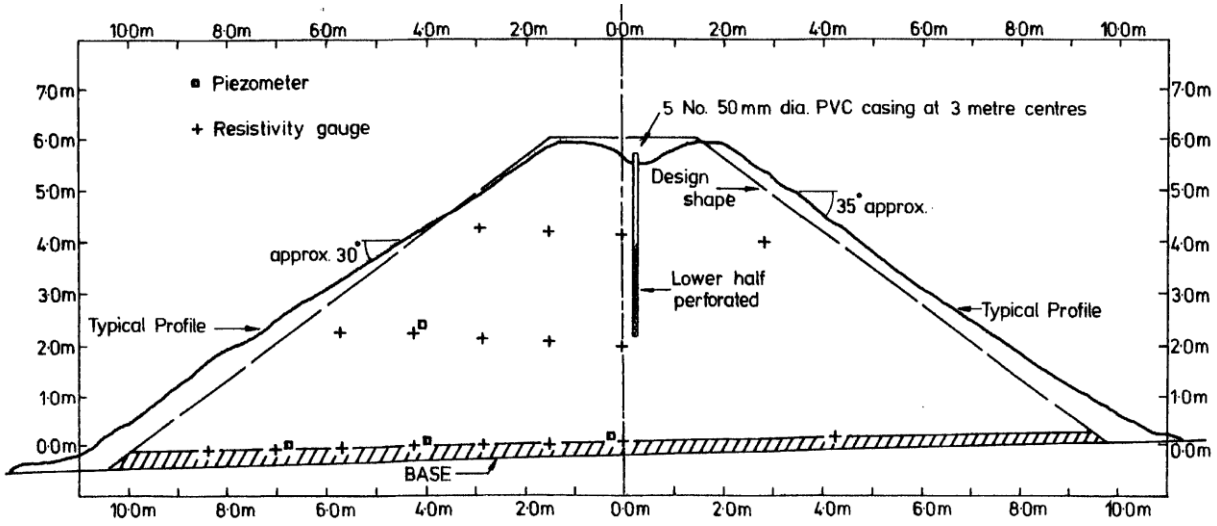

Figure 4: Cross-section AA: reinstated 1974 stockpile experiment (from Trollope & Wallace, 1975)

3.2 STABILITY ANALYSES

3.2.1 Analysis approach

The appropriateness of coal shear strength parameters selected using the laboratory data presented in Eckersley (2023) has been explored by way of slope stability analyses for conditions at failure (Section 3.2.6) and as constructed (Section 3.2.4). Stability analyses have been performed using SLOPE/W (GEO-SLOPE International, 2017). Spencer's method for handling inter-slice forces was adopted with initially circular slips and final optimization to a non-circular slip.

Attention has been focussed on the ultimate flowslide and not the earlier shallow slips that followed initial slope wetting by artificial rain. This was done since interest at the time of the experiment was primarily on the deep-seated flowslides previously observed at Hay Point. There was also no shallow instrumentation in the stockpile surface to provide data on shallow suction changes.

When originally constructed, the steepest average slope for the 6 m stockpile was 38º to 39º so stability of initial conditions was based on a slope at 38.5º. For conditions at failure, analyses have been based on the cross-section in Figure 4 and the last pore pressure records approximately 40 minutes before collapse.

Bulk unit weights adopted were 9.6 kN/m^3 for the as-constructed stockpile, 10 kN/m^3 for unsaturated coal after wetting, and 11.7 kN/m^3 for the saturated coal. The heavily compacted subgrade was assumed to be impenetrable to failure surfaces.

Since the objectives of the stability analyses were to confirm reasonableness of the data presented in Eckersley (2023) and investigate the questions raised in Sections 1 and 2 above, selection of shear strength parameters is outlined in the following paragraphs. Saturated coal forming the lower part of the stockpile was treated as a separate material zone from the unsaturated coal.

3.2.2 Saturated strength

For the saturated layer, dry density would probably have increased from 0.88 t/m^3 to approximately 0.94 t/m^3 (approximately 6.5% loss of volume – see data in Eckersley, 1986) as a result of saturation. Using the combined critical state line (CSL) in terms of dry density in Figure 7 of the companion paper (Eckersley, 2023) and an average (octahedral normal) effective stress p' of approximately 50 kPa at the stockpile base, the dry density and effective stress imply that the saturated coal would be prone to liquefaction with a density state parameter of 60 kg/m^3. From Figure 10 in Eckersley (2023) this corresponds to $\phi' = 24^o$ (with c' = 0). A similar value results from using the preliminary design line in Figure 8 of the same paper. Given the uncertainties involved, $\phi' = 24^o$ to 28^o might be reasonable.

3.2.3 Unsaturated strength

For the unsaturated coal the average moisture content increased from 11% as constructed to approximately 16% at collapse (by adding the contribution from total volume of added water less water in the saturated zone). SEEP/W modelling of the experiment was not attempted in view of the complex (and three-dimensional) wetting history. Instead, apparent cohesion values were assessed for the unsaturated coal using average moisture content and density. Vanapalli

et al.'s (1996) equation was used to assess the effective stress parameter for unsaturated soil X (see Equation (6) in Eckersley, 2023). Residual volumetric moisture content was taken as 0.065 and the saturated volumetric moisture content allowed for 5% entrapped air voids (consistent with Eckersley, 2022). Average suction through the stockpile was estimated to be (-)13.9 kPa at 11% moisture content (as constructed) and (-)1.8 kPa at 16% (after wetting), using the unsaturated moisture-suction relationship derived in Eckersley (2022). The estimated as-constructed value is considerably higher than initial suctions measured by piezometers at the stockpile base (4 to 5 kPa). These measured values may reflect higher dry density at the base and some wetting due to redistribution of initial moisture. The impact of an average suction of approximately 4.5kPa is discussed further below.

Considering Questions 2 and 3 raised in Section 1 and the associated discussion in Section 2, the following options for unsaturated shear strength were then considered:

a. Total stress parameters c = 11.7 kPa, ϕ = 37.2º, assessed from the triaxial results at peak deviator stress in Figure 11 in Eckersley (2023) for the lowest dry density tested (825 kg/m^3) with 15% moisture content.
b. To investigate the possibility that effective strength mobilized at 1.2% strain should be used (as for the saturated loose coal): ϕ' = 24º (and c' = 0) with apparent cohesion 0.88 kPa as constructed (11% moisture content) and 0.28 kPa at collapse (16% moisture content after wetting).
c. To investigate the possibility that unsaturated effective strength parameters should reflect the slope of the loosely tipped coal: ϕ' = 39º (and c' = 0, approximating the critical state value) with apparent cohesion 1.6 kPa as constructed and 0.5 kPa after wetting (from average suctions of 13.9 kPa and 1.8 kPa respectively). It is noted that based on data for coal used in the stockpile and LA coal (referred to in Eckersley, 2000, 2023), ϕ' = 37º to 39º would be reasonable.

Inspection of the unsaturated strength data at 1.2% axial strain in Figure 12 of Eckersley (2023) suggests that selection of total stress parameters appropriate for this case would involve substantial uncertainty. However, provided average normal stresses are less than around 50 kPa, ϕ = 40º (with c = 0) might be a reasonable assumption, and results would then be similar to those adopted for option c above. That these values are comparable may be coincidental.

3.2.4 Results: as-constructed conditions

Prior to considering the main case of the slope at the point of collapse, it is worth briefly considering implications from the observed stability of the as-constructed slope. When originally constructed, the steepest average slope for the 6 m stockpile was 38º to 39º and coal was placed without deliberate compaction. For comparison, Trollope and Wallace (1975) noted that stockpile side slopes were typically 36º to 37º and that as initially stacked, slopes in the mid-1970s varied from 35º to 41º depending on initial moisture and stacking peculiarities.

Stability analyses for the as-constructed 1974 stockpile gave the following results for unsaturated strength Options b and c:

b: $FoS_{min} = 0.82$

c: $FoS_{min} = 1.48$

The slope was clearly stable (therefore implying FoS $\geq$ 1) before wetting (by the sprinklers, overnight rain and infiltration from wells). The factor of safety of 0.82 for Option b parameters therefore seems unrealistic, and suggests that the ϕ' value adopted was too low. The result for Option c seems high, and partly results from the estimated suction of 13.9 kPa. If 4.5kPa is used to better reflect the measured suctions, a minimum factor of safety of 1.24 results. In any case, neither result implies slope failure.

Overall, this tentatively suggests that using unsaturated strength parameters based on ϕ' for loose saturated coal (with peak deviator stress occurring at low strains) is unreasonable. An alternative possibility may be that the method used to assess the suction contribution to shear strength substantially underestimates the true value.

3.2.5 Shallow slips

As foreshadowed in Section 3.2.1, the shallow slipping observed in response to artificial rain has not been analysed. However, it is noted that:

- If Option b parameters were adopted, factor of safety would be even less than 0.82.
- If Option c parameters were adopted (based on ϕ' = 39º) and a thin surface layer of near-saturated coal with zero apparent cohesion modelled, a minimum factor of safety of close to 1.0 would result for shallow slipping of the near-saturated coal. Option a parameters would lead to a similar result if apparent cohesion is reduced to zero for a shallow near-saturated zone.

3.2.6 Results: conditions at collapse

Minimum factors of safety for analysis of conditions at collapse with unsaturated coal strength Options a, b and c (as defined in Section 3.2.3) are as follows:

a: $FoS_{min} = 1.36$

b: $FoS_{min} = 0.79$

c: $FoS_{min} = 0.99$

Option a represents a substantial over-estimate, b an under-estimate, and c is close to the value of 1.0 expected at failure. A stability plot for option c showing the critical slip surface is presented in Figure 5, with minimum safety factor (FoS) of 0.99 after optimization. To reiterate, this represents the case of conditions at collapse with $\phi' = 24^o$ for the saturated zone and $\phi' = 39^o$ for the unsaturated coal with a corresponding apparent cohesion. This is an encouraging result since FoS = 1.0 would be expected at the point of failure.

To explore the impact of suctions and apparent cohesions being based on the measured 4 to 5 kPa instead of estimated values (as discussed in Section 3.2.3), the Option c analysis was repeated with apparent cohesion in the unsaturated coal at 16% moisture content $c_a = 0.16$ kPa based on a suction of 0.6 kPa. Minimum factor of safety was then 0.97 with critical failure surface approximately 2/3 of the stockpile height.

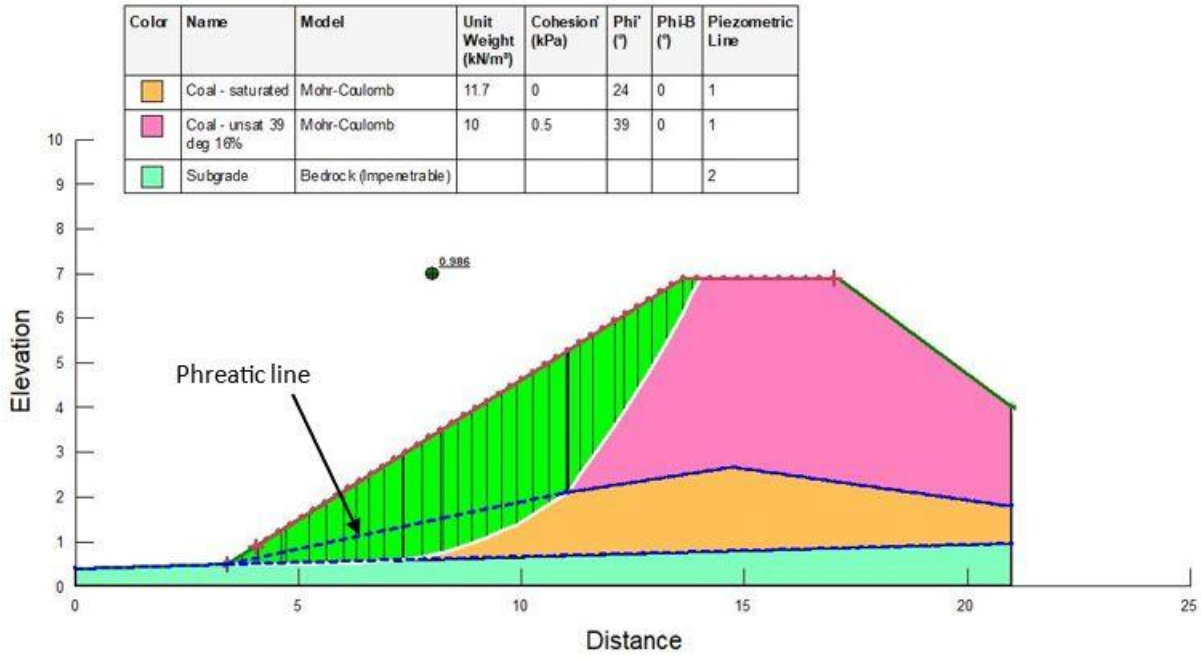

Figure 5: Stability plot from SLOPE/W analysis: reinstated 1974 stockpile experiment at failure

If apparent cohesion is removed entirely ($c_a = 0$), FoS = 0.95 and the critical failure surface is localized at the toe of the slope (approximately 1 m high). In this case retrogressive failure of the whole slope would be likely since FoS was still less than 1 for slip surfaces up to the top of the slope. The result suggests that the detailed failure sequence and the possibility of retrogressive slipping can be sensitive to apparent cohesion in the unsaturated coal as well as shape of the phreatic line near the stockpile toe (whether concave or convex). Laboratory scale stockpile experiments demonstrating this point are reported by Eckersley (1986, 1990b). Unfortunately for the 1974 stockpile experiment the actual collapse was not observed, but since coal slurry had not been pushed ahead of the flowing coal the author's view is that failure was probably not retrogressive.

It is noted that while the apparent cohesion values used are relatively small, if assumed to be zero, analyses will frequently show critical failure surfaces to be very localised slips at the toe of the slope. This is especially the case if the water table has a convex shape near the toe. An inexperienced analyst might then either assume that the small slips are inconsequential or over-emphasize the low FoS.

Importantly, when $\phi' = 24^o$ is used within the unsaturated coal (Option b above) FoS is much less than 1, as foreshadowed in Section 3.2.4. This would be expected by those with experience in stability analysis for slopes with little cohesion. This ϕ' value therefore either represents a poor assessment of strength within the unsaturated coal, or that apparent cohesion in the unsaturated coal is much greater than implied by the assessment used above and proposed by Eckersley (2023).

If strength of the saturated coal is increased slightly to $\phi' = 26^o$, FoS for analysis Option c increases to 1.05 and lower strength would be required for the unsaturated coal to achieve FoS = 1.0. This might be reasonable since it is noted above (Section 3.2.23) that $\phi' = 37^o$ to 39^o could apply for coal in the stockpile.

3.3 CONCLUSIONS: STABILITY ANALYSES OF 1974 STOCKPILE

The results presented above support a preliminary conclusion that saturated strength for the loose coal selected using data in Eckersley (2023) together with unsaturated strength represented by ϕ'_{CSL} (with $c' = 0$) and apparent cohesion assessed using the Vanapalli et al. (1996) expression provide a reasonable basis for slope stability analysis of the 1974 experimental coal stockpile.

It is noted that this does not represent a unique solution since there are too many variables. However, it seems a reasonable approach until there is better data for shear strength of unsaturated coal. It is also noted that the apparent cohesion values assessed are quite low. While it is considered important that they are included for the unsaturated coal (as discussed in Section 3.2.6), ϕ' for the saturated base and ϕ or (ϕ') for the unsaturated coal play a more significant role, and so conclusions about use of the Vanapalli et al. (1996) expression have to be treated as tentative.

Importantly, it seems reasonable to conclude from these analyses that:

1. Strength in the base of the stockpile after saturation seems reasonably modelled by $\phi' = 24^o$ (from CIU triaxial tests on saturated coal).
2. For unsaturated coal forming the bulk of the stockpile above the saturated zone, a ϕ' value close to the critical state value (and similar to the slope angle for loosely tipped coal) seems to provide a reasonable result.
3. Total stress parameters based on peak deviator stresses from the triaxial tests on unsaturated coal reported by Eckersley (2023) appear to over-estimate strength, at least for this relatively small stockpile.

4 STABILITY ANALYSES OF 1991 EXPERIMENTAL STOCKPILE

4.1 1991 STOCKPILE – CONSTRUCTION AND HISTORY

Analysis of the 1974 experimental stockpile in Section 3 provides significant encouragement that the approach followed predicts failure where a low dry density stockpile base is fully saturated. However, would stability be correctly inferred from analysis of a stockpile in which failure did not occur?

An instrumented 12 m high, 14700 tonne coking coal stockpile at average 12.2% initial moisture content was constructed at Hay Point from LA coal (Eckersley 2000, 2022) and monitored for 2 months from October to December 1991. Note that "LA" is the code used in Eckersley (2000) for one of the coking coal products tested as part of ACARP Project C4057. Coal forming the stockpile was sampled and tested, pore water pressures in the stockpile base were measured, and in-situ density and moisture content testing were performed as the stockpile was reclaimed in layers.

The stockpile did not suffer an overall collapse. It was not subjected to artificial wetting, and was constructed primarily so that the redistribution of moisture initially in the stockpile could be measured. Instability was limited to significant surface erosion that resulted from approximately 160 mm of rain. This is not analysed in the current paper, which focusses instead on overall stability of the stockpile as constructed, and at the point of maximum recorded pore water pressures.

The experiment is described in reasonable detail by Eckersley (1994, 2000), and analyses of moisture movements within the stockpile using SEEP/W are presented by Eckersley (2022). The analyses found that to adequately model the moisture redistribution and growth of saturated zone at the stockpile base required inclusion of a thin zone above the stockpile subgrade with permeability 7 times the saturated permeability of the bulk of the stockpile. Inclusion of this zone was justified by particle segregation observed during stockpile placement. This analysis was labelled as "Case C" in Eckersley (2022).

Peak pore water pressure heads of around 200 mm were measured above the subgrade 7 to 9 days after coal placement. Slightly higher peak pressures resulted in the SEEP/W model (Case C), and with a slightly delayed peak (10 days).

4.2 STABILITY ANALYSES

4.2.1 Approach and parameters

The approach taken was to use pore pressures in the saturated zone and suctions in the unsaturated coal modelled by SEEP/W analyses (Case C in Eckersley, 2022, as noted in Section 4.1) as input to SLOPE/W stability modelling. This was done since pore pressures in the saturated zone above the subgrade were close to those measured, and there were no suction measurements throughout the stockpile that could be used as a basis for stability analyses. It also provided a useful test of the combination of seepage and stability analyses.

Some details of the analysis inputs are as follows:

1. Cross-section geometry of the 12 m stockpile is as used for the SEEP/W model, with the 1:40 sloping subgrade being treated as impenetrable for stability modelling.
2. For the unsaturated coal at 12.2% moisture content and average dry density 0.97 t/m^3, average bulk density was assumed to be 10.6 kN/m^3.
3. Strength of the unsaturated coal was modelled using the Vanapalli et al. (1996) expression as implemented in SLOPE/W, with c' = 0, residual volumetric water content 0.065, and suctions taken from the SEEP/W analysis (as noted above). Effective friction angle was assumed to be $\phi' = 40^o$, consistent with the value assessed from triaxial testing for LA coal at steady state shear (critical state).
4. The saturated zone above the subgrade was assumed to have average dry density 0.99 t/m^3 – equivalent to average in-situ dry density from tests approximately 1 m above the subgrade. Assuming that average (octahedral normal) effective stress p' at the stockpile base beneath the full 12 m height is approximately 70% of the vertical stress (ie. 90 kPa), state parameter in terms of density change is approximately 30 kg/m^3 and therefore $\phi' = 33^o$ using Figures 7 and 10 respectively from Eckersley (2023). A higher ϕ' value would result for stresses assessed at less than full stockpile height.
5. As for the 1974 experiment, analyses used circular slips with Spencer's method for interslice forces, and the failure surface with minimum FoS was then optimized, forming a non-circular surface.

It is noted that the effective stress and dry density values for coal in the saturated zone plot above the critical state line in Figure 7 of Eckersley (2023), and so imply potential for liquefaction should shear failure initiate.

4.2.2 Results

A stability plot of the analysis at the time of peak water level (10 days) is shown in Figure 6. Note that the saturated zone is barely visible given the scale of the figure since maximum pore water pressure head at the stockpile base was approximately 200 mm. The critical failure surface has typically 1.5 m to 2.5 m vertical thickness, and through most of the unsaturated part of the slip surface moisture suction pressure was (-)5 to (-)6 kPa. Minimum FoS after optimization was 1.25. This is consistent with the observed history of stability throughout the life of the stockpile (apart from surface erosion after heavy rain).

The following are also noted:

- If effective friction angle within the unsaturated bulk of the stockpile was substantially reduced to reflect possible contractant behaviour (eg. $\phi' = 33^o$) as considered by Question 3 in Sections 1 and 2, safety factors less than 1 would result since the slope angle was approximately 38º.
- Analysis using pore water pressures (and suctions) at 0.5 days (ie. virtually at construction when there was not yet a saturated zone at the stockpile base) and the same parameters as above gave minimum FoS = 1.23, with suctions on the potential failure surface typically (-) 2.6 kPa.

The critical condition in this case was therefore at construction when suctions were smallest, even though a saturated zone had not yet developed. While not significant in practical terms since failure would be unlikely in either case, this is an unusual result since most critical conditions would normally be expected at the time of peak pore pressures.

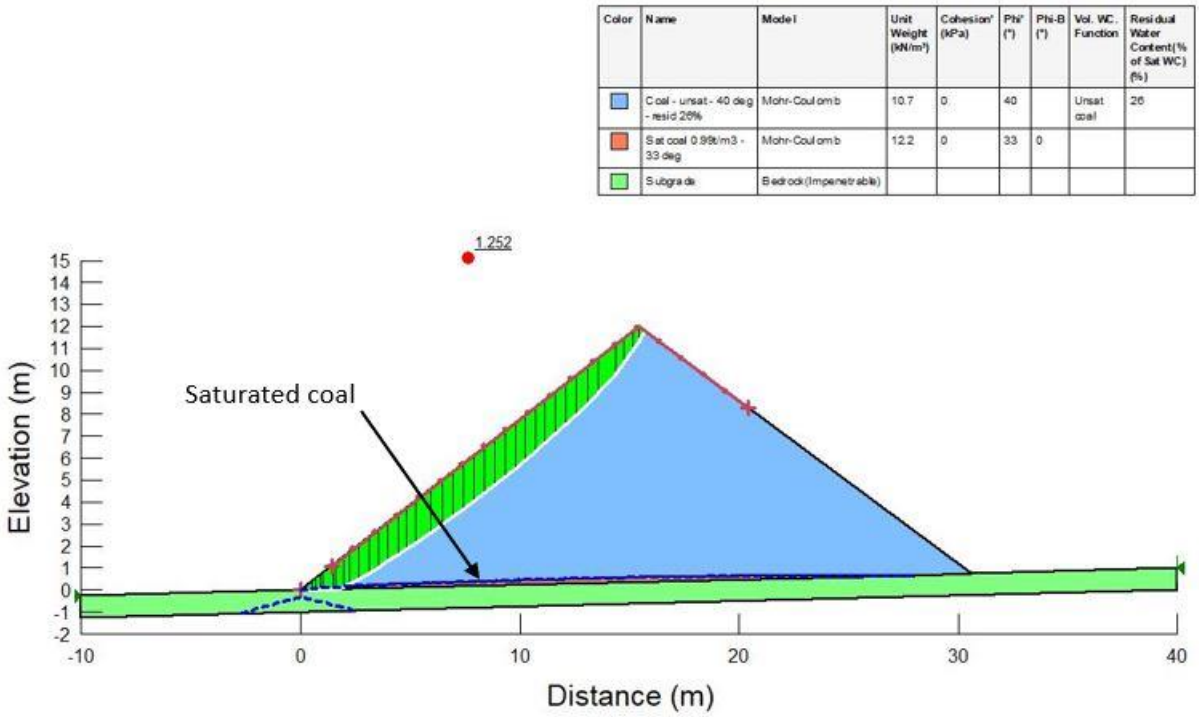

Figure 6: Stability plot from SLOPE/W analysis: 1991 stockpile experiment at 10 days

In summary, slope stability analysis using the parameters and approach outlined in this paper result in safety factors consistent with the observed stability of the slope. Even though ϕ' in the saturated zone corresponds to contractant, potentially liquefiable coal, the very low water table from moisture redistribution within the stockpile in this case resulted in a factor of safety of approximately 1.25, consistent with overall stability of the stockpile.

It is also clear that while not analysed here, heavy rain (with rainfall rate exceeding the saturated permeability) would reduce suctions to near zero in a shallow zone below the slope surface and so would lead to erosion and shallow slipping since ϕ' is similar to the slope angle.

5 SUMMARY AND CONCLUSIONS

Eckersley (2022) presented a basis for analysis of transient moisture movements in coal stockpiles with the objective of permitting realistic slope stability analyses for coal stockpiles where the product is prone to flowsliding. The ultimate objective is development of rational stockpile management procedures that simultaneously address the need for appropriately low risk of significant instability and the need for practical and cost-efficient handling of coal products.

Eckersley (2023) presented a summary of shear strength data for coking coal to provide a basis for selecting strength parameters for stockpile stability analyses and critical assessment of results from testing products not previously investigated. It was clear from the data that in-situ density and moisture content of coal stockpiles need to be considered in assessing appropriate strength parameters, and that these will be strongly influenced by the processes used in forming the stockpile. The paper then raised a series of significant questions relating to the selection of shear strength parameters for coal stockpiles, answers to which are not necessarily obvious.

The current paper then presents slope stability analyses of two experimental stockpiles conducted as part of previous research at James Cook University (in 1974 and 1991) to provide further insight into selection of parameters and provide at least tentative answers to the questions raised in Sections 1 and 2 above.

Stability analyses of the two experimental stockpiles – one of which was brought to failure by introducing water – provide at least preliminary confirmation that effective strength parameters for the saturated coal can be assessed as outlined above, and that for loose coal the ϕ' value appropriate within the saturated zone at initiation of failure (ie. at low strains) is not appropriate for use within the unsaturated bulk of the stockpile. It is tentatively concluded that the

processes typically used in stockpile formation imply that close to the sloping face ϕ' will approximate the critical state value.

It is noted that since there are too many variables to attempt a unique solution these conclusions remain tentative. However, the approach seems reasonable until there is better data for shear strength of unsaturated coal. It is also noted that the apparent cohesion values assessed are quite low. It is considered important that they are included for the unsaturated coal (as discussed in Section 3.2.6) and not just neglected. However, ϕ' for the saturated base and ϕ or ϕ' for the unsaturated coal play a more significant role. Conclusions about use of the Vanapalli et al. (1996) expression are therefore considered to be tentative.

6 ACKNOWLEDGEMENTS

BHP Australia Coal and its predecessor companies provided the opportunity for the research conducted at James Cook University over many years, with substantial financial support and encouragement. The Australian Coal Association Research Program provided specific support and several member companies (including BHP) provided opportunity to investigate their stockpile conditions and test selected products during the period 1995 to 2000. Since that time (while working for Coffey and AECOM) the author has had opportunity to review and observe stockpile conditions at numerous BHP and Glencore coal operations. The support and encouragement from these organisations and their staff at the times of that work are gratefully acknowledged.

The author's involvement in coal stockpile work would not have commenced without the pioneering work of (the late) Dr Keith Wallace and (the late) Professor Hugh Trollope at James Cook University. In particular, Dr Wallace mentored the author during 1975 to 1986 and provided insightful review comments on this paper prior to his death in June 2022. I remain most grateful for their contribution. More recently Dr John Simmons has provided helpful input.

The author is also grateful for comments provided by reviewers during the submission of this paper.

James Cook University provided the physical context in which this work could take place – mostly from 1975 to 2000, but more recently in providing access to software. Associate Professor Nagaratnam (Siva) Sivakugan assisted greatly in facilitating recent arrangements.

7 REFERENCES

Been, K. (2016). "Characterizing mine tailings for geotechnical design." Australian Geomechanics, Vol.51, No.4, December 2016, pp.59-78.

Castro, G. (1969). "Liquefaction of sands." Ph.D. Thesis. Harvard University.

Davies, P, Zargarbashi, S and McQueen, L 2013, "Flow failure in coal stockpiles – how to reduce risk', in PM Dight (ed.), *Slope Stability 2013: Proceedings of the 2013 International Symposium on Slope Stability in Open Pit Mining and Civil Engineering*, Australian Centre for Geomechanics, Perth, pp. 881-895.

Eckersley, J.D. (1977). "Transient moisture movements in stockpiled granular materials", M.Eng.Sc. Thesis, James Cook University of North Queensland.

Eckersley, J.D. (1985). "Flowslides in stockpiled coal", *Engineering Geology*, Vol.22, pp.13-22. (Originally published in 4th Australia - New Zealand Conference on Geomechanics, Perth, May 1984, Vol.2, pp.607-611.)

Eckersley, J.D. (1986). "The initiation and development of slope failures with particular reference to flowslides", Ph.D. Thesis, James Cook University of North Queensland, Dec. 1986.

Eckersley, J.D. (1990a). "Flowslide hazards in coal stockpiles", *Mechanical Engineering Transactions, I.E.Aust*., Vol. ME 15, No.4, Dec. 1990, pp.302-306. (Originally published in Institution of Engineers, Australia, 1990 International Coal Engineering Conference, Sydney. June 1990, pp.35-39.)

Eckersley, J.D. (1990b). "Instrumented laboratory flowslides", *Geotechnique*, Vol.40, No.3, pp.489-502.

Eckersley, J.D. (1994). "Moisture movement in coal stockpiles - 2: instrumented stockpile experiment". *Australian Coal Journal*, No.44, pp.9-25.

Eckersley, J.D. (2000). "Moisture Changes & Stability Problems in Coal Stockpiles", ACARP Report C4057, June 2000.

Eckersley, J.D. (2022). "Moisture movement analyses for coal stockpiles". *Australian Geomechanics*. Vol.57, No.3, September 2022, pp.33-48.

Eckersley, J.D. (2023). "Shear strength of stockpiled coking coal – existing data." *Australian Geomechanics*. Vol.58, No.3, September 2023. (https://doi.org/10.56295/AGJ5831).

GEO-SLOPE International (2017). "Stability modelling with GeoStudio", GEO-SLOPE International Ltd.

Jefferies, M.G. (2019). "Utility of critical state soil mechanics". In *Proceedings 13th Australia New Zealand Conference on Geomechanics* – Acosta-Martinez & Lehane (Eds). Perth, April 2019. Australian Geomechanics Society, pp.51-56.

Leeder, R., Howey, C., Todoschuk, T., Gransden, J., Giroux, L. and Ng, K.W. (2014). "Coal stockpile moisture and cokemaking". *AISTech - Iron and Steel Technology Conference Proceedings*. 1. 357-365.

Standards Australia (2001). "Australian Standard AS1038.1-2001 – Coal and coke – Analysis and testing. Higher rank coal – Total moisture." Standards Australia Ltd, Sydney. 2001.

Standards Australia (2005). "Australian Standard AS1289 - Methods of testing soils for engineering purposes. Method 2.1.1: Soil moisture content tests – Determination of the moisture content of a soil – Oven drying method (standard method)." Standards Australia Ltd, Sydney. 2005.

Trollope, D.H. and Wallace, K.B. (1975). "The stability of coal stockpiles at Hay Point, Queensland." (Confidential) Report to Utah Development Company, Dept. of Civil & Systems Engineering, James Cook University of North Queensland.

Vanapalli, S.K., Fredlund, D. and Pufahl, D.E. (1996). "The relationship between the soil water characteristic curve and the unsaturated shear strength of a compacted silt." ASTM International, Vol.19, No.3, pp.259-268.

Engineering the best solutions

In addition to our materials testing services, we offer a complete package of engineering support services to ensure the best outcome for your project.

Our 75+ geotechnical engineers and environmental scientists are part of a leading multi-disciplinary team of over 950 staff in 50 locations across Australia and New Zealand.

Find out more about our engineering and graduate positions at constructionsciences.net/careers

member of group kiwa

Construction Sciences

P: 1300 165 769 H/O: 60 Kingsford Smith Drive, Albion, QLD 4010
E: info@constructionsciences.net W: www.constructionsciences.net

FINANCIAL REVIEW BOSS
MOST INNOVATIVE COMPANIES

THE EARTH IS CORE TO OUR BUSINESS

At Geofabrics, we are working to protect, contain, and secure the physical environment using smart geosynthetics. With a view towards creating a sustainable future, we have set carbon emission targets in our manufacturing plants in Australia. This initiative aims to minimise our impact on the planet while delivering quality solutions that help our customers mitigate risks and build smarter infrastructure.

Visit **geofabrics.co**or call 1300 60 60 20

GEOFABRICS®
Sustainable solutions

CHADWICK GEOTECHNICS

Chadwick Geotechnics is a leading supplier of testing, drilling and engineering services to the Geotechnical, Civil and Environmental disciplines across Australia and throughout the Asia Pacific region.

Key capabilities include:

Field Engineering

- Construction Engineering Services
- Logging
- Factual Investigations & Reporting
- Earthworks Supervision (including Level 1)

Laboratory

- NATA Accredited
- Construction Materials Testing
- Triaxial and Consolidation Testing
- Thermal Resistivity Testing
- Remote Laboratory Establishment

Drilling

- Sonic/Solid/Percussion/Direct Push
- Geotechnical and Environmental Systems
- NDD (Non Destructive Digging)

Instrumentation

- Supply
- Installation
- Monitoring

Think Act Be Safe

bsi. AS/NZS 4801:2001 Occupational Health and Safety Management

Engineering • Laboratory • Drilling • Instrumentation

Head Office and VIC Laboratory: Melbourne **QLD Laboratory: Sunshine Coast**

www.chadwickgeotechnics.com.au | **info@chadwickgeotechnics.com.au**

THE ROLE OF PROGRESSIVE BRITTLE FRACTURE IN THE 1931 LANDSLIDE AT DOGFACE ROCK, KATOOMBA

Zack Tuckey
Jacobs Group (Australia) Pty Ltd

https://doi.org/10.56295/AGJ5833

ABSTRACT

The 1931 Dogface Rock landslide in Katoomba NSW was a complex, progressive cliff collapse with a failure volume in the order of 100,000 m^3 that was triggered by the extraction of remnant coal pillars from the Katoomba Colliery, about 200 m below the top of the escarpment. Although underground coal mining is generally accepted as a cause of the rockslide, previous studies have not explicitly investigated the role of progressive brittle fracture in the collapse. This paper presents an integrated study which incorporates remotely piloted aircraft photogrammetry with a discrete element method numerical investigation of the landslide, and thereby explores the role of progressive brittle fracture, and re-examines the failure mechanism and runout motion of this multi-stage landslide.

Remotely piloted aircraft photography is used to build a georeferenced 3D model of the site with Structure-from-Motion photogrammetry software. A digital geotechnical mapping workflow is demonstrated to investigate the morphology of the landslide scar, extract statistics on discontinuity orientation, persistence, and spacing, and undertake trace mapping of newer brittle fractures that interacted with pre-existing high persistence joints as the landslide rupture surface developed. A series of discrete element method numerical laboratory tests are used to calibrate bonded block contact properties that reproduce laboratory scale intact rock index parameters including UCS and tensile strength. Upscaled rock block contact parameters are then applied to a cliff-scale model that investigates the progressive development of rock mass damage induced by mining. Following extraction of the remnant pillars, rock mass damage develops mostly by extensile strains that produce tension cracks. Brittle fractures propagate upwards from the mine level and eventually initiate toppling of massive sandstone slabs defined by high persistence pre-existing subvertical joints. The investigation illustrates how the integration of photogrammetry with discrete element numerical methods can be used to characterise progressive brittle failure and runout of large rock slope failures.

1 INTRODUCTION

In early 1931, a series of complex rock slope failures occurred at Dogface Rock in Katoomba. The two largest collapse events involved a failure volume of about 100,000 m^3 that was mostly comprised of Triassic age Banks Wall Sandstone. Massive slabs of high strength sandstone up to about 20 m thick detached from the 200 m high cliff, separating along pre-existing subvertical joints and new brittle fractures. Historical records show that the failures were progressive and multi-stage: after the appearance of a 100 m long tension crack at the crest of the cliff in December 1930, weeks passed as the tension crack continued to propagate and dilate, with many minor precursory rockfalls occurring before the largest collapse events occurred on 28 and 29 January 1931 (Cameron-Smith, 2019).

The cliff failure is generally accepted to have been triggered by extraction of remnant underground coal mine pillars below the escarpment in June or July 1930, about six months before the cliff collapse events (Pells et al., 1987; Seedsman and Pells, 2014). Previous studies have proposed that the failure occurred by basal rock mass yielding of weaker claystone layers under gravitational loading (Pells, 2008). More recently, researchers have used numerical models to back-analyse a similar mining-induced landslide at Nattai North, about 36 km south of Katoomba, using conventional discrete element method (DEM) techniques (Salmi et al., 2017; Mostyn et al., 1997) and the Discontinuous Deformation Analysis (DDA) method (Do and Wu, 2020). However, the conventional DEM approach does not explicitly simulate the process of progressive brittle fracture initiation, propagation, and failure surface coalescence that occurs before the initiation of overall slope collapse. Although the DDA investigation did consider the role of mining-induced fractures at Nattai North, the analysis was limited to simulation of shear fractures localised at the toe of the cliff; the global role of tensile fracture of intact rock, driven by extensile strains, was not examined.

This investigation demonstrates an approach for integrating digital photogrammetry mapping with numerical modelling techniques to characterise the role of progressive brittle fracture in the Dogface Rock cliff failure, including brittle tension fracture of intact rock blocks. Structure-from-Motion (SfM) photogrammetry software is used to build a 3D model of the site from Remotely Piloted Aircraft (RPA) photography. Digital geotechnical mapping techniques are used to demonstrate evidence of interaction between pre-existing discontinuities and newer brittle fractures. Next, the UDEC-Trigon approach is used to calibrate laboratory and field scale rock block shear strength and stiffness parameters. The calibrated parameters are applied to a conceptual back analysis of the failure that explicitly simulates progressive rock

mass damage accumulation by tensile and shear fracturing, clearly demonstrating the dominant role of progressive tensile fracturing in the cliff collapse.

2 GEOLOGICAL AND PHYSIOGRAPHIC SETTING

The Dogface Rock landslide occurred in the Blue Mountains world heritage area at Katoomba, about 100 km inland from Sydney near the western margin of the Permian-Triassic Sydney Basin. The escarpment at Katoomba is formed by an uplifted sandstone tableland that has been deeply incised by rivers, with cliffs up to about 200 m high comprised of Triassic age Narrabeen Group sandstone. The geomorphological setting is characterised by active escarpment retreat processes, with frequent rockfalls initiating from the escarpment cliffs, and debris slides occurring in the slopes below. Slope failures vary in scale from minor discrete block falls up to deep-seated landslides with volumes exceeding 100,000 m^3. Figure 1 shows a plan view of the area around Katoomba, highlighting the locations of Landslide Lookout at the crest of the escarpment (directly above the landslide detachment scar) and the popular Federal Pass walking track that traverses across the colluvium covered slope about 230 m below the lookout.

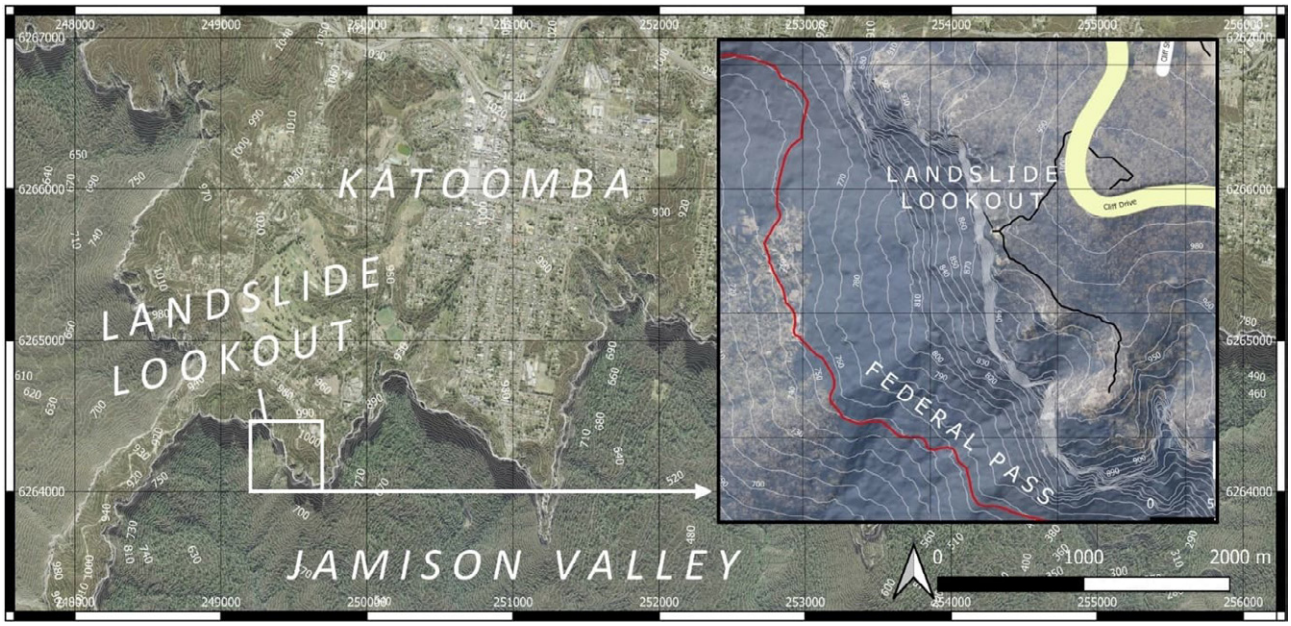

Figure 1: Location plan showing Katoomba, Landslide Lookout, and Federal Pass walking track

Landslide Lookout is on the crest of the cliff at elevation 980 m AHD, overlooking the Jamison Valley below. Figure 2 shows an annotated RPA image of the cliff face and a simplified, interpreted geological cross section.

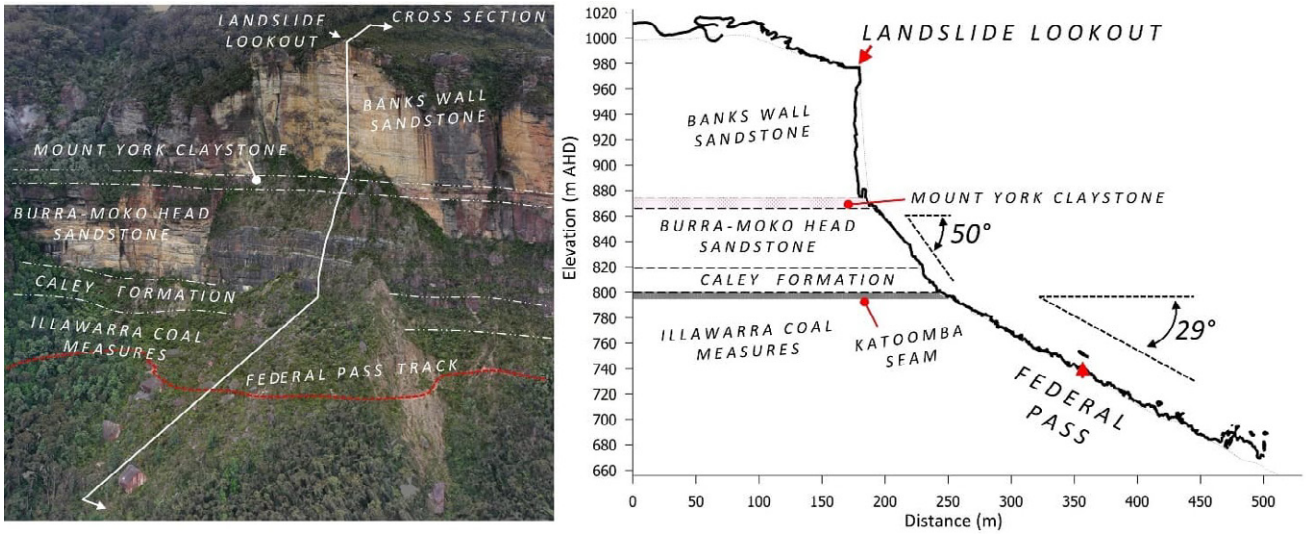

Figure 2: Annotated RPA image and interpreted geological cross section through Landslide Lookout

The upper cliffs are vertical and comprise Triassic age Banks Wall Sandstone, a strong and widely bedded to massive quartzose sandstone that contains ironstone bands, occasional conglomerate beds, and claystone lenses. The Banks Wall Sandstone is underlain by the Mount York Claystone, a narrow but very continuous band of weak red claystone that can be traced horizontally for many kilometres across the escarpment. The lower half of the cliff has a slope of about 50° and is formed by the quartzose to quartz-lithic Burra-Moko Head Sandstone, which is more closely bedded and contains more frequent claystone layers than the Banks Wall Sandstone. The Burra-Moko Head Sandstone is underlain by interbedded sandstone, shale, and claystone of the Caley Formation, forming the base of the Narrabeen Group and the boundary between the Permian and Triassic. The Illawarra Coal Measures underly the Caley Formation, outcropping along the base of the cliffs and extending beneath the 29° colluvial slope, including the Katoomba Seam that was historically mined in the late 1800s and early 1900s using the room-and-pillar method.

3 HISTORICAL COAL MINING AT KATOOMBA

From the late 1800s through the early 1900s numerous underground coal and torbanite (oil shale used to produce kerosene) mines were developed throughout the Blue Mountains region. The Katoomba Colliery mined the Permian coal measures under the Triassic sandstones; the coal measures rocks outcrop near the base of the escarpment cliffs throughout the Jamison Valley. By 1890 the colliery had developed extensive room-and-pillar mine workings below Dogface Rock and Malaita Point, extracting panels of coal from the sub-horizontal Katoomba Seam, which is about 200 m below the top of the escarpment and typically 1.5 m to 3 m thick. Pells and Hammon (2009) summarised the history of the mining developments in Katoomba, noting that by 1890 most of Malaita Point had been mined, leaving remnant pillars of coal to support the roof of the workings.

Mining ceased in 1905 and the colliery was inactive until 1925, when a new syndicate of investors leased the mine and restarted production. Around June or July 1930, miners extracted remnant coal pillars directly beneath and on the downslope side of the cliff line at Dogface Rock (Pells et al., 1987). Pells and Hammon (2009) summarised available historical records, suggesting that mining proceeded until excessive roof displacements and floor heave caused the miners to pull out of this area. They reviewed a 1930 mine plan and concluded that complete pillar extraction occurred over an area of about 40 m by 40 m; however, given the expected low degree of accuracy in these historical drawings, and the snap-shot nature of such surveys, the pillar extraction area may have been much more extensive. Figure 3 shows a mine plan prepared by Pells et al. (1987) with the colliery workings from the 1890s through to the pillar extraction in June 1930 (left) and annotated 1931 photographs of the cavernous tension crack that developed above Dogface Rock. A fault is mapped parallel to the cliff and the landslide rear release surface, described by Pells and Hammon (2009) as a subvertical fault that offset the Katoomba Seam. The magnitude of offset is uncertain, and the fault does not appear on current geological maps; however it is possible that this structure preconditioned the cliffline in this area to the complex toppling failure that initiated in 1931.

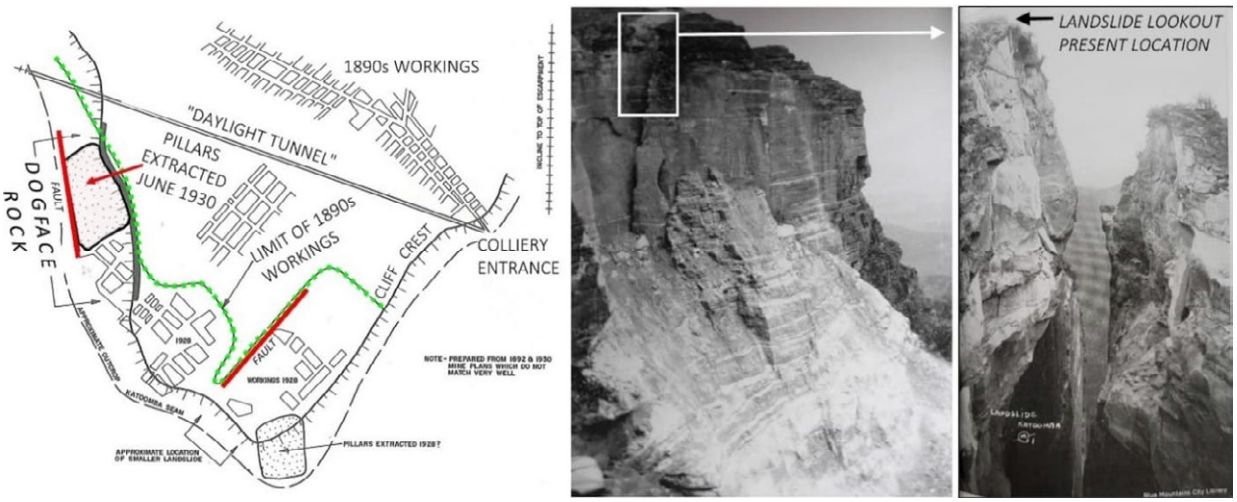

Figure 3: Mine plan at Malaita Point showing Dogface Rock in June 1930 (Pells et al. 1987) and photographs of the mining-induced tension cracking of the cliff face in early 1931 (Cameron-Smith, 2019)

The extraction of remnant coal pillars under Dogface Rock triggered a large-scale progressive brittle failure of the cliffs above the mine; however no visible surface displacements were detected for about six months. Cameron-Smith (2019) researched archived publications from newspapers including the Sydney Morning Herald, the Blackheath Bulletin and others in an attempt to constrain the chronology of the cliff failure. The earliest indication of incipient instability was

apparently observed by a local mine worker who reported the appearance of a 15 cm wide tension crack at the crest of the cliff in December 1930, six months after pillar extraction. Within 24 hours the tension crack dilated up to 1.8 m wide and propagated up to 90 m deep; several weeks later the tension crack widened to a 4 m aperture.

Historical newspaper records describe how tourists from Sydney began travelling to Katoomba, hoping to witness the collapse. The tension crack continued to grow during January 1931, and visitors to the site reported hearing periodic loud cracking or bursting noises as new tension fractures initiated, propagated, and widened, causing minor peripheral rockfalls to occur, evidenced by occasional dust clouds observed around the site as of 24 January 1931. These precursory cracking events and rockfalls suggest progressive development of extensile strain and rock mass damage as the cliff crest began to tilt into the valley, with rock mass damage accumulating as the eventual failure surface began to propagate and coalesce. Cameron-Smith concluded that the largest cliff failures included four main collapse events:

- **First Collapse**: 28 January 1931 – The southern side of Dog Face Rock collapsed at about 8:30 pm; the next collapse occurred about 7.5 hours later, involving several tens of thousands of cubic metres.
- **Second Collapse**: 29 January 1931 – The northern section of the cliff collapsed at about 4 am, the failure volume was perhaps 40,000 m^3 and this caused enough vibration and noise to wake some Katoomba residents.
- **Third Collapse**, 2 May 1931 – Three months passed before the main part of the 'leaning rock' in the central cliff collapsed at about 2 pm on Saturday 2 May 1931; the estimated volume was about 100,000 m^3.
- **Fourth Collapse**, 20 June 1931 – Pells and Hammon (2009) describe a fourth collapse of some remaining or peripheral portion of the detachment zone on 20 June 1931.

4 SITE INVESTIGATION USING RPA PHOTOGRAMMETRY

The following sections present observations from an RPA photogrammetry and discrete element method numerical modelling investigation of the landslide with focus on the morphology of the landslide detachment scar and evidence for the role of brittle fracture in the progressive cliff collapse events.

4.1 RPA SURVEY METHODOLOGY

The site was photographed using a Mavic 2 Pro quadcopter RPA equipped with a one-inch (13.22 mm x 8.8 mm) CMOS sensor with 20 MP resolution, flown manually around the site to capture a total of 879 photographs from oblique and nadir (downward-facing) viewing angles. Georeferencing was achieved using a series of nine ground control points marked in temporary chalk across outcrops and large boulders on the colluvial slope and at the crest of the cliffs around Landslide Lookout, surveyed using differential GPS to achieve an average spatial accuracy of 22 mm.

The Structure-from-Motion (SfM) photogrammetry software *ContextCapture* (Bentley, 2022) was used to build a 3D model of the site. Sequential photographs overlap by about 80% and the median ground sample distance (GSD) or resolution of a pixel on the ground is 24 mm. The resulting model has a mean RMS reprojection error under 0.5 pixels, with a maximum reprojection error of 1.9 pixels, suggesting spatial accuracy is in the order of 50 mm or better. Figure 4 shows an isometric view of the constellation of RPA locations and a typical ground control point marked in chalk.

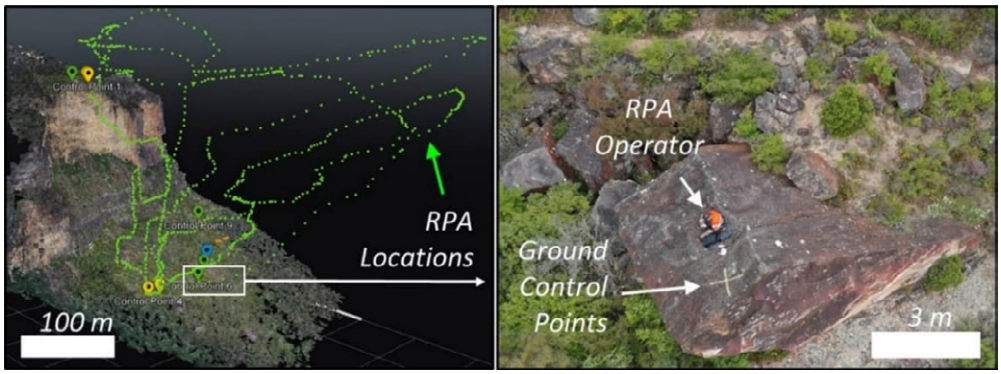

Figure 4: Isometric view of RPA survey setup and example of ground control point in the debris field

4.2 DIGITAL GEOTECHNICAL MAPPING

The photogrammetry outputs included a dense colourised point cloud and a coloured 3D mesh for digital discontinuity trace and plane mapping. First, 3D discontinuity mapping was undertaken using the point cloud mapping software *PointStudio* (Maptek, 2020). The author trialled the software's workflow for semi-automated and manual delineation of discontinuity surfaces, developing an inventory of over 3500 measurements of orientation and persistence (maximum trace length). For comparison, a detailed manual 3D mapping exercise was then carried out using the 3DM Analyst geotechnical mapping software (ADAM Technology, 2022), manually fitting 2D discs to a smaller but representative sample of discontinuity traces and planar exposures (n = 186). Figure 5 compares the discontinuity segments identified in each software package, along with the corresponding stereographic plot of the main discontinuity sets, and histogram of discontinuity trace length or disc diameter.

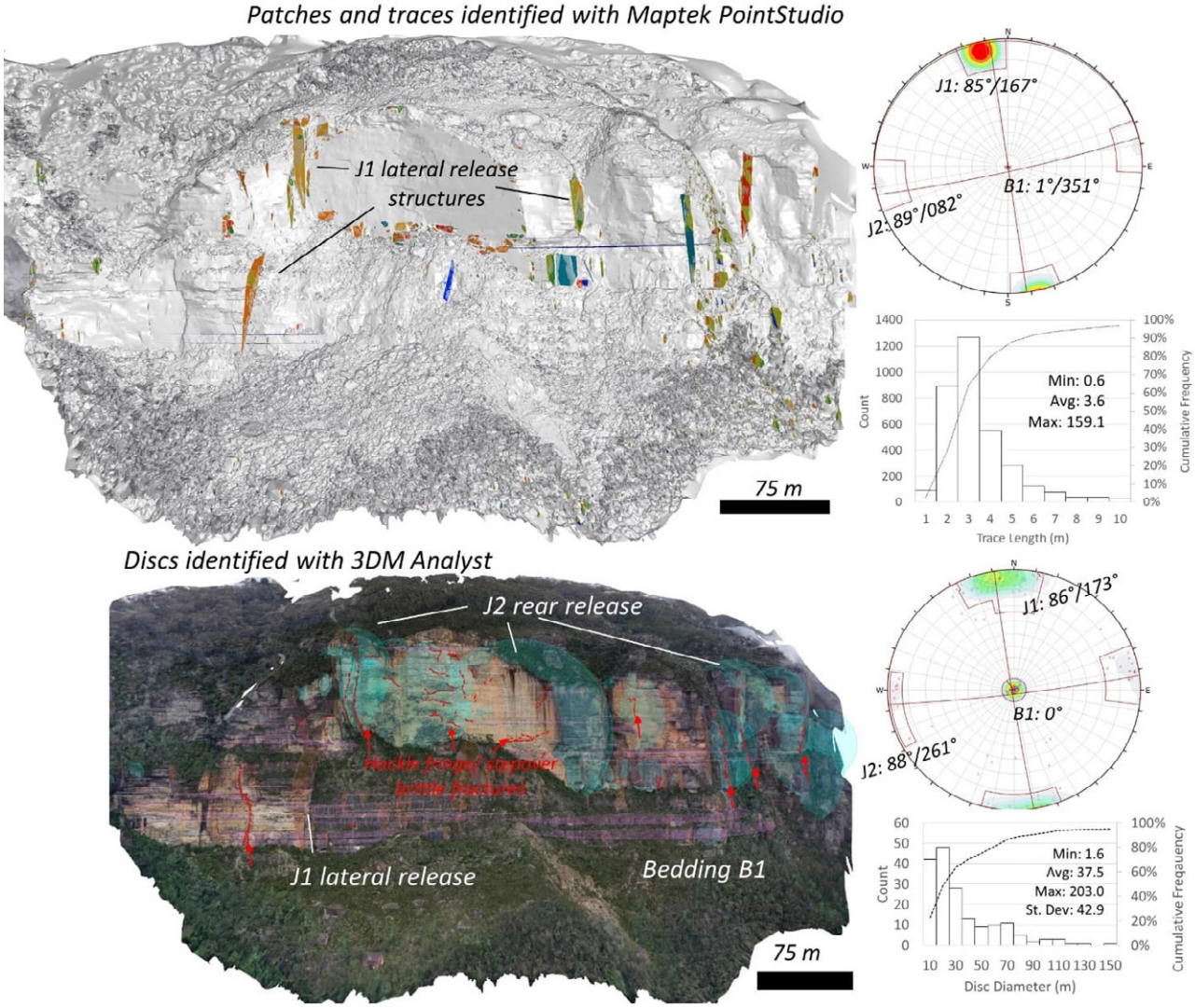

Figure 5: Digital discontinuity mapping of the 3D photogrammetry model (looking east)

The two main joint sets are subvertical and trend WSW-ENE and NNW-SSE, parallel and perpendicular to the landslide detachment scar, suggesting that these played a key role in the development of the lateral and rear release surfaces of the 1931 landslide. Brittle fractures traced in red using 3DM analyst show how the landslide failure surface developed by propagation across pre-existing bedding and joints; the northern (left side of Figure 5) lateral release surfaces are subvertical, following the overall orientation of joint set J1, but at the overall slope scale are curved and irregular, suggesting that although pre-existing joints provided initial kinematic potential for lateral release, there was a significant component of brittle fracture of intact rock involved in the propagation of pre-existing joints, culminating in the coalescence of the eventual rupture surface.

The mean orientations are similar in both datasets, despite an order-of-magnitude difference in sample size. In contrast, the discontinuity trace length and disc diameter data are markedly different between the two datasets: the *PointStudio* data include many small, automatically identified discontinuity patches with low persistence, with the histogram showing a peak at a trace length of 3 m and a 50th percentile trace length of about 2.5 m. In contrast, the manually mapped *3DM Analyst* data reflect an intentional focus on mapping the most persistent bedding traces and joint planes exposed in the cliff face, with a peak frequency and 50th percentile disc diameter of about 20 m.

In this geological setting, the author considers that the geotechnical site model should treat bedding discontinuities as fully persistent and represent the persistence of the two main joint sets based on upper-bound estimates derived from measuring the longest traces and largest planar exposures in the cliff face. These results highlight the importance of skilled geological interpretation of rock mass structure before undertaking semi- or automated mapping of the slope.

Discontinuity spacing was measured using an algorithm built into the *3DM Analyst* package that first generates a mean plane for each structural set, and then constructs an array of scanlines normal to the plane, with at least 400 scanlines passing through the smallest disc in the set. For each scanline, the algorithm records the distance from the mean set plane to each intersected discontinuity in order to collect an inventory of many discrete spacing measurements. Figure 6 illustrates the concept of the algorithm, plotting distances to joint intersections at D1 and D2 along a scanline perpendicular to the mean set plane, and three plots showing the change in median, first quartile (Q1) and third quartile (Q3) spacing produced by artificially increasing the diameter of every mapped disc to from 100 m to 500 m to approach an adverse case of fully persistent discontinuities.

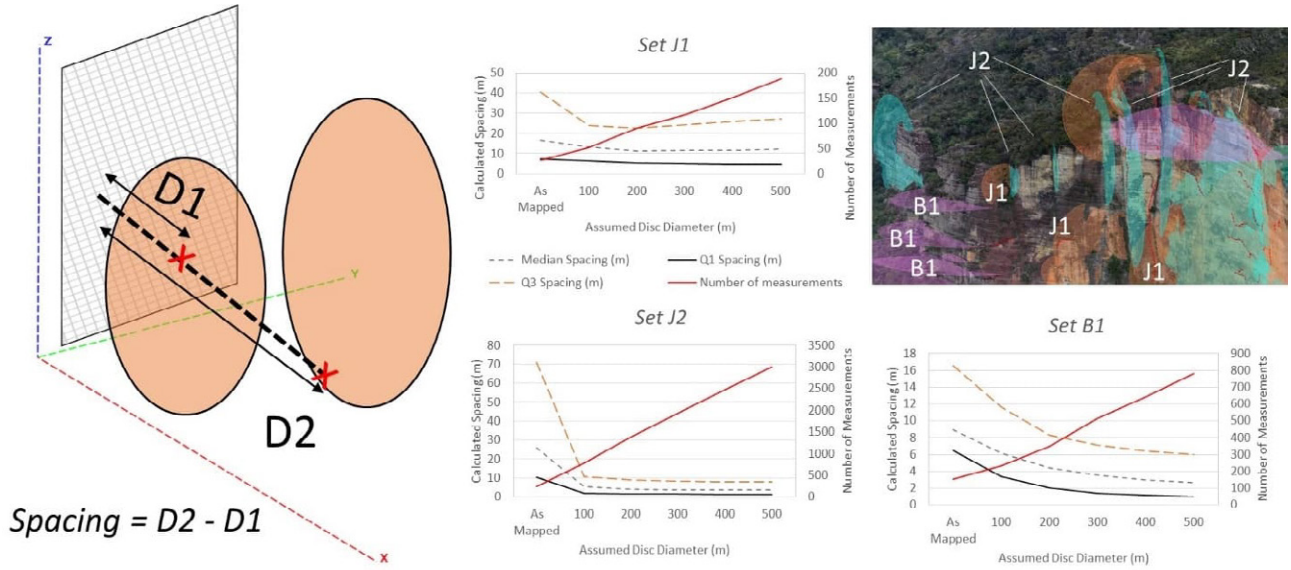

Figure 6: Estimation of discontinuity spacing using scanlines perpendicular to the mean set plane

The graphs in Figure 6 show how increasing the disc diameter (i.e. artificially increasing the size of the mapped discontinuities) increases the likelihood that any given scanline will intersect more discontinuities, therefore increasing the fracture frequency or P_{10} (Dershowitz and Herda, 1992) along the scanline and reducing the apparent spacing. Third quartile estimated spacing decreases by about 50% when the discs are increased from the "as mapped" persistence up to an artificial value of 100 m, while further increases in disc diameter have a less pronounced effect. The author suggests that increasing disc diameter to 100 m for a mapping domain of these dimensions produces a reasonably conservative estimate of discontinuity space for incorporation into discrete element method numerical models.

The photogrammetry model also shows clear evidence of irregular brittle fractographic features on the landslide detachment scar that suggest discrete episodes of brittle fracture initiation and subsequent propagation were associated with the progressive development of the 1931 failure surface:

- The upper vertical cliff face shows evidence of high persistence curved and stepped irregular brittle fractures traces that appear to have propagated both horizontally and vertically, suggesting interaction between persistent bedding discontinuities and incipient, non-persistence subvertical joints from set J1 and J2

- The main vertical rear release surface of the landslide is a composite surface comprised of two major planar surfaces oriented 88°/257° and 87°/086° (dip/dip direction) that merged during the progressive failure leading up to the collapse. The hinge or transition zone between these two major surfaces is characterised by very high persistence traces of irregular and curved step-over brittle fractures that resemble a hackle fringe; these are fractographic features typically occurring on the fringes of a propagating tension fracture (Mandl, 2005).

Recently formed strata-bound tension fractures in sedimentary rock tend to terminate against older bedding foliation; however, this does not always occur, as tension joints may also propagate directly across bedding foliation, or step sideways along bedding before continuing into adjacent strata (Mandl, 2005). The fractographic features of the landslide scar suggest that brittle tensile fracture played a prominent role in the development of the release surface in the propagation of lateral and rear release surfaces in the upper Banks Wall Sandstone, and in the next section a 2D discrete element method numerical model is developed to investigate the relative contributions of shear and tension fractures in the coalescence of the failure surface and the subsequent landslide runout.

5 DISCRETE ELEMENT MODELLING WITH THE BONDED BLOCK METHOD

5.1 THE BONDED BLOCK-TRIGON METHODOLOGY

The bonded block method (BBM) is a subset of the discrete element method, where intact material is represented using an assembly of 2D polygons or 3D polyhedra with strong, stiff contacts; breakage of the contacts in shear or tension simulates process of brittle fracture. This study applies the trigon BBM methodology in *UDEC*, which was first introduced by Gao (2013) who developed custom-built scripts for *UDEC* and *3DEC* that converted continuum meshes into assemblies of discrete triangular or tetrahedral blocks. Gao used the trigon method to simulate UCS and Brazilian test results on weak coal measures rock, and to analyse roof failure of underground coal mine roadways. The trigon discretisation functionality was later incorporated directly into the *UDEC* and *3DEC* programs.

The functionality of the BBM approach for modelling brittle rock failure has been researched in diverse geological environments. Turichshev (2016) used a 3DEC-BBM workflow to simulate triaxial tests on veined andesite from El Teniente mine in Chile. Ghazvinian (2015) used a modified approach with 3D elongated Voronoi grains, modelled after the Cobourg Limestone in Canada. Azocar (2016) compared UCS and tunnel-scale brittle failure mechanisms in tetrahedral and Voronoi BBM models, showing how the interlocking shape of Voronoi models produces a stiffer macroscopic response than triangular or tetrahedral models with equivalent contact parameters. Azocar also showed how failure of Voronoi models tends to occur by localised tensile failure, producing rough, irregular failure surfaces. In contrast, triangular and tetrahedral models are predisposed to shear failure of contacts and tend to form smooth failure surfaces, making this discretisation approach well suited to simulation of shear failure in weaker rock (Tuckey, 2020).

For this investigation, the BBM-trigon approach is used to simulate two rock types: (1) the massive quartzose sandstone making up the upper cliffs, and (2) the more closely bedded and jointed, weaker interbedded shale, sandstone, and laminite horizons of the underlying Burra-Moko Head Sandstone, Caley Formation, and Illawarra Coal Measures. The laboratory scale simulations aim to reproduce published UCS and tensile strength for the Triassic sandstone and shale formations found in Sydney. The target parameters of the upper sandstone unit are based on a Class I Sandstone and the underlying interbedded sandstone/shale unit is simplified as a Class I/II shale according to the Sydney Rock Mass Classification System (Oliveira, 2014; Bertuzzi and Pells, 2002). Contact stiffness is calibrated by setting the normal stiffness j_{kn} based on the target intact rock deformation parameters. Christianson et al. (2006) and Itasca (2011) developed recommendations for estimating contact normal stiffness in 2D bonded Voronoi models according to the typical minimum grain edge length:

$$j_{kn} = n\left(\frac{K+\frac{4}{3}G}{\Delta Z_{min}}\right) \tag{1}$$

Where K and G are the bulk and shear moduli of the simulated material and Δz_{min} represents the bonded block length. This investigation found an n value of 25 was able to match the Young's Modulus of the reference intact rock materials. In setting the shear to normal stiffness ratio, Gao and Stead (2014) and Kazerani and Zhao (2010) showed how contact shear stiffness can be related to the ratio of Shear Modulus to Young's Modulus of the reference intact rock:

$$\frac{j_{ks}}{j_{kn}} \approx \frac{G}{E} \tag{2}$$

After adopting an assumed friction angle (Gao and Stead, 2014), the contact c/σ_t ratio is fixed, and the input c value is varied until the reference UCS is achieved; potentially requiring refinement to the c/σ_t ratio to achieve the target uniaxial tensile strength. To promote stress localisation and brittle fracture initiation, the models need to introduce heterogeneity into the BBM contacts, so that contacts with lower cohesion and tensile strength create preferred sites for fracture initiation. The numerical models presented here assign contact cohesion and tensile strength according to a normal distribution with standard deviation equivalent to 10% of the mean.

5.2 SIMULATED LABORATORY TEST RESULTS

The laboratory scale models simulate a rock specimen 50 mm wide and 100 mm tall, with bonded elastic trigon blocks of 2 mm edge length, bounded by frictionless steel platens. All tests apply axial load with a constant upper and lower platen velocity of 1 mm/s for UCS tests and 0.1 mm/s for direct tension tests (numerical time). Table 1 summarises the target intact rock and calibrated model parameters. Scaled values of the shear strength parameters are indicated in parentheses, representing "rock block scale" parameters for the larger 2.5 m bonded trigon blocks applied to the cliff-scale back analysis of the 1931 landslide; the scaled parameters downgrade the target UCS and tensile strength by adopting an equivalent "block scale" GSI of 90; the scaling approach is discussed further in the next section.

Table 1: Summary of geotechnical material parameters

Material Parameters		**Upper Unit: Sandstone**	**Lower Unit: Interbedded Sandstone/Shale**
Target Intact Rock Parameters *(Rock block scale; GSI = 90)*	UCS (MPa)	25 (14.3)	10 (5.7)
	σ_t (MPa)	2.5 (0.7)	1.0 (0.6)
	E_i (MPa)	6000	3000
Laboratory Scale Bonded Block Contact Parameters *(Rock block scale; GSI = 90)*	Mean σ_t (MPa)	3.6 (2.1)	1.6 (1.0)
	Mean c (MPa)	11.1 (6.4)	5.1 (2.9)
	φ	35°	30°
	k_n (Pa/m)	9.0×10^{13} (7.2×10^{10})	4.5×10^{13} (3.6×10^{10})
	k_s (Pa/m)	1.8×10^{13} (1.4×10^{10})	9.0×10^{12} (7.2×10^{9})
	Measured UCS (MPa)	25.9 (14.1)	10.0 (5.9)
	Measured UTS (MPa)	2.5 (1.4)	1.0 (0.7)

Figure 7 shows results for the laboratory-scale simulations on the upper sandstone rock (top) and the lower shale unit (bottom). Plots of axial stress and cumulative crack length versus axial strain are presented next to images of the post-peak cracked condition of each specimen. Crack length is plotted on a logarithmic scale to highlight how fracture initiation in UCS tests begins with tension cracks occurring at about 50% of peak strength, within the typical range reported by Diederichs and Martin (2010).

The UCS failure mechanism is characterised by pre-peak accumulation of tensile damage starting after axial stress exceeds 40% to 50% of UCS, with shear crack length increasing rapidly as the tensile cracks begin to interact at an apparent crack damage threshold σ_{cd} of about 80% of UCS. In contrast, the UTS failure mechanism is involves rapid propagation of a tensile failure surface at peak tensile strength. These results conform to mechanism described by Diederichs (2007) that failure in bonded particle UCS tests occurs via a "group effort" of tensile crack damage accumulation, interaction, and coalescence. In contrast, when rock is loaded in direct tension, the first crack "wins". In the next section, these calibrated parameters are adapted for a rock mass scale trigon simulation of the mining-induced collapse of the cliff at Dogface Rock in 1931.

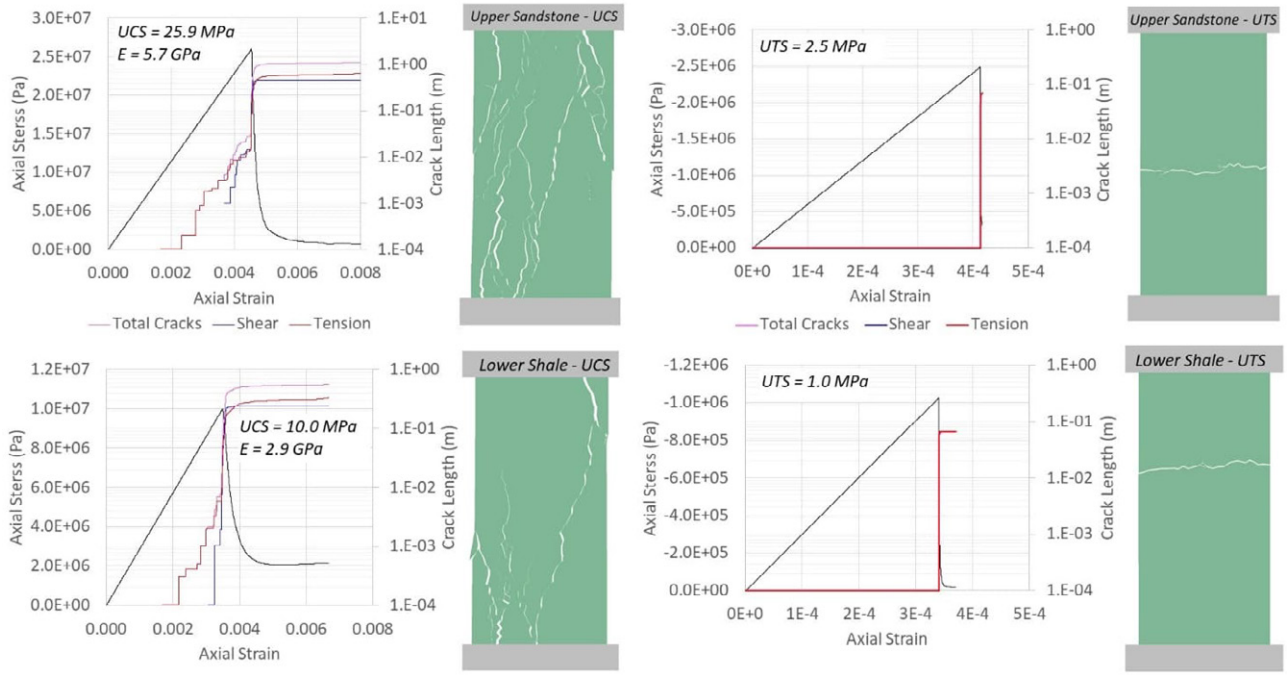

Figure 7: Stress and cumulative crack length versus axial strain for simulated UCS and UTS calibration

5.3 BACK ANALYSIS OF MINING INDUCED CLIFF COLLAPSE

A 2D discrete element model of the landslide was developed from a cross section through the georeferenced photogrammetry model. The cross section is aligned with the present-day location of Landslide Lookout, roughly in the centre of the main detachment scar; the pre-failure cliff surface is extrapolated 20 m horizontally out from the current cliff. Figure 8 shows the setup of the model domains, displacement history points where modelled displacement versus calculation step was recorded, and the discretisation area of bonded trigon blocks with 2.5 m edge length.

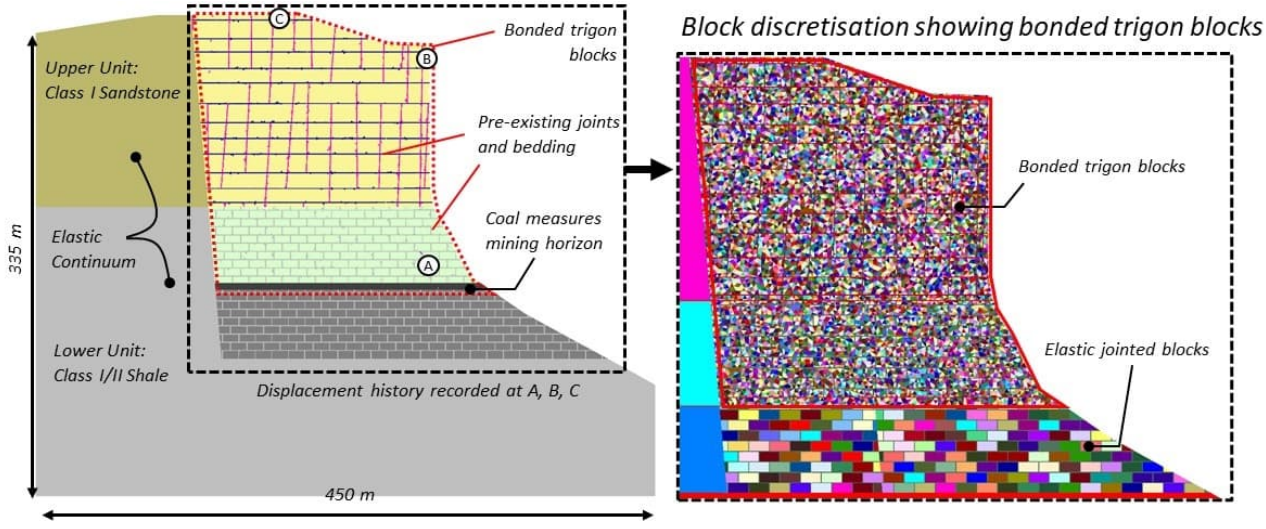

Figure 8: Model domains (left) and discretisation of individual blocks (right)

The far field elastic domain is bonded to the trigon domain using construction joints with artificially large values of cohesion and tensile strength to ensure smooth transfer of stress and displacement across this artificial interface. Rock fracturing is monitored by recording the number and cumulative length of bonded trigon contact failures in tension and shear. The upper sandstone unit has pre-existing horizontal bedding and very high persistence, widely spaced subvertical joints reflecting the mapping data from the photogrammetry model; whereas the lower unit is modelled on Class I/II Shale and is modelled with a regular, closer spaced network of joints and bedding.

The 2.5 m bonded trigon blocks are too large to represent laboratory scale intact rock free of any discontinuities; instead, they represent larger *in situ* rock blocks that contain discontinuities that are too small to resolve explicitly. As a consequence, the bonded trigon contact parameters have been scaled to account for the reduction in expected shear strength and stiffness of these rock blocks relative to laboratory scale specimens. Figure 9 illustrates the "effective block" concept of Bandis (2004), where in this case the effective block is discretised into a bonded trigon assembly with scaled shear strength and stiffness parameters.

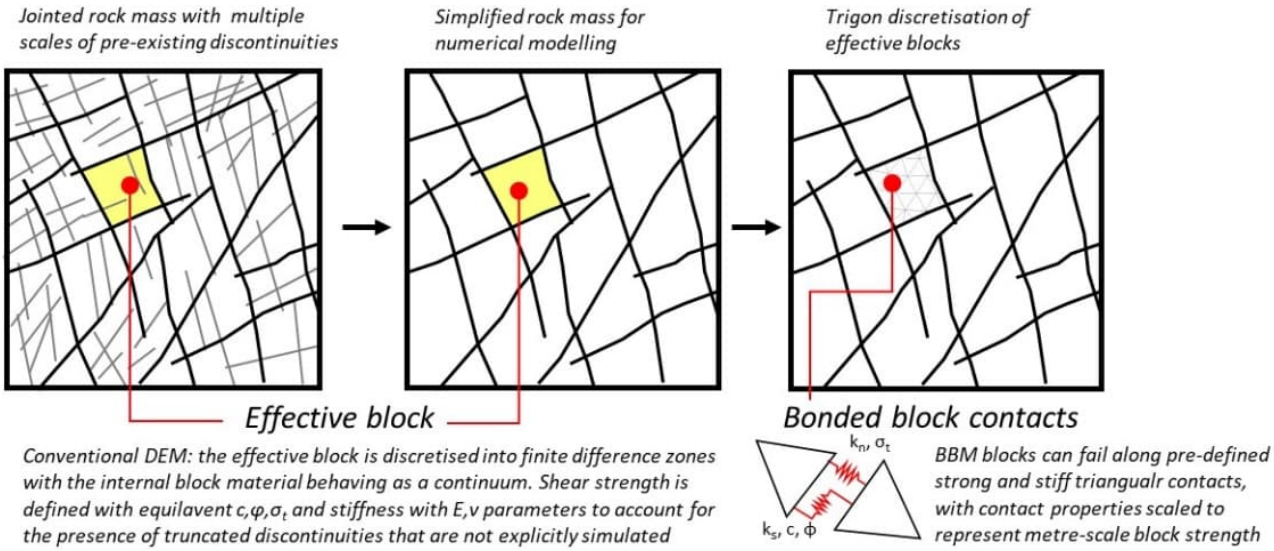

Figure 9: Conceptual illustration of an "effective block" for numerical modelling (after Bandis, 2004)

The target rock block strength is estimated using the Hoek-Brown criterion: whereas the laboratory scale simulations consider an effective GSI of 100, the 2.5 m block is downgraded to a GSI of 90, after the approach described by Oliveira (2014), thus reducing the block scale UCS and tensile strength. Table 2 summarises the rock block and discontinuity material parameters adopted in the cliff scale model.

Table 2: Summary of cliff scale model material parameters

Model unit	Material parameters	Cohesion (MPa)	Friction angle (°)	Stiffness parameters
Upper Sandstone Unit	Joints	0	36	j_{kn} = 10 GPa/m j_{ks} = 1 GPa/m
	Bedding	0.02	32	j_{kn} = 6 GPa/m j_{ks} = 0.6 GPa/m
	Elastic continuum blocks	-	-	E = 4 GPa υ = 0.25
	Bonded trigon blocks	-	-	E = 6 GPa υ = 0.25
Lower Interbedded Shale/Sandstone Unit	Joints and Bedding	0	28	j_{kn} = 6 GPa/m j_{ks} = 0.6 GPa/m
	Elastic continuum blocks	-	-	E = 2 GPa υ = 0.25
	Bonded trigon blocks	-	-	E = 3 GPa υ = 0.25

The bonded block stiffness parameters are scaled by decreasing the stiffness according to equation (1) where Δz_{min} reflects the 2.5 m block size. The left and right boundaries of the model are fixed in the horizontal direction, and the base of the model is fixed in the vertical direction. Pre-mining *in-situ* stresses are initialised according to the overburden height, with the out-of-plane stress set to $0.61\sigma_v$ after Oliveira and Parker (2014) who undertook a comprehensive review of published *in situ* stress measurements throughout the Sydney Basin.

High horizontal compressive stresses are present elsewhere in the region; however, it is expected that topographic effects of the cliff line produced local stress relief around the Katoomba Colliery near its interface with the valley slope. While the author recognises that high horizontal stresses have been measured in colliery roofs such as at Nattai North (Enever and McKay, 1980), these areas of high stress are typically concentrated under the floor of incised valleys. The Katoomba Colliery is at an elevation of approximately 800 m AHD, and the valley slope continues down to approximately 570 m AHD, about 230 m below the mining horizon. The location of the colliery well above the valley floor, and within about 100 m of the slope face, suggests that the pre-mining in situ stresses should more closely approximate a lithostatic condition than a condition of high horizontal major principal stress σ_1.

After initialising the stresses, the model is cycled to equilibrium using elastic material parameters, before applying the plastic Mohr-Coulomb properties to the discontinuities and bonded block contacts, and then cycling again to equilibrium. Figure 10 shows the displacement contours and failed trigon contacts at the initial pre-mining equilibrium, including a gridded heatmap of fracture intensity P_{21} (fracture length per square metre) measured across the model domain using 10 m square grid cells to highlight the spatial distribution and intensity of induced rock mass damage.

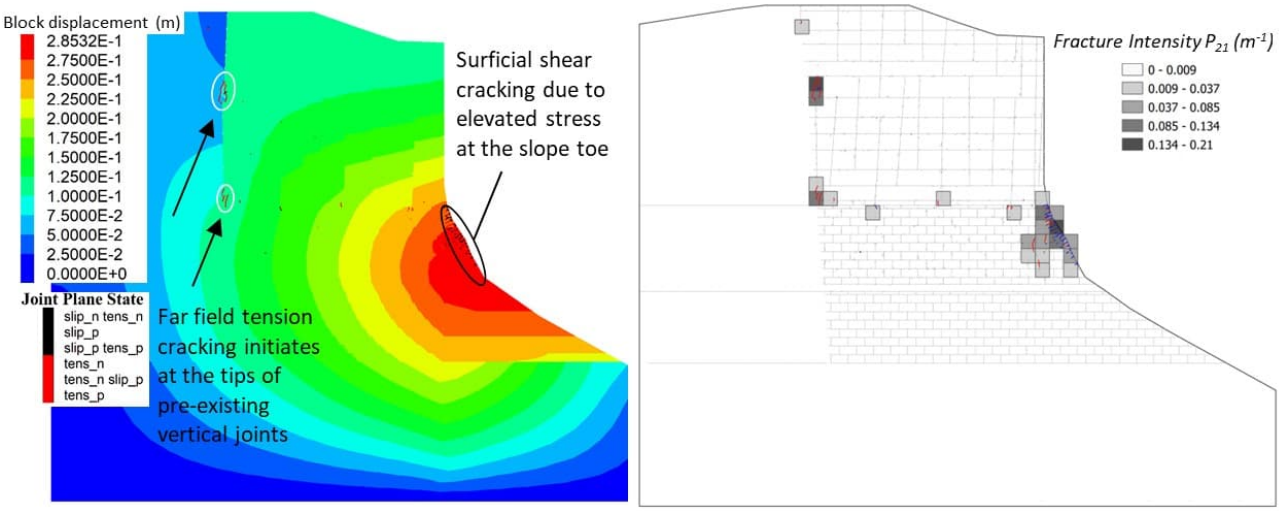

Figure 10: Displacement contours and fracture intensity map at pre-mining equilibrium state

Far-field tensile fracturing initiates from the tips of pre-existing vertical joints near the boundary of the bonded trigon discretisation zone. This behaviour may partially be attributed to boundary effects occurring at the interface between the far-field elastic continuum zone at the left side of the model, and the finely discretised trigon area. However, this may also be indicative of the mechanisms of slope damage that can develop under long-term gravitational loading and slope relaxation that is expected to occur as part of the escarpment retreat process.

After equilibrium is reached, model displacements are re-initialised to zero to monitor the magnitude of mining-induced displacement. The mine workings are excavated from the coal measures layer at the base of the bonded trigon zone, about 175 m below the crest of the cliff. Five mining panels of 10 m width and 5 m height are excavated in sequence, separated by 10 m wide pillars, solving the model to equilibrium after each mining stage. The precise dimensions of the historical mine workings are uncertain; however, it is likely that the Katoomba Seam was not more than 3 m thick at this location. The enlarged dimensions of the workings are a necessity of the numerical model resolution, and although the modelled panels are slightly taller than the true dimensions of the historical workings, it is expected that the simulated rock mass response will involve similar magnitude and orientation of induced of stress redistribution, fracturing, and rock mass failure mechanisms in the mine roof and pillars. Figure 11 presents displacement contours and fracture intensity maps for the equilibrium states reached after the first and fifth stage of mining respectively.

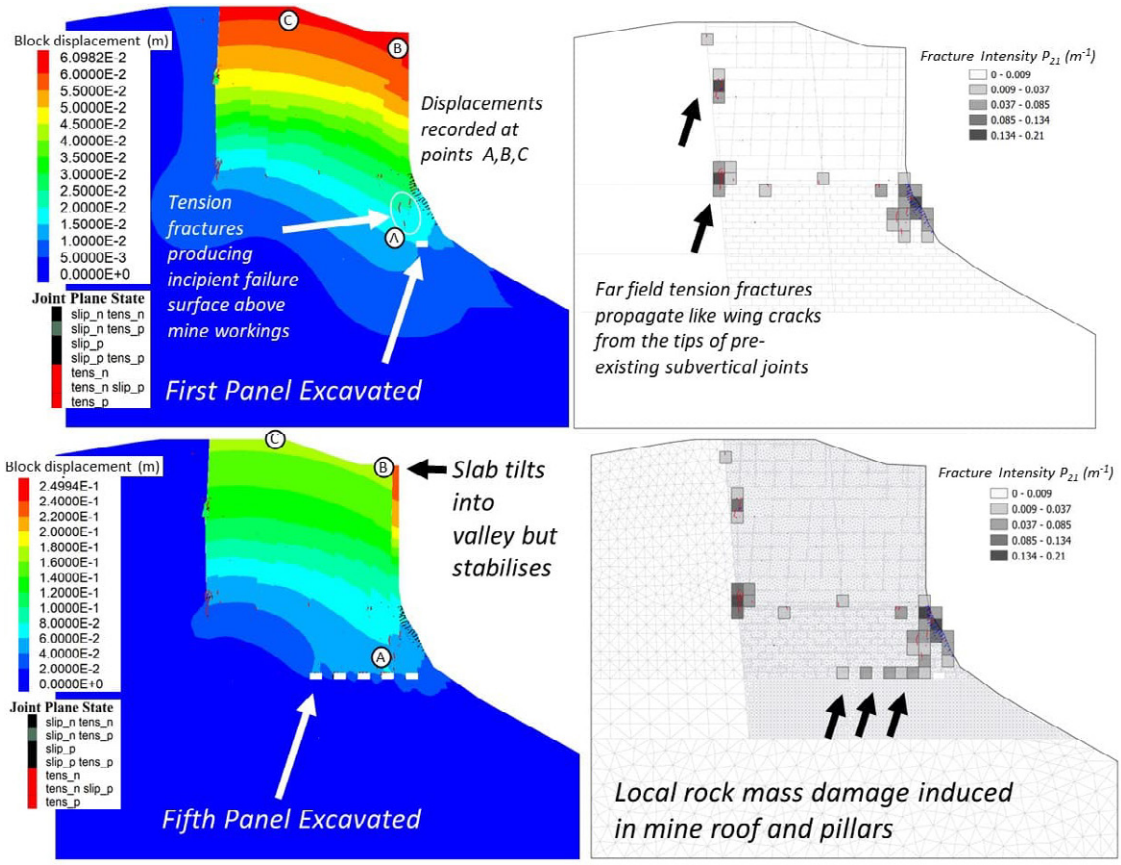

Figure 11: Displacement contours and fracture intensity map at first and fifth stages of panel excavation

After mining the fifth panel, the model converges to an apparently stable equilibrium with an unbalanced force ratio less than 10^{-6} and displacement and cumulative crack length trending towards constant values. The results show how progressive excavation of the mining panels causes fracturing (rock mass damage) to develop in the mine roof and pillars, and also around the toe of the slope, above the mine workings, where the pre-mining state was already pre-conditioned with damage induced during the initial pre-mining equilibrium solution.

A displacement hotspot develops at the crest of the cliff, where a stochastically generated subvertical joint produced a slab of sandstone 5 m thick that begins to tilt 250 mm into the valley before reaching equilibrium. Figure 12 shows the displacement versus calculation step at points A, B, and C (as shown in Figure 11), highlighting the calculation step where each panel is excavated, showing the corresponding increases in the rate of cracking and slope displacements (horizontal displacement *dx* and vertical displacement *dy*) after every mining stage.

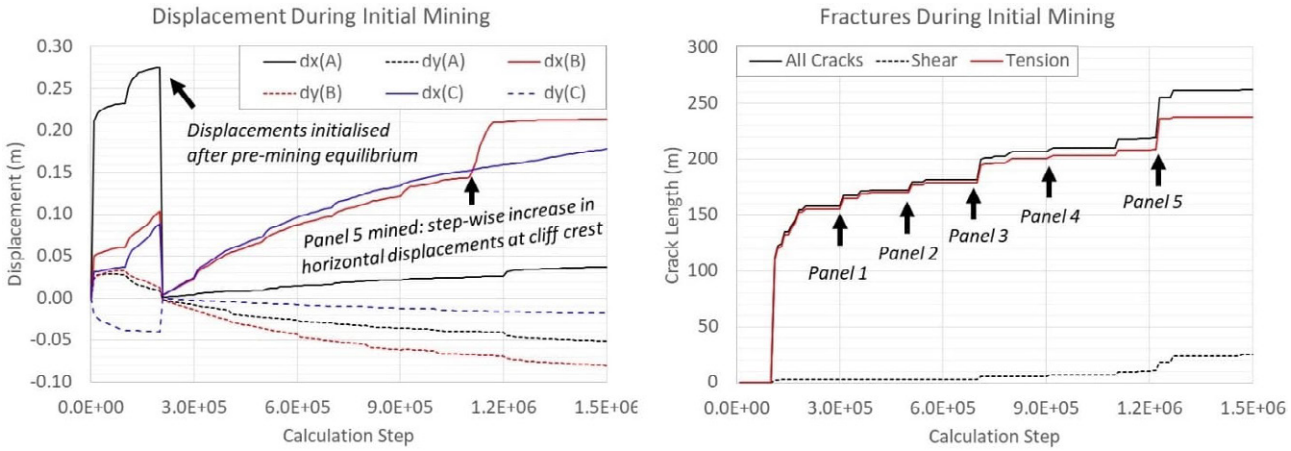

Figure 12: Displacement and cumulative crack length during five stages of initial mining

After the five mining panels are excavated, the model is solved to equilibrium, with this state conceptually representing the condition of the colliery after mining stopped in 1905, but before the resumption of mining in 1925 and the pillar robbing that occurred immediately under and downslope of the cliff crest in mid-1930. The slope is at equilibrium, despite the induced displacements at the cliff crest. The next modelling stage simulates extraction of a single 10 m wide pillar on the downslope side of the workings, below the cliff crest, as occurred around June or July 1930 (Figure 13).

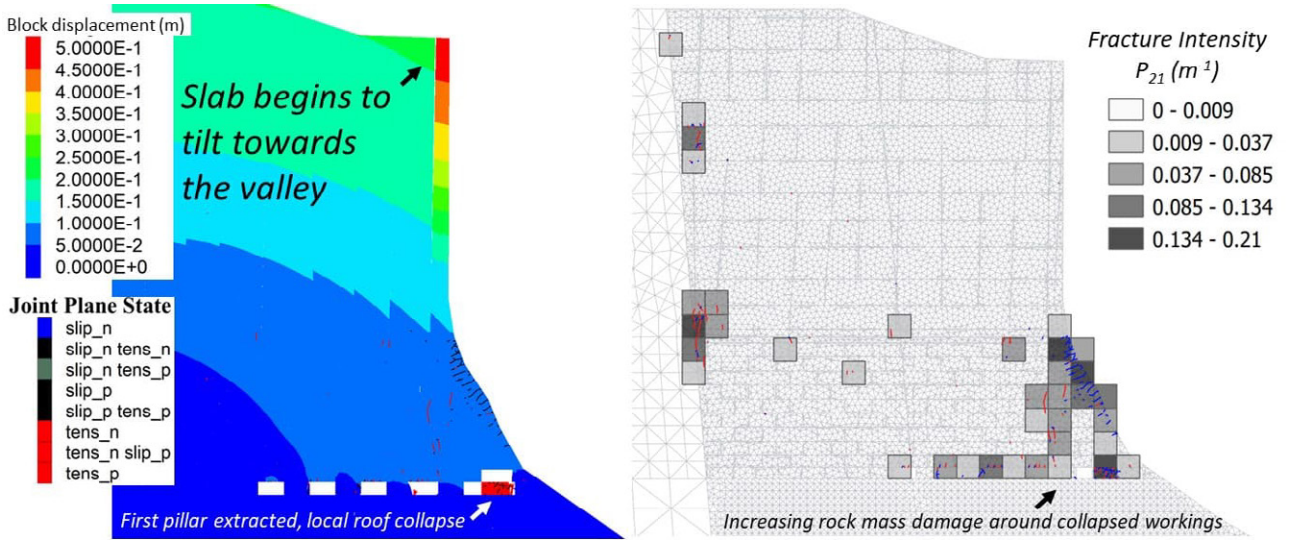

Figure 13: Displacement contours and fracture intensity map after extraction of the first pillar

A roof collapse occurs above the extracted pillar, and the fracture intensity around the mine workings undergoes a small stepwise increase. It is important to consider that no ground support elements are included in the model; this is considered appropriate as the passive timber props likely used during mining were not sufficient to support the excavation, as indicated by Pells and Hammon (2009) who described how excessive displacements developed in the mine, and caused the miners to pull out of this area after pillar extraction began. Horizontal displacement at the crest of the cliff (history point B in Figure 11) begins to increase and reaches approximately 0.43 m before the model reaches equilibrium with an unbalanced force ratio of 10^{-6} which broadly indicates global stability.

After the model reaches equilibrium, a second pillar was then extracted from the down-slope side of the cliff, which leads to rapid increase in the crack rate and initiation of the global collapse, with the horizontal displacement at the cliff crest reversing direction back towards the escarpment, suggesting the initiation of a "reverse toppling" mechanism as described by Cunningham (1988) for a similar mining-induced cliff collapse at nearby Nattai North in the 1970s. Figure 14 shows the displacement and crack histories after the extraction of the first and second pillars down-slope of the cliff, and then for a further 140 million calculation timesteps during the subsequent collapse and runout.

Global collapse initiates after the second pillar is extracted. Four stages of the landslide can be delineated based on the rate of bonded trigon contact failure (stages A, B, C, and D in Figure 14). Stage A encompasses the first 10 million calculation timesteps, during which trigon contact failure rapidly increases as the basal rupture surface begins to propagate and coalesce. Stage B extends from 10 M to 27 M calculation steps, where the rate of crack growth decreases as the basal rupture surface is fully formed, and new fractures occur mostly within the basal unit of interbedded shale and below the massive sandstone of the upper cliff.

Stage C occurs between 27 M and 64 M calculation steps, where the rate of crack growth again decreases as the "reverse topple" transitions to a rock avalanche, with the failure volume travelling downslope; new crack growth occurs mostly via the breakup of the collapsing upper sandstone slab. Stage D occurs after 64 M calculation steps, with crack growth decreasing again; new cracks appear to mostly involve further comminution of the slide mass during runout. Notably, during all stages of the model, from initial mining through to landslide runout, fracturing is dominated by tensile failure of bonded block contacts, with tensile crack length exceeding shear crack length by a factor of 3 to 5. The result highlights how the landslide develops by damage accumulation, characterised by local tensile fracture initiation, propagation, and interaction, before these cracks coalesce to form macroscopic shearing surfaces.

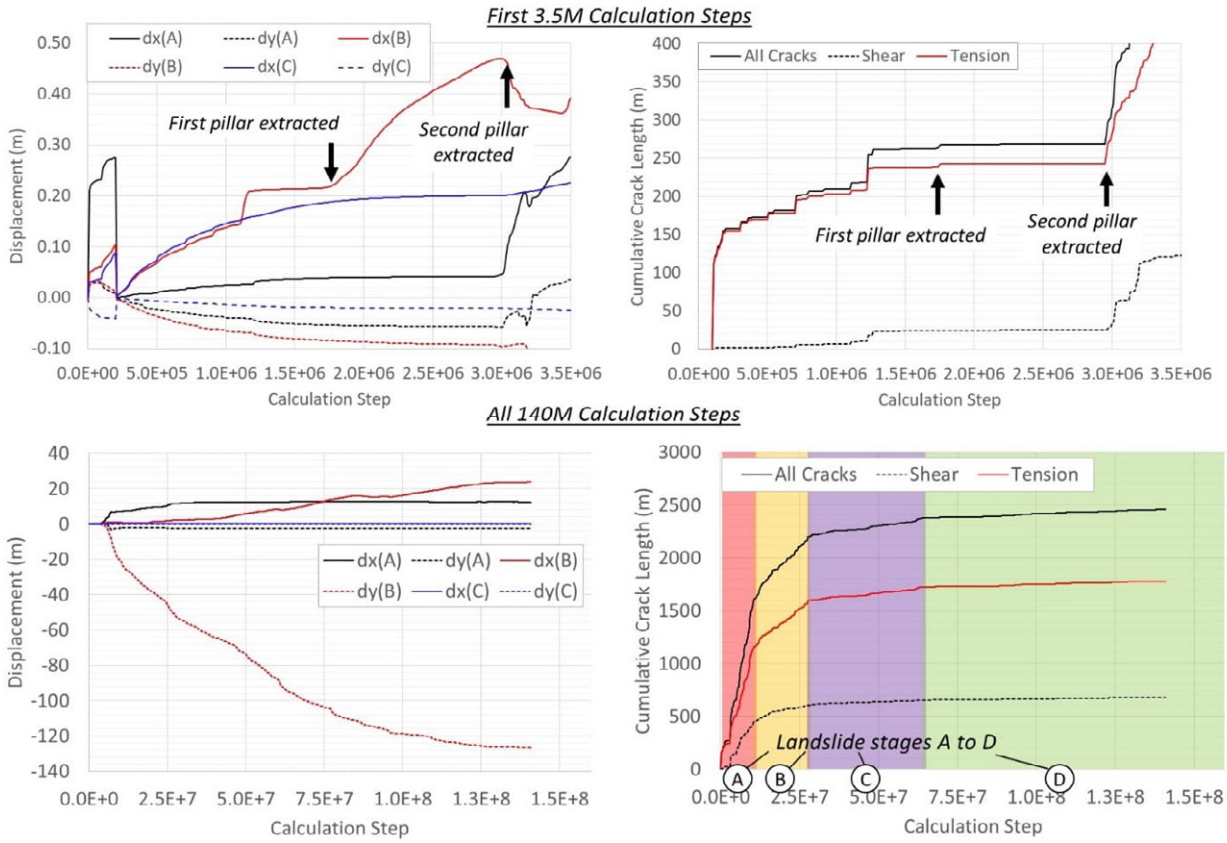

Figure 14: Displacements and cumulative crack length during pillar extraction and subsequent collapse

Figure 15 shows representative plots of displacement and fracture intensity maps at each stage of the landslide after the second pillar extraction, up to a maximum of 140 million cycles. The fracture heat maps are based on the instantaneous state of bonded trigon contacts failed in shear and tension at the pictured timestep.

The plots highlight how the failure of bonded block contacts in tension leads to the formation of the basal rupture suface in Stage A, followed by intense fracturing and dilation of the lower shale rock unit, enabling kinematic freedom to develop for a complex toppling failure that transitions into a rock avalanch as the failure volume disintegrates and flows downslope.

The collapse sequence involves initial failure of an outer sandstone slab 5 m thick, before progressively opening along another pre-existing vertical joint a further 10 m behind the initial cliff face. Although the model is not calibrated to real time, this retrogressive slab failure broadly reflects a historical report from 31 January 1931 that noted "…another crack has started [to open] about 25 yards back the original fissure" (Blue Mountains Star, 1931), suggesting that an outer slab began to detach before the initiation of a larger failure a further 10 m behind the initial tension crack.

The upper sandstone rock mass descends vertically as the basal shale unit disintegrates and runs out onto the talus slope. The sandstone eventually breaks apart into large boulders that are transported along the upper surface of the runout debris, forming large cubic to rectangular blocks with edge length up to 10 m. The block sizes of the debris broadly reflect observations of massive cubic to rectangular prismatic boulders of up to 10 m deposited in the debris field. After 140 M calculation steps the runout debris is not completely at rest; the runout angle is about 57° measured from the crest of the cliff to the furthest runout block, compared with 42° measured from crest to maximum debris extent in the photogrammetry model, suggesting that further calculation steps would be required to model the full extent of runout.

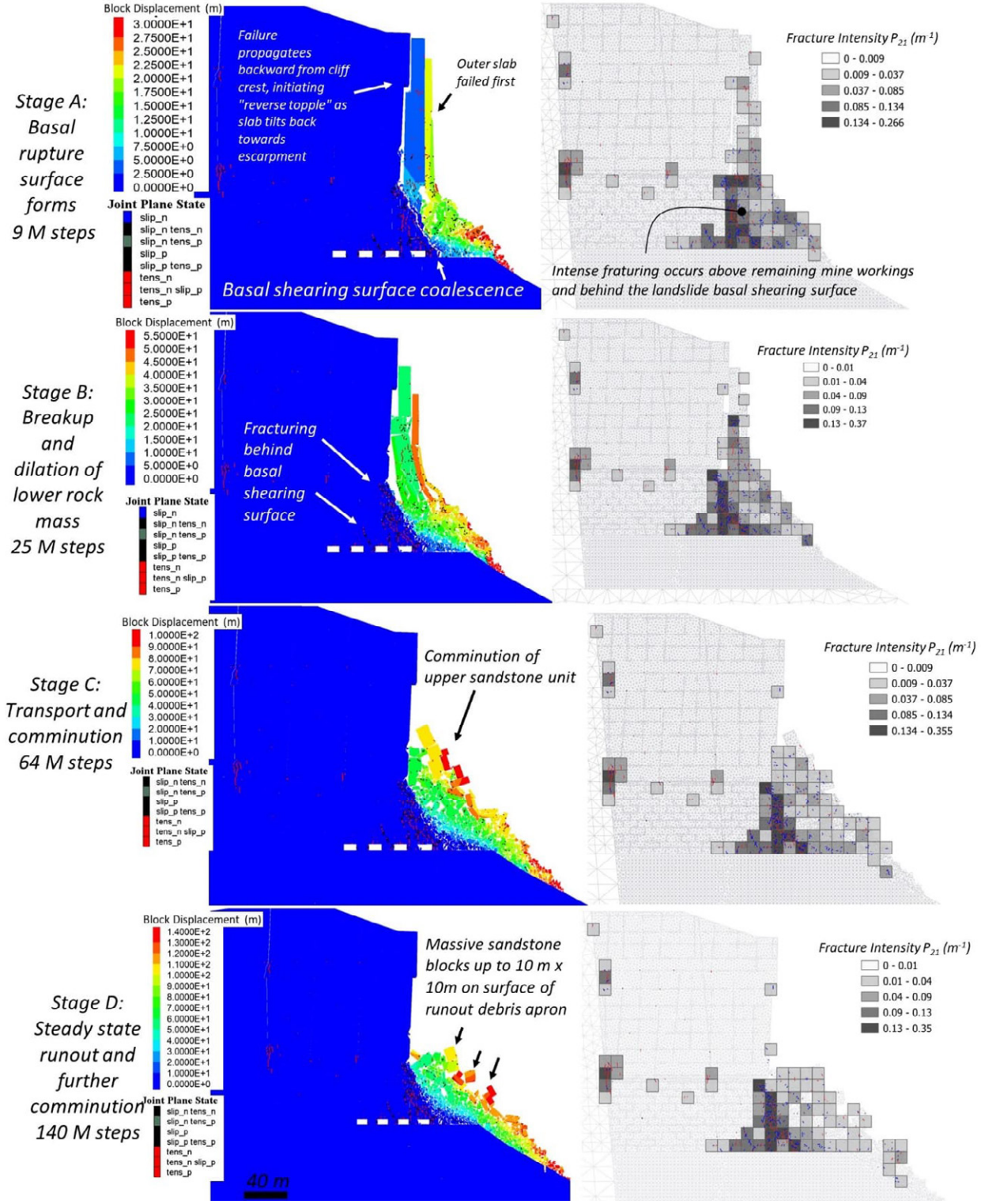

Figure 15: Displacement contours and fracture intensity maps for each stage of the simulated landslide

6 DISCUSSION

The bonded trigon analysis of the landslide shows how global failure likely developed by the progressive formation of a basal shearing surface through the interbedded shale and sandstone unit above Katoomba Colliery workings, underlying the massive Banks Wall sandstone of the upper cliffs. Pells (2008) interpreted that shearing occurred mainly through the Burra Moko Head Sandstone and partly through the underlying interbedded sandstones and mudstones, and the numerical modelling supports this conclusion.

One of the new insights provided by the bonded block back analysis is that tensile failure of bonded block contacts dominates over shear failure, by a factor of 3 to 5. Even though triangular shaped trigon blocks tend to fail more readily in shear than well-interlocked polygonal or Voronoi grains, the simulations in this investigation clearly demonstrate the role of tensile failure of rock blocks bounded by pre-existing discontinuities. The results suggest that the landslide mechanism at Dogface Rock was driven by extensile strains (evidenced by tilt of the cliff towards the valley, triggered by mining) driving tensile fracture initiation, eventually leading to fracture interaction and coalescence to form a macroscopic shearing surface.

The existence of very high persistence subvertical joints on the landslide rear release surface and lateral margins likely predisposed the cliff to this type of complex rock toppling failure, with global collapse triggered after mining-induced strains caused the crest of the cliff to tilt into the valley. As the basal shear surface begins to coalesce, the upper sandstone mass tilts back towards the escarpment, agreeing with the "reverse toppling" mechanism described by Cunningham (1988) at Nattai North. The failure then transitions into a rock avalanche as the landslide volume progressively disintegrates during transport.

7 CONCLUSIONS

This investigation has shown how RPA photogrammetry, digital geotechnical mapping tools, and discrete element method numerical modelling can be used in a holistic workflow to characterise the role of progressive brittle fracture in complex rock slope failures. The 2D bonded trigon modelling approach can be used to produce calibrated simulations of laboratory-scale intact rock parameters, and scaling these target UCS and tensile strength values using the Hoek-Brown criterion makes it possible to model brittle failure of larger metre-scale rock blocks at the overall slope scale. The simulation of a mining-induced cliff collapse at Dogface Rock shows how failure develops in a progressive manner that can be quantified by tracking the rate of crack growth, represented by the failure of bonded trigon block contacts.

Although this investigation focussed on the role of mining-induced brittle fracture in cliff collapse, the trigon approach shows promise for the assessment brittle-fracture induced landslide initiation and subsequent runout more generally. Future work will investigate the application of the shear strength reduction (SSR) approach to estimate Factor of Safety and potential landslide or rockfall runout distance for rock slopes where the failure is triggered by long-term subcritical crack growth driven by weathering and gravitational loading.

8 REFERENCES

Azocar, K.D., 2016. *Investigating the mesh dependency and upscaling of 3D grain-based models for the simulation of brittle fracture processes in low-porosity crystalline rock*. Master's Thesis, Queen's University.

ADAM Technology, 2022. 3DM Analyst Edit Station Enhanced Edition. Build 2.6.6, August 2022.

Bandis, S. C., 2004. Numerical modelling of discrete materials in rock mechanics: developments and engineering applications. In: *Proceedings of the 1st Int. In UDEC/3DEC Symp*. 2004.

Bentley Systems Incorporated, 2022. ContextCapture Desktop Edition, v 20.1.5562

Bertuzzi, R. and Pells, P.J., 2002. Geotechnical parameters of Sydney sandstone and shale. *Australian Geomechanics*, 37(5), p.41.

Blue Mountains Star, 1931. *The Blue Mountains – Nature and Structure: The Dog Face Rock Slide*. Saturday, 31 January 1931, page 7. Accessed from Trove, the National Library of Australia: http://nla.gov.au/nla.news-article190102885.

Cameron-Smith, B., 2019. The 'Leaning Rock' of Katoomba: Tragedy of Nature or Man-made Landslide?

Christianson, M., Board, M. and Rigby, D., 2006, January. UDEC simulation of triaxial testing of lithophysal tuff. In Golden Rocks 2006, *The 41st US Symposium on Rock Mechanics (USRMS)*. American Rock Mechanics Association.

Cunningham, D.M., 1988. A rockfall avalanche in a sandstone landscape, Nattai North, NSW. *Australian Geographer*, 19(2), pp.221-229.

Diederichs, M.S. and Martin, C.D., 2010, June. Measurement of spalling parameters from laboratory testing. In *ISRM International Symposium-EUROCK 2010*. OnePetro.

Diederichs, M.S., 2007. The 2003 Canadian Geotechnical Colloquium: Mechanistic interpretation and practical application of damage and spalling prediction criteria for deep tunnelling. *Canadian Geotechnical Journal*, 44(9), pp.1082-1116.

Dershowitz, W.S. and Herda, H.H., 1992, June. Interpretation of fracture spacing and intensity. In *The 33rd US Symposium on Rock Mechanics (USRMS)*. OnePetro.

Do, T.N. and Wu, J.H., 2020. Simulating a mining-triggered rock avalanche using DDA: A case study in Nattai North, Australia. *Engineering Geology*, 264, p.105386.

Gao, F. and Stead, D, 2014. The application of a modified Voronoi logic to brittle fracture modelling at the laboratory and field scale. *International Journal of Rock Mechanics and Mining Sciences*, 68, pp.1-14.

Gao, F., 2013. *Simulation of failure mechanisms around underground coal mine openings using discrete element modelling*. Doctoral dissertation, Simon Fraser University, Department of Earth Sciences.

Ghazvinian, E., 2015. *Fracture initiation and propagation in low porosity crystalline rocks: implications for excavation damage zone (EDZ) mechanics*. Doctoral dissertation, Queen's University.

Itasca Consulting Group, 2011. UDEC version 5 Manual.

Kazerani, T. and Zhao, J., 2010. Micromechanical parameters in bonded particle method for modelling of brittle material failure. *International journal for numerical and analytical methods in geomechanics*, 34(18), pp.1877-1895.

Mandl, G., 2005. *Rock joints*. Springer-Verlag Berlin Heidelberg.

Maptek, 2022. PointStudio: Point cloud processing, modelling and analysis tools for mining and industrial survey. Build Version: 9.3.0.18317, 10 May 2022.

Mostyn, G., Helgstedt, M.D. and Douglas, K.J., 1997. Towards field bounds on rock mass failure criteria. *International Journal of Rock Mechanics and Mining Sciences*, 34(3-4), pp.208-e1.

Oliveira, D., 2014. An alternative view on geotechnical parameters for tunnel design in Sydney. *Australian Geomechanics*, 49(3), pp.95-108.

Oliveira, D., and Parker, C., 2014. An alternative approach for assessing in situ stresses in Sydney. In: *Proceedings of the 15th Australian Tunnelling Conference*. Sydney NSW, 17-19 September 2014.

Pells, P.J.N. and Hammon, P.J., 2009. The Burning Mists of Time: A Technological and Social History of Mining in Katoomba.

Pells, P.J.N., 2008. Assessing parameters for computations in rock mechanics. In *Proceedings of the First Southern Hemisphere International Rock Mechanics Symposium* (pp. 39-54). Australian Centre for Geomechanics.

Pells, P.J.N., Braybrooke, J.C., Mong, J. and Kotze, G.P., 1987. Cliff line collapse associated with mining activities soil slope instability and stabilization. In: *Soil Slope Instability and Stabilisation*; Eds. Walker & Fell, Balkema, Rotterdam.

Salmi, E.F., Nazem, M. and Karakus, M., 2017. Numerical analysis of a large landslide induced by coal mining subsidence. *Engineering Geology*, 217, pp.141-152.

Seedsman, R. and Pells, P.J.N., 2014. On the deception in requiring and providing singular accurate predictions for surface subsidence, tilt and strain. *Proceedings of the 9th triennial conference on mine subsidence* (p. 63).

Tuckey, Z., 2020. Modelling brittle fracture in weak rock with the bonded block method, from laboratory to tunnel scale. *Australian Geomechanics*, Vol. 55(2), June 2020.

Douglas Partners

Geotechnics / Environment / Groundwater

60 years of providing practical solutions

Understanding the Earth and delivering practical solutions to enhance outcomes for our clients, community and environment.

Over **500** staff across **20** branches, including **15** NATA registered laboratories.

Best Provider

Winner of the Client Choice Awards 2022

Finalist Best provider to property in the Client Choice Award 2022

Client Choice Awards finalists for 14 years

www.douglaspartners.com.au

ABN: 75 053 980 117

TERRASCAN

Terrascan was created to deliver technical excellence for the geotechnical and resource industries.

We offer a variety of specialist services under one roof, bringing you industry leading results in a convenient, cost effective package.

TERRASCAN OFFERS

- Borehole imaging
- Rig Supervision
- Core Logging
- Cone Penetration Testing

www.terrascangroup.com.au | 0408 723 340

A CASE STUDY ON THE VARIABILITY OF THE COEFFICIENT OF CONSOLIDATION AND ITS DESIGN RELIABILITY

Burt G. Look
FSG – Geotechnics and Foundations, Brisbane

https://doi.org/10.56295/AGJ5834

ABSTRACT

The consolidation characteristics of cohesive soils are estimated using established relationships between the coefficient of consolidation (c_v) and index tests, as well as laboratory oedometer tests. While the design c_v is preferred from the field dissipation tests, the conversion from a horizontal to vertical value needs to be considered. A trial load was used to verify the consolidation parameters during a Queensland Road upgrade, which involved both road widening and raising of the existing embankments over compressible soils. Construction was done in 4 stages, and with preloading and surcharging in selected areas. Settlement monitoring and Asaoka plots were used to validate the design, and "moderately conservative" design values were adopted. This case study is used to show the large variability of the c_v by the various test methods. While 99% of the site settlement was within the magnitude and time predicted during design, a 25 m length was not consistent with the data and performance of the rest of this site within the flood plain. The back-calculated c_v was below the lowest test value and even data from nearby settlement plate monitoring from adjacent stages. In situ tests were located within 25m of this unconforming area and given that stratigraphy was consistent then the c_v value adopted may not be representative. The lessons learnt show the various verification and validation process required to envelope risks, but all conditions with a "moderately conservative" design may not be covered.

1. INTRODUCTION

When a soil is loaded in an undrained manner, the pore pressures increase. The time for consolidation is dependent on a non-dimensional time factor (T_v), the drainage path length (H_{dr}) and the coefficient of vertical consolidation (c_v) by:

$$t = \frac{T_v H_{dr}^2}{c_v}$$

The c_v can be estimated by laboratory (oedometer) or insitu testing methods (CPTu porewater dissipation tests). The laboratory consolidation tests underestimate the field c_v value due to the presence of macro fabric within the soil structure such as silt and sand lenses, which lead to faster drainage in the field. For this reason, values determined from porewater dissipation tests are typically used for design purposes. In addition, the c_v is also dependent on the over-consolidation ratio (OCR). For over-consolidation soils the c_v is higher than for normally consolidated soils. The c_v for a normally consolidated soil can be considered a lower bound. The stress state prior to and following construction is therefore considered in the adopted design c_v.

Index properties, such as the liquid limit (LL) are also typically used to help define the expected range of c_v values for a given soil. NAVFAC (1986) provide a well-cited correlation between the liquid limit of a soil and c_v (Figure 1). Designs using c_v derived from such index tests may be misleading, as seen when Queensland consolidation data is compared with this graph (Figure 2 from Look, 2023).

This case study compares the c_v results obtained using

1. Index tests based on LL and laboratory consolidation test values using 2 different standard methods
2. In situ dissipation tests and 2 trial loading during design
3. Additionally, a probabilistic risk analysis was conducted for the range of c_v values
4. Back analysis during construction using Asaoka plots

Designers may use either the coefficient of compression (C_c) or the coefficient of compressibility (m_v) method to calculate the magnitude of settlement. The latter is stress dependent while the C_c should be corrected for sample disturbance. Both sets of parameters can be obtained from oedometer tests. Rowe (1972) highlight how size of sample affects drainage in consolidation tests. Oedometer tests provide rigid lateral confinement which is not found in the field. Consolidation settlements calculated from oedometer testing should be corrected with the Skempton – Bjerrum correction factor which is dependent on the type of clay. Typical correction values are provided in Tomlinson (1995).

The paper highlights that selection of an input design value is no trivial matter, with this case study used to highlight some of the many considerations for consolidation settlement, given its significant associated risk.

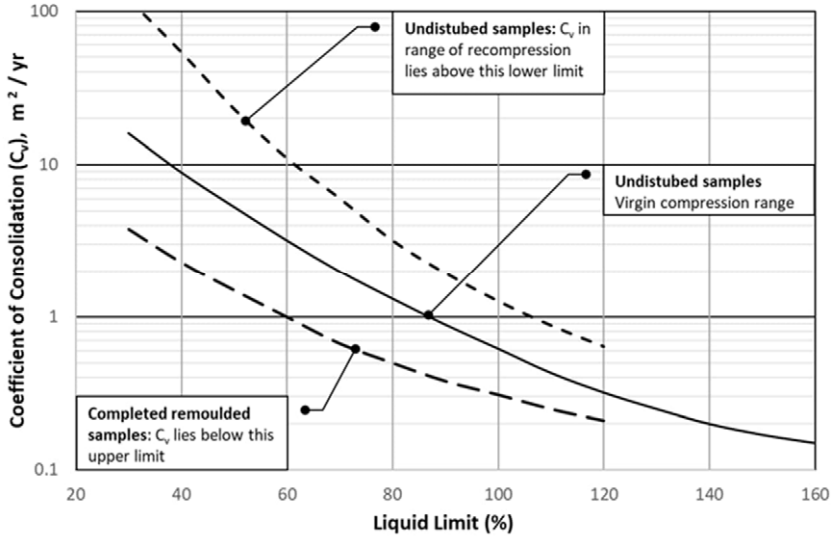

Figure 1: NAVFAC (1986) correlation of c_v vs. LL

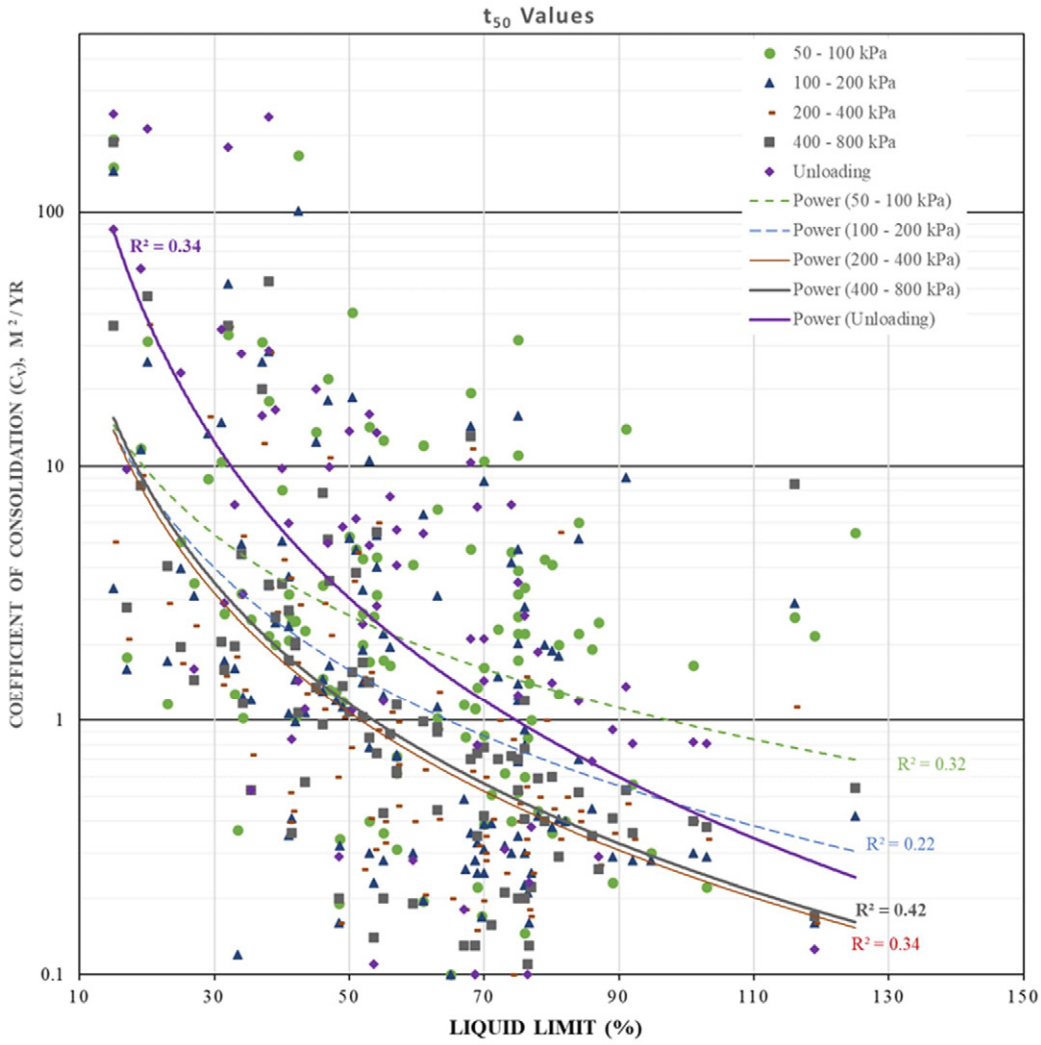

Figure 2: Queensland consolidation data (126 consolidation tests) using Casagrande's t_{50} approach

2. PROJECT BACKGROUND

The project site is located on the Ipswich Motorway between Rocklea and Darra (R2D). The compressible clay section discussed is within the Oxley Creek floodplain, bounded by Oxley Creek in the east and Little Doris Creek in the west. The floodplain comprises three watercourse crossings, Oxley Creek, Oxley Creek Overflow and Little Doris Creek. These creeks feed into the Brisbane river with quaternary age materials deposited over the 900 m width floodplain. The upgrade consisted of road widening with 2 service roads (north and south) and raising the levels of the existing road embankments for flood immunity. Thus 4 X 900 m = 3,600 m of road embankment traverse compressible clays. Ground improvements consisted mainly of surcharging and preloading, with load transfer platforms at services areas.

The project is further described by Kemp et al. (2019) who highlight the importance of avoiding generalised site wide geotechnical models for site characterisation. The grid-based mapping software "Surfer" was used both as a data analysis and visualisation tool. Settlement calculations were undertaken at each of the investigation points and the results were gridded, using kriging techniques in Surfer (Kemp et al. (2019). The maps developed using this method provide a visual tool of identifying constraints and opportunities within the alignment and ground improvement measures required.

Figure 3 shows two of the many inputs in ground characterisation prior to settlement analysis. The contouring readily identifies hot spots where more than 3 months of preloading is required, and where higher magnitudes of settlement are expected. This case study compares the reliability of the various methods in predicting settlement vs the measured settlements, at the one highlighted area shown in Figure 4 over the 900m flood plain.

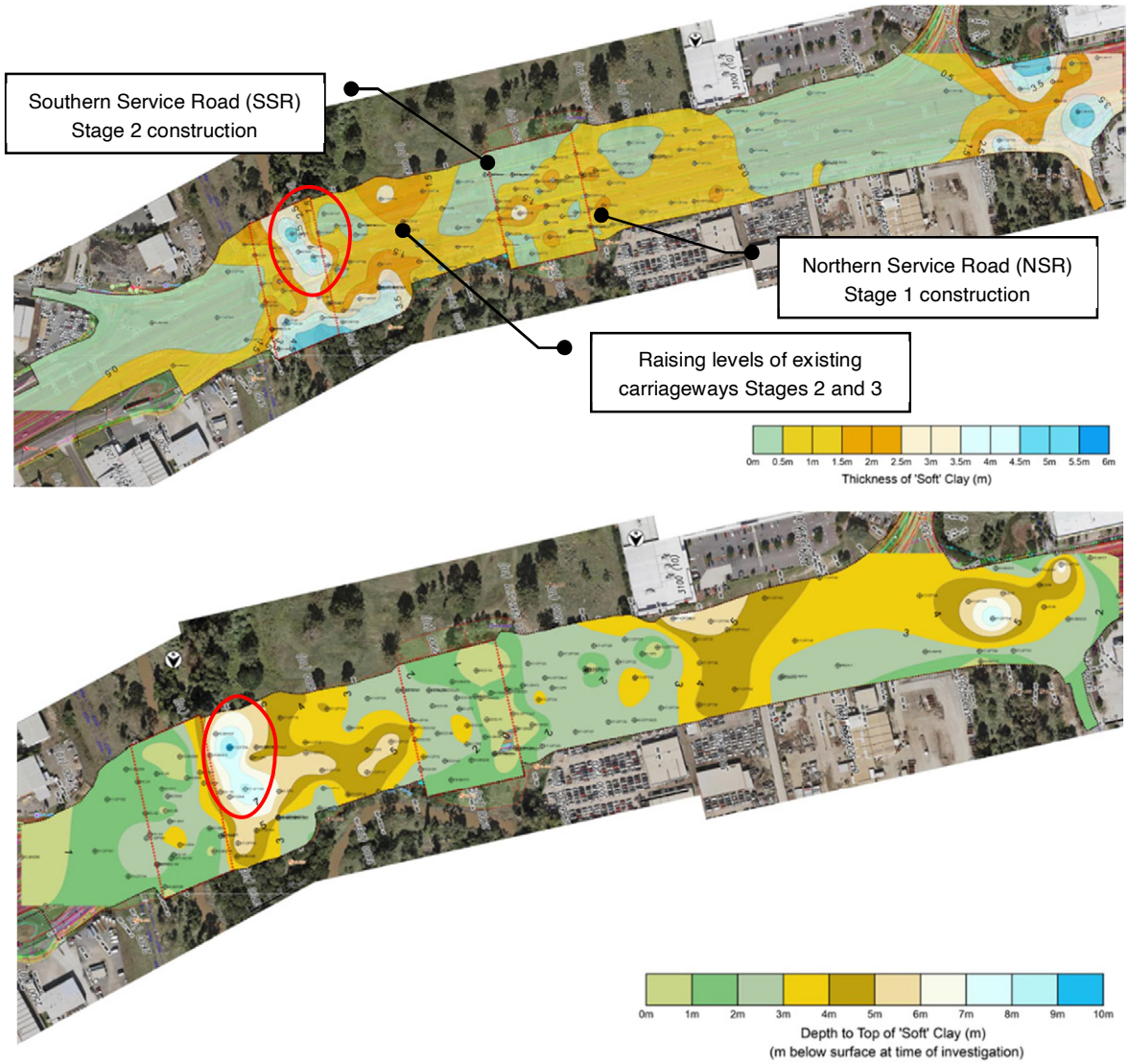

Figure 3: Hot spot (a) thickness and (b) depth to compressible clay layer for settlement analysis. Highlighted circled area raising the existing embankment is the subject of this paper

3. TEST DATA

3.1 INDEX PROPERTIES

Based on site wide Atterberg Limits testing of the compressible layer, the typical range of liquid limits is 50-70%. Using the NAVFAC (1986) correlation this results in a possible range of c_v values of 2 to 5 m^2/yr for normally consolidated clays and 6 to 20 m^2/yr for over-consolidated clays (Figure 1). Based on the oedometer and CPT testing undertaken, combined with the additional applied embankment load, the clays are expected to be within the lightly over-consolidation range, therefore the latter range applies. This varied with both depth and area of the site.

3.2 PORE PRESSURE DISSIPATION AND LABORATORY CONSOLIDATION TESTS

At the R2D site, 24 lab tests data on 75mm undisturbed samples, over several phases of the project, and 9 dissipation tests were carried out during detailed design. The lab tests were mainly during the preliminary design, while the dissipation tests were carried out several years later during the detailed design phase. There were 7 other historical test which were considered unreliable / insufficient time to determine the t_{50} value. The 2017 dissipation tests were carried out overnight initially, although later tests were generally performed over 1 to 4 hrs. As this was a highly trafficked road, the tests were carried out at the toe of the existing road embankments for safety reasons, and therefore the dissipation test are representative of the NSR and SSR and not the existing carriageway. The following is observed from this site data:

- Median and mean in situ c_h = 20 m^2/yr and = 23.3 m^2/yr, respectively from 9 dissipation tests (Figure 4). Using a lognormal probability density function (PDF), 90% of values would be above c_h = 4.9 m^2/yr. A normal PDF is inappropriate as a statistical distribution as that would calculate 14% of values ≤ 0 m^2/yr. The normal PDF is clearly incorrect for statistical analysis of this data. Look (2015) and Look and He (2022b) highlighted the pitfalls of using a normal PDF in statistical assessment of a design value. In this case the value of 77 m^2/yr is a clear outlier, and in visual assessments would typically be removed from analysis. Yet in statistical analysis removal of data points is often criticised as cherry picking.

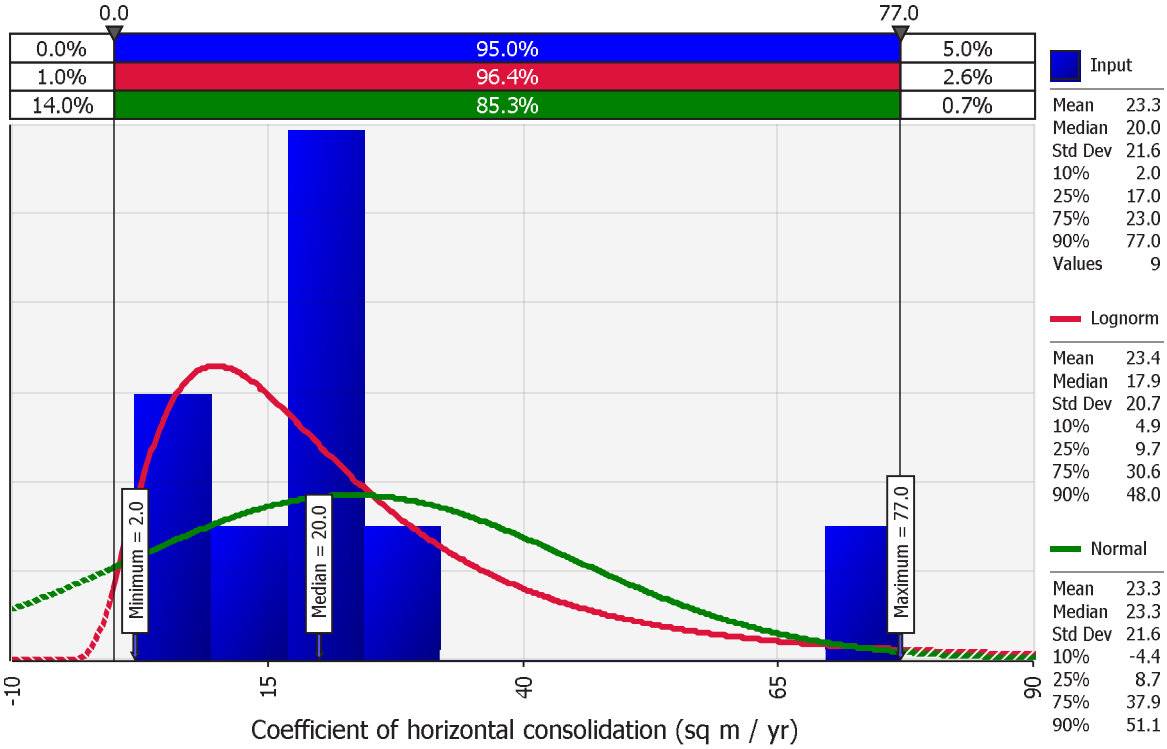

Figure 4: Dissipation tests (9 No.) at R2D site

- Laboratory median c_v varied from 0.5 to 15.7 m^2 / yr for the 2 stress ranges and two laboratory "standard" approaches. At this site the additional load on the compressible clay varied from 50 kPa to 125 kPa. Loaded stress level at 50 – 100 kPa has a typical c_v value ~ 3.3 – 5.0 times the value (typically) at the 100 to 200 kPa stress increment based on these consolidation tests (Table 1). This would vary depending on what "moderately conservative value" is used in design. The field tests (highlighted in red) are used in practice

- The Overconsolidation ratio (OCR) varies from 2 to 3.4 for the compressible clay layer

Table 1: Comparison of laboratory and field values of the coefficient of consolidation (R2D site)

Method used	No. of tests	Stress Range	Coefficient of consolidation (m^2 / yr)				Typical ratio
			Lower 10%	Lower Quartile	Median	Mean	
C_v Lab t_{50}	24	50 – 100 kPa	0.6	1.1	2.3	13.2	~ 3.3
C_v Lab t_{50}	24	100 – 200 kPa	0.2	0.3	0.5	7.8	
C_v Lab t_{90}	11	50 – 100 kPa	2.3	11.1	15.7	70.2	~ 5.0
C_v Lab t_{90}	11	100 – 200 kPa	0.6	0.7	2.5	33.2	
C_h Dissipation test (Lognormal PDF)	9	In situ	4.9	9.7	17.9	23.4	
C_v based on LL in NAVFAC charts	23 LL results	NC	1	2	5	3	~3.3
		OC	2	6	20	10	

Table 1 shows the difficulty the designer is faced in choosing a "moderately conservative" value for design. Type of test and variation of test results provide wide variability of results. Even when using dissipation tests this c_h must be factored for conversion to a c_v value that varies from 1 to 10, but typically 2 typically assumed (Jamiolkowski et. al., 1985). The effect of the increased stress (varies from 3 to 5 for this site) should also be factored. Using a lower bound value, with a high anisotropy conversion and high effect of stress increase leads to an overly conservative design varying by two orders of magnitude. Yet no clear guidance is given in the literature for this critical evaluation. The field test values are preferred to account for the site drainage layers, which laboratory size samples would not represent.

This site data suggests that c_v Lab using the t_{90} approach is approximately the field c_h dissipation test. The dissipation tests were carried out in the compressible clay layer at 4 – 6 m depth (approximately 60 kPa effective overburden pressure). Further details on the site characterisation are provided in Kemp et al. (2019).

A sensitivity analysis in a deterministic approach does not envelope full risk. A risk evaluation requires an appropriate statistical distribution to be meaningful. Such an approach is discussed for this case study in later sections. Look and He (2022a) discuss the benefits of simulation in risk analysis to guide these uncertainties using the wide possibilities of input, rather than selecting a singular design.

3.3 TRIAL LOAD DURING DESIGN

The test data in Table 1 represents a site wide summary of test data, and a designer should also consider zonation of the site, especially with a COV of consolidation typically about 235% for this site. Asaoka plots using data from several settlement plates and 2 test load sections showed the c_v varied from 10 to 25 m^2 / yr, for most of the site, but with one local area with $c_v < 5$ m^2/yr.

During the detailed site investigation and design period, two trial areas were loaded with precast concrete barriers (PCBs). This consisted of 2 levels of PCBs stacked on 2 concrete slabs (Figure 5). Safety consideration would not allow greater stacking heights. Both trials were near the northern services road; one trial was near the Oxley creek bend, and the Oxley creek bridge. At the existing motorway, additional fill heights of between 2.5 m and 3.7 m were used, while the trial load represents an equivalent fill height of 2.8 m.

The trial loads were placed at a representative area (after the rived bend) and a "critical" as defined by the results of CPTUs. It was recognised the trials did not represent the full loading for the high embankments for the widening. This was due to the limitation of space and stacking heights for safety requirements. This load was more representative of the areas of raising the heights for the existing carriageway embankments at stages 3 and 4, although not located directly at such locations.

The result of this trial is described in Kemp et al. (2019). The settlement stabilised at 45 days, which was within the 90-daty stipulated period for the fill heights at the stages 3 and 4 over the existing motorway.

Based on the slope of the settlement data in the Asaoka plot and the drainage path length, the coefficients of vertical consolidation, c_v, were estimated as 22 m^2/yr and 25 m^2/yr for the Oxley Creek Bridge and Oxley Creek Bend sites respectively. These values are similar to the CPTu dissipation test results, which showed 50% (median) of CPTu test results at 18m^2/yr (lognormal PDF). The values suggest the use of c_h / c_v ~ 1 at this site. The in-situ dissipation test data

best represented the settlement behavior during construction, and with a c_h / c_v ~ 1 for this site, and without factoring for the load increase effect suggested by the laboratory tests.

Figure 5: PCB trial area located 25m to 50m from concern area

4. DESIGN VALUES

A comparison between the CPT traces shows the compressible layer having similar sandy clay properties, this is highlighted by the small spikes in the CPT cone resistance (q_c) which indicates the presence of sand lenses within the clay layer. No low pore pressure response suggests a layer that can drain quickly. The compressible layer thickness (H), varied across the site, with H_{max} = 4m at land areas, with nominally higher values within the river.

Based on the above testing a design c_v value of 5 m^2/yr was adopted as a sitewide parameter, with an upper bound of the thickness used in design. This value is conservative as it was not increased to account for the sandy nature of the material found at some locations. Values less than the ranges described above are outside of what is considered reasonable for an economical design. A sensitivity analysis used the lowest test c_v value of 2.0 m^2/yr.

Using the above parameters, a time for 90% consolidation of 2 months was determined, this implies that the settlement occurs mainly during the construction of the embankments. Settlement magnitudes in the order of 80mm to 100mm were estimated. The northern service road was identified as more critical, and surcharge was applied. Additionally, that NSR area was programmed to be constructed before the 3 other areas.

Due to the rapid settlement, no preloading beyond the 3 months or surcharge was required at the other areas, as design and the 2 trial loads indicated the settlement would occur during the embankment construction. The finished asphalt surface would then be placed after a 3-month period, and future creep settlement was expected to be < 50mm.

Only the approach using the coefficient of volume compressibility (m_v) as used in the simulation analysis is discussed herein although the approach using the compression Index (C_c) was also used in the design.

4.1 SIMULATION ANALYSIS INPUT

Deterministic design approaches may not explicitly consider the ground uncertainty. Lower and/or upper bound estimates are applied in sensitivity analysis based on an estimate of likely variability, but this is not a full risk assessment as often many of the variables are set as fixed in the analysis, while one or 2 key variables are assessed. Simulation models allow the full spectrum of risk to be evaluated by evaluating probable / likely inputs together as described in Look (2022a). Monte Carlo (MC) simulation provides several advantages over deterministic "moderately conservative" analysis. The combined effect of multiple variables can be better assessed, with a focus on input variable risk. In deterministic models, different combinations of values for different inputs are not readily interrelated to see the effects of truly different scenarios. An enhancement to Monte Carlo simulation is the use of Latin Hypercube (LH) sampling as discussed in Look and He (2022a).

For example, the coefficient of volume compressibility varies with stress levels as shown in Figure 6. Selection of the best fit probability density function (PDF) is no trivial matter. The use of a normal PDF should be avoided in simulation analysis as shown in Look and He (2022b). In Figure 6 (50 – 100kPa stress level), the Logistic is the best fit PDF but has a 7.2% probability of having a negative value (similar to normal PDF). The lognormal although not the best fit does avoid this discrepancy and was adopted for assessing realistic input to the simulation analysis.

A conservative design value of $c_v = 5.0$ m^2/yr was used in the R2D design. This contrasts with both the "likely" and full range of test values used in the simulation analysis which provides a more realistic risk profile for time required for settlement during construction monitoring. Laboratory tests showed the effect of the increased stress varies with the higher stress level having the lower c_v value and considered in the simulation input values used.

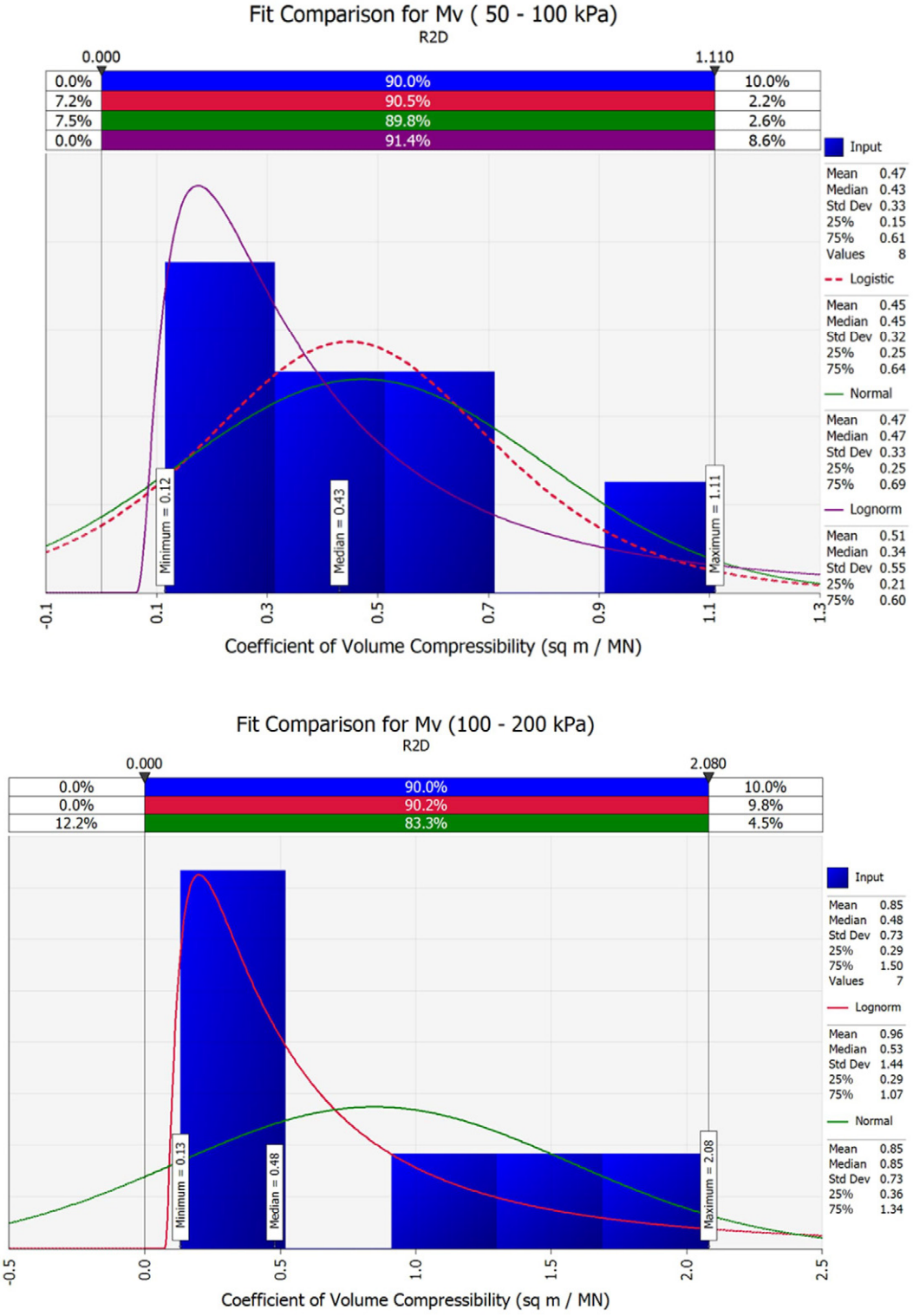

Figure 6: Variation of coefficient of compressibility with stress level

Following similar statistical analysis of the site data Table 2 provides a summary of the input for the various soil parameters used in the analysis. Compressibility is highly stress dependent, and using the higher stress range would result

in almost twice the settlement prediction from the range of values shown. However, Table 1 compared the coefficient of consolidation between laboratory and field values and only the 50 – 100 kPa stress range for the t_{90} corresponds to the dissipation field tests and the 2 loading trials carried out. This is due to the inter-relationship of c_v to the coefficient of compressibility (m_v) as shown with the permeability (k) and unit weight of water (γ_w).

$$c_v = \frac{k}{m_v \ \gamma_w}$$

Simulation analysis adopted that 50 – 100 kPa stress range as compatible with the field tests recognising c_v and m_v are linked by the equation above. A program evaluation and review technique (PERT) PDF was adopted (Look, 2023) as shown in Table 3 for the simulation input of the various parameters that affect the output results. The upper bound layer thickness was conservatively adopted in design, but the variation is included in the simulation analysis.

Note that the unit weight is the parameter with the most certainty, yet it can produce variation of predicted settlement by 10% . One should not only assume a unit weight of 20 kN/m^3. This effect of density input with stability and settlement of embankment fill is discussed in Look (2021).

Only the 3m high embankment where raising the road levels above flood levels are discussed further in the simulation analysis. The trial load at 2 critical areas provide confidence on the parameters to be adopted for design. Both time and magnitude of settlement were critical to the 4 stages of construction.

Table 2: Comparison of laboratory and field values for design assessment (R2D site)

No. of tests	Stress Range	Method used	Min. Test	Lower 10%	Lower Quartile	Median/ Mean	Upper Quartile	Upper 10%
8	50 – 100 kPa	M_v Lab (m^2/MN)	0.12	0.15	0.21	0.34/ 0.51	0.60	1.11
7	100 – 200 kPa		0.13	0.12	0.36	0.53/0.96	1.34	2.08
9	In situ $C_v \sim C_h$ from in situ trial	C_h Dissipation test (Lognormal PDF) (m^2/yr)	2.0	4.9	9.7	17.9 /23.4	30.6	77.0

Table 3: Simulation values adopted

Parameter	Lowest likely ~ 10% value	Most likely (median)	Highest likely ~ 90% value
Thickness of compressible layer (m)	2.5	3.0	4.0
Depth to top of layer (m)	5.0	6.0	7.5
Unit weight of fill (kN/m^3)	19.5	20.5	22
Stress influence factor	0.96 (bottom of layer)	0.96	0.995 (top of layer)
Skempton – Bjerrum correction factor	0.75	0.9	1.0
M_v (m^2/MN)	0.12 (minimum test value)	0.34	1.1
$C_v \sim C_h$ (m^2/yr)	2.0 (min) / 5.0 (10%)	18	31

4.2 SIMULATION ANALYSIS OUTPUT

Figure 7 shows the input variables most affecting the analysis given the input range and with 5,000 LH simulation analysis. Thus, the designer needs to focus on the m_v input parameter to minimise risk in the settlement analysis. The effect of the depth to the compressible layer although included in the simulation is not shown in the tornado output as it is least affected in this case due to the wide embankment and is a subset to the influence factor. The baseline settlement of 71mm has a range of 30 to 126 mm based on this analysis but does not account for the high and low 5 percentile. This

relative effect would not be apparent in deterministic analysis, even with sensitivity analysis of highest and lowest credible values.

The range of predicted settlement is 35 mm to 112 mm for the 90% to 10% probability, i.e., there is less than 10% probability that 112mm settlement would be exceeded at this location for 3 m of fill (Figure 8). Note the large range of settlements at the site, although a deterministic analysis would use a conservative one value input, there is often a false expectation by site engineers that design values is the expected value. A design value envelops risks, while a "predicted" value represent what would most likely happen on site during construction monitoring.

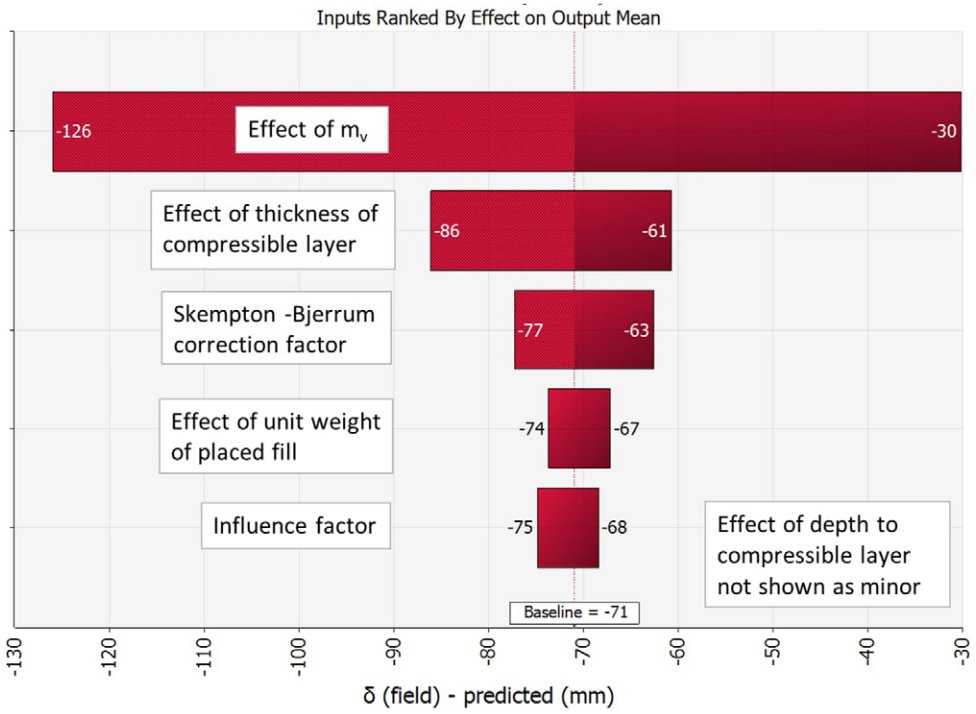

Figure 7: Simulation output – tornado graph showing relative effects on analysis at western bridge abutment location with 3 m fill height

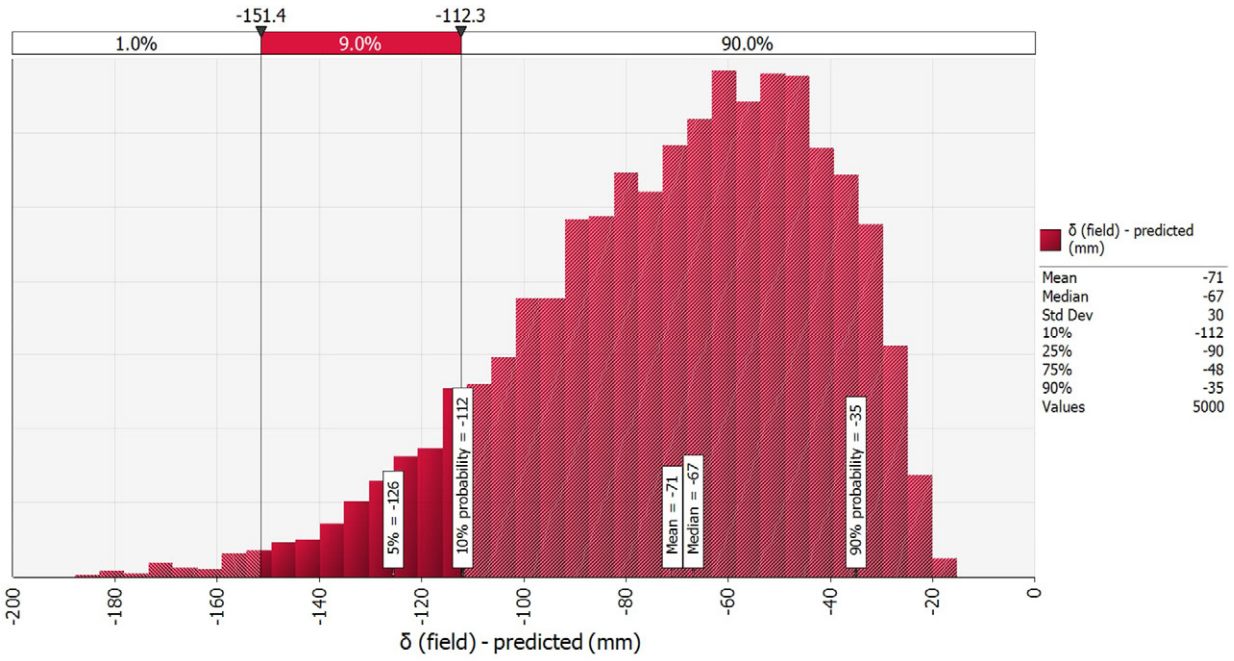

Figure 8: Simulation output – at western bridge abutment location with 3 m fill height

The time for consolidation is as important as the magnitude. The simulation analysis using the site data was carried out using both the minimum test value (Figure 9 output), and the 10% risk value (Figure 10 output), These are in areas where 3 m of fill is placed.

Figure 9 shows there is a 1% probability that 3.4 months of consolidation is exceeded if a minimum likely c_v of 5 m^2/yr is used. This design used 3 months as the expected time frame, and which is expected to be achieved in over 95% of the site, based on this analysis.

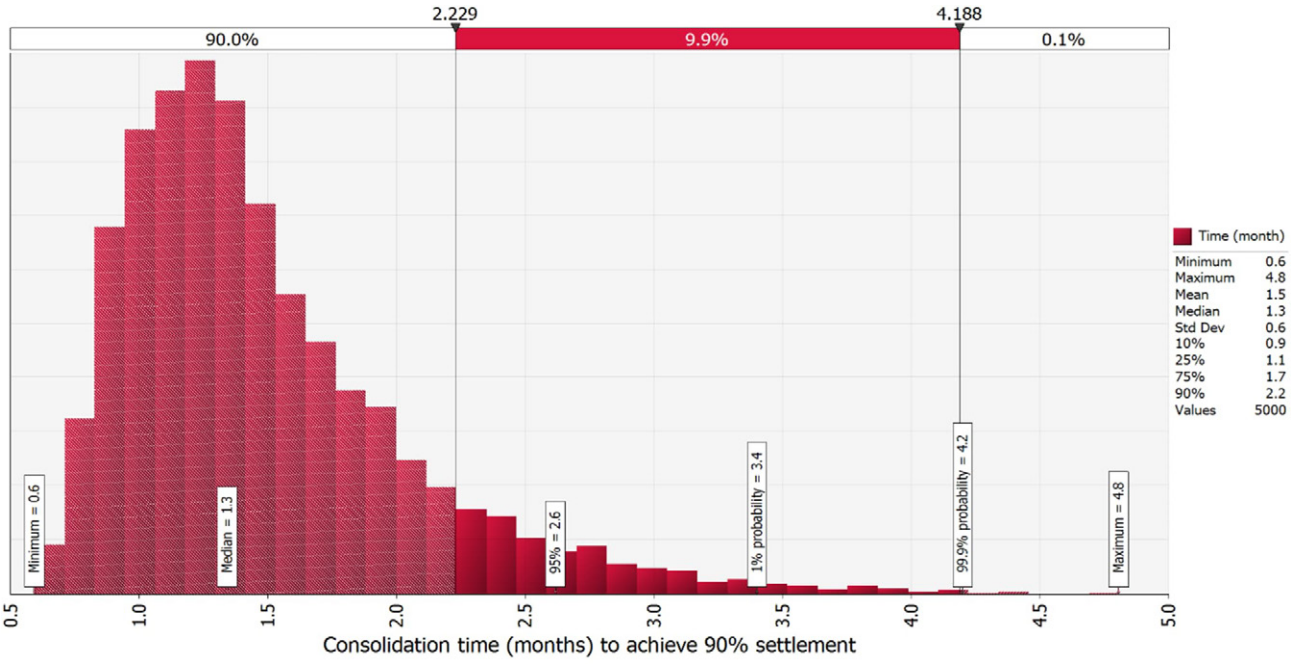

Figure 9: Simulation output – consolidation time probability using likely minimum c_v= 5 m^2 /yr

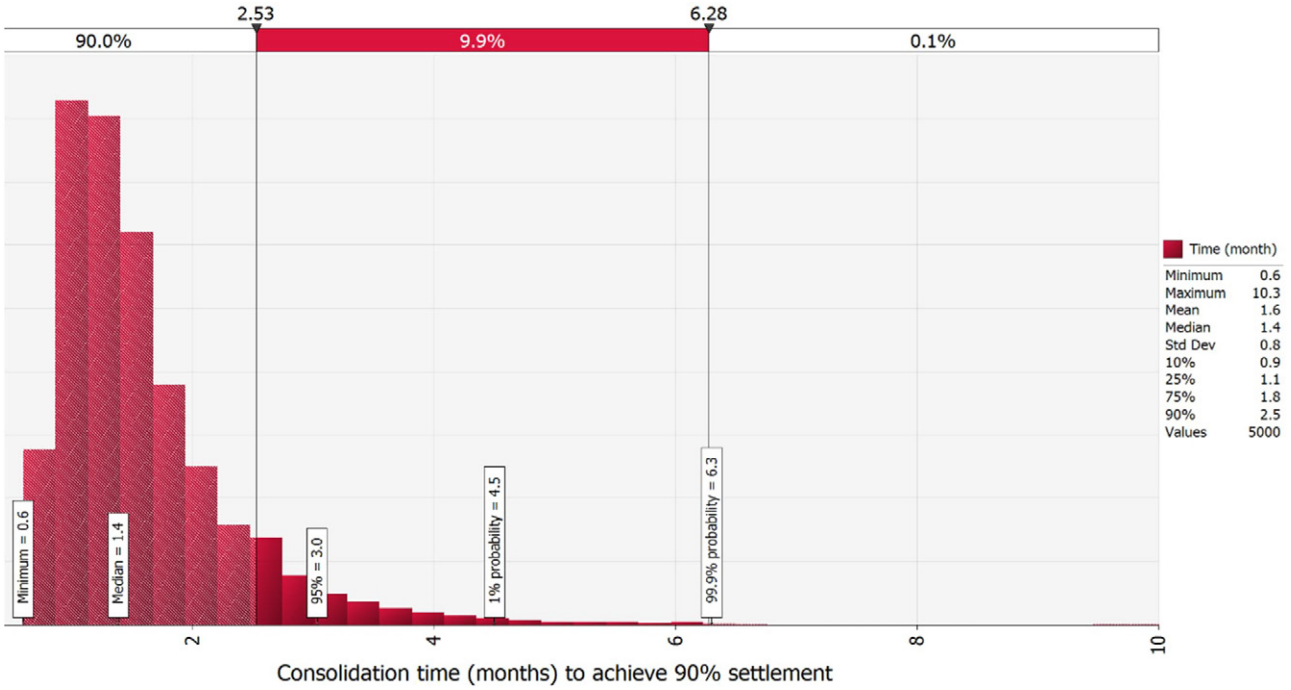

Figure 10: Simulation output – consolidation time using minimum test value of c_v = 2 m^2 /yr

Figure 10 is the output if the minimum test value c_v of 2 kPa is used in the analysis. This now shows there is a 1% probability that 4.5 months of consolidation is exceeded. This selection of a minimum likely vs a minimum test value does influence the simulation result although both provides confidence in a 3-month design basis. Note that the highest test value was excluded from analysis. The maximum calculated time for 90% consolidation now increases from 4.8 to

10.3 months with this "minor" input change. Agon this highlights how our single value input in a deterministic value does not capture risks apparent in variability in site test data.

5. CONSTRUCTION MONITORING

5.1 REVIEW OF PERFORMANCE ON SOUTHERN SERVICE ROAD (SSR)

The results of the settlement plate monitoring at SP-1 and SP-3 at the SSR are shown in Figure 11 (6m fill) and Figure 12 (3 m fill), respectively. CPT tests are located close to the settlement plates. In both case settlement was achieved in less than 2 months.

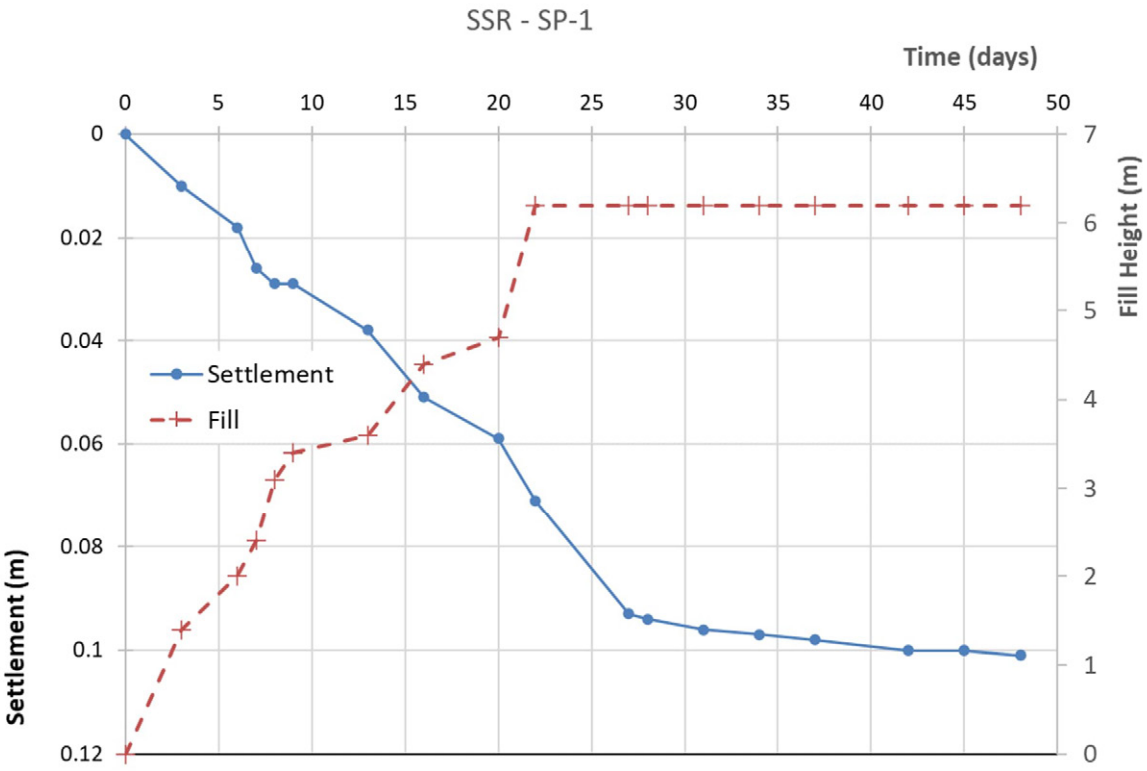

Figure 11: Comparison SP-1 Settlement Plate Results

The following key points can be highlighted based on the settlement plate results:

- Settlement at both locations was rapid with over 75% of the settlement occurring during the embankment construction. This rapid settlement aligns with the expected, sandy, geotechnical conditions described by the CPTs. The magnitude of settlement was 100 mm and 120 mm for SP-1 and SP-3 respectively. This was within the range expected for these locations.
- A back-analysis of the settlement plate results was undertaken using the Asaoka method. This method can be used to determine the percentage consolidation (U%) at a given timeframe and the coefficient of vertical consolidation (c_v) based on an assumed drainage path length
- Using the Asaoka method and the above drainage path lengths the following coefficients of vertical consolidation were estimated based on the actual settlement data:
  - SP-1 – c_v = 37.5 m^2/yr; SP-3 – c_v = 10 m^2/yr
- Both estimates were greater than the assumed design value of 5 m^2/yr, and compares with the expected value of 20 m^2/yr. Again, this shows the wide variability of results that occurs at a given site, and the failings of a "one value" applied in a deterministic design approach.

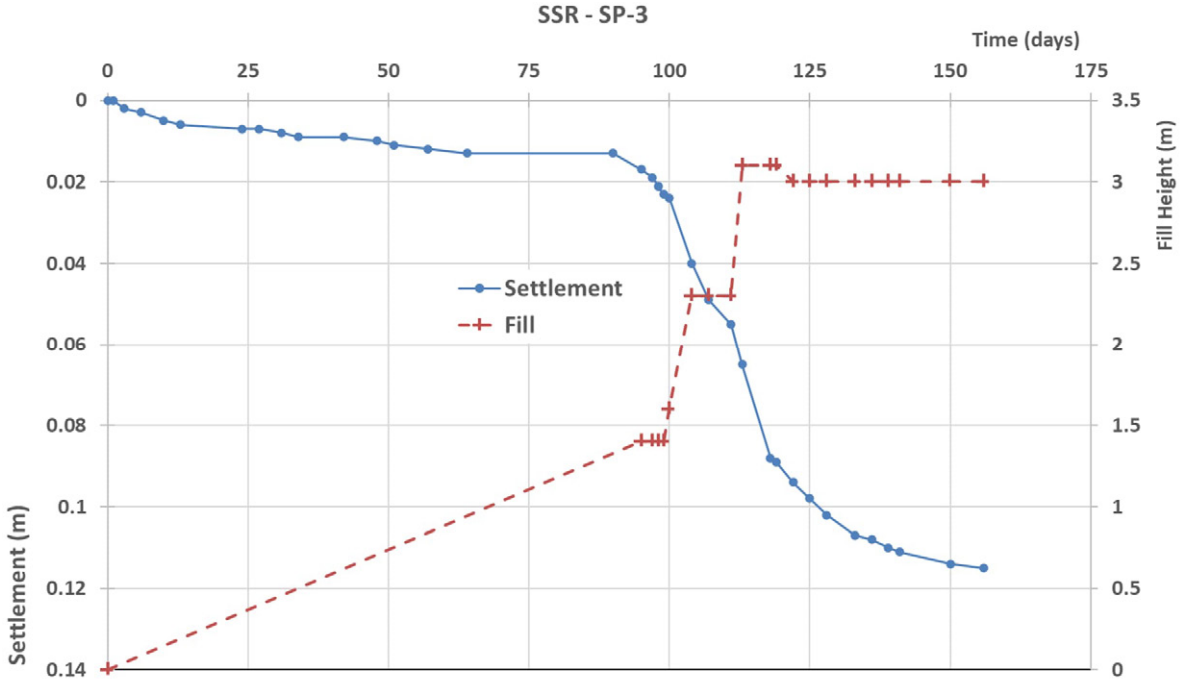

Figure 12: Comparison SP-3 Settlement Plate Results

5.2 REVIEW OF SETTLEMENT PLATE AT BR03 ABUTMENT B DURING CONSTRUCTION

The NSR and SSR were constructed in the first 2 stages as those areas with higher embankment heights were considered more critical in terms of settlement times. Construction of BR03 Abutment B (circled area in Figure 3) commenced following the SSR and NSR. The eastbound carriageway was completed prior to the westbound. Embankment construction was completed in the areas within the structure zone first and the area immediately behind the abutment was the last section of embankment filled.

Settlement plate, SP-11, was installed within the BR03 Abutment B Structure Zone, on the inbound side. Although there was not a formal preload or surcharge in this zone, the settlement plate was used to monitor settlement performance during embankment filling. At the settlement plate location, 2m of fill was placed over 11 days and settlement monitoring continued for a further 30 days. Figure 13 presents the settlement plate results.

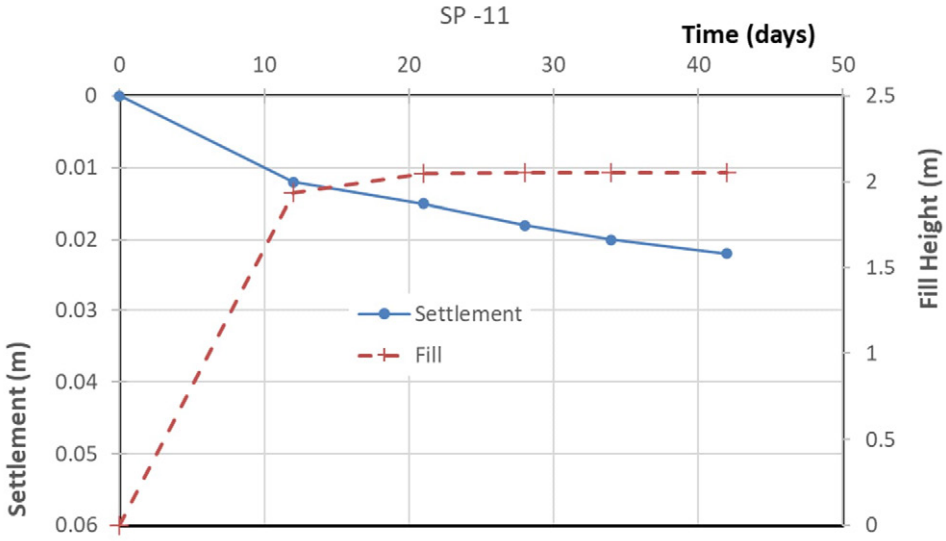

Figure 13: Settlement Plate Results SP-11

The following key points can be highlighted based on the settlement plate results:

- Initial settlement was rapid across the first 11 days. Asphalt was placed at the settlement plate location a further 39 days after the last recorded settlement plate monitoring point.
- Using the Asaoka method and the above drainage path lengths the following coefficients of vertical consolidation were estimated based on the actual settlement data:
- SP-11 – c_v = 7.8 m^2/yr
- A review of the SP-11 settlement performance indicated similar performance as SP-1 and SP-3 on the adjacent SSR, that was in line with the geotechnical model expectations for a sandy clay material with sufficient drainage paths.

5.3 POST CONSTRUCTION SETTLEMENT OF BR03 ABUTMENT B

Following construction of the final pavement layers at the BR03 – Abutment B, a sag/dip adjacent to the abutment relieving slab was observed. Post construction settlement monitoring was undertaken at 10m chainage intervals to monitor settlement performance. Figure 14 present the results of this monitoring. The following key points can be highlighted based on the settlement monitoring results:

- The current maximum settlement on the inbound and outbound alignment is approximately 120mm and 80mm, respectively. The magnitude of settlement observed at both abutment locations is within reasonable expectations based on the geotechnical model. Yet this occurred months after settlement was thought to have been completed based on a nearby settlement plate (Figure 13). Using the Asaoka method and the drainage path lengths determined from the nearby CPT, the following coefficients of vertical consolidation were estimated based on the actual settlement data:
- BR03 West - Inbound – c_v = 0.4 m^2/yr ; BR03 West – Outbound – c_v = 0.4 m^2/yr
- The back-calculated c_v shows a significantly lower value than that based on the available testing data (design value of 5 m^2/yr) and for a sandy clay (8 to 37 m^2/yr), which was identified at the three (3) settlement plate locations nearest to this BR03 Abutment B location.

Figure 14: BR03 West - Inbound and Outbound Settlement Results at chainages shown

6. IMPLICATION OF ACTUAL PERFORMANCE ON DESIGN

As shown for the NSR, SSR and other locations of embankments within the flood plain of this project, the design c_v value, and corresponding preloading or surcharging, was found to be reasonable at all settlement plate locations monitored. Yet settlement at abutment B of BR03 occurred after placement of the final surface pavement layers. This area represents 1.25% of the site area. The performance of the other (98.75%) embankments and abutments met design expectations. The back-calculated c_v value of 0.4 m^2/yr was outside the range of all field test results. This could not have been reasonably

expected at the time of design or from review of adjacent construction performance at the northern (stage 1) and southern service roads (stage 2).

Figure 15 provides a summary of test data, probability analysis and settlement monitoring. The back calculated c_v values from Asaoka plots show a lower c_v value at the lower loading. This contrasts with the laboratory tests which suggests the reverse i.e., a lower c_v value at the higher loading.

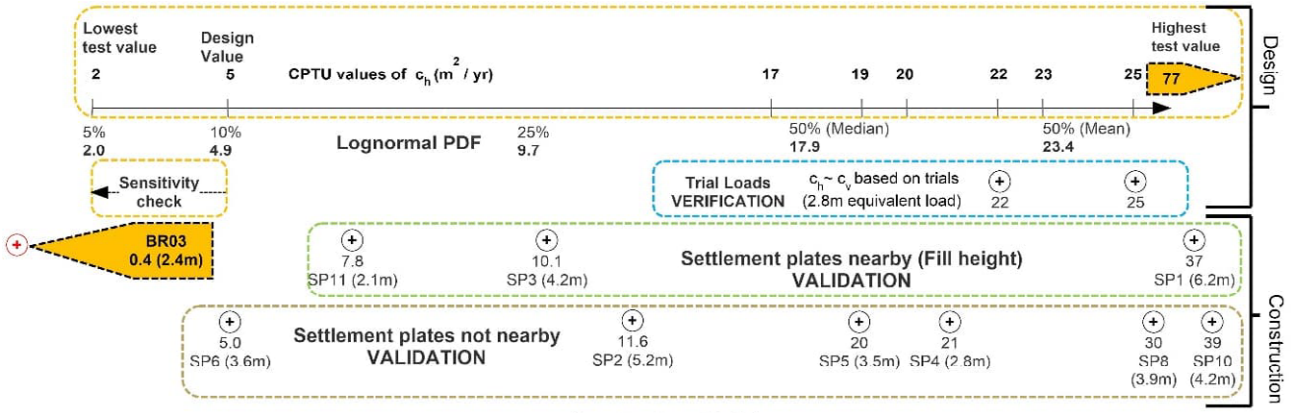

Construction SP data

Fill Height (m)	Height of Fill (m)	c_v median (m^2/yr)	c_v range (m^2/yr)	δ (mm)
> 3.6m	3.9 - 6.2	30	10.1 - 39	40 - 230
≤ 3.6m	2.1 - 3.6	20	5.0 - 25	24 - 51

Figure 15: Comparison of design and construction data analysis of C_v

The practical implication of adopting a c_v value of 0.4 m^2/yr and applied sitewide to other locations where permeable (sandy) clays were present. would have resulted in rigid ground inclusions (CMCs, CFAs or similar) getting specified for all locations. This would have resulted a significant cost to the project (circa $20 million+).

Comparison of analysis and field test data of c_v prior to, during and post construction is summarised in Figure 6. Laboratory tests do show such low c_v values, but in practice such lab values are disregarded in favour of field dissipation test values as drainage is not represented in small sample lab tests.

Three (3) investigation points are located within 25 m of Abutment B, with a further four (4) within 25-50 m. Four of the 7 tests at this area are historical data provided at the time of tender. Overall, the stratigraphy at this area is consistent. All investigation points consistently show a predominantly sandy profile where the clay is described either as clayey sand or sandy clay and the CPT traces show significant interbedding of sand layer. These profiles indicated a higher permeability material and fast consolidation times.

A survey of the bridge BR03 has not shown any significant movement. Other causes such as collapse settlement, embankment instability was discounted. The factor of safety for both the short and long term were not a concern and supported by adjacent inclinometers monitored during construction. Thus, a blocked drainage path was the most likely explanation.

Overall, the magnitude of settlement is within design expectations. The key issue being that this occurred after placement of final running surface, after the road opening. This had contractual issues.

A few key lessons from this unconforming location in hindsight are:

- The c_v input being over an order of magnitude less than other locations seem improbable
- Two-way drainage was used throughout due to the upper and lower sand layers in all CPTs and boreholes. The drainage path length is related to the time for consolidation as H_{dr}^2 (Section 1). A few test locations had to be relocated when drilled through the old embankment as a concrete slab was intersected at the base. In hindsight, perhaps this may also be located at this anomaly location and impedes the drainage. This is an unknown
- In the variability of the depth to and thickness of the compressible layer was used in the simulation analysis, while a "conservative" upper bound of layer thickness was adopted in design. This accounts for vertical spatial

variability only. Horizontal spatial variability could also account for this outlier as the nearest test location was 20m distance

Unlike strength-based analysis settlement analysis does not have factor of safety. A safety of factor of 1.5 would typically be associated with less than 1% chance of failure. The simulation risk analysis prediction during design (using the site test data) was for less than 1% probability of exceeding 4.2 months and with less than 0.1% risk of exceeding 7 months. Yet at this location (representing 1.25% length of site) settlement took up to 18 months. This is 4 times the 1% probability and halving the drainage path does also increase the time by a factor of 4. Thus, the hypothesis on the most likely cause of a blocked drainage at this location.

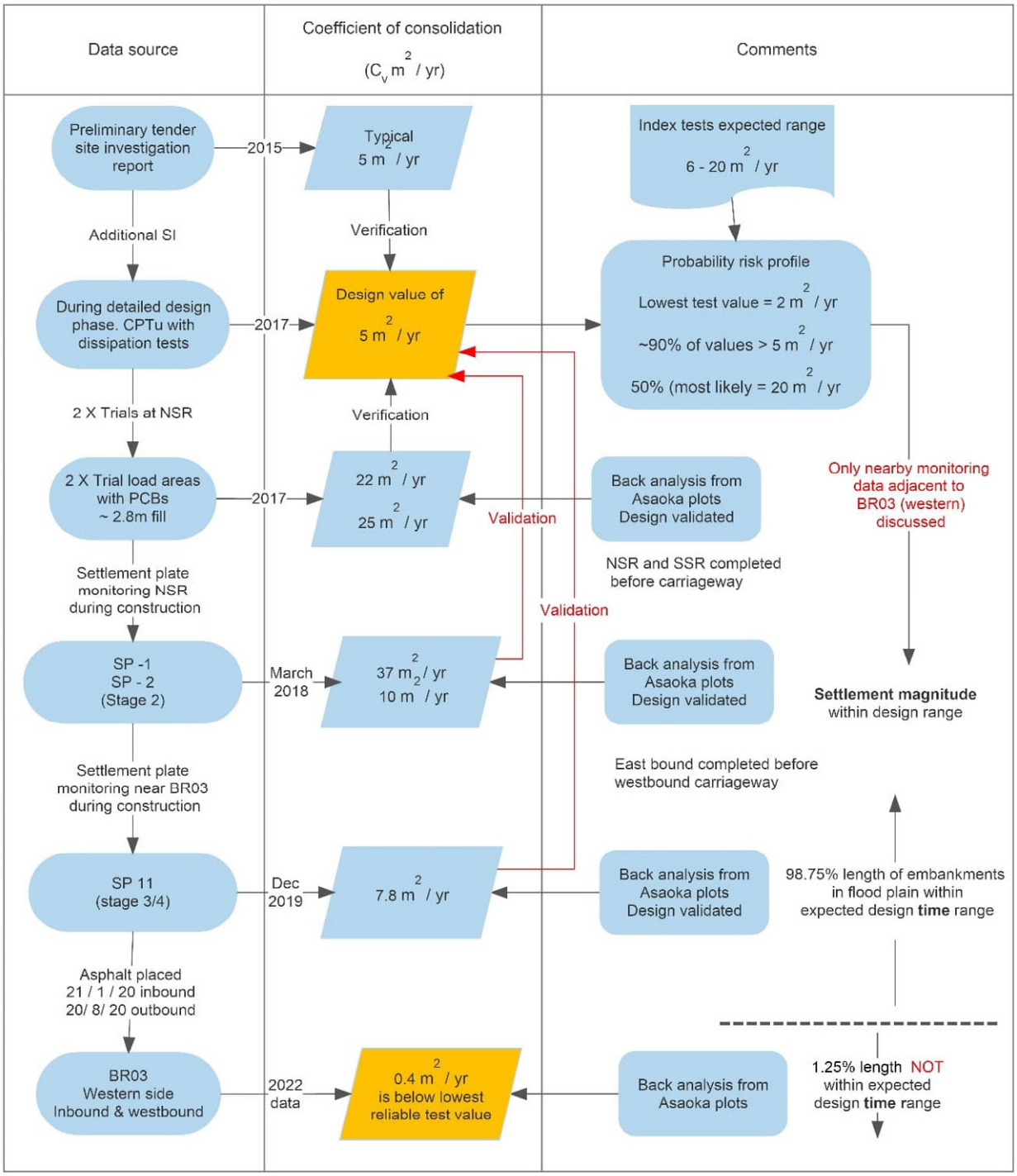

Figure 16: Comparison of analysis and test data of C_v prior to, during and post construction

This paper highlights even with a site-specific data, conservative design values and with sensitivity checks, simulation risk models, trial sections, and settlement monitoring during construction of adjacent and earlier stages, that settlement time in this case was exceeded.

As an advocate for simulation models to envelope risk (Look,2022) in a way that sensitivity analysis is not able to evaluate, and given limited data on most projects, this case study was written to show the journey is far from over with respect to time for settlement. Strength based simulations have not had this anomaly (so far as known). The data input assessment remains critical, and this consolidation case suggests stepping beyond actual test results. This is not technically rationale. Of course, the usual geotechnical plea for additional and high-quality testing still applies, but time and cost constraints are the reality in any project. Highlighting and detailing lesson learnt for this case study where risk was not fully enveloped in the simulation analysis, should not detract from its benefits.

7. CONCLUSIONS

This case study provides an insight into the wide variation of test results and considerations in selecting a design value. Selection of a moderately conservative design value for settlement analysis requires rigour before analysis should proceed. The benefits of simulation analysis typically envelopes the risk associated with compressible clays. Specifically, time for settlement can be highly variable.

The risk of time prediction and assignment of the c_v value must be given due consideration to envelope the wide variability of field and laboratory results. Using an overly conservative value has significant cost implications. The requirement of field observation should be mandatory in such compressible materials, and yet this case study highlights how settlement times may still stray outside prediction models and adjacent construction monitoring data. Ultimately models are as only as good as the quantity and quality of the data input.

A back-analysis of the settlement data was undertaken to determine the coefficient of vertical consolidation observed following construction. The geotechnical design has been validated by 98.75% of the motorway site. However, at BR03 (western abutment) the settlement time is not consistent with the data and performance of the rest of this site within the flood plain. This settlement time has occurred is in excess of the 3-month period assumed as part of the detailed design at this area. The risk seems reasonable within the data available for a design engineer, and was validated (mostly) during construction, but client expectations are different.

This comparison shows that back-calculated coefficient of vertical consolidation could not have been reasonably selected at the time of design, using the data that was available. The back calculated c_v value is lower than test values provided prior to design, and the additional testing carried out during the detailed design phase, as well as from verified from 2 trial test load areas and validated from back analysis of settlement plates data during construction. Neither moderately conservative with sensitivity analysis with lower bound values nor simulation models for risk analysis predicted this time possibility.

The magnitudes of settlement were all within the design and risk model prediction at this site. Time for settlement remains the greater unknown in a design prediction. This case study highlights how simulation analysis was used to envelope data variability and associated risk. A black swan event was also shown in this case study. However, such an outlier should not detract from the benefits of including the wide variability of data in a simulation model versus the selection of a singular deterministic design value.

8. ACKNOWLEDGEMENTS

Adam Kemp was active in the analysis and reporting of some of the data presented in the project phase.

9. REFERENCES

Jamiolkowski M, Ladd C.C., Germaine J.T. and Lancelotta R. (1985). New developments in field and laboratory testing of soils, *11th International Conference on Soil Mechanics and Foundation Engineering* (San Francisco)

Kemp A, Look B and Lacey D (2019). Integration of geotechnical models with data visualisation tools for the Ipswich Motorway Upgrade – Rocklea to Darra. *13th Australia New Zealand Conference in Geomechanics*, Perth

Look, B.G. (2015). Appropriate distribution functions in determining characteristic values. *12th Australia New Zealand Conference in Geomechanics*, Wellington, New Zealand, P014.

Look, B. G (2021). Compaction density of residual soils and weathered rock. *Australian Geomechanics*, Vol 56, No.1, pp 61 – 75.

Look, B.G. and He, W (2022a*)*. Simulations used in geotechnical practice: Part 1 – comparing Monte Carlo ad Latin hypercube sampling. *8th International Symposium on Geotechnical Safety and Risk* (ISGSR 2022) Newcastle, Australia, 14–16 December, pp 1003 – 1008.

Look, B.G. and He, W (2022b). Simulations used in geotechnical practice: Part 2 – comparing normal and non-normal PDF in sampling. *8th International Symposium on Geotechnical Safety and Risk* (ISGSR 2022) Newcastle, Australia, 14–16 December, pp 1009 – 1014.

Look, Burt G (2022). Managing geotechnical uncertainty with simulation models: An introduction. *Australian Geomechanics,* Vol 57, No. 4, pp 25 – 44.

Look, Burt G (2023). Assessment of the coefficient of consolidation with Queensland data. *Australian Geomechanics*. Vol 58, No. 2, pp 105 – 120.

NAVFAC (1986). *Soil mechanics – Design manual 7.1*, Department of the Navy, Naval Facilities Engineering Command, U.S. Government Printing Office, Washington, DC

Rowe, P.W. (1972), The relevance of soil fabric to site investigation practice. *Géotechnique*, Vol. 22, No. 2, pp 195 – 300.

Tomlinson M.J. (1995). *Foundation design and construction*, Sixth Edition, Longman Publication.

NATURAL HAZARD PROTECTION? SURE!

Tested to the world's toughest standards and beyond, our systems provide the level of protection you need. Whether from rockfall, landslides, debris flows, or coastal erosion. Whether standard or special solutions. Learn more: **www.geobrugg.com**

MANUFACTURED IN AUSTRALIA

Geobrugg Australia Pty Ltd
300 Victoria Road | Malaga WA 6090
T +61 8 9249 9939
www.geobrugg.com.au

Regional offices
Sydney NSW, T +61 400 845 289
South Melbourne VIC, T +61 488 044 708
Brisbane QLD, T +61 488 044 003
Perth, WA +61 477 470 064

BRUGG
Geobrugg

Safety is our nature

TERRATEST

SITE INVESTIGATION DRILLERS

From the pint-sized XC to CPT, from Queensland, to Newcastle, Sydney, and down to Melbourne, Terratest has the tools to get the job done and the staff to ensure it's done safely.

Sydney

Jon Maguire
E: jon@terratest.com.au
M: 0468 952 248

Newcastle

Paul Barker
E: paul@terratest.com.au
M: 0412 488 953

Queensland

Dave Coleman
E: dave@terratest.com.au
M: 0429 987 271

Victoria

Simon Hamilton
E: simon@terratest.com.au
M: 0412 496 672

CPT

Marten Sweeney
E: marten@terratest.com.au
M: 0412 272 953

Trilab

Accurate Quality Results

For tomorrow's engineering

Australia's Leading Independent Supplier of Specialised Soil & Rock Testing

Trilab is the specialised testing supplier of choice to some of the world's largest mining, civil construction, and infrastructure projects. Our soil and rock mechanics testing services and technical assessment of soil and rock characteristics are used by our global clients to make critical decisions for their projects.

Trilab uses the latest geomechanical equipment, new testing methods, software and data acquisition systems.

Our full-service laboratories in Brisbane and Perth are accredited by NATA to perform rock and material testing to Australian and ASTM standards. We also offer ISO/IEC 17025 certified calibration and instrumentation support services for a large range of engineering metrology equipment including troubleshooting of existing software used in the automation of laboratory test methods.

Soil

- UU/CU/CD Triaxial
- CSL/Ko Triaxial
- Oedometer
- Permeability
- Texas Triaxial
- Direct Shear & Torsional Ring Shear
- CRS & Rowecell Consolidation
- UCS/QU with Young's Modulus
- CBR & Compaction
- Dispersion & Chemical Testing
- Classification & Index Testing
- Cyclic & Monotonic Direct Simple Shears

Rock

- High Pressure Rock Triaxial Testing System
- Rock UCS with Young's Modulus and Poisson's Ratio
- Direct Shear
- Triaxial
- P and S Wave / Sonic Velocity
- Point Load Index
- Brazilian (Indirect Tensile Strength)
- Slake Durability and Dispersion
- Cerchar Abrasivity
- Direct Tensile Strength

Calibration

- NATA calibration of wire woven and plate sieves to AS, ASTM and ISO specifications
- Dial gauges to NATA CMT and AS2103 requirements
- Load Cells / Proving Rings
- Extensometers
- Concrete and material testing machines
- Electronic balances up to 60kg
- Pressure gauges / transducers
- Vernier calipers
- Rubber hardness for AS1289.3.1.1

Trilab

Brisbane
346A Bilsen Road,
Geebung QLD 4034
+61 7 3265 5656

Perth
2 Kimmer Place,
Queens Park WA 6107
+61 8 9258 8323

National Association of Testing Authorities, Australia (NATA, Accredited Laboratory No. 9926)

ISO/IEC 17025 Certified Laboratory Systems for Testing and Calibration Services

Member of Australian Geomechanics Society and International Society of Rock Mechanics

www.trilab.com.au

Established 1994 | Over 40 Expert Staff | Critical Design Partner

WORKING PLATFORMS AND BEARING CAPACITY ASSESSMENTS OF SAND OVERLYING CLAY USING FINITE ELEMENT LIMIT ANALYSIS

Sean J Goodall[1] and Richard S Merifield[1,2]

[1] Douglas Partners Pty Ltd, Newcastle. [2] The University of Newcastle, Australia

https://doi.org/10.56295/AGJ5835

ABSTRACT

The bearing capacity of shallow foundations on layered soils is typically based on empirical models assuming a strip footing. Shape factors are then applied to the strip footing solution to account for the specific geometry of the foundation being considered. A common practical application of this methodology is when the ultimate bearing capacity of a granular working platform constructed over a clay subgrade is estimated using the Working Platforms for Tracked Plant BRE-470 guideline. Previous studies using finite element limit analysis have been undertaken to examine a strip footing on a layered soil and how the resulting bearing capacity compares to that derived from BRE-470. This paper presents an extension of previous work by the authors using finite element limit analysis to investigate the three-dimensional influence on the bearing capacity of square and rectangular footings on sand over clay. The finite element limit analysis solutions are used to produce charts to assist designers with estimating the ultimate bearing capacity of granular working platforms overlying clay. The paper also aims to highlight some important considerations when adopting the BRE-470 guideline to design granular working platforms overlying clay.

1 INTRODUCTION

The bearing capacity of a footing resting on sand overlying clay is a classic geotechnical engineering problem, commonly encountered in the design of a working platform. Working platforms normally comprise a good quality granular material, such as fine crushed rock, that is placed and compacted in a controlled manner, over a weak clay subgrade. The design of a working platform aims to determine the thickness and strength of the granular layer such that a minimum factor of safety against bearing capacity failure is achieved.

Several studies (Shiau et al 2003, Salimi Eshkevari & Abbo 2015 and Salimi Eshkevari et al 2019a) using Finite Element Limit Analyses (FELA) have investigated the bearing capacity of a footing resting on sand overlying clay. These studies have indicated that the bearing capacity depends on the relative strength of the two layers, which differs from what is assumed in the commonly used design guideline BRE-470 Working Platforms for Tracked Plant (BRE 2004) method (ie the bearing capacity contributions of each layer are decoupled). Whilst these previous studies are insightful to the behaviour of a footing resting on sand overlying clay, they have been limited to plain strain conditions which limits the use of the solutions in engineering practice.

The objective of this paper is to investigate the three-dimensional bearing capacity of square and rectangular footings resting on sand overlying clay using FELA. The results of the modelling are used to develop dimensionless design charts for a range of commonly encountered geotechnical conditions, working platforms and more generally footings resting on sand overlying clay. Comparisons with the BRE (2004) method are also provided for some selected cases. It is emphasised that it is not the intention of this paper to advocate or criticise the BRE-470 guideline, rather it aims to provide an alternative to compare the method with and to provide additional tools for geotechnical engineers to design working platforms, in particular, for situations that may fall outside the scope of the BRE-470 guideline.

2 LITERATURE REVIEW AND BACKGROUND

2.1 BEARING CAPACITY OF LAYERED SOILS

2.1.1 Empirical methods

In the authors' experience, the most frequently cited method to estimate the bearing capacity of sand overlying clay comes from Meyerhof (1974) and Hanna & Meyerhof (1980). These methods assume that a rigid block of sand is pushed down into the underlying clay and is commonly referred to as a punching shear model. In this instance, the ultimate bearing capacity of a strip footing is assessed using the following Equation 1.

$$q_u = s_u N_c + \frac{\gamma D^2}{B} K_p \tan(\delta) \leq q_s \quad (1)$$

Where s_u is the undrained shear strength of the clay layer, N_c is a bearing capacity factor (typically taken as equal to 5.14 for strip footings with no embedment), γ is the unit weight of the sand, D is the thickness of the sand, B is the width of the footing, K_p is the coefficient of passive earth pressure, δ is the average mobilised frictional angle and q_s is the ultimate bearing capacity of the same footing resting on a layer of uniform sand with the same friction angle and unit weight. Meyerhof (1974) indicated that the average mobilised friction angle δ was a function of the friction angle of the sand φ', and varied between φ'/2 to 3φ'/4. Meyerhof (1974) proposed an average value of 2φ'/3 for practical applications.

An alternative to the punching shear model is the load spread model (Terzaghi and Peck 1948). This bearing capacity model assumes that the load is distributed through the upper sand resulting in a hypothetical footing of an equivalent width resting on the clay layer beneath. The method ignores any contribution from the strength of the overlying sand. The bearing capacity of a strip footing is then assessed using classical bearing capacity theory as shown in the following equation:

$$q_u = s_u N_c \frac{B'}{B} \quad (2)$$

Where B' is the effective width of the hypothetical footing as defined in the following equation:

$$B' = B + 2Dtan(\theta) \quad (3)$$

Terzaghi & Peck (1978) proposed θ be taken as 26.6°, which is commensurate with a 2V:1H stress distribution. Later studies have indicated 2V:1H assumption may not be appropriate where a layered soil profile is present as the angle is a function of the relative strength of the upper and lower layers (Burd & Frydman 1997). Further discussion on the load spread angle is provided in Burd & Frydman (1997) and Salimi Eshkevari et al (2019a).

2.1.2 Numerical methods

Although conventional displacement finite element analysis can be used to predict the ultimate bearing capacity of a footing on layered soil, the estimate obtained is neither a lower nor upper bound (Shiau et al 2003). Furthermore, a phenomenon referred to as 'locking' can occur and is characterised by a constantly rising load deformation curve and can lead to inaccurate estimates of the ultimate bearing capacity (Sloan & Randolph 1982 and Shiau et al 2003). One method to overcome these limitations is to apply the limit analysis theorems to estimate the rigorous plasticity solutions using linear finite elements (commonly referred to as finite element limit analysis or FELA). Further details on the background and theory of FELA applied to bearing capacity problems is provided in Merifield et al (1999), Shiau et al (2004), Salimi Eshkevari et al (2019a) and Salimi Eshkevari et al (2019b).

FELA has been successfully applied to estimate the bearing capacity of strip footings on layered clays (Merifield et al 1999), sand over clay (Shiau et al 2003 and Salimi Eshkevari et al 2019a) and layered sands (Salimi Eshkevari et al 2019b). However, to the authors' knowledge, limited studies using FELA have considered three-dimensional footing effects on the resulting ultimate bearing capacity of a layered soil. For example, solutions appear to be limited to Merifield & Nguyen (2006) who provide the ultimate bearing capacity for square and circular footings resting on a layered clay.

2.2 WORKING PLATFORM THICKNESS DESIGN

In Australian practice, it is common to refer to the design guideline 'Working Platforms for Tracked Plant', published by the Building Research Establishment (BRE 2004) for guidance when designing a working platform. Even though BRE (2004) is aimed at tracked plant, it has found its way into routine working platform assessments for both tracked and outrigger plant without much consideration of the limitations or applicability of the design guide.

Even though the BRE (2004) approach has proven to be useful in assessing and preparing the design of working platforms, some authors have indicated that BRE (2004) can result in both thick working platforms and over predictions of the

bearing capacity (Corke & Gannon 2010 and Eshkevari & Abbo 2015). It is important to highlight that, even though the method has been shown to yield conservative working platforms, there are many other factors that may contribute to the perceived conservatism of the BRE (2004) method. For example, pessimistic / lower bound subgrade strengths adopted in design and that the friction angle of the granular layer is usually much higher than what is adopted in design. From a designer's perspective, this should seem sensible, since most of the time the subgrade strength is assessed using simple methods (eg a dynamic cone penetrometer or pocket penetrometer to assess subgrade strength is common) and the friction angle of the granular material is not normally determined from laboratory testing. This would usually be acceptable on simple sites for routine working platform assessments, however, where large / high risk lifts are proposed or there are difficult / poor ground conditions, a more rigorous assessment of the geotechnical parameters should be considered.

In the authors experience, there also appears to be some misunderstandings or misconceptions in industry regarding the track bearing pressure and loading geometry for working platform thickness design. All too often, we (consultants) receive requests like 'just design the working platform for 300 kPa', without any information on how or what situation the track pressures are to be considered. And when queried, or clarifications requested, responses like 'this has not been an issue in the past, why can't you just design it for 300 kPa' or 'here is the technical drawing for the rig, just use the track dimensions' or 'what do you mean travelling / standing and drilling / extracting load cases'. From a geotechnical perspective, it is apparent that the resultant thickness of any working platform is directly proportional to the magnitude and geometry of the loading. It is also very apparent from BRE (2004) how important what situation the loading occurs in. Unfortunately, this message is either not always conveyed or understood by contractors and designers alike and has the potential to lead to both unsafe and overly conservative situations.

Further discussions on BRE (2004) can be found in Look & Honeyfield (2016) and the accompanied discussion paper by Buttling (2016). Although not discussed further here, these two references include an insightful case study, discussions around the limitations of BRE (2004) and issues of conservatism and how these might be managed.

The general approach in BRE (2004) for assessing the bearing capacity of a granular layer overlying clay has been based on the work of Meyerhof (1974) and Hanna & Meyerhof (1980) (eg punching failure bearing capacity model) and adopts the average mobilised friction value proposed by Meyerhof (1978). BRE (2004) qualifies this by stating that a simple approach to assess the ultimate bearing capacity of a working platform of a relatively shallow thickness placed on a weak subgrade is to adopt a punching shear model. However, BRE (2004) provides limited guidance or background to determine if the granular layer is considered 'relatively shallow', and only states the punching shear model is not appropriate when the ratio of D/B is larger than 1.5. Where a cohesive subgrade is being assessed, BRE (2004) states that it is limited to clay subgrades with undrained shears strengths between 20 kPa to 80 kPa.

BRE (2004) adopts the following equation to calculate the ultimate bearing capacity:

$$q_u = s_u N_c s_c + \frac{D^2 \gamma}{B} K_p \tan(\delta) s_p \quad (4)$$

Where s_c and s_p are shape factors as defined in the following equations:

$$s_c = 1 + 0.2\left(\frac{B}{L}\right) \quad (5)$$

$$s_p = 1 + \left(\frac{B}{L}\right) \quad (6)$$

Where L is the length of the footing.

The value of the shape factor s_c has been derived from experimental data from Meyerhof (1951), Meyerhof (1963) and Skempton (1951). The shape factor intends to account for the additional slip surfaces in front and behind the footing (Salgado et al 2004). More recently, the shape factor s_c has been derived numerically (Salgado et al 2004 and Zhu et al 2005). The shape factor s_c derived from the various authors and equations presented above are illustrated in Figure 1 (a).

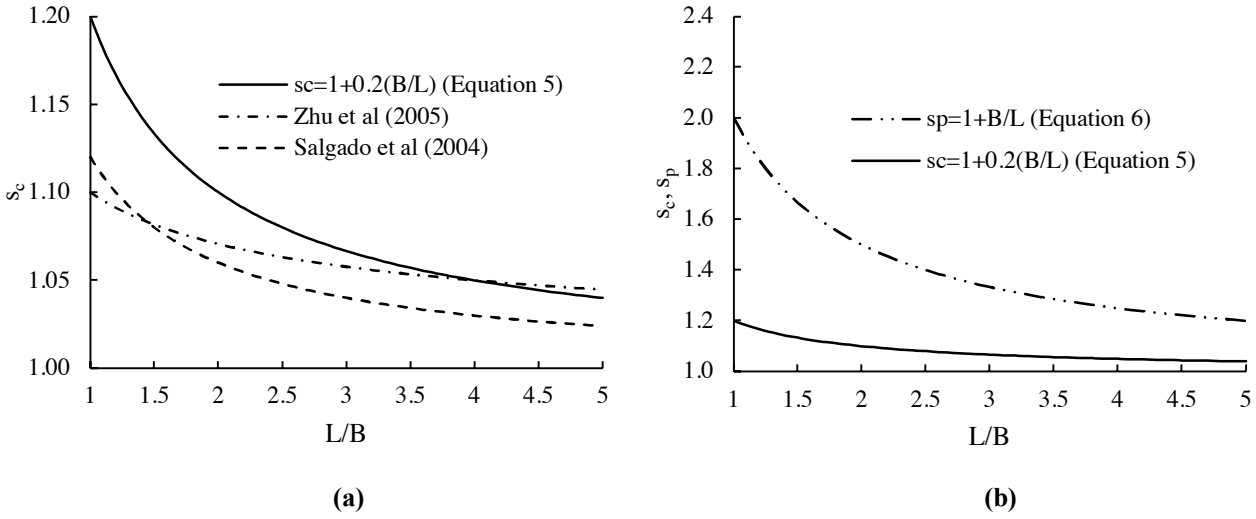

Figure 1: Shape factors from various authors:

(a) after Meyerhof (1951), Salgado et al (2004), Zhu et al (2005). (b) , BRE (2004)

Figure 1 (a) shows that the relationship after Meyerhof (1951) (Equation 5), as adopted in BRE (2004)) is only comparable to the numerically derived shape factors for large *L/B* ratios beyond about 3.5, which is typical of tracked plant. However, when considering outrigger plant, which typically have outrigger pads with *L/B* ratios of between 1 and 2, Meyerhof (1951) leads to unconservative estimates of the ultimate bearing capacity in the order up to about 10%.

The shape factor s_p proposed in BRE (2004) is said to be based on the volume of soil undergoing punching shear. To the authors' best knowledge, the shape factor s_p has not been proven either experimentally or numerically, and in comparison to the shape factor s_c, is some 15% to 70% larger for *L/B* ratios ranging between 1 to 5 (see Figure 1 (b)). Historically, shape factors have only been developed to be used with the general bearing capacity formula of a strip footing resting on a uniform homogenous soil. In the authors opinion, the applicability of using shape factors in a layered soil problem is dubious and should be undertaken with caution. It is important to point out BRE (2004) provides no discussion or evidence for the use of shape factors in calculating the ultimate bearing capacity of a footing resting on sand overlying clay.

Whilst not the aim of this paper, another relevant consideration is the factor of safety (FoS) adopted in the design of working platforms in order to derive the allowable (or safe) bearing capacity. Some guidance may be obtained from BRE (2004) on the choice of a FoS according to the design case being considered, although readers should be mindful that the definition presented in BRE (2004) is in the context of a load factor, which varies according to the load case being considered and also whether a working platform is required (ie the load factor varies between 1.2 to 2.0). In the authors experience, the FoS adopted in design of a working platform thickness can vary between 1.3 to 3.0. Ultimately, the FoS adopted for working platform design needs to be assessed and determined by the designer since this depends on many considerations including but not limited to the consequence of failure, the amount and quality of geotechnical data, design method / philosophy etc.

3 FINITE ELEMENT LIMIT ANALYSIS

3.1 PROBLEM DEFINITION

A series of FELA simulations were performed using the software OptumG2 and OptumG3 (Optum CE). Over 250 analyses were conducted from which values of limit loads were estimated for a range of geometric and material parameters (Table 1) and assumptions (rough and smooth footings). OptumG2 was used to assess the lower and upper bound limit loads for strip footings. The analyses in OptumG3 were performed using a mixed element type to assess the limit loads for square and rectangular footings. The mixed element type is based on the requirements of the upper and lower bound theorems and is found to be very accurate (Olsen & Krabbenhoft 2021). It is also the recommended element in Optum G3 (Optum 2020). Further discussion on the validation and application of the mixed element is given by Optum (2020) and Olsen & Krabbenhoft (2021). Both analyses have considered adaptive meshing. A simple schematic of the problem is given in Figure 2 along with examples of a typical upper bound mesh for a strip footing and mixed element mesh for a square footing.

Table 1: Problem Variable Considered

Parameter	Values
Friction angle of sand, φ' (°)	35, 40 and 45
Undrained shear strength of clay, s_u (kPa)	10, 20, 30, 40, 50, 60, 80, 100
Unit weight of sand, γ (kN/m^3)	18
Sand thickness, D (m)	0.25, 0.5, 1.0 and 2.0
Foundation width, B (m)	1.0
Foundation length, L (m)	1.0, 2.0 and 5.0

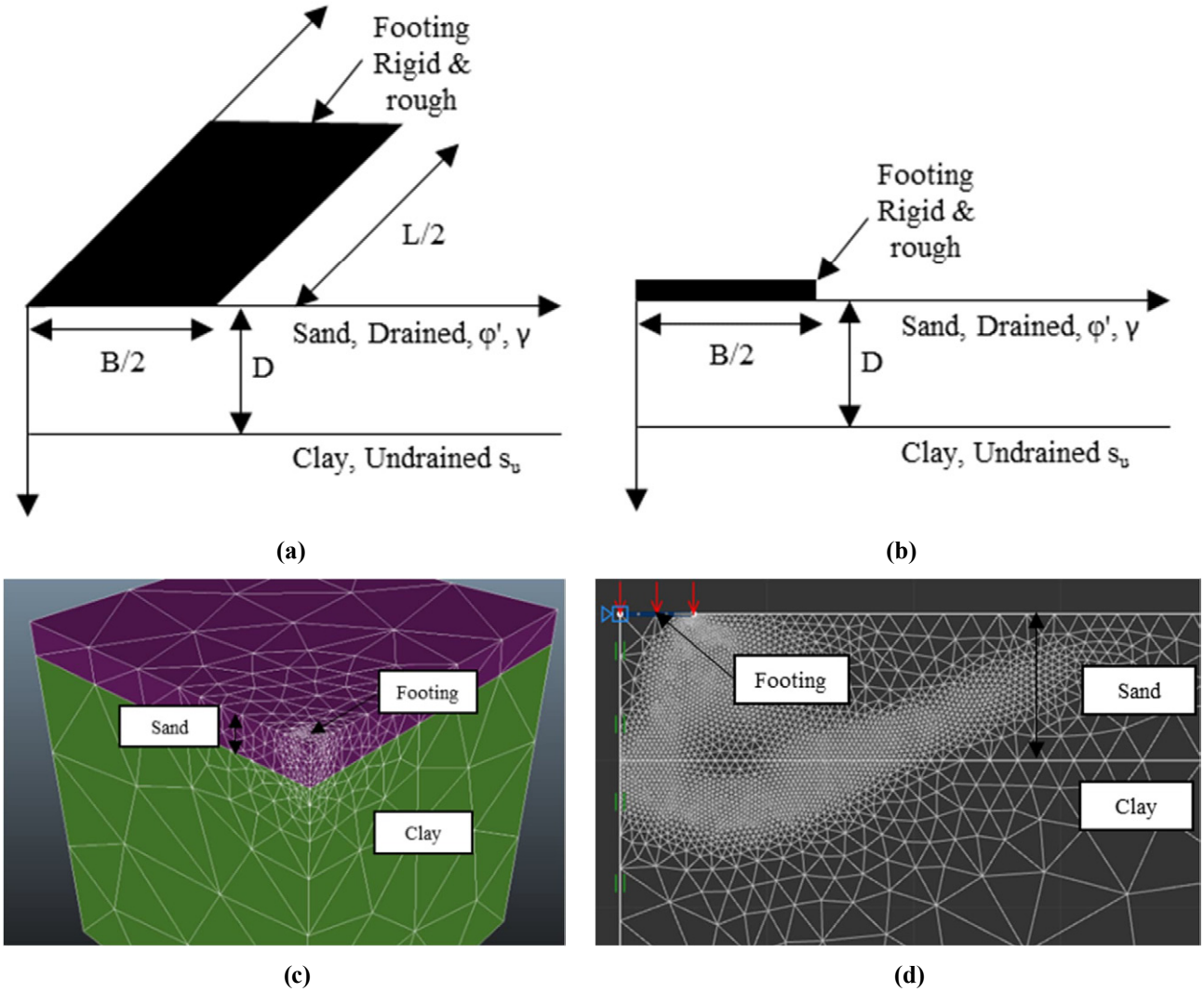

Figure 2: Problem definition and typical meshes:

(a) Three-dimensional problem definition. (b) Plain strain problem definition.

(c) Mixed element mesh in three-dimensional analysis. (d) Upper bound mesh in plain strain analysis

The sand and clay layers were modelled using Mohr-Coulomb and Tresca models respectively. The analysis is based on an associative flow rule. This assumption is considered reasonable since the problem is not strongly constrained due to the freely deforming ground surface and semi-infinite domain (Sloan 2013). The footing was modelled using a weightless shell / plate element and was assumed to be perfectly rigid and rough for the majority of the analyses. Due to symmetry a quarter of the foundation has been modelled in the three-dimensional analyses where possible. The 2D analyses of strip

footings considered half of the footing width where possible. The analyses have been limited to footings resting on the surface.

The ultimate bearing capacity from the FELA for the strip footing ($q_{u,\ strip}$) is taken as the average of the lower and upper bound limit loads (Salgado et al 2004). The relative error in the solution was assessed using the following equation and was found to be generally less than about 5 %, with the maximum relative in the order of about 10 %.

$$error\ \% = \frac{q_{u,upper\ bound} - q_{u,lower\ bound}}{q_{u\ ,upper\ bound} + q_{u,lower\ bound}} \times 100 \qquad (7)$$

3.2 BENCHMARKING AND COMPARISON WITH PUBLISHED DATA

There is limited data available to compare the current study with, however, analyses were undertaken for various cases and benchmarked against available published solutions for a square footing resting on a uniform sand layer (Martin 2005, Meyerhof 1951, Meyerhof 1963), for a strip footing resting on sand overlying clay (Michalowski & Shi 1995, Burd & Frydman 1997, Shiau et al 2003 and Salimi Eshkevari et al 2019a), and centrifuge data of strip and circular footings resting on sand overlying clay (Okamura et al 1997). The results from the benchmark / validation exercises are presented in Figure 3 (a) to (d).

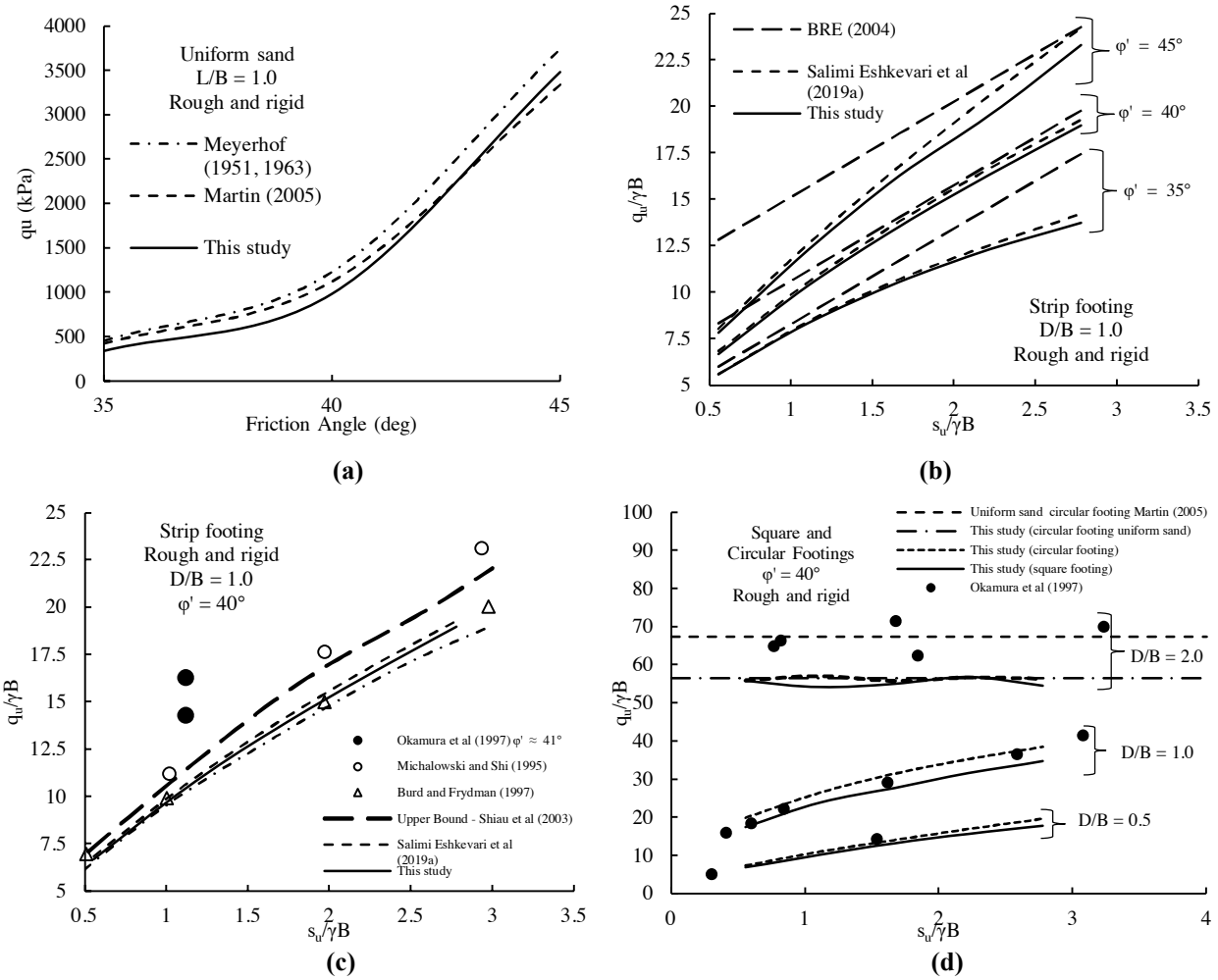

Figure 3: Results of benchmarking and comparisons with published data:
(a) Square footing on uniform sand – This study, Meyerhof (1951), Meyerhof (1963) and Martin (2005).
(b) Strip footing *D/B* = 1.0 – This study, BRE (2004) and Salimi Eshkevari et al (2019a)
(c) Strip footing *D/B* = 1 φ' = 40° – This study, Michalowski & Shi (1995), Burd & Frydman (1997), Okamura et al (1997), Shiau et al (2003) and Salimi Eshkevari et al (2019a).
(d) Square and circular footing φ' = 40° – This study, Okamura et al (1997) and Martin (2005).

The bearing capacity estimated from this study for the various cases considered can be seen to compare reasonably well with other available published results and data.

Although not presented here, the benchmarking exercises included comparisons of the resulting limit loads from lower, upper and mixed element types in the three-dimensional analyses for selected cases. The relative error between the mixed element and those obtained from the averaging of the upper and lower bounds was found to be generally less than about 3 %, with the maximum relative error in the order of about 10 %.

3.3 RESULTS AND DISCUSSION

3.3.1 Parametric study and ultimate bearing capacity

A parametric study based on the Table 1 parameters was undertaken to estimate the limit loads for rough and rigid, strip, square (L/B = 1) and rectangular (L/B = 2 and 5) footings resting on sand overlying clay. The results of the analysis have been presented in Figure 4 to Figure 8 and Table 2 to Table 4. It is acknowledged some results exhibit some minor oscillating / variation, albeit very small, and is likely to be attributed to minor variations in numerical convergence.

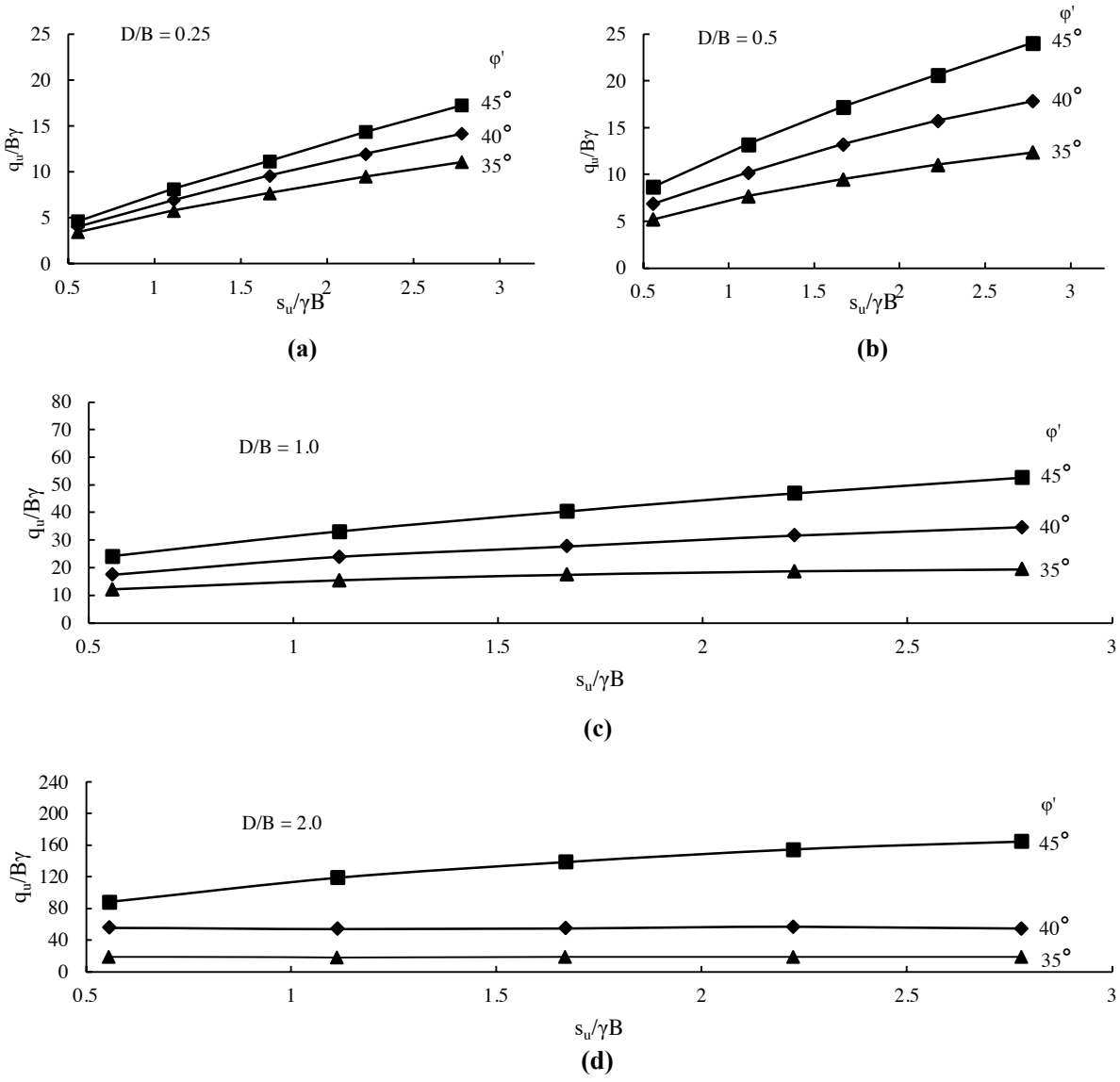

Figure 4: Ultimate bearing capacity ($q_u/B\,\gamma$) for rough rigid square footings (L/B = 1.0) on sand overlying clay: (a) D/B = 0.25. (b) D/B = 0.5. (c) D/B = 1.0. (d) D/B = 2.0.

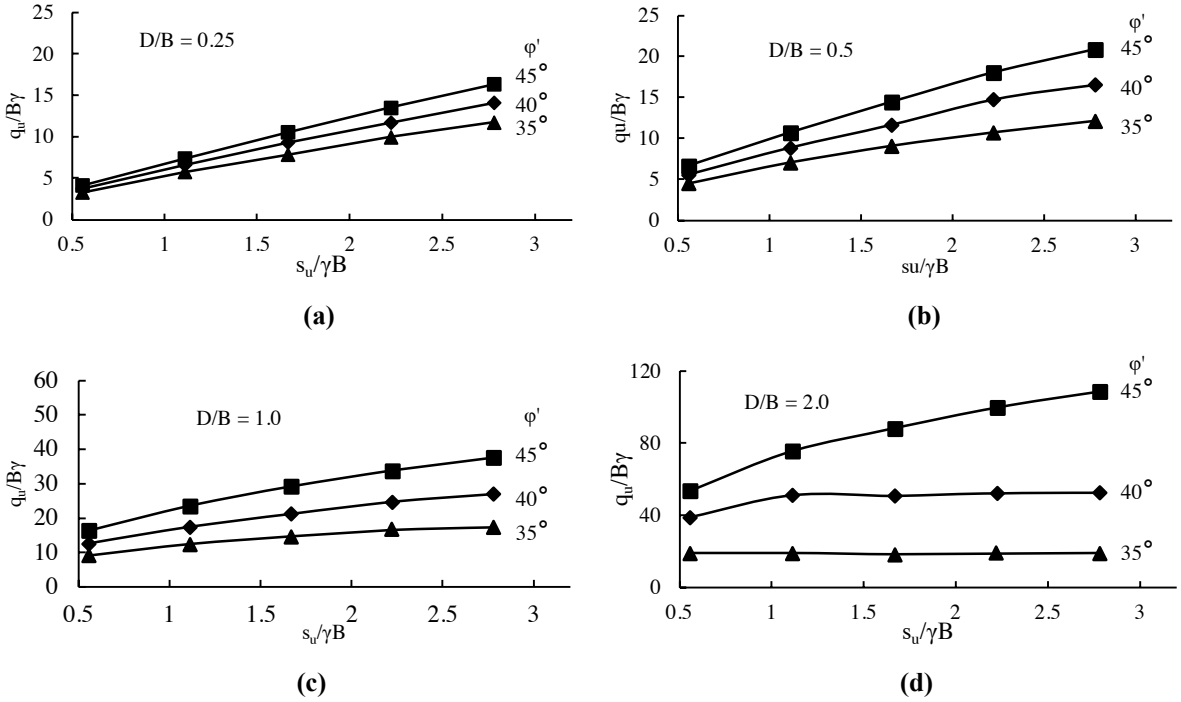

Figure 5: Ultimate bearing capacity ($q_u/B\ \gamma$) for rough rigid rectangular footings (L/B = 2.0) on sand overlying clay:

(a). D/B = 0.25. (b) D/B = 0.5.

(c) D/B = 1.0. (d) D/B = 2.0.

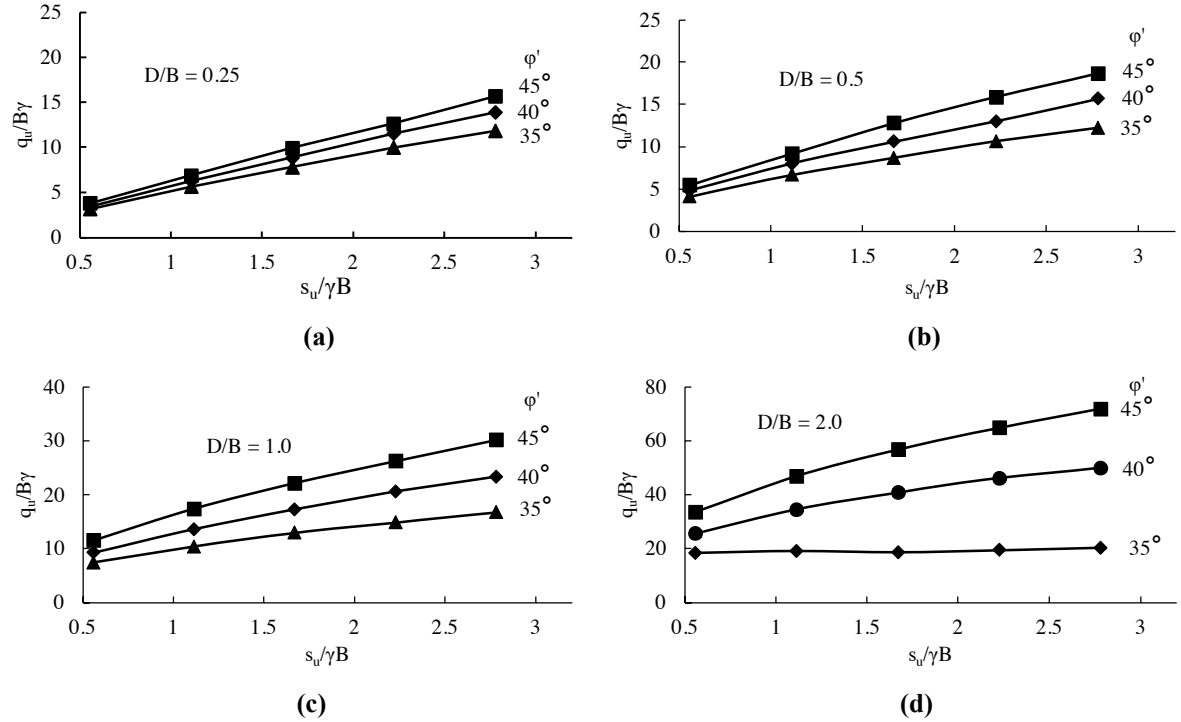

Figure 6: Ultimate bearing capacity ($q_u/B\ \gamma$) for rough rigid rectangular footings (L/B = 5.0) on sand overlying clay:

(a) D/B = 0.25. (b) D/B = 0.5.

(c) D/B = 1.0. (d) D/B = 2.0

Table 2: Values of ultimate bearing capacity ($q_u/B\,\gamma$) rough rigid footings φ' = 35 °

D/B	$s_u/\gamma B$	Ultimate bearing capacity ($q_u/B\,\gamma$)			
		Square Footing (*L/B* = 1.0)	**Rectangular Footing (*L/B* = 2.0)**	**Rectangular Footing (*L/B* =5.0)**	**Strip Footing (*L/B* = ∞)**
0.25	0.56	3.43	3.28	3.17	2.90
	1.11	5.78	5.75	5.64	5.31
	1.67	7.68	7.83	7.80	7.51
	2.22	9.48	9.97	9.97	9.60
	2.78	11.10	11.74	11.84	11.59
0.5	0.56	5.24	4.54	4.11	3.53
	1.11	7.71	7.06	6.68	5.96
	1.67	9.50	9.09	8.71	8.04
	2.22	11.03	10.76	10.65	9.87
	2.78	12.41	12.14	12.25	11.57
1.0	0.56	12.21	9.27	7.41	5.61
	1.11	15.43	12.50	10.40	8.46
	1.67	17.53	14.72	12.97	10.72
	2.22	18.73	16.63	14.88	12.55
	2.78	19.46	17.47	16.75	14.22
2.0	0.56	18.93	19.11	18.44	11.84
	1.11	18.53	19.11	19.10	15.99
	1.67	18.64	18.37	18.62	16.67
	2.22	18.67	18.81	19.39	16.57
	2.78	18.65	19.13	20.27	16.55
Uniform Sand	-	18.98	19.06	18.92	16.53

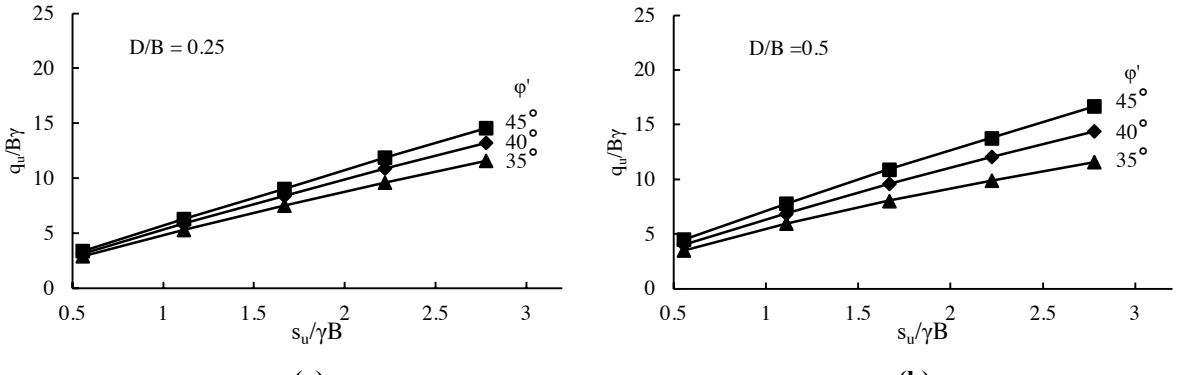

(a) **(b)**

Figure 7: Ultimate bearing capacity ($q_u/B\,\gamma$) for rough rigid strip footings on sand overlying clay: (a) *D/B* = 0.25. (b) *D/B* = 0.5.

Table 3: Values of ultimate bearing capacity ($q_u/B\,\gamma$) rough rigid footings φ' = 40 °

D/B	$s_u/\gamma B$	Ultimate bearing capacity ($q_u/B\,\gamma$)			
		Square Footing (*L/B* = 1.0)	**Rectangular Footing (*L/B* = 2.0)**	**Rectangular Footing (*L/B* =5.0)**	**Strip Footing (*L/B* = ∞)**
0.25	0.56	4.03	3.73	3.44	3.17
	1.11	6.92	6.60	6.28	5.85
	1.67	9.57	9.29	8.88	8.38
	2.22	11.95	11.71	11.55	10.88
	2.78	14.18	14.11	13.91	13.21
0.5	0.56	6.93	5.59	4.82	4.01
	1.11	10.22	8.88	8.03	6.85
	1.67	13.26	11.67	10.62	9.59
	2.22	15.74	14.77	13.01	12.04
	2.78	17.87	16.57	15.69	14.40
1.0	0.56	17.55	12.74	9.28	6.69
	1.11	23.92	17.53	13.61	10.39
	1.67	27.79	21.31	17.27	13.55
	2.22	31.68	24.77	20.60	16.35
	2.78	34.73	27.16	23.35	18.99
2.0	0.56	55.80	39.00	25.58	14.45
	1.11	54.17	51.31	34.55	20.97
	1.67	55.06	50.87	40.84	26.21
	2.22	56.79	52.35	46.20	29.81
	2.78	54.60	52.66	49.93	33.51
Uniform Sand	-	54.81	50.12	49.05	40.91

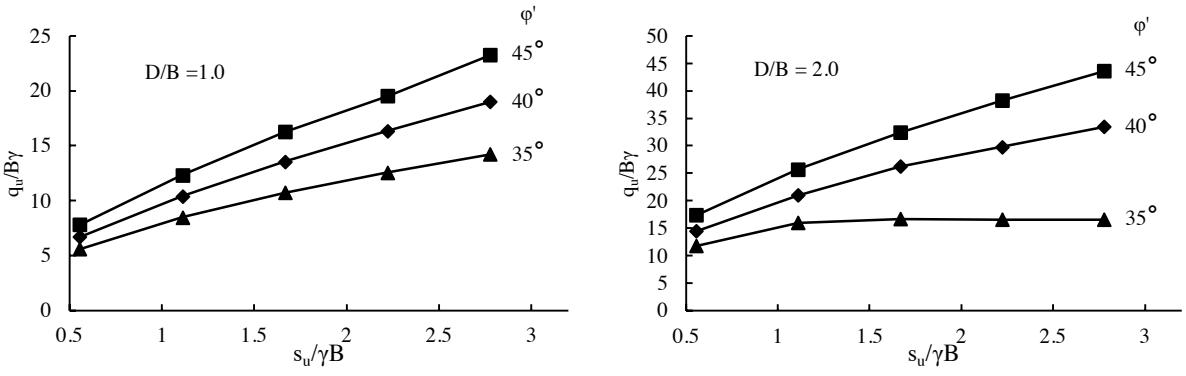

(a) **(b)**

Figure 8: Ultimate bearing capacity ($q_u/B\,\gamma$) for rough rigid strip footings on sand overlying clay: (a) *D/B* = 1.0. (b) *D/B* = 2.0.

Table 4: Values of ultimate bearing capacity ($q_u/B\gamma$) rough rigid footings φ' = 45 °

D/B	$s_u/\gamma B$	Ultimate bearing capacity ($q_u/B\,\gamma$)			
		Square Footing (*L/B* = 1.0)	**Rectangular Footing (*L/B* = 2.0)**	**Rectangular Footing (*L/B* =5.0)**	**Strip Footing (*L/B* = ∞)**
0.25	0.56	4.63	4.12	3.78	3.37
	1.11	8.12	7.36	6.90	6.29
	1.67	11.17	10.55	9.92	9.04
	2.22	14.35	13.48	12.64	11.88
	2.78	17.26	16.35	15.68	14.58
0.5	0.56	8.71	6.66	5.48	4.50
	1.11	13.24	10.73	9.18	7.78
	1.67	17.24	14.49	12.81	10.89
	2.22	20.65	18.08	15.90	13.76
	2.78	24.10	20.90	18.68	16.64
1.0	0.56	24.23	16.56	11.56	7.83
	1.11	33.18	23.66	17.43	12.32
	1.67	40.43	29.34	22.13	16.27
	2.22	46.99	33.88	26.22	19.54
	2.78	52.69	37.76	30.15	23.29
2.0	0.56	88.12	53.79	33.58	17.44
	1.11	119.00	75.77	46.82	25.71
	1.67	138.97	88.43	56.74	32.40
	2.22	154.82	99.95	64.86	38.26
	2.78	164.78	108.82	71.78	43.62
Uniform Sand	-	193.57	160.25	141.75	112.51

The results shown in Figure 4 to Figure 8 indicate that the ultimate bearing capacity from the FELA have an almost linear variation with the undrained shear strength of the clay for low *D/B* ratios. However, as *D/B* increases, this tends to a power law, particularly for higher friction angles of the sand. A similar behaviour for strip footings was observed by Shiau et al (2003) and Salimi Eshkevari et al (2019a).

For *D/B* = 2.0, the FELA analysis indicates for φ' < 40°, the failure mechanism is generally constrained to the sand (ie the constant ratio of $q_u/B\gamma$), refer Figure 4 (d), Figure 5 (d) and Figure 6 (d). However, for the same *D/B* and when φ' = 45° (refer Figure 4 (d), Figure 5 (d) and Figure 6 (d)) the lower clay layer is still having an appreciable effect on the ultimate bearing capacity. This indicates that there is a critical ratio of *D/B* and that there is a likely a transitional failure mechanism (eg from a general bearing failure within the sand to a punching failure into the clay) that is influenced by the relative shear strength of the upper and lower layers, and the geometrical aspects of the loaded area. Similar behaviours have been discussed by Michalowski & Shi (1995), Shiau et al (2003), Merifield & Nguyen (2006) and Salimi Eshkevari et al (2019b). It is also of interest to highlight that the limiting values of the ultimate bearing capacity observed are similar to $N_\gamma/2$ obtained from Martin (2005) ($N_\gamma/2$ = 17.23 to 42.78 for φ' = 35° and 40° respectively) and Meyerhof (1951, 1963) ($N_\gamma/2$ = 18.58 to 46.85 for φ' = 35° and 40° respectively), albeit with some slight variation which would be attributed to the footings three dimensional geometry.

3.3.2 Comparisons with BRE (2004)

The results of the analysis in Section 3.3.1. have been compared to an equivalent BRE (2004) assessment. The BRE (2004) assessment has been based on Equations 4 to 6. Where relevant, the BRE (2004) assessment has considered a limiting ultimate bearing capacity based on a uniform sand layer and the procedures in BRE (2004) (eg assuming uniform granular layer with a load applied at the surface). The comparisons are presented in Figure 9 and Figure 10 for the selected cases of a square footing (L/B = 1.0) and rectangular footing (L/B = 5) respectively.

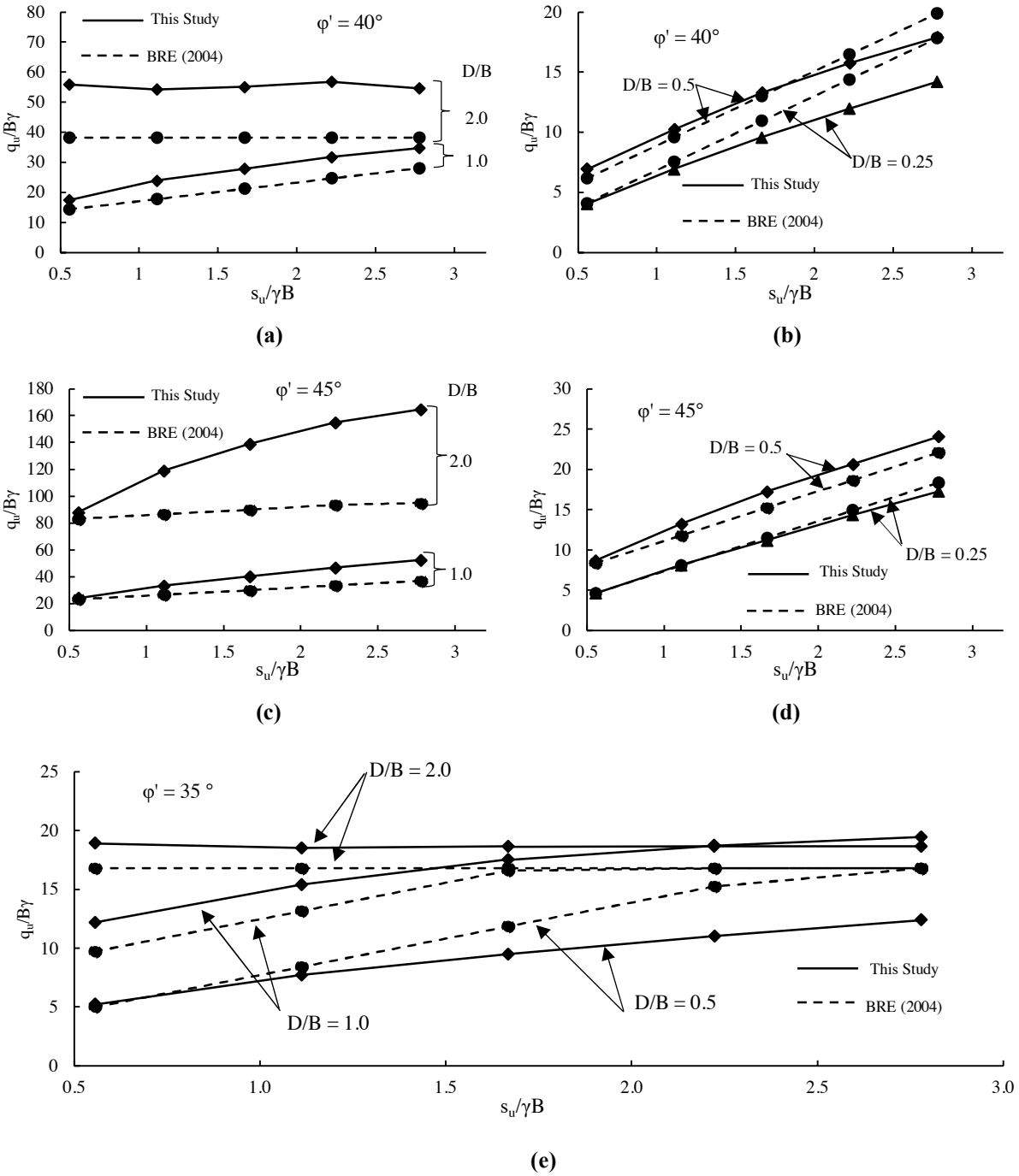

Figure 9: Comparisons with BRE (2004) and the effect of sand thickness for a rigid rough square footing (L/B = 1.0):

(a) φ' = 40° with D/B = 1.0 and D/B = 2.0. **(b) φ' = 40° with D/B = 0.25 and D/B = 0.5.**

(c) φ' = 45° with D/B = 1.0 and D/B = 2.0. **(d) φ' = 45° with D/B = 0.25 and D/B = 0.5.**

(e) φ' = 35° with D/B = 0.5, D/B = 1.0 and D/B = 2.0.

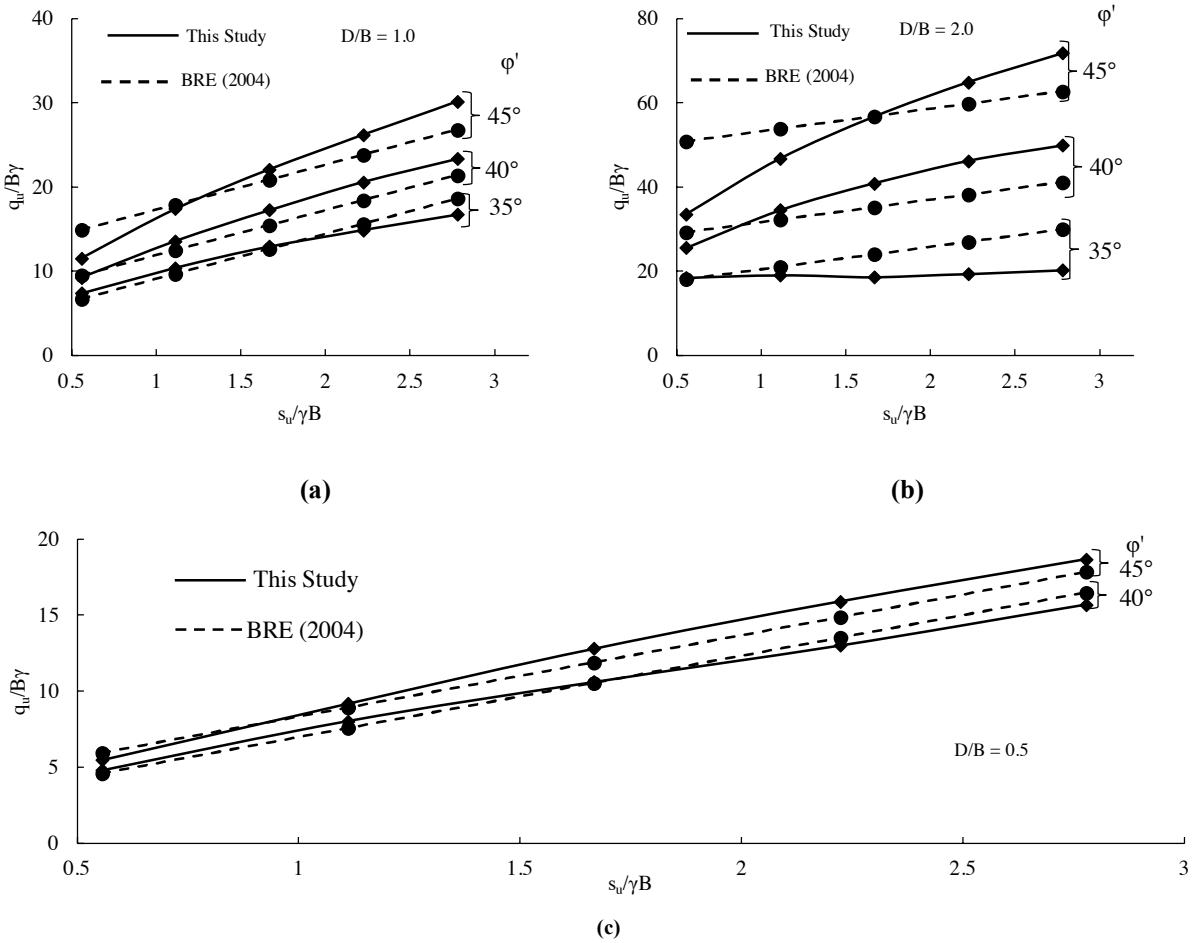

Figure 10: Comparisons with BRE (2004) and the effect of friction angle for rigid rough footing (*L/B* = 5)

(a) *D/B* = 1.0. (b) *D/B* = 2.0. (c) *D/B* = 0.5

Figure 9 (b) and (d) and Figure 10 (c) show that the ultimate bearing capacity from BRE (2004) is generally comparable to or slightly less than the FELA results for $\varphi' \geq 40°$ for $D/B \leq 0.5$ for the L/B ratios considered in this study. Although, as the strength of the clay increases, BRE (2004) tends to overestimate the bearing capacity for the case of $\varphi' = 40°$ (refer Figure 9 (b)).

As the working platform thickness increases, Figure 9 (a) and (c) and Figure 10 (a) and (b) show that the ultimate bearing capacity from BRE (2004) tends to be underestimated compared to the FELA (in the order of about 10% to 30% for $D/B = 1.0$ and 50% to 70% for $D/B = 2.0$). Whilst not all presented here, the results from the FELA for $L/B \leq 2.0$ are different to the those from Salimi Eshkevari et al (2019a), who indicated that for a strip footing, the BRE (2004) method tends to overestimate the ultimate bearing capacity of clay subgrades of strengths lower than 55 kPa, with high friction angles ($\varphi' > 40°$). However, as L/B increases to 5.0 (refer Figure 10 (a) and (b)) it is clear that BRE (2004) tends to overestimate the ultimate bearing capacity for $s_u/\gamma B$ less than about 1.11 to 1.67 and $D/B \geq 1.0$. This is similar to the results obtained by Salimi Eshkevari et al (2019a) (refer to Figure 3 (b)) which shows BRE (2004) strip footing results compared with the strip footing of this study and Salimi Eshkevari et al (2019a)).

Where thin platforms are constructed out of lower frictional material ($\varphi' = 35°$), it can be seen in Figure 9 (e) that BRE (2004) tends to overestimate the ultimate bearing capacity compared to the FELA, and is generally only comparable for the case of $L/B = 5.0$ and $D/B = 1.0$. Such a situation where a working platform is constructed out of a low frictional material is arguably not within the scope of the BRE (2004) guideline. However, depending on location and material availability, crushed rock from quarries may not be available and designers may need to consider a poorer quality source (eg river won gravel that may be rounded to sub rounded).

Whilst a direct comparison with BRE (2004) is not shown here, it is of interest to point out a special case where $D/B = 2.0$ and $\varphi' = 40°$, where the cases for $L/B \leq 2.0$ (refer Figure 4 (d) and Figure 5 (d)) are compared with the strip footing results in Figure 8 (b). It is clear from the analysis that the failure mechanism from the three-dimensional FELA is constrained to the upper sand layer (ie the FELA has converged to a constant ratio of $q_u/B\gamma$), albeit with a minor amount

of numerical variation. However, the values of $q_u/B\gamma$ derived from the analysis of a strip footing indicate that the clay layer is still having an appreciable effect on the resulting bearing capacity. Such a situation highlights the caution required when considering applying shape factors to a layered bearing capacity problem, as is done in the BRE (2004) method. Inspection of the shear dissipation plots from the FELA further emphasises this, where a punching mechanism is observed in the plain strain model (refer Figure 11 (a)), whereas the square and rectangular footings indicate the failure mechanism is a general bearing failure constrained to the sand (refer Figure 11 (b)). This is likely to be attributed to the greater influence depth of a strip footing compared to that of a square or rectangular footing. Further discussion on the effect of footing geometry is provided in Section 3.3.3.

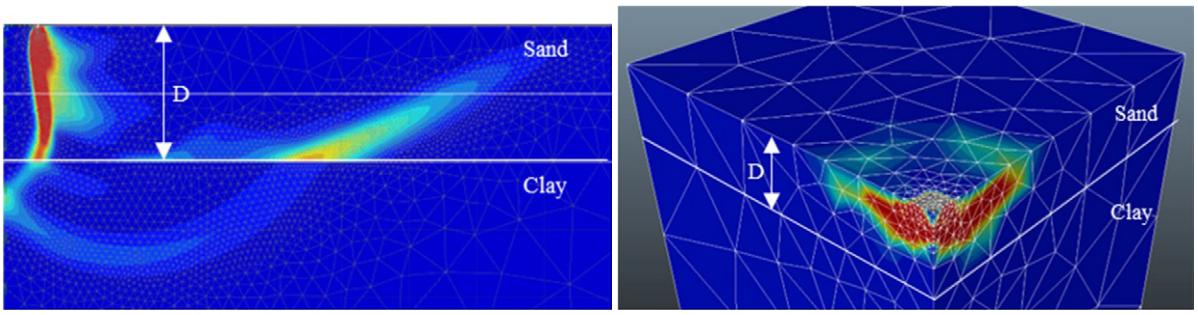

(a) **(b)**

Figure 11: Shear dissipation plots for D/B = 2.0, φ' = 40° and $s_u/\gamma B$ = 1.11.

(a) Plain strain with B = 1.0 m. (b) Square footing (L/B = 1.0)

The FELA has indicated that for many practical situations where thin working platforms, eg $D/B \leq 0.5$, are proposed to be constructed out of good quality fine crushed rock with φ' > 40° (preferably 45°) over a soft to firm clay, the BRE (2004) guideline generally provides estimates of the ultimate bearing capacity within about 10 % of the FELA. However, for thicker working platforms, BRE (2004) may not yield reliable estimates of the ultimate bearing capacity and may potentially be either overly conservative or unconservative. Some circumstances where the undrained shear strength was low ($s_u/\gamma B < 1.11$), the FELA indicated that the BRE (2004) method can provide reasonable estimates of the ultimate bearing capacity. Although, the FELA has also indicated that there are possible combinations of platform material strength, thickness and load geometry where BRE (2004) yielded conservative and unconservative ultimate bearing capacities. BRE (2004) states that the ultimate bearing capacity using a punching shear model is not appropriate when the ratio of D/B is larger than 1.5, however, based on the results of the FELA, it is suggested to be less, and no larger than D/B of about 0.5 to 1.0, although this depends on the ratio of L/B and the relative shear strength of the sand and clay.

3.3.3 Effect of footing dimensions

As noted in Section 3.3.2, caution should be exercised when considering the modification of the ultimate bearing capacity of a strip footing using shape factors for a layered bearing capacity problem. To further investigate the effect of footing dimensions on the ultimate bearing capacity, Figure 12 presents the ultimate bearing capacity ($q_u/B\gamma$) as a function of the aspect ratio L/B for various ratios of D/B, $s_u/\gamma B$, and friction angles. The results have also been extrapolated out to the ultimate bearing capacity from the plain strain analysis. For illustrative purposes, an L/B of 1000 has been adopted for the plain strain case (ie ideally plain strain).

Figure 12 indicates for cases where $D/B \leq 1.0$ and $L/B > 5.0$, the ultimate bearing capacity is tending to that of the plain strain solution. This indicates that in situations where $D/B \leq 1.0$ and $L/B > 5.0$, the use of shape factors to modify a plain strain solution may not be justified for a layered soil problem. Similar behaviours have been observed by Merifield (2002) for plate anchors and Salgado et al (2004) for uniform clays. Where $D/B = 2.0$ it can be seen the aspect ratio is still having an appreciable effect on the ultimate bearing capacity ($q_u/B\gamma$). It is relevant to highlight that the shape factor s_c used in BRE (2004) derived from Equation 5 for $L/B = 5.0$ is only 1.04, indicating that the overall geometrical contribution from the clay layer is small in this instance (but only if the shape factor is valid). However, the shape factor s_p from Equation 6 is 1.20 for $L/B = 5.0$, indicating that BRE (2004) assumes that there is still an appreciable contribution from the footing geometry within the granular layer.

Finally, it can also be seen that as the relative thickness of the upper sand reduces, the influence the aspect ratio has on the ultimate bearing capacity reduces.

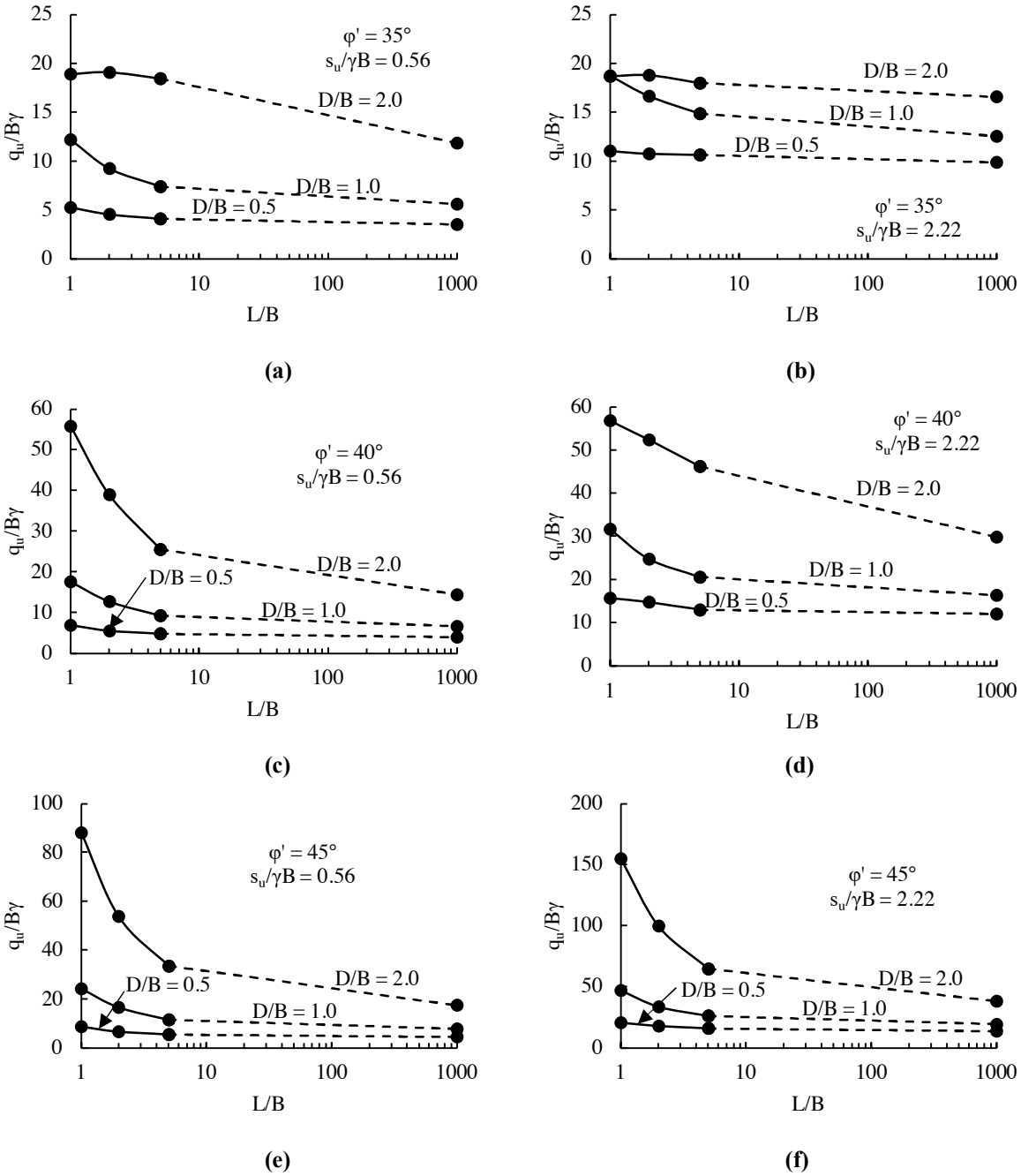

Figure 12: Effect of footing dimensions:
(a) φ' = 35° and $s_u/\gamma B$ = 0.56. (b) φ' = 35° and $s_u/\gamma B$ = 2.22.
(c) φ' = 40° and $s_u/\gamma B$ = 0.56. (d) φ' = 40° and $s_u/\gamma B$ = 2.22.
(e) φ' = 45° and $s_u/\gamma B$ = 0.56. (f) φ' = 45° and $s_u/\gamma B$ = 2.22.

An alternative way to examine the geometrical contributions and aspect ratio of a footing resting on sand over clay is to use the FELA results to derive a shape factor. Historically, shape factors have been derived by dividing the ultimate bearing capacity of a circular, square or rectangular footing by the ultimate bearing capacity of the strip footing for uniform soil problems, as defined in the equation below. A similar approach was adopted by Salgado et al (2004) for evaluating the shape factors s_c for rectangular, square, and circular footings resting on uniform clay soils.

$$s^* = \frac{q_{u,square\ or\ rectangle}}{q_{u,strip}} \quad (8)$$

For the current study, Equation 8 is adopted since the contribution of the sand and clay layers to the overall bearing capacity cannot be separated in the FELA. It should be noted that this implies that the geometrical contributions to the bearing capacity from each layer are the same, however, in the authors opinion this is unlikely.

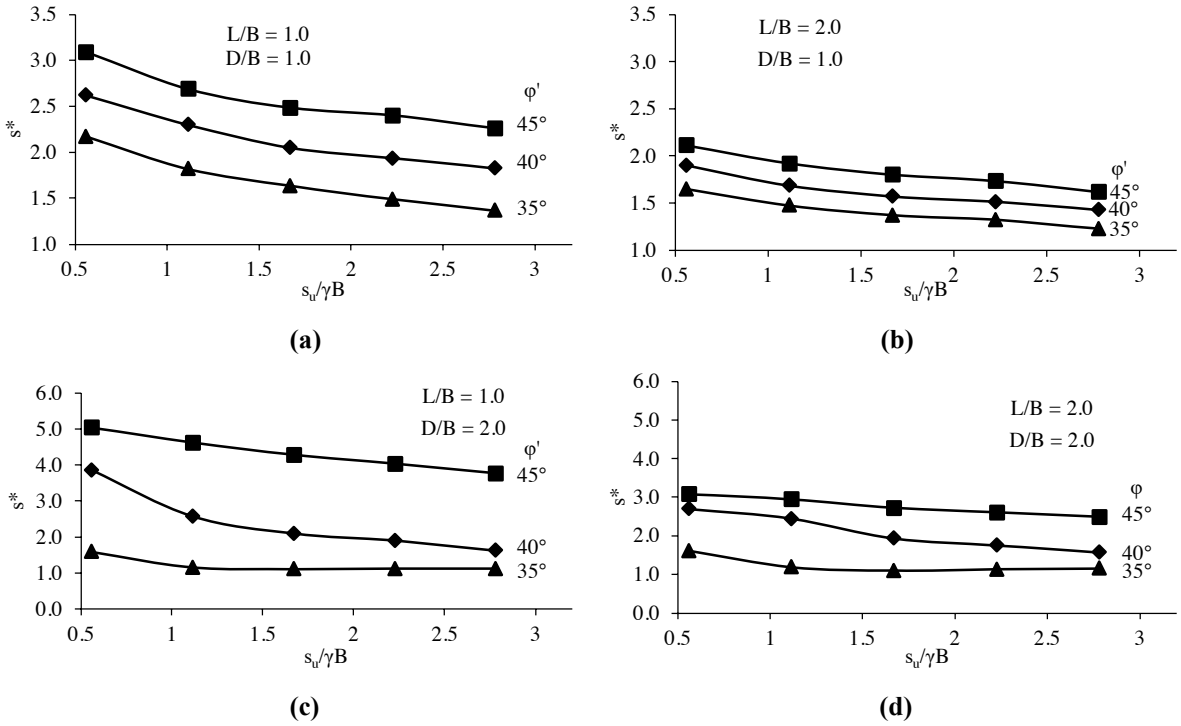

Figure 13: Preliminary shape factors for sand over clay:

(a) *L/B* = *D/B* = 1.0. **(b) *L/B* = 2.0 and *D/B* = 1.0.**

(c) *L/B* = 1.0 and *D/B* = 2.0. **(d) *L/B* = *D/B* = 2.0.**

It is apparent from the FELA results in Figure 13 that the shape factor s* for square and rectangular footings depends not only on the aspect ratio *L/B* and relative shear strength of the upper and lower layers, but also the relative thickness *D/B*. These results are not unexpected since many previous studies have shown for the simplest case of a footing resting on a uniform cohesionless soil, the shape factor varies according to the geometry and friction angle (Meyerhof 1963, De Beer 1970 and Zhu et al 2005). Furthermore, Salgado et al (2004) demonstrated for a uniform clay layer, the shape factor for square, circular, and rectangular footings was non-linear and varied according to footing embedment. The results of Merifield & Nguyen (2006) have also indicated the calculated bearing capacity factors for square and circular footings vary according to the relative thickness of the upper clay layer and the relative shear strength of the clay layers.

It must be noted, however, the validity of shape factors derived using Equation 8 and as presented in Figure 13 may depend on the prevailing failure mechanisms in the respective plain strain and three-dimensional analyses. Review of the results for $L/B = 2.0$, $D/B = 2.0$ and $\varphi' = 40°$ in Figure 5 (d) and Figure 13 (d) provide one example of where s* may not be valid. Figure 5 (d) shows that $q_u/B\gamma$ has converged to a constant value which indicates the underlying clay is having no appreciable effect on the ultimate bearing capacity, whereas Figure 13 (d) still indicates the shape factor is reducing. For this same circumstance, review of the plain stain results shown in Figure 8 (b) also clearly show the underlying clay is influencing the ultimate bearing capacity. In this instance, it would only seem reasonable to compare the results to a strip footing resting on a uniform layer of sand, rather than the results for the layered plain strain problem, to derive the true geometrical contribution from the footing. It is postulated that some degree of similarity should be maintained between the observed failure mechanisms from both plain strain and three-dimensional analyses in order for Equation 8 to be valid. Future studies are proposed to further investigate and attempt to better establish the importance of the prevailing failure mechanism and resulting shape factors. Consequently, it is not recommended the shape factors presented in Figure 13 are used in design.

3.3.4 Effect of sand thickness

As noted in Section 3.3.1, there is a critical ratio of *D/B* where the failure mechanism is constrained to the upper sand. To further investigate this critical ratio, Figure 14 presents the ultimate bearing capacity ($q_u/B\gamma$) as a function of *D/B* for various ratios of *L/B* and $s_u/\gamma B$ and friction angles. The results have also been extrapolated out to the ultimate bearing capacity for the case of a uniform sand. For illustrative purposes, a *D/B* of 1000 has been adopted for the uniform sand case. Figure 15 reproduces Figure 14 for D/*B* up to 2.0.

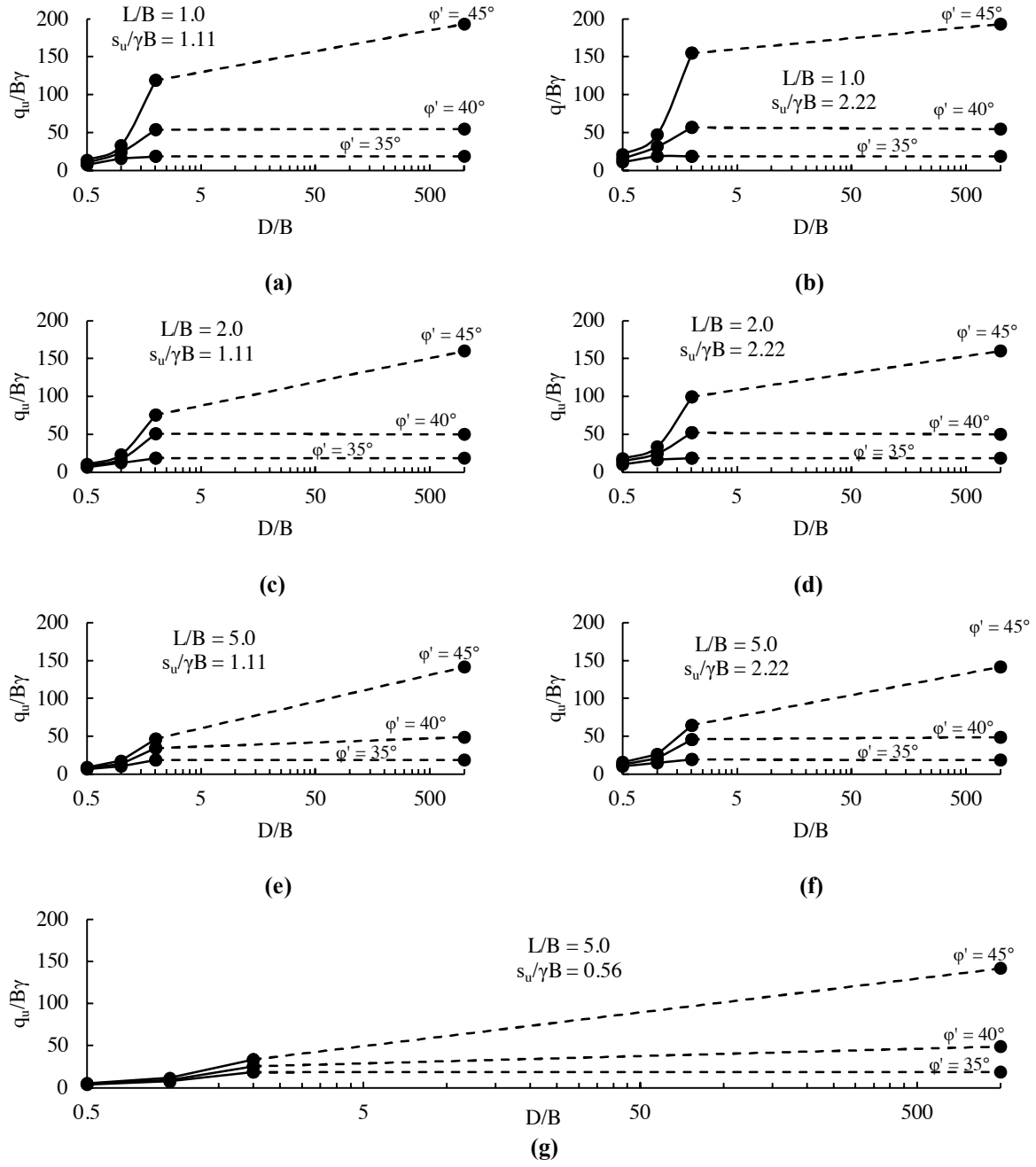

Figure 14: Effect of sand thickness:

(a) $s_u/\gamma B$ = 1.11 and *L/B* = 1.0. (b) $s_u/\gamma B$ = 2.22 and *L/B* = 1.0.

(c) $s_u/\gamma B$ = 1.11 and *L/B* = 2.0. (d) $s_u/\gamma B$ = 2.22 and *L/B* = 2.0.

(e) $s_u/\gamma B$ = 1.11 and *L/B* = 5.0. (f) $s_u/\gamma B$ = 2.22 and *L/B* = 5.0.

(g) $s_u/\gamma B$ = 0.56 and *L/B* = 5.0.

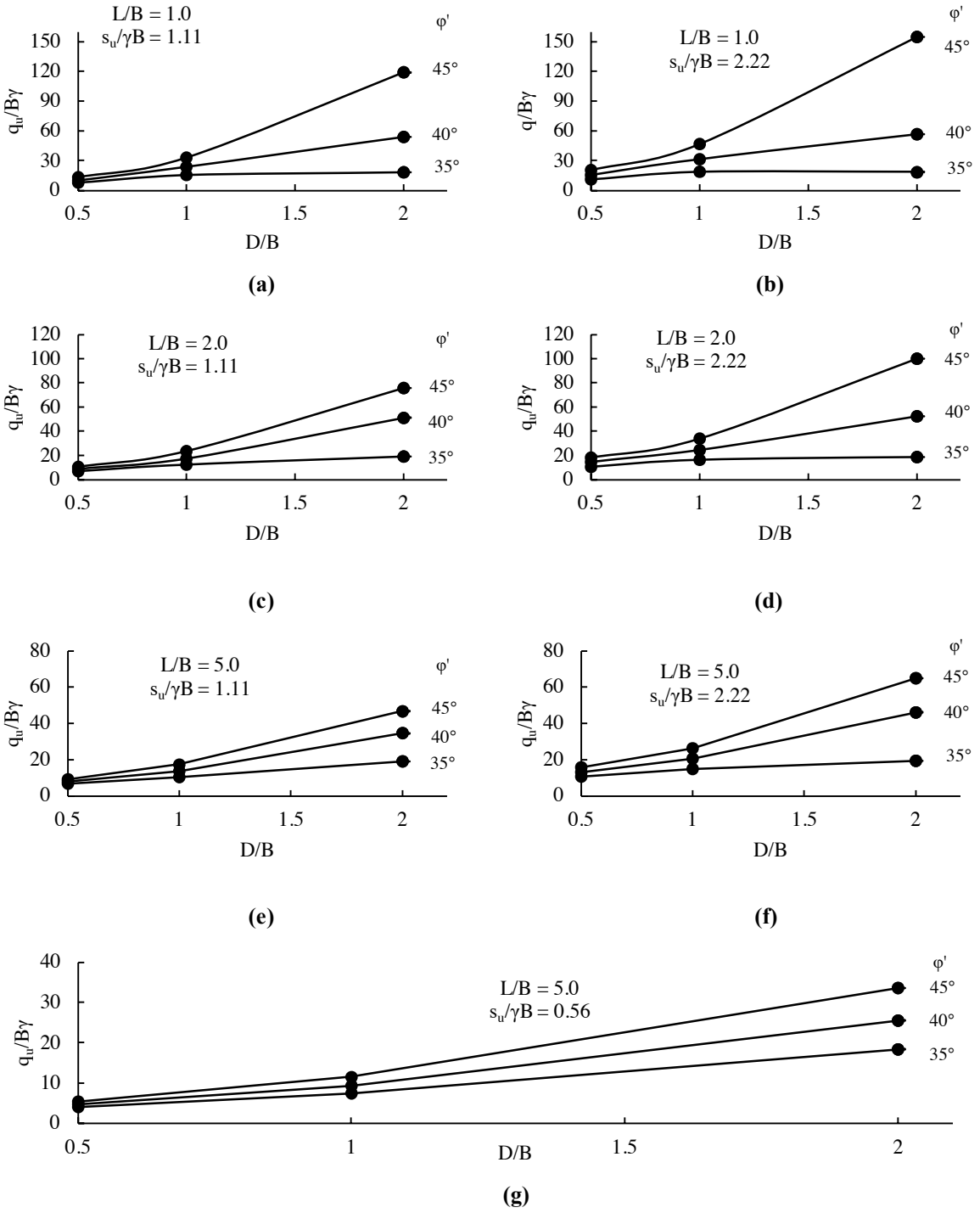

Figure 15: Effect of sand thickness for up to D/B = 2.0

(a) $s_u/\gamma B$ = 1.11 and L/B = 1.0. (b) $s_u/\gamma B$ = 2.22 and L/B = 1.0.

(c) $s_u/\gamma B$ = 1.11 and L/B = 2.0. (d) $s_u/\gamma B$ = 2.22 and L/B = 2.0.

(e) $s_u/\gamma B$ = 1.11 and L/B = 5.0. (f) $s_u/\gamma B$ = 2.22 and L/B = 5.0.

(g) $s_u/\gamma B$ = 0.56 and L/B = 5.0.

Figure 14 generally indicates that when φ' $\leq$ 40°, the critical thickness ratio for the cases presented here is around D/B = 1.5 to 2.0. This is indicated by the asymptotic value of $q_u/B\gamma$. Comparison to a Prandtl type mechanism indicates for φ' = 35° to 40°, the critical D/B is in the order of about 1.52 to 1.71. However, when φ' = 45° a critical thickness has not been

identified in the current study, and Figure 14 clearly indicates that the underlying clay is still having an appreciable influence on the ultimate bearing capacity. For the case of φ' = 45°, the critical thickness based on a Prandtl mechanism would be about 1.93, which is clearly much less then what would be obtained from the FELA. Where a working platform is being considered, it is obvious that the critical thickness for φ' = 45° far exceeds what would be encountered in practice.

Whilst not a clear or direct comparison, it is of interest to highlight similar behaviours have been observed for pile groups founded in a competent upper stratum underlain by a weaker layer (see Merifield et al (2021)). It can be seen that where the upper stratum is appreciably stiffer, the underlying weak layer has a greater influence on the settlement performance of the pile group.

3.3.5 Effect of footing roughness

To investigate the effect of footing roughness on the ultimate bearing capacity, Figure 16 presents the ultimate bearing capacity ($q_u/B\gamma$) as a function $s_u/\gamma B$ for various friction angles and ratios of D/B and L/B.

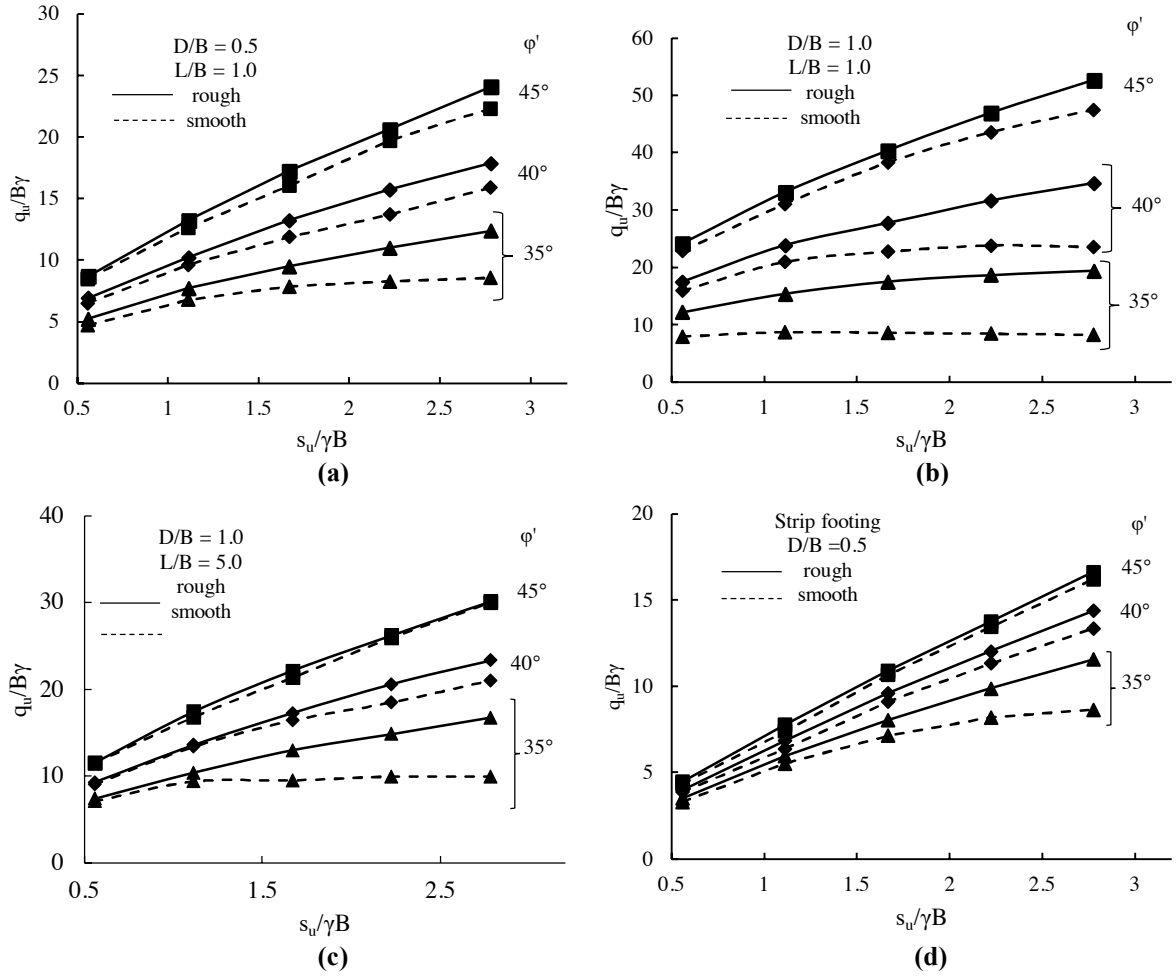

Figure 16: Effect of footing roughness for selected cases:

(a) D/B = 0.5 and L/B = 1.0. (b) D/B = L/B = 1.0.

(c) D/B = 1.0 and L/B = 5.0. (d) D/B = 0.5 Strip Footing.

Figure 16 indicates that generally when φ' ≤ 40°, the footing roughness has the most influence on the ultimate bearing capacity, although the overall impact reduces with increasing L/B. This result is not unexpected since the cases where the overall failure mechanism is more likely to be constrained to the upper sand layer the roughness is expected to have the largest influence (eg L/B = 1, D/B>0.5 and φ' ≤ 40°). This is consistent with previous studies after Chen (1975) and Martin (2005), where it was demonstrated that the bearing capacity factor N_γ for a perfectly smooth footing is about half of the perfectly rough case for the case of a uniform cohesionless soil. Similar behaviours for strip footings on sand overlying clay were also observed by Shiau et al (2004).

4 APPLICATION OF THE SOLUTIONS TO PRACTICAL PROBLEMS

4.1 EXAMPLE 1 – 600 T CRAWLER CRANE USED TO INSTALL BRIDGE GIRDERS

A 600-tonne crawler crane was proposed to lift bridge girders into place. The maximum working ground bearing pressure for the crane was estimated to be a peak of 670 kPa at the toe of the 1.35 m wide tracks, which linearly reduced to zero over a length of 6 m. This load was advised to be during the crane lifting a girder and is considered commensurate with Load Case 1 (eg handling a lift) as per BRE (2004). Due to the appreciable loads, it was proposed to use 3.8 m wide load spreading mats. Accordingly, based on the methods of Meyerhof (1953) and the proposed load spread mats, the design equivalent uniform bearing pressure to consider for the working platform thickness was estimated to be about 180 kPa over a design length of 4 m. Cone penetration testing had indicated that the subgrade comprised firm clay with a typical s_u of about 30 to 40 kPa. The working platform was proposed to be constructed mostly from a non-spec ballast with a particle size ranging from 20 mm to 75 mm with a skim layer of DGB20 to provide a level / trafficable surface. Placement and compaction of the ballast would comprise end dumping by truck and then track rolling with excavators.

BRE (2004) is proposed to be used to obtain a first pass of a minimum platform thickness, which can then be checked using the FELA charts for $q_u/B\gamma$. The material and geometrical parameters input to the assessment have been summarised in Table 5. Based on the non-dimensional parameters in Table 5, the results of Figure 4 (a) and (b) may be used. For convenience in assessing the bearing capacity, power laws have been fit to the relevant data from Figure 4, as shown in Figure 17. The results are summarised in Table 5.

Table 5: Summary of input and results for 600t crane example

Inputs	Input Values
Length of Load, L	4 m
Width of Load, B	3.8 m
Thickness of Platform, D from BRE (2004)	First pass check ~ 1.3 m for Load Case 1
L/B	1.05 (check L/B = 1.0)
D/B	0.34 (check D/B = 0.25 to 0.5)
φ'	40°
γ	16 kN/m^3
s_u	35 kPa
$s_u/\gamma B$	0.58
$q_u/B\gamma$	~ 4.1 to 7.1 (refer Figure 17)
q_u	~ 250 kPa to 430 kPa. Noting that D/B is 0.34, using linear interpolation, indicates an ultimate bearing capacity of about 315 kPa. This gives a FoS of about 1.9, which would be considered acceptable if using the BRE (2004) loading factors as a guide.
Summary	Indicating the 1.3 m thick platform is adequate, albeit slightly thicker than needed (depending on the factor of safety adopted).

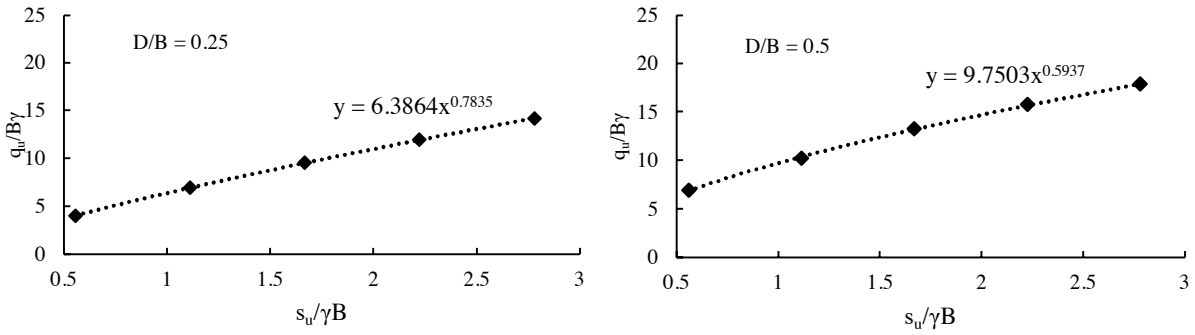

Figure 17: Charts for Example 1

4.2 EXAMPLE 2 – FUNDEX 3500 PILING RIG

A Fundex 3500 piling rig has maximum design ground bearing pressures as summarised in Table 6.

Shear vane testing indicated that the subgrade at the site comprised a soft clay with a characteristic s_u of about 15 kPa. The working platform was proposed to be constructed from a well graded crushed rock (eg DGB20). Placement and compaction of the working platform would comprise end dumping by truck, spreading with excavators and compaction with a 10 tonne roller. Even though the current problem does not fall within the BRE (2004) guideline it is proposed to be used to obtain a first pass of a minimum platform thickness, which can then be checked using the FELA charts for $q_u/B\gamma$. The material and geometrical parameters input to the assessment have been summarised in Table 6.

Based on the non-dimensional parameters in Table 6, the results of Figure 5 (b) and (c) and Figure 6 (c) may be used. For convenience in assessing the bearing capacity, power laws have been fit to the relevant data, as shown in Figure 18. The results are summarised in Table 6.

Table 6: Summary of input and results for Fundex 3500 piling rig example

Inputs	**Input Values**	
	Load Case 1	**Load Case 2**
Applied Pressure	261 kPa	270 kPa
Design Length, L	3.5 m	2.9 m
Width of Load, B	0.9 m track width	1.3 m padfoot width
Thickness of Platform, D from BRE (2004)	First pass check ~ 1 m (based on BRE (2004))	First pass check ~ 1 m (based on BRE (2004))
L/B	3.9 (check L/B = 2.0 to 5.0)	2.2 (check L/B = 2.0)
D/B	1.1 (check D/B = 1.0)	0.77 (check D/B = 0.5 to 1.0)
φ'	45°	
γ	21 kN/m^3	
s_u	15 kPa	
$s_u/\gamma B$	0.79	0.55
$q_u/B\gamma$	~ 14.2 to 19.8 (refer Figure 18)	~ 6.6 to 16.5 (refer Figure 18)
q_u	~ 270 kPa to 370 kPa This is noting that L/B is 3.9, using linear interpolation indicates an ultimate bearing capacity of about 330 kPa. This gives a FoS of about 1.26 which would not be considered acceptable for Load Case 1 if using the BRE (2004) loading factors as a guide.	~ 180 kPa to 450 kPa This is noting that D/B = 0.77, using linear interpolation indicates an ultimate bearing capacity of about 325 kPa. This gives a FoS of 1.20 which would be considered acceptable for Load Case 2 if using the BRE (2004) loading factors as a guide.
Summary	The proposed thickness of 1 m is not considered suitable for Load Case 1, and consideration should be given to increasing the thickness. By trial and error it can be shown that a working platform of about 1.2 m thickness would satisfy a minimum FoS of 1.6, which would normally be accepted for Load Case 1 (if using BRE (2004) load factors as a guide).	

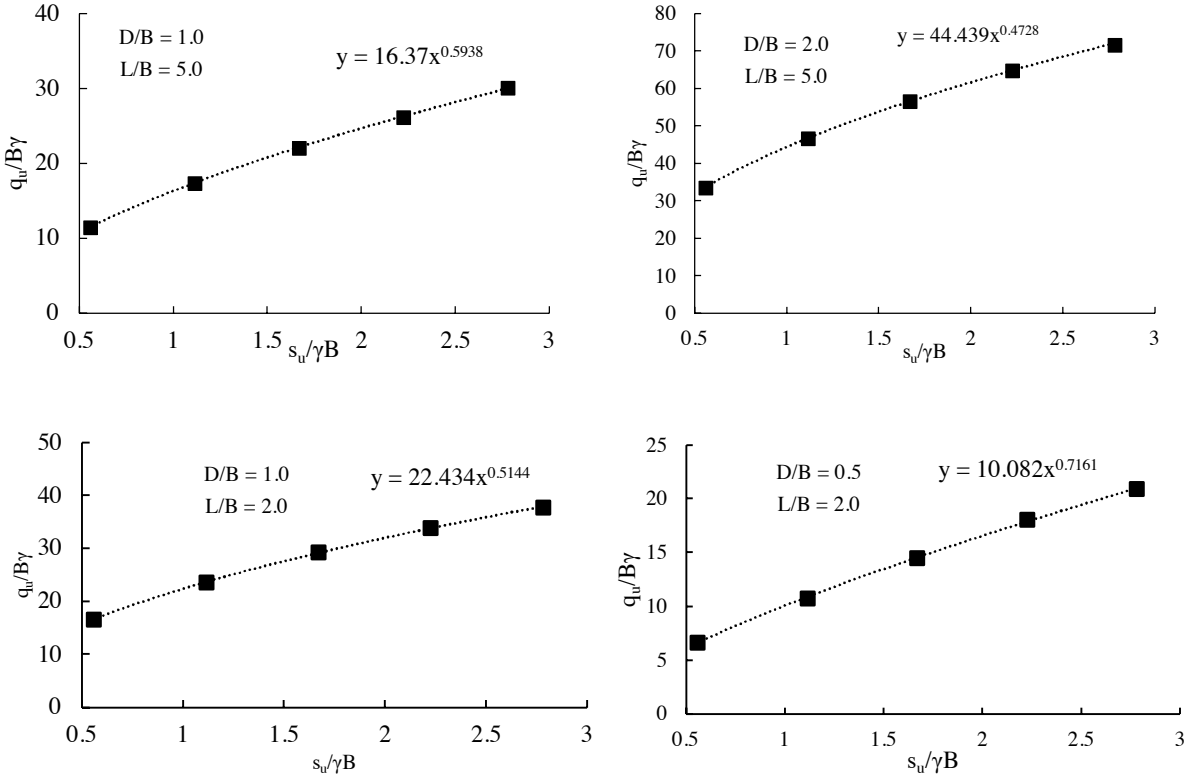

Figure 18: Charts for Example 2

5 CONCLUSIONS

This paper presents the results of a study using FELA to investigate the ultimate bearing capacity of a footing resting on sand overlying clay. Solutions for strips, square and rectangular footings were developed and, where possible, compared with other available published data and case studies. Comparisons with the available published data and case studies show good agreement and provides confidence in the results of the study.

A range of geometric and material parameters were considered in the study. The results of the parametric study were used to develop design charts where it is hoped that many of the more commonly encountered cases of working platforms in practice can be readily assessed using the design charts. The study also included sensitivity analyses to assess the influence of footing dimension, sand thickness and footing roughness.

Comparisons were made with the commonly used design guideline BRE-470 (BRE 2004). The FELA indicated that for many practical situations where a thin working platform, eg D/B of ≤ 0.5, is proposed to be constructed out of good quality fine crushed rock with $\varphi' \geq 40°$ over a soft to firm clay, BRE (2004) generally provides estimates of the ultimate bearing capacity within about 10 % of the FELA. However, numerous situations were presented where BRE (2004) may yield estimates of the ultimate bearing capacity that may either be potentially conservative or unconservative. BRE (2004) also indicates that the ultimate bearing capacity using a punching shear model is not appropriate when the ratio of D/B is larger than 1.5, however, the FELA indicates this may be less, and may more appropriately be no larger than D/B of about 0.5 to 1.0, although this depends on the ratio of L/B and the relative shear strength of the upper and lower layers. An attempt was made to derive shape factors from the FELA, however this study has indicated that it is unlikely to be a straightforward ratio between the ultimate bearing capacity from the respective two and three-dimensional analyses (ie plain strain and true rectangular loading). The FELA has indicated that in situations where $D/B \leq 1.0$ and $L/B > 5.0$, the use of shape factors to modify a plain strain solution may not be justified for a layered soil problem. This highlights that caution is required when applying shape factors to layered bearing capacity problems, as is done in the BRE (2004) method.

Some simple examples of how the design charts could be used were presented. The examples included a situation where the FELA charts may be used as a cross check against BRE (2004), and a situation where the FELA charts indicated that the working platform thickness from BRE (2004) was inadequate. The FELA charts are also suited to situations where

BRE (2004) leads to an overly conservative working platform thickness, and a more efficient / sustainable thickness needs to be justified.

6 ACKNOWLEDGEMENTS

The authors acknowledge the support from Douglas Partners Pty Ltd and the University of Newcastle Australia.

7 REFERENCES

Building Research Establishment, 2004. Working Platforms for Tracked Plant: Good Practice Guide to the Design, Installation, Maintenance and Repair of Ground Supported Working Platforms, s.l.: s.n.

Burd, H. J. & Frydman, S., 1997. Bearing Capacity of Plain Strain Footings on Layered Soils. *Canadian Geotechnical Journal*, Volume 34, pp. 241-253.

Chen, W. F., 1975. Limit Analysis and Soil Plasticity. Elsevier, Amsterdam.

Corke, D. & Gannon, J., 2010. Economic Design of Working Platforms for Tracked Plant. *Ground Engineering*, Volume 43, pp. 29-31.

De Beer, E. E., 1970. Experimental Determination of the Shape Factors and the Bearing Capacity of Sand. *Géotechnique*, Volume 20, pp. 387-411.

Hanna, A. M. & Meyerhof, G. G., 1980. Design Charts for Ultimate Bearing Capacity of Foundations on Sand Overlying Soft Clay. *Canadian Geotechnical Journal*, Volume 17, pp. 300-303.

Martin, C. M., 2005. Exact Bearing Capacity Calculations using the Method of Characteristics, s.l.: Oxford University.

Merifield, R. S., Sloan, S. W. & Yu, H. S., 1999. Rigorous Plasticity Solutions for the Bearing Capacity of Two Layered Clays. *Géotechnique*, 49(4), pp. 471-490.

Merifield, R. S., 2002. Numerical Model of Soil Anchors. Thesis for the Degree of Doctor of Philosophy. The University of Newcastle, Australia.

Merifield, R. S. & Nguyen, V. Q., 2006. Two and Three Dimensional Bearing Capacity Solutions for Footings on Two Layered Clays. *Geomechanics and Geoengineering*, 1(2), pp. 151-162.

Merifield, R. S., Goodall, S. J., and McFarlane, S. A, 2021. Finite Element Modelling to Predict the Settlement of Pile Groups Founded Above Compressible Layers. *Computers and Geotechnics*, Volume 134.

Meyerhof, G. G., 1951. The Ultimate Bearing Capacity of Foundations. *Géotechnique*, 2(4), pp. 301-332.

Meyerhof, G. G., Struct 1953. The Bearing Capacity of Foundations under Eccentric and Inclined Loads. *Proceedings of the 3rd International Conference on Soil Mechanics*, Zurich, Vol 1, pp. 440-445.

Meyerhof, G. G., 1963. Some Recent Research on Bearing Capacity of Foundations. *Canadian Geotechnical Journal*, Volume 1, pp. 16-26.

Meyerhof, G. G., 1974. Ultimate Bearing Capacity of Footings on Sand Overlying Clay. *Canadian Geotechnical Journal*, Volume 11, pp. 223-229.

Michalowski, R.L., and Shi, L. 1995. Bearing capacity of footings over two-layer foundation soils. *Journal of Geotechnical Engineering*, ASCE, 121(5): 421–428.

Okamura, M., Takemura, J. & Kimura, T., 1997. Centrifuge Model Tests on Bearing Capacity and Deformation of Sand Overlying Clay. *Soils and Foundations*, 37(1), pp. 73-88.

Olsen, C., L, and Krabbenhoft, K. 2021. Case study on advanced 3D finite element limit analysis of counter-acts installed at Ormen Lange. Proceedings of the International Conference on Computational Methods & Ocean Technology and Oil and Gas Technologies in Cold Climate, pp 1-9.

Optum G2 and G3 [Computer Software]. 2020. Optum CE. Copenhagen, Denmark.

Salgado, R., Lyamin, A. V., Sloan, S. W. & Yu, H. S., 2004. Two and Three Dimensional Bearing Capacity of Foundations in Clay. *Géotechnique*, Volume 54, pp. 297-306.

Salimi Eshkevari, S. N. & Abbo, A. J., 2015. Punching Shear Coefficients for the Design of Working Platforms. Leiden, Proceedings of the 14th International Conference of International Association for Computer Methods and Recent Advances in Geomechanics, pp. 317-322.

Salimi Eshkevari, S., Abbo, A. J. & Kouretzis, G., 2019a. Bearing Capacity of Strip Footings on Sand over Clay. *Canadian Geotechnical Journal*, Volume 56, pp. 699-709.

Salimi Eshkevari, S., Abbo, A. J. & Kouretzis, G., 2019b. Bearing Capacity of Strip Footings on Layered Sands. *Computers and Geotechnics*, Volume 114.

Shiau, J. S., Lyamin, A. V. & Sloan, S. W., 2003. Bearing Capacity of a Sand Layer on Clay by Finite Element Limit Analysis. *Canadian Geotechnical Journal*, Volume 40, pp. 900-915.

Skempton, A. W. 1951. The Bearing Capacity of Clays. Proceedings of the Building Research Congress, Vol. 1, pp. 180–189.

Sloan, S. W., & Randolph, M.F. 1982. Numerical prediction of collapse loads using finite element methods. *International Journal for Numerical and Analytical Methods in Geomechanics*, Volume 6, pp. 47-76.

Terzaghi, K. & Peck, R. B., 1948. Soil Mechanics in Engineering Practice. New York: John Wiley and Sons.

Zhu, M., Radoslaw, L. & Michalowski, F., 2005. Shape Factors for Limit Loads on Square and Rectangular Footings. *Journal of Geotechnical and Geoenvironmental Engineering*, Volume 131, pp. 223-231.

BLACK
INSITU TESTING

GEOTECHNICAL TESTING SPECIALISTS

BLACK INSITU TESTING WAS FORMED IN 2008 AS A SPECIALISED CONE PENETRATION TESTING COMPANY.

The company founders are experienced geotechnical engineers who were motivated to create Black Insitu Testing by recognising a need for high quality CPT tests to aid accurate and economic geotechnical investigations.

In addition to CPT, we provide an extensive range of other insitu testing and soil sampling services. We have 9 CPT rigs that can access a wide range of site conditions.

Detailed information on our testing services and CPT rigs is available on our website

www.blackinsitutesting.com.au

Join a firm that offers real opportunities to be part of a growing team providing engineering solutions on challenging projects.

You might know Senversa as a leading Australian employee-owned contaminated land, waste management and environmental consultancy, but did you know that we also have an established Engineering Workgroup that provides geotechnical, geological, hydrogeological and civil/environmental engineering solutions to meet our clients' needs? We have a unique broad-based employee ownership model and a commitment to growing our engineering offering nationally.

- We have a recognised brand for providing quality advice and services.
- We deliver solutions for all things below ground and environmental.
- We embrace diversity and a teaming culture.
- We offer a unique opportunity to share in the ownership and growth of the firm.

We are currently looking for Principal, Senior, mid-level and junior geotechnical and civil engineers to work in our people-focused, culture-driven Workgroup.

If interested, please visit senversa.com.au/careers/

Senversa is Climate Active certified and an award-winning B Corp organisation, specialising in combined services projects - balancing the needs of engineering solutions with protection of the environment.

Climate Active NETWORK MEMBER

Certified B Corporation

Your geotechnical future starts with GHD

→ Our global technical expertise, multidisciplinary and integrated **geoprofessional experience**, alongside our local presence, allows us to **deliver engineering geology and geotechnical engineering excellence** both in the field and in the office.

Our client-focussed work often uses **innovative ideas and technological advancements** combined with various technical and traditional applications. We are proud of our Award-winning efforts, including recently being named as **finalists in the 2022 Bentley's Going Digital Awards in the Geoprofessional category.**

At GHD, **we go beyond the ordinary** to solve complex social and economic issues for our clients beyond the earth beneath our feet. Creating lasting community benefit is our legacy. **Come join us!**

Discover more at ghd.com/geosciences

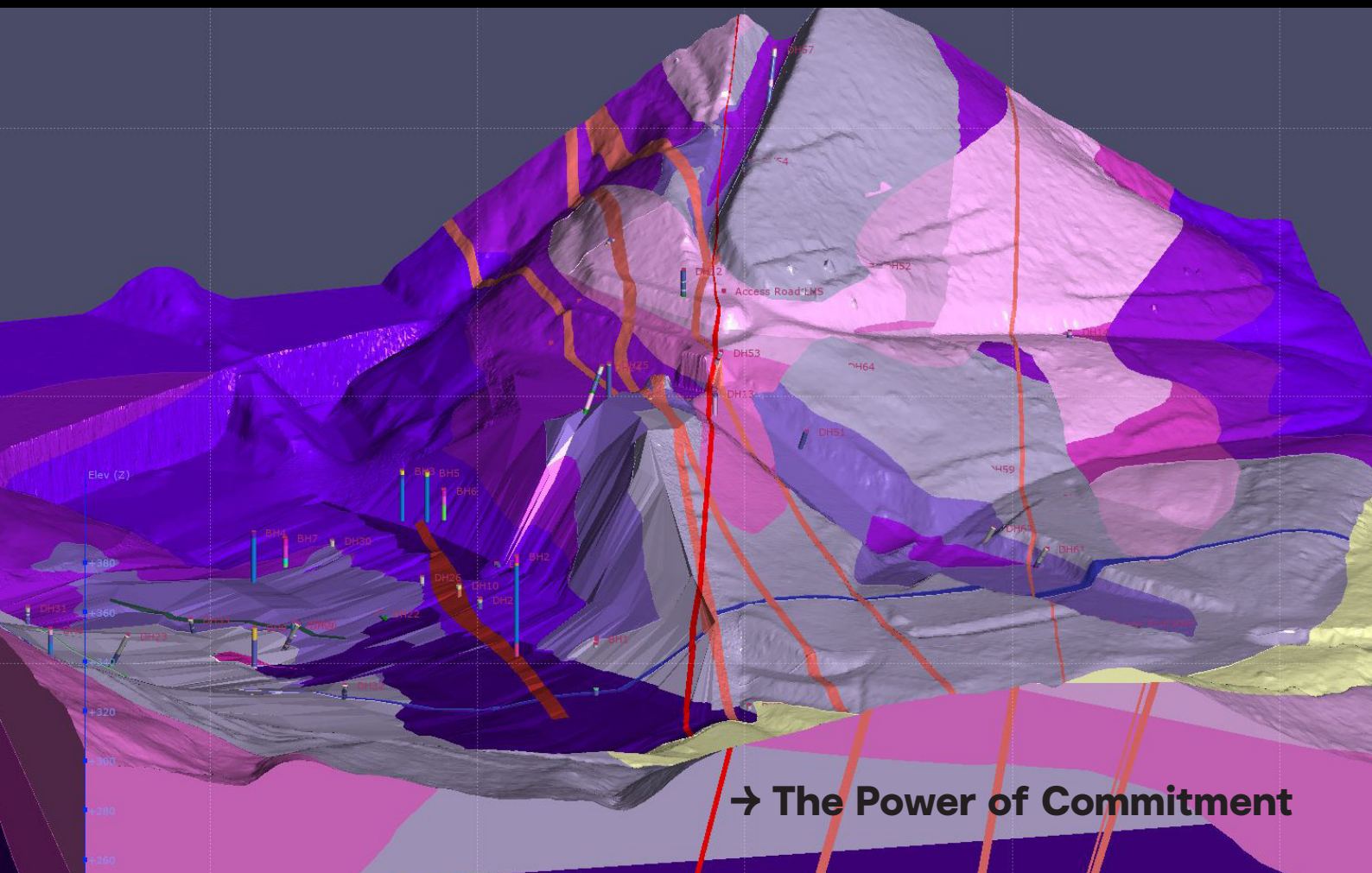

COMPARISON OF MOHR-COULOMB AND HARDENING SOIL CONSTITUTIVE MODELS FOR SIMULATION OF SETTLEMENTS IN THE KARKHEH EARTH DAM

Hossein Samadi-Boroujeni[1], Amir Haghshenas-Adarmanabadi[2], Mohammad Shayannejad[2] and Hadi Khabbaz[3]

[1] Shahrekord University, Iran [2] Isfahan University of Technology, Iran [3] University of Technology Sydney (UTS)

https://doi.org/10.56295/AGJ5836

ABSTRACT

This paper presents the settlement behaviour of Karkheh earth dam during its construction and operation stages. Karkheh is one of the largest earth dams in the world in terms of its reservoir capacity and body volume. The settlement of such a large body of soil can affect the performance of the dam elements and endanger downstream areas; should a breach or failure occur in the dam, more than two million people will be affected. It is crucial to know the settlement behaviour of this structure and use the existing results to predict its future settlements and calibrate the existing stress-strain models. For anticipation of dam settlement the measured displacement from the portable probe anchor magnets installed in the dam body are compared to the results of numerical simulations. The available data cover a period of 12 years including construction, and two material impounding and operation periods of the dam. The numerical analysis is performed in 2D plane-strain conditions and two material models are used, including Mohr-Coulomb (MC) and Hardening Soil (HS) models. The comparison between the calculation results and the measured vertical deformations in the dam site reveals that the accuracy of model for the deformations in the middle levels of dam is better than those of the crest for both applied material models in construction and impounding stages. The maximum settlement differences between computed and observed values are 0.05 m for MC model and 0.01 m for HS model. For the operation stage, the error of calculated settlements for the MC model is smaller; hence the results of this model might be more reliable for prediction of future dam settlements. The similar trends, obtained from both material models, exhibit the suitability of the model parameters used in the simulations.

1 INTRODUCTION

For several years, earth dam designs were based on the seepage control and the stability of dam slopes. Recently, it has been found that the settlements of the dam body play an important role in the dam safety (Mirghasemi 2006). Non-uniform settlement causes cracks in the dam body, whereas uniform but excessive unpredicted settlement may lead to breach; both can endanger the overall stability of the dam. Therefore, prediction of settlements in the dam is essential to ensure in the long term the dam is safe. The prediction of settlement in an earth dam is a complicated process because different parameters should be considered: the non-linear time- dependent behaviour of materials, effect of degree of saturation on the soil behaviour and interaction between the dam and its foundation (Ozcoban et al 2007). One of the available methods for calculation of the settlements in the body and foundation of earth dams is employing the finite element method (FEM). This numerical method is also widely used for the seepage analysis (Szostak-Chrzanowski and Massiera 2006; Uromeihy and Barzegari 2007) and the slope stability analysis of earth dams (Berilgen 2007), arching (Esmaeilzadeh et al. 2017) and seismic analysis (Han et al. 2016) of earth dams. Numerical modeling of the seepage and stability analyses of the considered earth dam using finite element method showed that an increase in the Young's modulus of core and shell resulted in the decrease of the maximum crest displacement. According to Athania et al. (2015) the variation in the angle of internal friction plays a vital role in the fulfillment of the overall stability criteria. Comparison of the post-construction settlement methods and the three life-cycle phases settlement methods reviled that that the latter approach is more precise and highly practical to estimate the rock fill deformation mechanisms (Kermani et al. 2017).

Settlement analysis using FEM analysis is very common for the most earth dams (Athania et al 2015). However, the comparison between FEM results and measured data are usually limited to construction and impounding stages (Talebi et al. 2013), while some unusual behaviours have been observed according to the long-term monitoring data (Dolezalova and Hladik 2011). Very few studies have been conducted on the long-term settlement behaviour of earth

dams because of incomplete and unreliable monitoring data. Comparison between the simulation results from FEM analysis and the actual measured data at the dam sites is useful for monitoring of dam stability and regular maintenance operation. In addition, these comparisons can be used in verifying the design parameters, such as geotechnical parameters, which are the most important parameters, and may be useful for the future structures (Gikas and Sakellariou 2008a; Szostak-Chrzanowski et al. 2008; Zoorasna et al 2008; Xu et al 2003).

The deformation of earth fill dams with time have been investigated by a number of researchers. The long-term crest deformation of Kouris dam in Egypt was studied by Pantazis et al. (2019) based on the crest movement indicators and geodetic network. However, no inclinometer was installed in the dam body for monitoring of internal displacement. The same study was performed by Michallis and Pytharoli (2016) on the Pournari-I dam in Greece. Wen et al. (2017) discussed on behaviour of Miaojiaba concrete face rock fill dam built in river gravel foundation in China on the basis of in-situ measurement records and FEM analysis. That study covered the stages of dam construction, initial reservoir filling and first year of operation. The associated FEM modeling results were in good agreement with measured deformation. Furthermore, the long-term deformation of Shuibuya concrete face rock fill dam in China was analyzed by Yao et al. (2019).

The calibration of soil models used in the FEM analysis for reproduction of the soil settlement has a great importance in numerical analysis [22]. One of the effective and more practical ways for calibrating a soil model is the inverse-analysis for minimizing the difference between the measured data and simulated results (Calvello and Finno 2004).

According to Dolezalova and Hladik (2013),numerical study on the rate of arching parametrically of Darian earth dam showed that increasing the elastic modulus, Poisson's ratio, internal friction angle, and the proportion of core thickness to filters thickness, will result in decreased arching.

Han et al. (2016) simulated the seismic response of a well-documented Chinese rockfill dam, Yele dam using the dynamic hydro-mechanically (HM) coupled finite element (FE) method. The results showed that the predicted seismic deformation of the Yele dam is in agreement with field observations that suggested that the dam operated safely during the Wenchuan earthquake.

In this paper, the settlements, monitored by the magnetic inclinometers installed in the body of the Karkheh earth dam were compared to the results obtained from a numerical inverse-analysis. The monitoring settlements consists a 12-year data set covering the construction, impounding and operation stages of the dam. For numerical modeling the 2D finite element analysis in the plane-strain conditions was used. For modeling of settlements in the dam body the Mohr-Coulomb (MC) and Hardening soil (HS) models were used for materials behaviour. Then the results of the construction and the operation stages of the dam were compared. The purpose of this paper is to study and explain the settlements observed in the dam body, by means of the geotechnical behaviour of materials. In addition this study includes the comparison of the results of numerical analyses (using different material models) in different stages of dam lifetime with measured data and calibration of the employed models.

2 CHARACTERISTICS OF THE KARKHEH DAM AND ITS FOUNDATION

Karkheh dam is the largest earth dam in terms of body volume and reservoir capacity in Iran, built on the Karkheh River (Figures 1 and 2). The dam is located in a wide U-shaped river valley and has 127 m height above the foundation with a 3030 m crest length. The dam foundation consists of several layers of permeable conglomerates, which are slightly-moderately cemented and are stratified by nearly horizontal mudstone layers with 3 to 9 m thickness (Heidarzadeh et al. 2019). Because of the zones of discontinuity and open frame work gravels, the permeability of the conglomerate rock is estimated to be between 0.4 and 0.9 mm/s and the impervious mudstone has a permeability about 10^{-9} m/s. The geological and geotechnical characteristics of the Karkheh dam are shown in Fig 2. For the measuring of internal deformation of the dam body and its foundation, the inclinometers and anchor magnets with a portable probe are used (Kermani et al 2017).

Figure 1: Location of Karkheh earth dam on Iran's map [left]; an aerial view of Karkheh earth Dam [right] (after Mirghasemi, 2006)

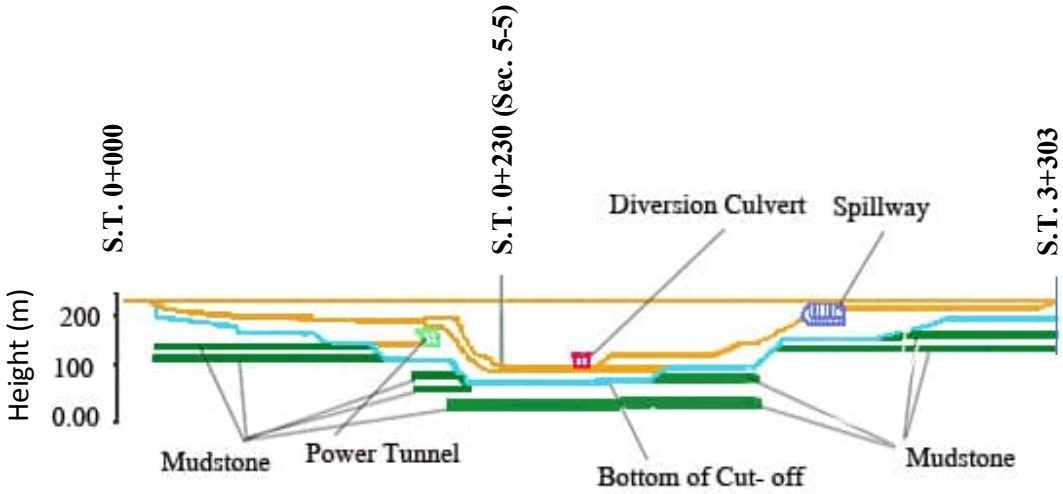

Figure 2: Longitudinal cross section of Karkheh earth dam

Nowadays, the core of embankment dams is constructed by aggregate-clay mixtures, avoiding noticeable settlement after construction and exploiting the arching effect across the core. This clay mixture is not as soft as pure clay and its permeability should be sufficiently low (Loupasakis 2009). The graded part of mixture supplies high shear stresses and a low compressibility; while the clay fraction governs the permeability of mixture. Miboro and Ohshirakawa dams in Japan, Sfikia earth dam in Greece (Loupasakis 2009), Taguaza dam in Venezuela and Masjedsoleiman and Karkheh earth dam in Iran are some examples of dams with aggregate-clay mixture cores. The mixture of Karkheh earth dam core consists of a combination of 60% clay materials and 40% sands and gravels (Jafari and Shafiee 1999; Shadravan et al 2004; Heidarzadeh et al 2019).

2.1 MONITORING AND ANALYSIS OF THE DAM

In order to monitor and control the dam behaviour and performance, a field instrumentation including a total of 278 vibrating wire piezometers, 134 stand-pipe piezometers, 510 earth pressure cells and 26 inclinometers were placed in the dam body and foundation. In addition, for monitoring of external deformation of dam a geodetic system with

reference stations that spread at the crest, abutment and downstream of the dam was used. This net also included the top point of inclinometers. The vertical displacements inside the dam body were measured using magnetic extensometer probes, together with inclinometers. The anchor magnets were placed approximately 3.5 m centre to centre distance from each other and the settlement measuring were performed in 14 cross sections of the dam.

The settlement trend of the dam core at Cross Section 5 (Figure 3) at the end of construction and operation stages is shown in Figure 4. The maximum settlement at the end of construction phase was 1.18 m (about 1% of the dam height), occurred in the middle levels (44% to 55% of the dam height from the base). This amount of settlement is considered to be at a common practice value reported by the United States Bureau of Reclamation (USBR, 2011). According to USBR in more than 20 constructed dams, the settlement at the end stage of construction was between 1% and 4% of the height of the dam (Sherard et al 1963). This is probably due to using a clay mixture core in the dam. The impounding of the Karkheh earth dam reservoir began in February 2000, when some elements of the dam was not completely constructed; hence it could be concluded that the reported value would be the post-construction and impounding cumulative settlement. At the end of 10 years from the commencement of operation, the maximum cumulative settlement was 1.46 m, which occurred at the level of 195 m (70% of the dam height from the base and in upper semi-part of the core). Therefore, the developed settlement in operation stage was about 20% of the total settlement of the dam; and more than 80% of the settlement occurred during the post construction and impounding time, indicating that the dam tended to stabilize.

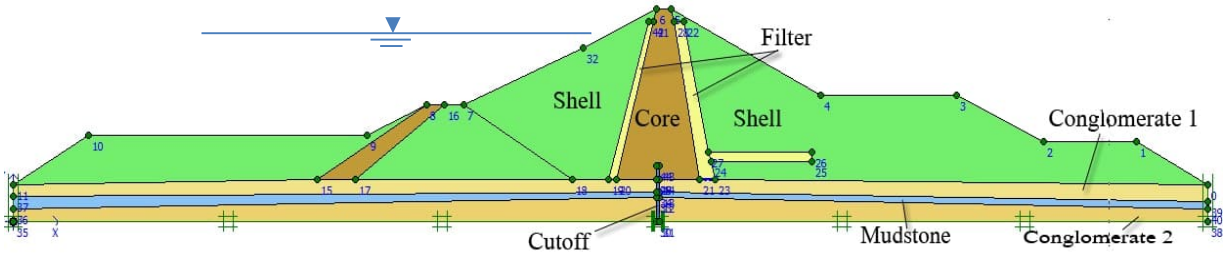

Figure 3: Geological and geotechnical characteristics at the Karkheh earth dam cross section in station 1+230

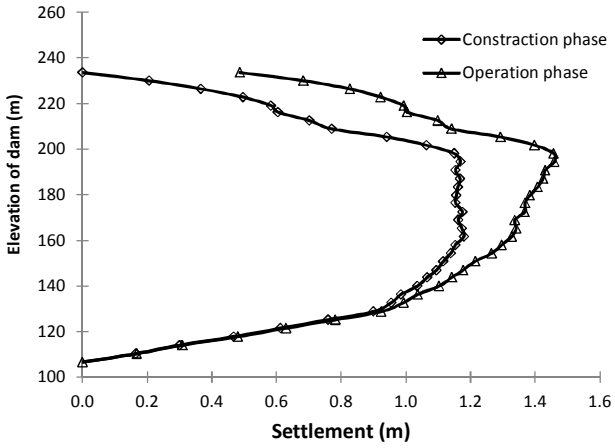

Figure 4: Observed settlements in the core of Karkheh earth dam at the end time of construction and during the operation period

Figure 5 presents the time series of settlement at the low, middle and the crest of the dam. It covers the whole lifetime of the dam, including the construction, impounding and operation stages. The largest amount of settlements occurred in the construction phase and impounding of the dam; and the rate of cumulating displacements decreased over the time and approached to their final values in all part of the dam. This decrease in settlement magnitude was evidence

that the dam approached to its stable state. Figure 5 also reveals that the settlements at the middle levels of the dam are larger than the settlements at the crest or at the low levels of the dam.

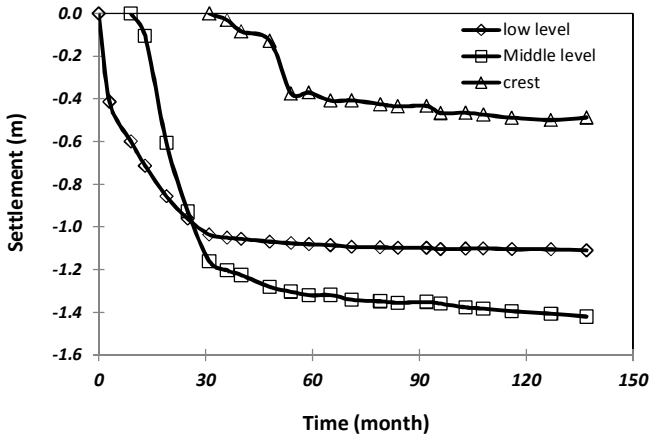

Figure 5: Time series of measured settlements in the low levels, in middle and at the crest of the Karkheh earth dam

3 FINITE ELEMENT MODELING

As it mentioned before, the Karkheh earth dam is located in a wide U-shaped river valley with a 3030 m crest length, hence the 2D analysis was performed for simulation of the dam behaviour. In order to model the settlement of the dam body, the FEM elasto-plastic analyses were performed using PLAXIS 2D software. PLAXIS 2D (version V8), developed by Delft University of Technology, is a FEM package for analysis of deformation and stability in geotechnical engineering projects. In this software, several models for simulating soil or rock behaviour (non-linear, time-dependent and anisotropic) is available (PLAXIS General Information, 2006). For better studying deformation behaviour, two FEM models were applied, the first model employed for construction and impounding and the second model used for the operation stage. These models are explained in the following sections.

3.1 CONSTRUCTION AND IMPOUNDING STAGES SIMULATION

To simulate the stress-displacement behaviour of the dam in construction and impounding stage, the geometry model of Cross Section 5 with 15 construction layers was used. The analysis was performed under plane-strain conditions and the elastic-plastic Mohr–Coulomb (MC) model and the hardening soil (HS) model were used to simulate the material behaviour; and then the acquired results from these two models were compared. In Mohr-Coulomb model the stress-strain behaviour of materials is a bi-linear curve and the user has to select a fixed value of Young's modulus (PLAXIS Material Models Manual, 2006). The modulus of stiffness changes by the stress level for real soils. In contrast, the hardening soil model uses a hyperbolic stress- strain curve and also controls the stress level dependency. The HS model is an advanced model which can be used for simulation of the behaviour of both stiff and soft soils (Loupasakis 2009; Schenaz 1999). It must be mentioned that the hardening behaviour used just for materials of the dam body.

The vertical boundaries of model were developed 500 m in both upstream and downstream. The FEM model includes more than 1,100 triangular 15-node elements and 9,000 nodes. The standard fixities was used for the boundary conditions that with it the lower boundary of the model has no strain and the side boundaries (with maximum and minimum x coordinates) assume to have zero horizontal strain. In order to simulating of dam construction, two phases of calculation consist of plastic (for loading of layer weight) and consolidating calculate (time dependent) were defined in PLAXIS for each layer similar to other investigations (Mirghasemi 2006). The applied time for the second phase was equal to real consolidation time based on the scheme of operational construction of the dam.

3.2 OPERATION STAGE SIMULATION

As mentioned earlier, the impounding of the Karkheh earth dam began when the dam was not completely constructed; hence, the operation model was defined from 2001, after first two impounding. This model contained more than 3000 nodes. The boundary conditions and material properties were the same in the construction model; furthermore the lower boundary was defined closed against seepage. In order to simulating dam behaviour, two plastic calculating phases (one for increasing and another one for decreasing the water level in the reservoir) were defined for each year and the defined water level in upstream of model was exactly equal to the maximum and minimum reservoir water level. In Figure 6, the changes in water level in the reservoir of Karkheh earth dam from the first impounding are shown. As can be seen in this figure, because of a severe drought the reservoir water level had a reducing trend in the years between 2008 and 2009, and therefore one calculating phase was defined for these years.

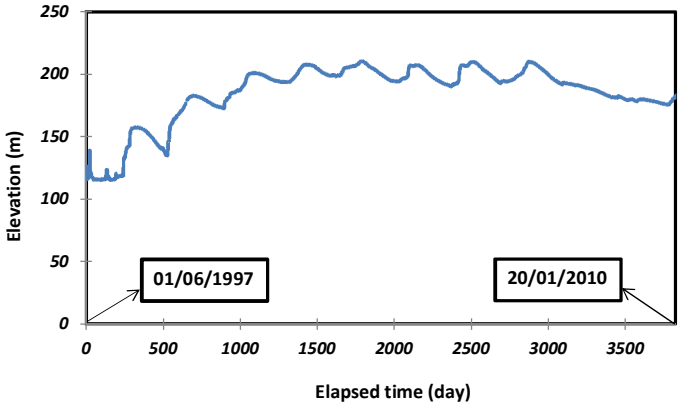

Figure 6: Time series of reservoir water level of Karkheh earth dam

3.3 CALIBRATION OF MODEL PARAMETERS

For calibrating of two employed numerical models the inverse analysis was used, according to Calvello and Finno (2004) approach. The inverse analysis was performed by changing the model input values iteratively until the output of the models match the observed data. For the initial definition of model geotechnical parameters of the dam body and foundation materials, the previous studies on the Karkheh dam were considered (Shafiee 2008; Shafiee et al 2008; Talebi et al 2013). The basic parameters of the MC model are E (the elastic modulus), ν (the Poisson's ratio), c (the cohesion), φ (the friction angle) and ψ (the dilatancy angle). The key HS model input parameters are E_{50}^{ref} (the secant stiffness in standard drained triaxial test), E_{oed}^{ref} (the tangent stiffness for primary oedometer loading), m (the power for stress level dependency of stiffness), and the advanced parameters for this model are E_{ur}^{ref} (the unloading-reloading stiffness), ν_{ur} (Poisson's ratio), P_{ref} (the reference stress for stiffness), R_f (the failure ratio) and K_0 (the value for the lateral earth pressure at rest for normally consolidated soil. The unit weight (γ) and the permeability of materials (K) are general inputs for both models.

Applying a sensitivity analysis, the more relevant parameters were determined in the displacement calculation of each model. Because of the HS model internal algorithm used in PLAXIS, which adjusts the values of E_{oed}^{ref} to produce a hyperbolic curve in a triaxial stress–strain space considering deviatoric stresses, this parameter could not be optimized by the inverse analysis (Calvello and Finno 2004). Figure 7 depicts the results of sensitivity analyses on other parameters. This figure also shows that in MC model, the elastic modulus and Poisson's ratio have a significant effect on the calculated settlements whereas, the c and φ effects are not notable. In the HS model the parameter m had more effect than the E_{50}^{ref} on the results, as it was reported by the other studies (Loupasakis et al., 2009).

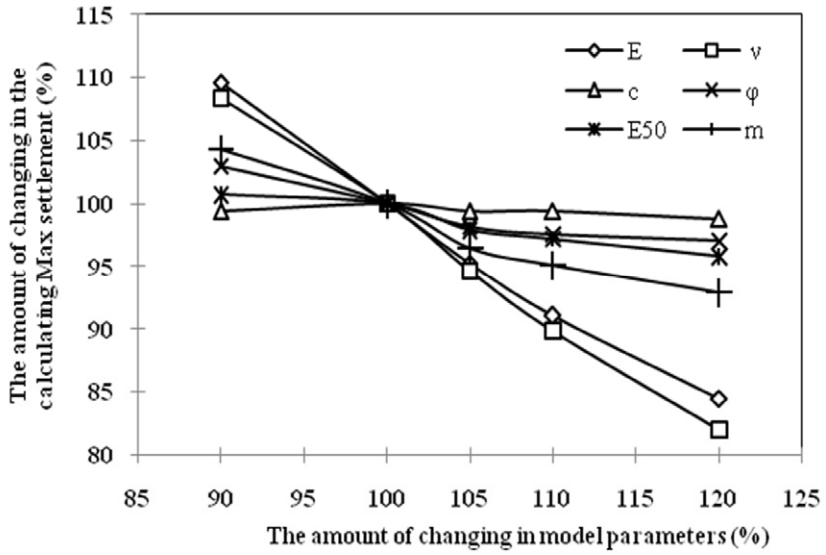

Figure 7: Results of sensitive data analysis on the parameters of MC and HS models

Table 1: The material properties used in the FEM analysis

Material Properties	Material Type						
	Conglomerate 1	Conglomerate 2	Core	Shell	Filter	Mudstone	Cut-off
$\gamma_{dry}\,(kN/m^3)$	21	21	17.4	20	19	19.5	21
$\gamma_{sat}\,(kN/m^3)$	23	23	20.2	22	20	21	22
K (m/day)	38.9	0.95	4.5×10^{-4}	0.085	0.85	4.5×10^{-5}	8.6×10^{-5}
E_{ref} (kN/m^2)	8×10^5	106	3.8×10^4	1.25×10^5	7.5×10^4	1.2×10^5	4×10^6
ν	0.25	0.25	0.37	0.28	0.3	0.3	0.25
c (kPa)	85	85	30	2	2	70	700
□ (deg.)	40	40	20	39	35	22	33
□ (deg.)	10	10	2	10	8	5	10
E_{50}^{ref} (kPa)	-	-	3.2×10^4	10^5	6.5×10^4	-	-
E_{oed}^{ref} (kPa)	-	-	3.5×10^4	1.1×10^5	7×10^4	-	-
E_{ur}^{ref} (kPa)	-	-	9.6×10^4	3×10^5	1.95×10^5	-	-
Power (m)	-	-	0.65	0.35	0.5	-	-
ν_{ur}	-	-	0.2	0.2	0.2	-	-
P_{ref} (kPa)	-	-	100	100	100	-	-
R_f	-	-	0.9	0.9	0.9	-	-
K_0	-	-	0.658	0.371	0.426	-	-

Regarding sensitivity analysis results, the inverse analysis was performed for optimization of the effective parameters, based on the measurement of settlement at the end of dam construction. The non-effective parameters generally set equal to the initial or PLAXIS suggested values. The final accepted values for material properties are listed in Table 1. It can be noted that the dam body in construction model was assumed dry and the consolidation occurred only by the upper layers weight.

4 RESULTS AND DISCUSSION

4.1 RESULTS OF FEM MODELING

For the two basic models stated above, the finite element analysis performed using PLAXIS 2D software and the stresses, the vertical and horizontal displacements of the dam were calculated. The calculations were conducted, concentrating on Cross Section 5. However, Cross Sections 4 and 7, located in the left and right sides of Section 5, respectively, also were used for comparison and validation of the results. Figure 8 represents the calculated vertical displacement in Section 5 at the construction and impounding stages using MC model and HS model. This figure also reveals that the settlements for both models have generally symmetrical distribution at the two sides of the vertical axis passing through the dam.

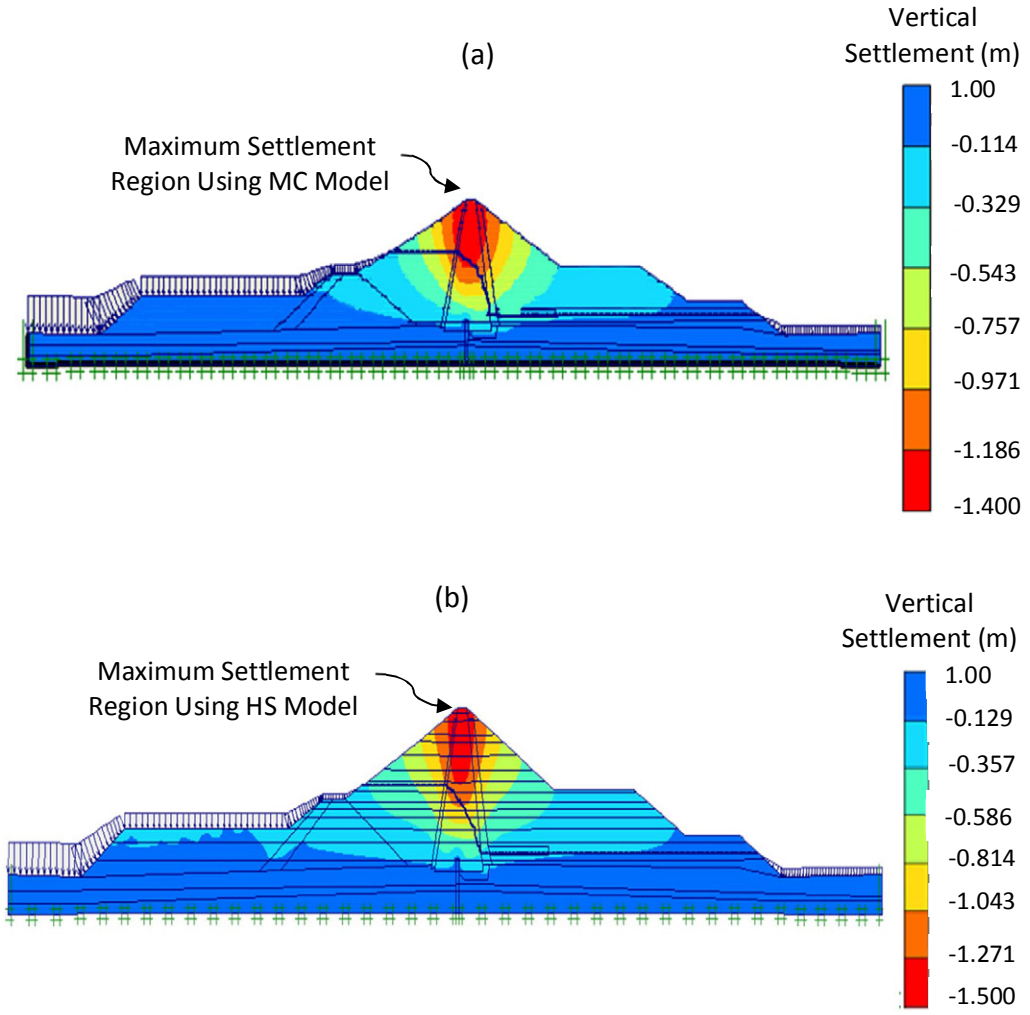

Figure 8: Computed vertical displacement by FEM analysis in Section 5 at the time of construction and impounding of the dam by (a) MC model, and (b) HS model

As can be seen in Figure 8, the maximum calculated settlement occurred at the core near the crest. The settlement at the operation stage is presented in Figure 9. As clearly shown in this graph, the maximum settlement is at the crest of dam and the displacements at the upstream shell are higher than the downstream, as expected. Similar graphs were created for Sections 4 and 7.

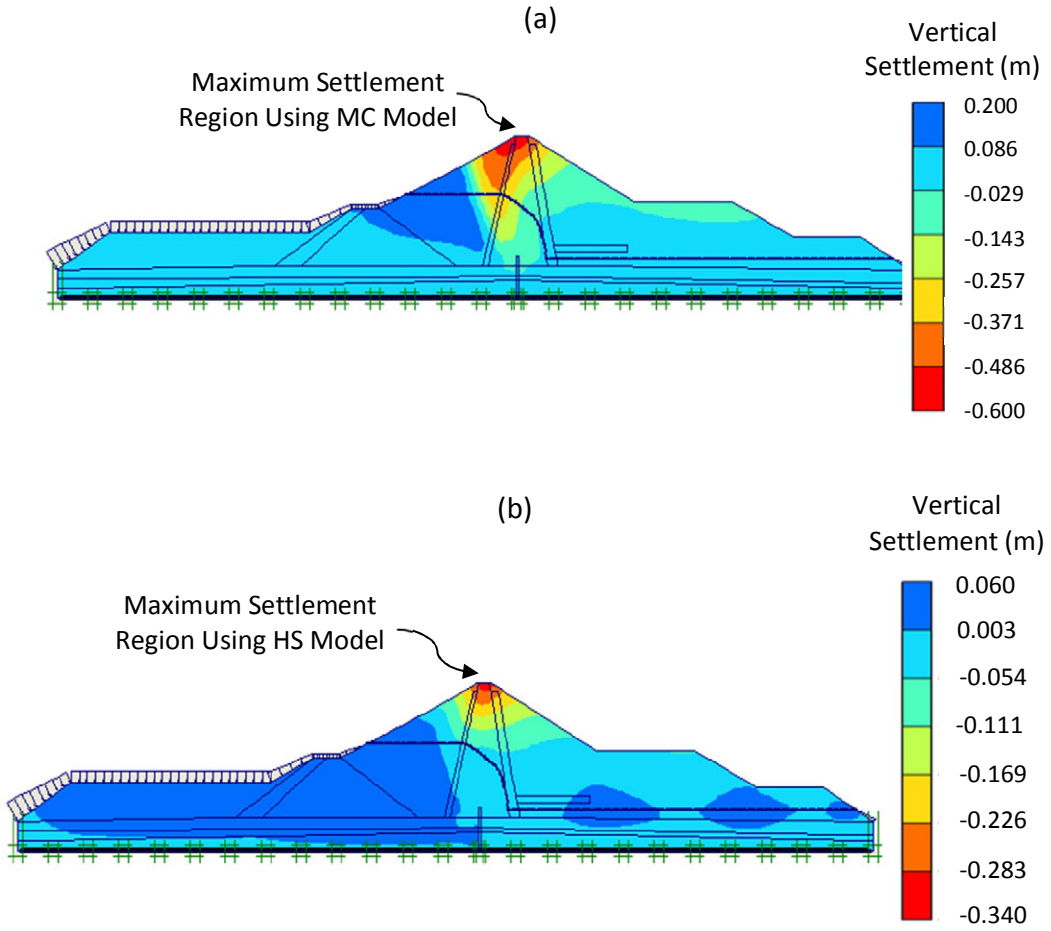

Figure 9: Calculated settlements by (a) MC model, and (b) HS model, in the body of the dam in Section 5 during the operation period

4.2 COMPARISONS, VALIDATION AND DISCUSSION

For comparing the results of numerical calculations with the measured data from the settlement monitoring, Cross Section 5 was considered. Figure 10 and Table 2 exhibit the measured and calculated settlements using MC and HS models at the end of construction in the core of dam at Section 5. The results depicted in Figure 10 show a good agreement between curves for both models. However, the differences between the measured and the calculated displacements are fairly large, except for the middle levels. The maximum settlement calculated by the MC model at the dam core was equal to 0.138 m, while applying HS model the value was 0.142 m.

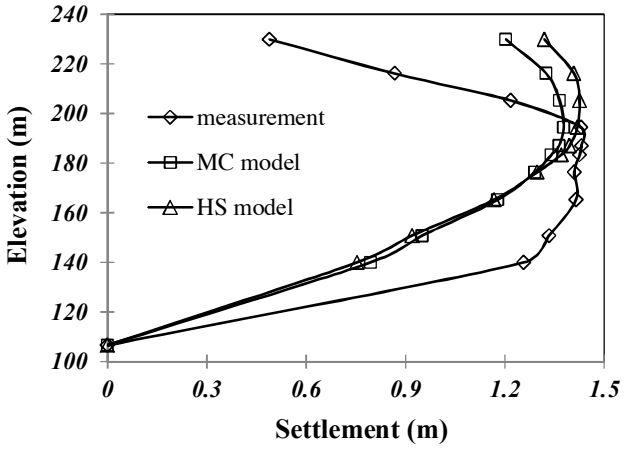

Figure 10: Measured and computed settlements with MC model and HS model in the core of the dam in Section 5 at the construction and impounding phases of the dam

Table 2: Comparison of measured and calculated settlements in the core of the dam in Section 5 at the construction and impounding phases of the dam

Elevation (m)	Measured Settlement (m)	MC Model Settlement (m)	HS Model Settlement (m)
106.6	0	0	0
140.0	1.256	0.794	0.753
150.8	1.333	0.95	0.919
165.3	1.415	1.178	1.167
176.4	1.40.9	1.290	1.297
183.3	1.426	1.340	1.370
187.0	1.431	1.363	1.395
194.5	1.429	1.377	1.419
205.3	1.217	1.365	1.425
216.2	0.867	1.324	1.408
229.9	0.489	1.202	1.319

Referring to the monitored data, the maximum vertical displacement at the end of construction phase was 0.143 m. Therefore, it could be concluded that the HS model in predicting the maximum settlement was more accurate in contrast with the MC model, which was more precise in calculating its level. In the higher levels the calculated settlements were more than the measured data. This could be attributed to the arching effect in the core, in those levels during construction of the dam. Arching caused by transferring of stresses from the soft clay core to the stiffer shell as a result of differential movements between shell and core (Talebi et al. 2013). The stress distribution at the end of construction and impounding stages along the core in Section 5 is depicted in Figure 11. The stresses in the core reduced due to arching effect; hence, this caused the reduction of vertical displacements. The overestimating of the crest settlement by the FEM analysis was also observed in other investigations (Gikas and Sakellariou 2008b).

In the lower parts, because of saturation of this part of dam during impounding, and hence, reducing of the elastic modulus and developing of buoyancy forces, the monitored settlements were higher than the calculated results. The same results were found by Szostak-Chrzanowski et al. (2008).

For validation of the suggested parameters, Sections 4 and 7 were modeled during the construction and impounding stages and the settlements were studied. The assumed constructed layers were 15 for both cross section models and the boundary conditions and calculation phases were the same as Section 5. The calculated and monitored settlements

in Sections 4 and 7 during the construction of the dam are shown in the Figure 11. The trends of computed settlements were similar to the measured data, but the observed vertical displacements were more in the lower levels, due to saturation of these regions during impounding of the dam. Studying the effects of saturation and pore pressures on the calculation results is complicated. The pore pressures in the core decrease the effective vertical stress, then the calculated settlements become to be less, while in this condition the stiffness (which depends on the stress levels) decreases in HS model. Thus, the calculated settlements using HS model is slightly greater than the MC model results. Because of arching on the higher levels of the core the monitored settlements were less than the computed results for both models. The most agreement between the measurement and calculated vertical displacements was being observed in the middle levels, which the maximum settlement occurred.

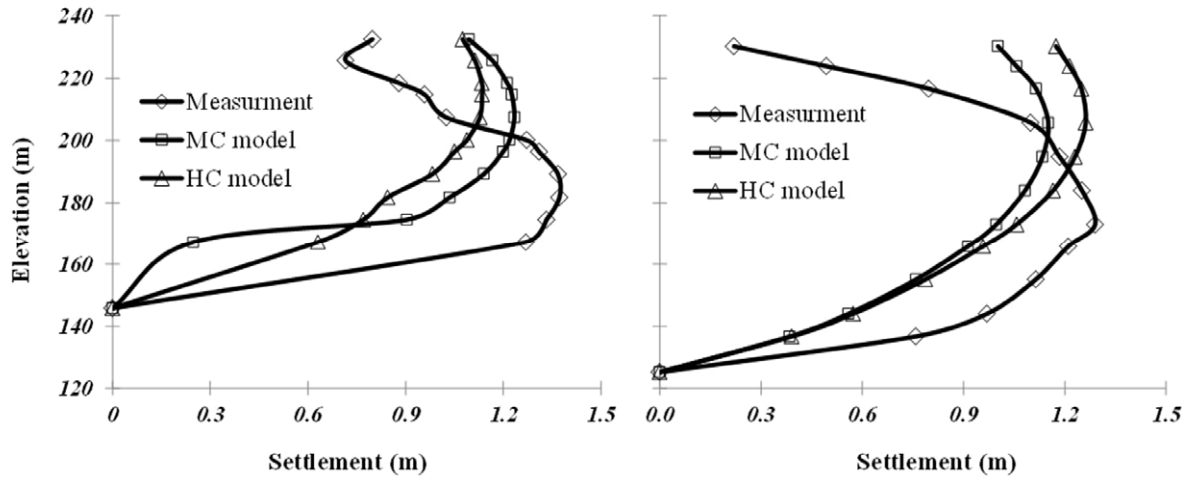

Figure 11: Monitored and calculated settlements, using MC model and HS model in Section 4 [left] and Section 7 [right], during the construction and impounding phases of the dam

The observed and computed crest settlements of the dam are depicted in Figure 12 during construction and operation stages. Referring to Figure 12., approximately 0.3 m difference could be observed between the measured data by the magnetic inclinometer and the results of FEM analysis for both models (the exact difference was 0.29 m for MC model and 0.32 m for HS model), indicating the crest settlement in the second impounding of the dam. It can be noted that the first impounding of the dam was performed before construction of the crest. The HS model results had less difference with the measured data. The crest settlement at the end of operation period (2009) was measured about 487 mm, while this value was calculated about 826 and 620.5 mm with the MC and HS model, respectively.

As expected, this difference was less for the middle levels. This point is shown in Figure 13. In this figure, the calculated and measured settlements in level 176 m (at the middle level of the dam) can be observed. It is clear that there is an apparent difference between the measured and calculated curves, particularly in construction and during the first impounding period, but with continuing the construction of dam and during the operation period the differences became to be less. It can be considers as a further confirmation for correcting the calculations. The difference due to construction of the dam was higher in this stage, due to more elapsed time of consolidation and the imposed weight of higher layers. As shown in Figure 11, the construction time of the middle layer of dam was about 2 years, before constructing the dam's crest layer. The computed settlements applying HS model in the operation period increased more than the observed data, whereas the results of MC model have a better match with them. Hence, it is expected that employing the MC model may yield a better simulation for the settlement of the dam in the future.

Figure 14 displays the vertical calculated and measured displacements in the crest of the dam in cross Sections 4 and 7 in the operation period. The trend of two graphs is similar to Cross Section 5. In Cross Section 4 with relinquishing of the settlement at the first impounding phase, the MC model was simulated a better trend for the displacements; and it sounds that this model might be more appropriate for prediction of the future behaviour of the dam. The result of the calculations in Cross Section 7 was similar to the other two sections.

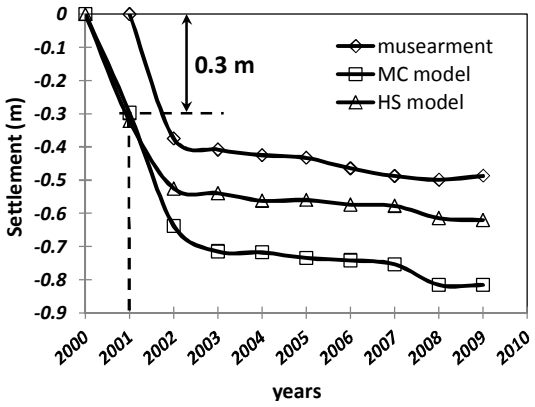

Figure 12: Total measured and calculated vertical displacement using MC model and HS model of the dam crest at the lifetime of the dam in Cross Section 5

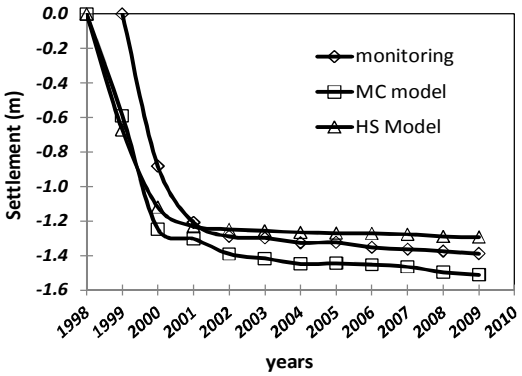

Figure 13: Total settlement of the middle of Dam (level 176 m) derived by the monitored data and FEM analysis in Section 5

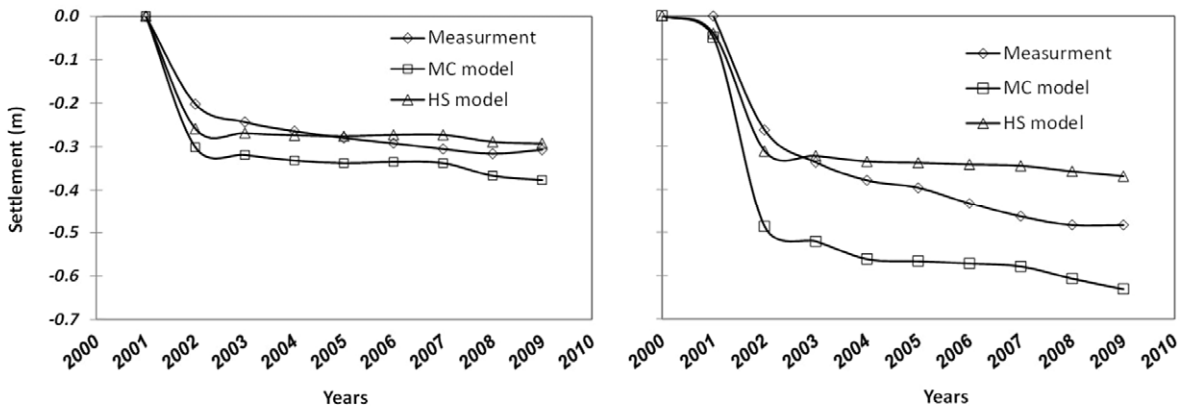

Figure 14: Comparison of measuring and computed vertical displacement in the crest of the Dam in cross Section 4 [left] and Section 7 [right]

The observed and computed vertical displacements at the operation stage at the crest and in middle levels along the length of dam have been shown in Figure 15. The curves in this figure are drawn by a linear interpolation between the settlement occurred in the three cross sections of the dam, as mentioned before. The calculated settlements by the numerical model have a similar trend to the monitored data and the differences in the crest of dam when using the MC model are less, particularly in the middle levels. Therefore, it could be concluded that unlike the construction stage model, the accuracy of the MC model in the crest was higher than the middle of the dam in operation stage, and the maximum difference observed was 0.031 m for the crest and 0.067 m for the middle of the dam, as both of them were related to Section 7. The results of HS model in the operation period had less accuracy than the MC model. In Cross Section 4, the difference was less, but in the other two cross sections the error was relatively high, especially for the crest of the dam. Referring to Figure 15, it can be seen that the settlements in the crest are significantly more than those in the middle of dam. By and large, the two applied FEM models simulated the settlement trend properly, and this might be an added confirmation for the suitability of the numerical modeling employed.

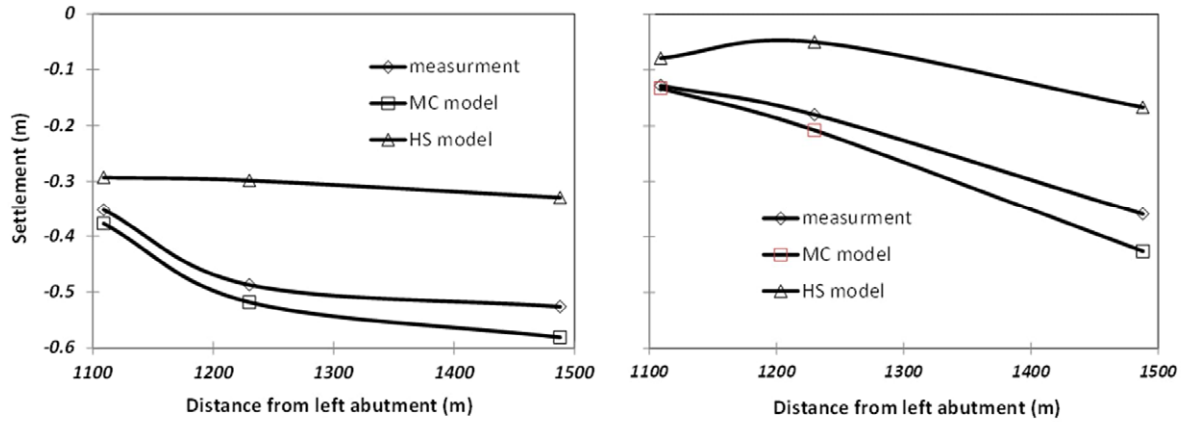

Figure 15: Vertical displacements obtained from site measurements and FEM analysis along the length of Dam at the crest [left] and at the middle [right] in the operation period

The cumulative monitored and computed vertical displacements at the end of 2009 in the three cross sections of the dam are presented in Figure 16. This figure shows the calculated settlements are less than measurement data in the lower levels because of pore pressures produced during impounding and operation stages of the dam and reducing of the effective stresses. In comparison with the construction phase model, the difference between the levels of maximum settlement was higher, especially for the HS model results. In the higher levels of the core the calculated settlements by both two finite element models were more than measured data.

The main reason for this difference could be due to the arching phenomenon in these levels of the dam during the construction stage. These figures reveal that using a single model for simulating the behaviour a dam in different phases of its lifetime may produce unreliable results, thus it is recommended to perform distinctive models for different stages of a dam lifetime.

The accuracy of the HS model during the operation stage was less than the MC model. This is probably due to the presence of pore pressures in the lower levels of the core. The pore pressure in some points of the low levels of the core was more than earth pressure, leading to a positive displacement (to the upward of the core). In the HS model, the reduction of the stiffness due to the presence of pore pressures and reduction of the effective stresses in these levels led to increase in these positive displacements. As explained earlier, the settlement of the crest is representing the cumulative displacements of the lower levels, hence these positive displacements in the lower levels reduce the calculating crest settlement with the HS model. In the MC model the stiffness does not change with the stresses then the strength of the soil against the positive displacement was more, then the reduction in the predicted settlements of the crest was less. Therefore, the behaviour of the HS model for simulating of the settlement of the earth dam core in the presence of the pore pressure can be complicated, and further research is required to study this occurrence.

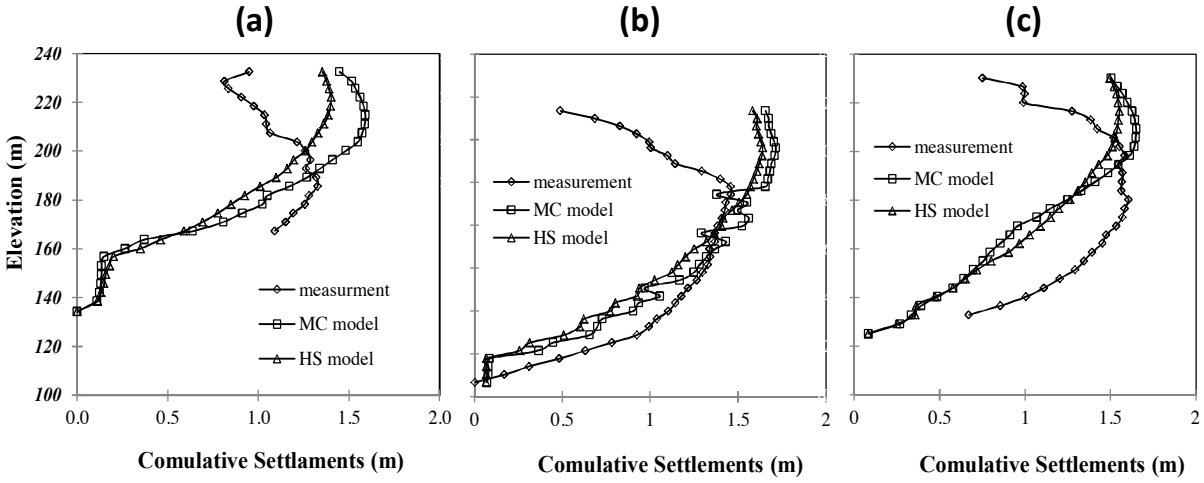

Figure 16: Observed and computed cumulative settlements (a) at Section 4, (b) Section 5, and (c) Section 7 of the dam at the end of 2009

One of the main goals for developing different numerical models in this study was prediction of the future behaviour of the dam. The settlement of the dam in the operation stage depends on the fluctuation of the reservoir water level. However, by assuming the pattern of the last fluctuation of the reservoir water level in the next ten years, the vertical displacement of the dam was computed. The displacement results for Cross Section 5 were a 171 mm using the MC model and 71 mm when applying the HS model for the crest of the dam, and with these values the cumulative settlement at the crest in this section reached to 658 and 558 mm based on the MC model and HS model, respectively. As mentioned before, the results of MC model during the operation stage had better agreement with measured data, and the anticipated settlements applying this model would be more reliable.

5 CONCLUSIONS

The investigation of monitored settlements in the body of Karkheh earth dam showed the maximum observed settlement after a 10 years operation was about 1.15 m, which more than 80% of the settlement was associated with the construction and impounding stages. The time series of settlements reveals the occurring a continuous consolidating behaviour in the dam body and the settlements are approaching to the final values with an exponential decreasing trend. Tow material models comprising the Mohr- Coulomb (MC) and Hardening soil (HS) models were used for simulating settlements in the dam body. The calculations were carried out in plane-strain conditions. The comparison of the results, obtained from FEM analyses with the measured data acquired using magnetic inclinometers installed on the dam body, represents a good consistency both along the height and the length of the dam. The maximum settlement of Karkheh earth dam at the end of construction phase was 0.143 m while this value was equal to 0.138 m by the MC and 0.142 m by the HS model. These findings confirm the suitability of the employed numerical modeling and the values accepted for the models parameters.

The results of the FEM modeling also showed a reasonable accuracy in predicting the maximum settlement and its level in the body of dam. The best agreement between the calculated vertical displacements and monitored data was observed in the middle levels of the dam. Although, the general accuracy of the two applied soil models in the construction and impounding stages was similar, the error of the computed settlements using the MC model was less than the HS model, particularly in the operation period. It may be associated with the presence of excess pore pressures in the lower levels of the core, reduction of the effective stresses, the stiffness value in the HS model and development of positive displacements in these levels. The maximum differences between calculated and observed settlement at the end of 10-years operation period were 0.031 m for the crest and 0.067 m for the middle of the dam by using of MC model. Therefore, the predicted settlements of the dam in the future employing the MC model might be more reliable. The results obtained in this study indicate that one of the proper methods for the calibration and validation of the geotechnical modeling can be combination of FEM analysis with exiting observed data. It could be useful in

interpreting the simulated results. It is also recommended to perform distinctive modeling for simulating the dam behaviour in different stages of its lifetime. In spite of many advantages, there are some limitations for the numerical modeling of settlement in the earth dams such as hydraulic fracture in the core materials during the long term operation period, which can be affected the dam settlement in the future. Hence, it is recommended to closely monitor the dam deformation with time in a long-term.

6 REFERENCES

Athania, S.S., Shivamantha, S., Solankia, C.H. and Dodagoudar, G.R. (2015). Seepage and Stability Analyses of Earth Dam Using Finite Element Method, Science Direct, Aquatic Procedia 4 (ICWRCOE, 2015) pp. 876 – 883.

Berilgen M.M. (2007). Investigation of Stability of Slopes under Drawdown Conditions. *Computers and Geotechnics* 34: pp. 81–91.

Calvello M. and Finno R.J. (2004). Selecting Parameters to Optimize in Model Calibration by Inverse Analysis. *Computers and Geotechnics* 31: pp. 411- 415.

Dolezalova, M., and Hladik, I. (2013). "Constitutive Models for Simulation of Field Performance of Dams." *Int. J. Geomech*., 11(6), 477-489.

Esmaeilzadeh, M., Talkhablou, M. and Ganjalipour, K. (2017). Arching Parametric Study on Earth Dams by Numerical Modeling: A Case Study on Darian Dam, *Indian Geotech Journal*, https://doi.org/10.1007/s40098-017-0290-2. pp. 1-18.

Gikas V. and Sakellariou M. (2008a). Horizontal Deflection Analysis of a Large Earth Dam by Means of Geodetic and Geotechnical Methods. *13th FIG International Symposium on Deformation Measurements and Analysis*, May 12-15, Lisbon, pp. 1-9.

Gikas V. and Sakellariou M. (2008b). Settlement Analysis of the Mornos Earth Dam (Greece): Evidence from numerical modeling and geodetic monitoring. *Engineering Structures*, 30: pp. 3074-3081.

Han B., Zdravkovic, L., Kontoe, S. and Taborda, D.M.G. (2016), Numerical Investigation of the Response of the Yele Rockfill Dam during the 2008 Wenchuan Earthquake, *Soil Dynamics and Earthquake Engineering*, 88: pp.124-142.

Heidarzadeh M. Mirghasemi A.A. Niroomand H. and Eslamin F. (2019). Construction and Performance of the Karkheh Dam Complementary Cut-off Wall: an Innovative Engineering Solution. International Journal of Civil Engineering 17:859–869.

Jafari, M.K. and Shafiee, A. (1999). Dynamic Properties of Core Materials for some Embankment Dams in Iran. Proceeding of third international conference on Seismology and Earthquake Engineering, May 17-19, Tehran, Iran, pp. 433-443.

Kermani, M., Konrad, J.M. and Smith, M. (2017). An Empirical Method for Predicting Post-construction Settlement of Concrete Face Rockfill Dams, Canadian Geotechnical Journal, 2017, Vol. 54, No. 6: pp. 755-767.

Loupasakis, C.J., Christaras, B.G., Dimopoulos, G.C. and Hatzigogos, T.N. (2009). Evaluation of Plasticity Models' Ability to Analyze Typical Earth Dams' Soil Materials. Geotech. Geol. Eng. 27: pp. 71–80.

Michallis P. and Pytharoli S.I. (2016). Long Term Deformation Patterns of Earth-fill Dams Based on Geodetic Monitoring Data: the Pournai I Dam Case Study. 3rd joint international Symposium on Deformation Monitoring (JISDM) Vienna, 30th March, 2016.

Mirghasemi A.A. (2006). Karkheh Dam Instrumentation System-Some Experiences. *Geotechnical Instrumentation News* (GIN) 1:32-36.

Ozcoban S. Berilgen M.M. Kilic H. Edil T.B. and Ozaydin I. K. (2007). Staged Construction and Settlement of a Dam Founded on Soft Clay. *Journal of Geotechnical and Geoenvironmental Engineering*, ASCE 133(8): pp.1003-1016.

Pantazis G. Skarlatos D. and Pelecanos L. (2019). Long-term Geodetic Monitoring of Seasonal Deformations of Earth dams and Relevant Finite Element Verification. *4th Joint International Symposium on Deformation Monitoring (JISDM)*, Athens, May 15-17, 2019.

Plaxis (2006). Version 8, http://www.plaxis.nl.

Schenaz, T., Vermeer, P.A. and Bonnier, P.G. (1999). The Hardening Soil Model: Formulation and Verification. Beyond 2000 in Computational Geotechnics, Balkema, Rotterdam, pp. 281-290.

Shadravan, B., Mirghasemi, A.A. and Pakzad, M. (2004). Karkheh Storage Dam Cutoff Wall Analysis and Design. Fifth international conference on case histories in geotechnical engineering, April 13-17, New York, N 2.71.

Shafiee, A. (2008). Permeability of Compacted Granule–clay Mixtures. Engineering Geology 97: 199–208.

Shafiee, A., Bahador, M. and Bahrami, R. (2008). Application of Fuzzy Set Theory to Evaluate the Effect of Pore Pressure Build-Up on the Seismic Stability of Karkheh Dam, Iran. *Journal of Earthquake Engineering* 12(8): pp. 1296-1313.

Sherard, J.L., Woodward, R.J., Gizienski, S.F. and Clevenger, W.A. (1963). *Earth and Earth-Rock Dams*. John Wiley and Sons. New York.

Szostak-Chrzanowski A. and Massiera M. (2006). Relation between Monitoring and Design Aspects of Large Earth Dams. *12th FIG Symposium*, May 22-24, Baden, pp. 1-10.

Szostak-Chrzanowski A., Chrzanowski A., Massiera M., Bazanowski M. and Whitaker C. (2008). Study of Long-term Behaviour of Large Earth Dam Combining Monitoring and Finite Element Analysis Results. *13th FIG International Symposium on Deformation Measurements and Analysis*, May 12-15, Lisbon, pp. 1-10.

Talebi, M., Vahedifard, F. and Meehan, C.L. (2013). Effect of Geomechanical and Geometrical Factors on Soil Arching in Zoned Embankment Dams. *Geo-Congress*, ASCE.

Uromeihy, A. and Barzegari, G. (2007). Evaluation and treatment of seepage problem at Chapar-Abad Dam, Iran. Engineering Geology, 91: pp. 219-228.

U.S. Bureau of Reclamation Technical Service Centre, (2011), Embankment Dams, Design Standards No. 13, DS-13(9)-17.

Wen L. Chai J. Xu Z. Qin Y. and Li Y. (2017). Monitoring and numerical analysis of behaviour of Miaojiaba concreteface rockfill dam built on river gravel foundation in China. Computers and Geotechnics 85: 230–248.

Xu Y.K., Unami, K. and Kawachi, T. (2003). Optimal Hydraulic Design of Earth Dam Cross Section Using Saturated–unsaturated Seepage Flow Model. Advances in Water Resources 26: pp. 1-7.

Yao F. Guan S. Yang H. Chen Y. Qiu H. Ma G. and Liu Q. (2019). Long-term Deformation Analysis of Shuibuya Concrete Face Rockfill Dam Based on Response Surface Method and Improved Genetic Algorithm. Water Science and Engineering, 12(3): 196-204.

Zoorasna, Z., Hamidi, A. and Ghanbari, A. (2008). Mechanical and Hydraulic Behaviour of Cut off-Core Connecting Systems in Earth Dams. EJGE 13 (bund. k): pp. 1-12.

WHY JOIN THE AUSTRALIAN GEOMECHANICS SOCIETY

Geomechanics is the application of engineering and geological principles to the behaviour of the ground and ground water and the use of these principles in civil, mining, offshore and environmental engineering in the widest sense.

The Australian Geomechanics Society (AGS), founded in 1970, has roots that go back to 1953. It exists as a Technical Society of the Institution of Engineers Australia to provide activities, technical conferences, symposia, meetings and events designed to stimulate, educate and inform all those with an interest in the field. Such activities occur both nationally and through its many active chapters located around Australia.

The AGS is run by its members, for its members and enthusiastic involvement is encouraged.

Entitlements

As a member of the AGS you receive:

- Free access to evening seminars run by your local chapter including national and international speakers
- Discounts to AGS run courses, workshops and conferences, including the quadrennial Australia New Zealand Conference on Geomechanics
- Four editions per year of our journal, *Australian Geomechanics*, either in print or electronic version. A reduced membership fee for electronic journal access only is available
- Regular networking opportunities
- Access to our website members' zone, including all past editions of *Australian Geomechanics* (to 1971), select seminar and conference proceedings
- Membership to one of our three affiliated international technical societies:
  - International Society for Soil Mechanics and Geotechnical Engineering (ISSMGE)
  - International Association for Engineering Geology and the Environment (IAEG)
  - International Society for Rock Mechanics (ISRM)

Student Membership is available at no cost for all undergraduate students which includes access to the members zone, AGS run seminars and an electronic version of *Australian Geomechanics*.

Corporate Membership is also available. Please contact the AGS secretary at *secretary@australiangeomechanics.org* for more information.

Eligibility

There are no restrictions on joining the AGS. Although AGS is a Technical Society of Engineers Australia, you do not need to be a member of Engineers Australia to be a member of AGS. Discounts apply to those with membership of both Engineers Australia and AGS.

Fees

Membership fees for the 2023/2024 membership period are set out below. The subscription period is from 1 July to 30 June. Fees can be adjusted pro-rata for members who join for part of the subscription period.

Category	EA Member	Non EA Member
Corporate Membership	**825.00***	**825.00***
Full Membership	**198.00***	**220.00***
PostGrad Student or Retired Membership	**99.00***	**110.00***
Undergraduate Student Membership (conditions apply)	**Free**	**Free**

*A reduction in fees of $22 is applicable if you only want access to the electronic version of the Journal and do not require a printed copy.

How to join

For information on how to become a member of the Australian Geomechanics Society, please visit:
http://australiangeomechanics.org/become-an-ags-member/

INTERNATIONAL SOCIETIES

INTERNATIONAL SOCIETY FOR ROCK MECHANICS AND ROCK ENGINEERING (ISRM)

Embracing Geomechanics for Sustainable and Resilient Infrastructure Development in Australasia

Dear Esteemed Colleagues,

It is with great honour and gratitude that I assume the position of Vice President for Australasia within the International Society of Rock Mechanics and Rock Engineering (ISRM) for the term spanning 2023-2027. I am currently an Associate Professor and Director of Research in the Department of Civil Engineering at Monash University. I am a Fellow (FIEAust) and Chartered Professional Engineer (CPEng) of Engineers Australia. I have been an Editor-in-Chief since 2019 of the Tunnelling and Underground Space Technology journal (Elsevier). I have 15 years of experience in experimental, analytical, and computational investigation of rock mechanics, tunnelling, and mining engineering.

I want to take a moment to express my appreciation to the AGS National Committee for the great support, and my predecessor, Dr Sevda Dehkhoda, for her efforts and dedication to the field.

We are witnessing fast-paced developments in our infrastructure and energy resources. It is essential to recognise the critical role that geomechanics plays in this progress. Our region has made remarkable strides in energy, transportation, water, and lifeline sectors, where the understanding and application of geomechanical principles played a key role. These have laid the foundation for the robustness and longevity of our constructions and resources.

Amidst the excitement of the post-pandemic infrastructure boom, we are met with new challenges. The emergence of construction automation and digital transformation technologies presents us with unprecedented opportunities to optimise processes and enhance efficiency. However, even with these advancements, we cannot overlook the fact that we are still building with natural materials and designing structures that must withstand the forces of nature, including natural hazards and extreme events. Recent seismic activity in Australia and New Zealand, serve as poignant reminders of the need for innovative solutions to bolster sustainability and resilience in our urban and mining infrastructures. Geomechanics, in conjunction with other engineering disciplines, holds the key to achieving this.

As ISRM Vice President for Australasia, I am dedicated to fostering collaborative efforts, cultivating innovative solutions, and promoting excellence in education. By engaging with the the ISRM Board and the AGS National Committee, along with our esteemed members, we will work together to overcome challenges and seize opportunities in our region's infrastructure development.

The 15th ISRM Congress will be held in conjunction with the 72nd Geomechanics Colloquium in Salzburg, Austria, between 9 and 14 October, 2023. I look forward to seeing many of you there!

Thank you for your support and dedication to our shared mission.

Sincerely,

Qianbing Zhang
ISRM Vice President for Australasia

AGS REPRESENTATION ON ISRM COMMISSIONS

COMMISION	PRESIDENT(S)	EMAIL	MEMBER(S) FOR AUSTRALIA
Coupled Thermal-Hydro-Mechanical-Chemical Processes in Fractured Rock	Jonny Rutqvist	jrutqvist@lbl.gov	Baotang Shen
Crustal Stress and Earthquake	Professor Furen Xie	xxiefr@263.net	
Design Methodology	Professor Xia-Ting Feng	xia.ting.feng@gmail.com	Mostafa Sharifzadeh
Deep Mining	Dr Abbas Taheri	abbas.taheri@adelaide.edu.au	Murat Karakus Ranjith PG
Discontinuous Deformation Analysis – DDA	Prof. Yu-Yong Jiao Prof. Gao-Feng Zhao Dr Fei Zheng	yyjiao@cug.edu.cn gaofeng.zhao@tju.edu.cn zhengfei@cug.edu.cn	Professor Guowei Ma
Planetary Rock Mechanics	Serkan Saydam	s.saydam@unsw.edu.au	
Radioactive Waste Disposal	Dr Ju Wang	wangju9818@163.com	
Rockburst	Prof. Manchao He	hemanchao@263.net	Chengguo Zhang Murat Karakus
Rock Dynamics	Prof. Jianchun Li	jcli@seu.edu.cn	Sevda Dehkhoda Prof Jian Zhao
Rock Grouting	Mohamed El Tani	md.eltani@rockgro.com	
Soft Rocks	Prof. Xiaoming Sun	sxmcumtb@163.com	Mostafa Sharifzadeh
Sorptive Rocks	Dr. Shimin Liu Dr. Yixin Zhao	szl3@psu.edu zhaoyx@cumtb.edu.cn	Zhongwei Chen
Testing Methods	Professor Resat Ulusay	resat@hacettepe.edu.tr	Sevda Dehkhoda
Underground Nuclear Power Plant	Professor Shunsuke Sakurai	ssakurai@kensetsuk.or.jp	

EDITORIAL POLICY

Australian Geomechanics is published quarterly, in March, June, September and December, by the Australian Geomechanics Society. The magazine is edited and produced by the Australian Geomechanics Society. It provides a journal and news magazine for matters of interest to the Australian geotechnical community. The statements made or opinions expressed do not necessarily reflect the views of the AGS.

Whilst the authors of papers retain copyright, submission of a paper for publication implies that the author gives AGS permission to copy and distribute papers in hardcopy format as well as in electronic format. Furthermore, permission is given for the sale of individual papers or compilations by AGS to benefit AGS members as well as for the supply of paper abstracts to third parties so that papers can be catalogued and made findable in bibliographic databases.

All technical papers submitted to *Australian Geomechanics* should be accompanied by a signed AUTHOR DECLARATION FORM which can be downloaded from the AGS website: https://australiangeomechanics.org/wp-content/uploads/2019/05/AG-author-declaration-form.pdf

No technical paper will be processed unless the form is submitted.

Material will be accepted at any time and published in the next available issue.

The Editorial Panel of *Australian Geomechanics* seeks contributions for future editions. The following comments are offered to assist would-be contributors.

Contributions can include: refereed technical papers; technical papers or notes; or news items and reports.

Technical papers can be refereed to ensure that they are of a standard similar to those published in international geotechnical journals. Authors should aim for a maximum overall length of no more than 10 pages, although shorter papers or technical notes are particularly welcome. Authors should indicate if they want their submission to be refereed; the status of the paper will be indicated on publication.

Refereed technical papers should be original and:

- Papers on geotechnical engineering, engineering geology and environmental geomechanics. Papers should be topical, practically oriented and preferably of national interest. Case studies describing innovative geotechnical work are particularly encouraged.
- Papers on geotechnical or geoscience research undertaken in Australia or of relevance to Australian Geomechanics. These should clearly indicate their practical relevance and limitations.
- Authoritative reviews of aspects of geotechnical practice or aspects of geotechnical education.

Technical papers or notes can be: Items as above but submitted for rapid publishing. These will not be refereed but will be reviewed. They will be accepted at the discretion of the editorial panel. The intention is to provide a source for rapid dissemination of technical material to the geotechnical community.

- Discussions on papers published in previous editions.
- News items and reports can be: Items describing significant projects, instructive failures, conferences, courses or other matters of general interest to the Australian geotechnical community.
- Geotechnical book reviews.
- Letters to the Editor.

It is preferable for contributors to submit formatted text, tables and figures in electronic format using Microsoft Word on Windows or Mac compatible hardware. If containing equations a PDF file should also be submitted.

It is preferable that submitted papers are presented in a specific format, detailed below. Papers that have not been properly formatted prior to submission, and are provisionally accepted, will be returned to authors to address peer review comments and proper formatting. A formatted template for technical papers in *Australian Geomechanics* is available for download from the AGS website: https://australiangeomechanics.org/journal/editorial-policy/

Details of the correct journal format are:

- Single column format on A4 paper.
- Left and right margins of 20 mm.
- A top margin of 30 mm and a bottom margin of 25 mm.
- 10 point character size of Times New Roman font with single (normal) line spacing.
- Text should be formatted to have 6 pt after paragraphs and after headings.
- No indent at the beginning of paragraphs.
- Title of Paper in 14 point Times New Roman, bold, uppercase, and centred in column.
- Main headings numbered 1, 2, 3…. etc. in 12 point Times New Roman, bold, upper-case and centred in the column.
- Sub-headings numbered 2.1, 2.2, 2.3 … etc. in 10 point Times New Roman, bold, upper-case and left justified.
- Minor headings numbered 2.1.1, 2.1.2 … etc. in 10 point Times New Roman, bold, lower-case and left justified

- Items in bulleted or numbered lists should not be separated by a line, but should be indented by 10 mm.
- Formulae typed and numbered (1), (2), (3) … etc. and centred in the column.
- Captions for figures should be placed beneath the item and numbered Figure 1.
- Captions for tables should be placed above the item and numbered Table 1:
- Figures and tables should be referred to in the text as Figure 1, Table 1, etc.
- Figures and tables should be centred in the column.
- Do NOT use page numbers, these will be added later.
- In text citation according to the Harvard system of author (year) or (author, year) as appropriate. Multiple references should be separated by semicolons (author 1, year 1; author 2, year 2)
- References should be listed at the end of the paper in alphabetical order using the Harvard system: Author (year) title, publication, volume, pages, publisher with a 10 mm hanging indent and no blank line between each.
- Underlining should be avoided and symbols shown in italics.

FIGURES AND TABLES

All the journal is published in colour.

Where possible figures and tables should be placed at the correct position in the text. Figures should be imported into the document as a single image and not constructed in the word document. These should be sharp and of the correct size for incorporation into the finished document. The width of these must be less than or equal to the width of the text column (165 mm).

Where images are included in the paper they should be sent as a separate JPEG file to improve the picture resolution.

Photographs should preferably be good contrast gloss prints and of the correct size for incorporation directly into the copy. Please ensure that all such items are clearly marked to indicate position in paper.

EDITORIAL CONTACTS

A new editor is to be appointed. The Editorial Panel consists of the Executive and State Chapter Representatives on the AGS National Committee.

The process of submission, peer review, discussion, re-submission, approval etc. of technical papers, is conducted using the peer review software Scholastica. Technical papers should be submitted via:

Submit Manuscript button on the AGS Scholastica website:
https://ags.scholasticahq.com
or
Submit using Scholastica button on the AGS website:
https://australiangeomechanics.org/journal/

Correspondence other than submission of, and queries about, technical papers, may be emailed to:

Editor, *Australian Geomechanics*
E-Mail editor@australiangeomechanics.org

ADVERTISING RATES

Every three months, *Australian Geomechanics* reaches more than 2000 professional geotechnical engineers and engineering geologists spread throughout Australia. Most of these are associated with significant site investigations, construction and computer analysis. So *Australian Geomechanics* provides a very targeted delivery for advertising.

Advertising rates include GST and from the 1st January 2020 are:

SIZE*	ONE ISSUE	TWO ISSUES	FOUR ISSUES
Cover Page	$1330	$1920	$3330
Full Page	$1030	$1760	$2640
Half Page	$530	$990	$1320
Quarter Page	$300	$480	$740

The prices quoted are for advertisements supplied in digital form as print resolution (240dpi or more) PDF, JPG or TIFF files.

* Files should be supplied at correct size with at least 3 mm bleed for designs that print to the edge of the page.

A4 Portrait – Width: 210 mm x Height: 297 mm (+bleed)
Half A4 Landscape – Width: 210 mm x Height: 148.5 mm (+bleed)
Half A4 Column – Width: 105 mm x Height: 297 mm (+bleed)
Quarter A4 Column – Width: 105 mm x Height: 148.5 mm (+bleed)

Inserts into an individual mail-out of *Australian Geomechanics* can be accepted at a minimum charge of $1330 (including GST).

Advertising queries should be addressed to:

Sara Lanesman, Email: *lanesman@optusnet.com.au*

ADVERTISEMENT DESIGN

If required AGS can arrange the design of adverts for *Australian Geomechanics*. The advertiser shall provide logo (high resolution), heading, text content, other images (photos) and style guide (if advertiser has one), otherwise styles and colours will be made similar to company's website styles or other provided media.

AGS will provide 1-2 design options and allow for two revisions of the chosen concept.

AD SIZE	APPROX. MAXIMUM WORD COUNT	COST
Full Page	250	$350
Half Page	150	$250
Quarter Page	75	$150

If design is required, material should be submitted no later than the first business day of February for the March issue, May for June, August for September and November for the December issue.

ISRM

ROCHA MEDAL 2025

Since 1982 a bronze medal and a cash prize have been **awarded annually by the ISRM** for an outstanding doctoral thesis in rock mechanics or rock engineering, to honour the memory of Past President Manuel Rocha while stimulating researchers.

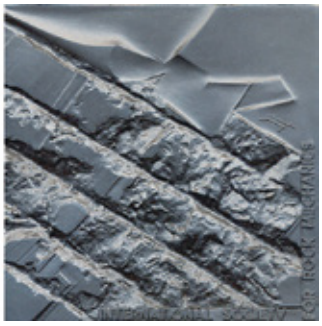

In addition to the Rocha Medal award to the winning submission, one or two runner-up certificates may also be awarded.

An invitation is now extended to the rock mechanics community for nominations for the Rocha Medal 2025.

Full details about the Rocha Medal are provided in ISRM By-law No. 7, and all relevant information can be obtained from the ISRM website - isrm.net.

Application

To be considered for an award the candidate must be nominated within two years of the date of the official doctorate degree certification.

Nominations shall be by the nominee, or by the nominee's National Group, or by some other person or organization acquainted with the nominee's work.

Nominations shall be sent electronically, addressed to the Secretary-General, and shall contain:

- a one page curriculum vitae, including nationality information;
- a written confirmation by the candidate's National Group that he/she is a member of the ISRM;
- a thesis summary, written in English, with between 5,000 and 10,000 words, detailed enough to convey the full impact of the thesis and accompanied by selected tables and figures, and information on word count;
- one copy of the complete thesis;
- one copy of the doctorate degree certificate;
- a letter of copyright release, allowing the ISRM to copy the thesis for purposes of review and selection only;
- an undertaking by the nominee to submit an article describing the work, for publication in the ISRM News Journal.

Application Deadline

The nomination must reach the ISRM Secretary-General by 31 December 2023.

Past Recipients

1982	A.P. Cunha	PORTUGAL	2003	L.M. Andersen	SOUTH AFRICA
1983	S. Bandis	GREECE	2004	G. Grasselli	ITALY
1984	B. Amadei	FRANCE	2005	M. Hildyard	UK
1985	P.M. Dight	AUSTRALIA	2006	D. Ask	SWEDEN
1986	W. Purrer	AUSTRIA	2007	H. Yasuhara	JAPAN
1987	D. Elsworth	UK	2008	Z.Z. Liang	CHINA
1988	S. Gentier	FRANCE	2009	G. Li	CHINA
1989	B. Fröhlich	GERMANY	2010	J.C. Andersson	SWEDEN
1990	R.K. Brummer	SOUTH AFRICA	2011	D. Park	REP. OF KOREA
1991	T.H. Kleine	AUSTRALIA	2012	M.T. Zandarin	ARGENTINA
1992	A. Ghosh	INDIA	2013	M. Pierce	CANADA
1993	O. Reyes W.	PHILIPPINES	2014	M.S.A. Perera	AUSTRALIA
1994	S. Akutagawa	JAPAN	2015	A.L. Bradley	ITALY
1995	C. Derek Martin	CANADA	2016	C.W. Boon	MALAYSIA
1996	M.P. Board	USA	2017	Bryan Tatone	CANADA
1997	M. Brudy	GERMANY	2018	M. du Plessis	SOUTH AFRICA
1998	F. Mac Gregor	AUSTRALIA	2019	Q. Lei	CHINA
1999	A. Daehnke	SOUTH AFRICA	2020	J. Shang	CHINA
2000	P. Cosenza	FRANCE	2021	Y. Yasuhiro	JAPAN
2001	D.F. Malan	SOUTH AFRICA	2022	R.S. De Silva	SRI LANKA
2002	M.S. Diederichs	CANADA	2023	J. Zhao	CHINA